# PPP2R1A regulates migration persistence through the WAVE Shell Complex

Yanan Wang

INSTITUT POLYTECHNIQUE DE PARIS

ECOLE DOCTORALE

ÉCOLE POLYTECHNIQUE

IP PARIS

NNT : 2022IPPAX044

Thèse de doctorat

# PPP2R1A regulates migration persistence through the WAVE Shell Complex

Thèse de doctorat de l'Institut Polytechnique de Paris
préparée à l'École Polytechnique

École Doctorale de l'Institut Polytechnique de Paris (ED IP Paris)
n°626
Spécialité de doctorat : biologie

Thèse présentée et soutenue à Palaiseau, le 20 juin 2022, par

**Yanan Wang**

Composition du Jury :

| | |
|---|---|
| Arnaud Echard<br>Directeur de Recherche CNRS,<br>Trafic membranaire et division cellulaire, Institut Pasteur, Paris<br>Professeur, École Polytechnique, Palaiseau | Président |
| Julie Plastino<br>Directrice de Recherche CNRS,<br>Laboratoire de Physique de l'Ecole Normale Supérieure (LP ENS),<br>Physico Chimie Curie, Institut Curie, Paris | Rapporteur |
| Maria-Carla Parrini<br>Ingénieur de Recherche,<br>Institut Curie, Centre de Recherche, Inserm U830, Paris | Rapporteur |
| Matthias Krause<br>Directeur de Recherche<br>Randall Centre for Cell and Molecular Biophysics,<br>King's College London, UK | Examinateur |
| Raphaël Guérois<br>Directeur de Recherche,<br>Institute for Integrative Biology of the Cell (I2BC), CEA, Saclay | Examinateur |
| Anna Polesskaya<br>Chargée de Recherche CNRS,<br>Laboratoire de Biologie Structurale de la Cellule (BIOC),<br>École Polytechnique, Palaiseau | Directeur de thèse |
| Alexis Gautreau<br>Directeur de Recherche CNRS,<br>Laboratoire de Biologie Structurale de la Cellule (BIOC),<br>Professeur, École Polytechnique, Palaiseau | Co-Directeur de thèse |

# Contents

# List of Abbreviations

| | |
|---|---|
| **ABI** | ABL interactor |
| **ARP2/3 complex** | Actin-related protein 2/3 complex |
| **Arpin** | ARP2/3 inhibitory protein |
| **BRK1** | BRICK1 subunit of SCAR/WAVE actin nucleating complex |
| **CDC42** | Cell division cycle 42 |
| **CP** | Capping protein |
| **CPI** | CP interaction |
| **CYFIP** | Cytoplasmic FMR1-interacting protein |
| **CYRI** | CYFIP-related Rac interactor |
| **ECM** | Extracellular matrix |
| **FAK** | Focal adhesion kinase |
| **FAs** | Focal adhesions |
| **HEAT** | Huntingtin, EF3, PP2A A subunit, and TOR1 |
| **HSPC300** | Hematopoietic stem progenitor cell 300 |
| **IRSp53** | Insulin Receptor Substrate of 53 kDa |
| **JMY** | Junction mediating regulatory protein |
| **MMPs** | Matrix metalloproteinases |
| **MT** | Microtubule |
| **NCKAP** | NCK-associated protein |
| **NHS** | Nance-Horan Syndrome protein |
| **NHSL1** | Nance-Horan Syndrome-like 1 protein |
| **NHSL2** | Nance-Horan Syndrome-like 2 protein |
| **NPF** | Nuclear promoting factor |
| **OA** | Okadaic acid |
| **PI3K** | Phosphatidylinositol 3-kinase |
| **PP2A** | Protein phosphatase 2A |
| **PRD** | Proline-rich domain |
| **RAC** | Ras-related C3 botulinum toxin substrate |

| | |
|---|---|
| **SCAR** | Suppressor of cyclic AMP receptor |
| **SFK** | Src family kinases |
| **SHD/WHD** | SCAR/WAVE homology domain |
| **SRA** | Specifically RAC1-associated protein |
| **ST** | Small tumor antigen |
| **STRIP** | STRN-interacting protein |
| **STRIPAK** | Striatin-interacting phosphatase and kinase |
| **STRN** | Striatin |
| **WASH** | Wiskott–Aldrich syndrome protein and SCAR homologue |
| **WASP** | Wiskott-Aldrich Syndrome protein |
| **WAVE** | WASP-family verprolin-homologous protein |
| **WH1** | WASP homology domain 1 |
| **WH2** | WASP homology domain 2 |
| **WHAMM** | WASP homolog associated with actin, membranes, and microtubules |
| **WIP** | WASP-interacting protein |
| **WMD** | WHAMM membrane interaction domain |
| **WRC** | WAVE regulatory complex |
| **WSC** | WAVE shell complex |

# Chapter 1

# Summary in French

La migration cellulaire joue un rôle essentiel dans divers processus physiologiques. Au cours de la migration cellulaire, des protrusions en forme de feuille (les lamellipodes), entraînées par des réseaux d'actine branchée, sont générées au niveau du bord avant de la cellule afin de fournir la force nécessaire pour avancer. La formation des lamellipodes est contrôlée par l'activité du complexe ARP2/3. Au bord des lamellipodes, la petite GTPase RAC1 active le complexe régulateur WAVE (WRC), qui active à son tour le complexe ARP2/3 pour nucléer les réseaux d'actine branchée. RAC1 maintient son activité lorsque l'actine branchée a déjà été polymérisée, ce qui constitue une boucle de rétrocontrôle positive. Ainsi, les cellules conservent leur capacité à migrer dans la même direction, un phénomène appelé « persistance de la migration ». Au bord du lamellipode, RAC1 active également ARPIN, une protéine inhibitrice d'ARP2/3, ainsi créant une boucle de rétrocontrôle négative, ce qui permet aux cellules de freiner et de tourner pendant la migration. En combinant les boucles de rétrocontrôle positif et négatif, la migration cellulaire est finement régulée. La formation de lamellipodes pilotée par RAC1-WRC-ARP2/3 est également requise pour l'haptotaxis, le processus de migration dirigée vers le gradient d'ECMs.

La voie RAC1-WRC-ARP2/3 est sous le contrôle de différents facteurs. Plusieurs ptotéines ont été identifiés pour s'associer au WRC et réguler la persistance de la migration cellulaire de différentes manières, comme le régulateur positif lamellipodine ou le régulateur négatif récemment identifié, NHSL1. Il a été démontré que CYRI/Fam49, un autre régulateur négatif de la migration cellulaire, entre en compétition avec le WRC pour la liaison avec le RAC1 via un domaine spécifique qui est structurellement similaire au domaine d'interaction avec le RAC1 de CYFIP. Cependant, les facteurs de régulation qui se lient spécifiquement au WRC n'ont pas été entièrement élucidés, en particulier dans le contexte d'une stimulation différentielle de la voie RAC1-WRC-ARP2/3.

Mon laboratoire d'accueil a conçu et réalisé un crible protéomique différentiel, pour les effecteurs potentiels de la signalisation RAC1-WRC-ARP2/3 dans des diverses conditions. Parmi les candidats issus de ce crible, PPP2R1A a été le plus fort, affichant une association réduite avec le WRC lorsque la migration est plus persistante. PPP2R1A est une des sous-unités du complexe phosphatase PP2A. La sous-unité catalytique du complexe phosphatase PP2A a été aussi trouvée dans le crible, mais n'a pas montré de variations dans les différentes conditions, ce qui suggère que PPP2R1A pourrait avoir un rôle indépendant de PP2A dans la régulation de la persistance de la migration cellulaire. PPP2R1A est également un gène associé au cancer, avec des mutants dans plusieurs types de cancer.

Mon projet de thèse visait à comprendre comment PPP2R1A régule la persistance de la migration dans les cellules normales et cancéreuses et à caractériser les mécanismes moléculaires de cette voie de régulation. Pour atteindre ces objectifs, j'ai réalisé des expériences de migration aléatoire et directionnelle de cellules en 2D et 3D. La purification par affinité en tandem a été utilisée pour explorer les partenaires potentiels de PPP2R1A. Un test de polymérisation de l'actine in vitro sur des billes recouvertes de GTPase a été établi pour examiner le rôle de PPP2R1A dans la régulation de la polymérisation de l'actine. Un essai d'acini en 3D pour imiter la structure du sein a été réalisé pour tester comment les mutations associées au cancer affectent la fonction de PPP2R1A.

Grâce à ces approches, j'ai montré que PPP2R1A est nécessaire à la persistance de la migration cellulaire. De manière surprenante, j'ai découvert que PPP2R1A régule la migration cellulaire en interagissant spécifiquement avec une nouvelle forme de complexe WAVE qui contient toutes les sous-unités du WRC, mais la sous-unité WAVE est remplacée par une protéine de la famille du syndrome de Nance-Horan, NHSL1. Ce nouveau complexe a été nommé le complexe WAVE Shell (WSC). De plus, en examinant l'effet des mutations de PPP2R1A associées au cancer dans les cellules, j'ai découvert que ces mutations interrompent considérablement l'interaction entre PPP2R1A et WSC et entraînent une persistance migratoire altérée et une morphologie anormale des acini en 3D.

Pour résumer, dans ce projet, j'ai caractérisé le rôle de PPP2R1A en tant que régulateur positif de la migration cellulaire directionnelle et démontré qu'un nouveau complexe multiprotéique, le complexe WAVE shell (WSC), est essentiel à cette fonction de PPP2R1A.

# Chapter 2

# Introduction

## 2.1 Cell migration

Cell migration is a fundamental process involved in a variety of physiological phenomena. During embryonic development, cell migration is required during different stages. In gastrulation, a large number of cells inside the blastocyst migrate collectively to form the three embryonic layers, the ectoderm, the mesoderm, and the endoderm. Cells from the three layers then migrate to specific locations for differentiation [1, 2]. During the immune response, leukocytes and macrophages rapidly migrate towards the damaged or infected tissues [3, 4]. To repair a blood vessel, platelets are activated and accumulated at the vascular injury site. Then, epithelial cells, macrophages and granulocytes migrate close to the injury site to heal the wound and to clean the pathogens, respectively [5, 6]. Abnormal cell migration contributes to many pathological processes, such as the cancer metastasis.

### 2.1.1 The modes of cell migration

Based on the cell types and the context of movement, cell migration can be roughly classified into single cell migration and collective cell migration, which allow cells to move from one location to another individually or as groups.

Despite the different patterns among diverse cell migration modes, the asymmetric spatial morphology is the typical feature in migrating cells. By forming protrusions at the leading edge and releasing attachment at the trailing edge, the asymmetric morphology generates the intracellular forces in migrating cells and leads to the translocation of cell body.

### Single cell migration

Single cell migration can be divided into amoeboid migration and mesenchymal migration (Figure 2.1).

- **Amoeboid migration**

  Amoeboid migration is a rapid single cell migration mode that is driven by hydrostatically generated blebs, actin-rich pseudopods, or reduced adhesion to the substratum [7].

  **Bleb amoeboid migration** is based on the bleb, which is a kind of spherical protrusion triggered by the hydrostatic pressure from the cytoplasm. This type of migration is evolutionally conserved and observed in various cell types, such as amoebae, embryonic cells, and some cancer cells [8]. The formation of blebs starts from the local detachment or disruption of the cortex on the plasma membrane. Then the fluid cytoplasm flows out from the damaged site, which leads to membrane expansion. The actin cortex under the bleb membrane is reformed during the expansion [9].

  On 2D substrates, the migrating cells form blebs at the leading edge. The blebs attach to the substrate through adhesion proteins on the membrane. Then the cell rear generates retraction force and detaches from the substrate to allow the cell body to move forward [10]. In the 3D environment, the blebs enable cells with reduced adhesion to squeeze through the gaps in the extracellular matrix network. This adhesion and traction independent migration mechanism is also known as 'chimneying' [11].

  **Pseudopodal ameboid migration** is a subtype of ameboid migration based on pseudopods, which are highly dynamic 3D arm-like membrane protrusions filled with actin filaments [12]. Pseudopodal migration is observed in the elongated fast moving cells ( $\sim 10 \mu m/min$ ) with low affinity adhesion to the 3D extracellular environment, such as neutrophils and dendritic cells [7, 13].

- **Mesenchymal migration**

  Mesenchymal migration is the most common mode of cell migration. Single cells with elongated, fibroblast-like, polarized morphology that can efficiantly adhere to the extracellular matrix (ECM), such as fibroblast, epithelial, and cancer cells use mesenchymal migration to move forward. Mesenchymal migration is a slow cell migration mode ( $\sim 1 \mu m/min$ ), which is mediated by the actin-rich protrusions (thin, sheet-like lamellipodial actin networks or finger-like filopodial actin bundles) at the leading edge

[14, 15]. To migrate in the tissue with mesenchymal migration, cells can secrete matrix metalloproteinases (MMPs) at the cell front and degrade the ECM to pass through the tissue [16].

Some cell types prefer to exclusively use either amoeboid migration of mesenchymal migration [17]. For example, zebrafish primordial germ cells prefer amoeboid migration [18], fish keratocytes cells prefer mesenchymal migration [19]. Many cell types are able to switch between different cell migration modes in response to the intracellular and extracellular cues [20, 21, 22]. For example, under the condition of confinement and low adhesion, mesenchymal cells can migrate with amoeboid mode, which is known as mesenchymal-amoeboid transition [23]. Neutrophils with the genetic deficiency in forming branched actin networks can switch from mesenchymal migration to bleb-based migration under the confined environment [24]. Cancer cells can display both amoeboid and mesenchymal migrations and switch between these two modes in response to the changes in the environment to promote cancer dissemination [25]. The plasticity of cell migration enables cells to adapt their migration mode in the complex environment.

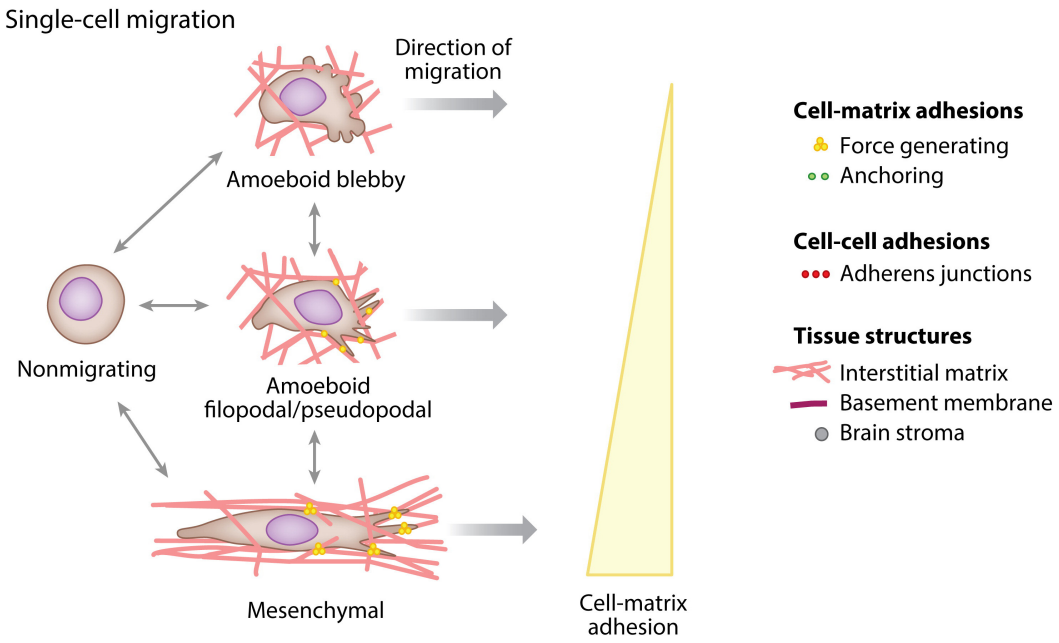


**Figure 2.1: Characterization of the modes of single cell migration.** Modified from [22]. Cells with a nonmigrating state can transition into diverse single cell migration modes. With amoeboid migration modes, cells show roundish or ellipsoid morphology with short trailing edges but highly dynamic front edges and weak adhesion towards the substrate. Cells with mesenchymal migration mode show elongated cell shape, strong adhesion and traction force.

### Collective cell migration

In contrast to single cell migration, in collective migration, cells still maintain cell-cell junctions and move as coordinated groups, in sheets, strands, tubes or clusters [17]. The collective morphology is dependent on the extracellular tissue environment and intercellular junction stability and types. Collective cell migration is an essential process during embryonic development, wound healing and tissue regeneration in multicellular organisms. Collective cell migration also contributes to tissue invasion in different cancer cells types [26].

Collective migration can be organized at different levels. At the cell level, with the low level of cell-cell coordination, cell-cell interactions only act as a way to hold the cells together and can not change the behavior of neighbor cells. The collective movement mainly depends on the activities of individual cells, such as the collective movement in the *Drosophila* follicular epithelium [13]. In this case, all the cells in the group contribute equally to the migration. Each cell regulates its front-rear polarity and generates its own protrusions and force for migration. With this migration mode, all cells are physically connected and required to move in the same direction, and cells in the group exhibit more efficient migration than single cells.

At the tissue level, the cooperation and coordination level of cells in the group is high. Cells communicate with others and affect the behaviors of the neighbor and faraway cells. In this case, the whole group can be considered as a single cell. This collective migration mode is also termed 'supracellular migration'. In this mode, the entire cell group exhibits front-rear supracellular polarity, the cells at the front of the migrating group (leaders) generate focal adhesions and protrusions to sense the environment cues and guide the group to move in the correct directions, which behaves like the front of an individual cell, and the cells at the rear (followers) generate high actomyosin contractility and traction forces, thus behaving like the rear of an individual cell [27] [28].

Single cell migration and collective cell migration modes can interconvert as well [26]. For example, the neural crest cells during the delamination phase reduce their cell-cell adhesions and migrate as mesenchymal cells with extensive migratory capabilities [29]. In addition, individual cells can detach from the group when the cell-matrix or cell-cell adhesions are weakened, leading to the collective to amoeboid transition [30] [31]. Moreover, epithelial cancer cells switch their movement from collective to amoeboid mode and promote cancer dissemination under hypoxia condition [32].

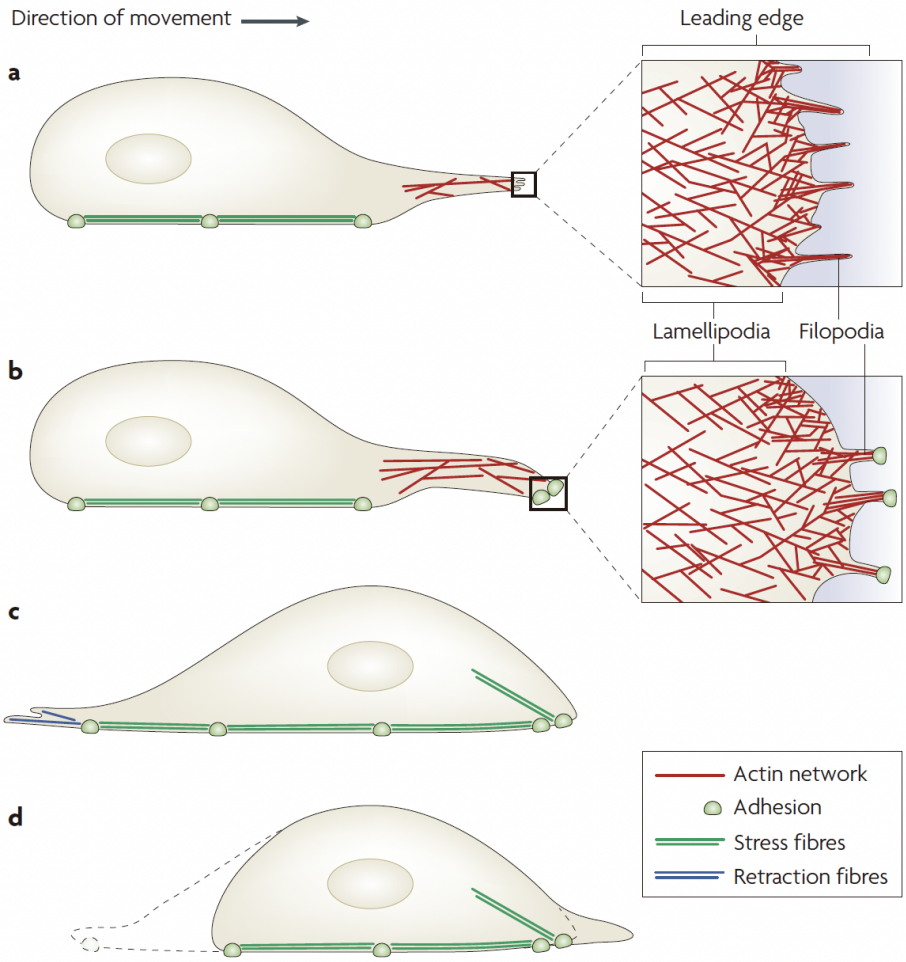


**Figure 2.2: Basic principles of cell migration** Modified from [33]. **A**, To initiate the migration, the cell generates the lamellipodia and filopodia protrusions at the leading edge. **B**, New adhesions to the substratum are formed under the leading edge. **C**, Next, the cell body translocates forward through the actomyosin-based contraction force. **D**, Last, adhesions at the trailing edge detach, and the cell rear retracts.

### 2.1.2 The principles of cell migration

#### Random cell migration

*In vitro*, cells have the intrinsic ability to migrate in the absence of extracellular cues, which is called random cell migration. But unlike Brownian motion, during random migration, cells prefer to sustain their movement in the same direction than to change, although this direction is randomly chosen at the beginning. The duration of a cell migrating in the same direction is called directional persistence [34].

The basic principles of adherent random cell migration are well studied (Figure 2.2). Firstly, the non-polarized cell distinguishes its front and rear and generates the actin-rich protrusions (flat, sheet-like lamellipodia and/or finger-like filopodia) at the leading edge, to initiate the migration. Then the new adhesions are formed at the leading edge to anchor the cell front to the substrate. Next, the new adhesions associate with the actomyosin-based stress fibers to produce contractile force and translocate the nucleus and cell body forward. Finally, the old adhesions disassemble and detach from the substrate at the trailing edge, the traction force pulls the rear of the cell forward [35, 36, 37].

#### Directional cell migration

*In vivo*, cells have to sense and respond to various environmental cues and migrate towards or away from the cues to complete their mission during different physiological and pathological processes. In contrast with random cell migration, cells exhibit directed migration to sense and migrate towards the external cues [38, 36]. Based on the nature of the external cues, different types of directed migration are defined. Chemotaxis refers to cell migration in response to the gradient of diffusible chemical cues [39], durotaxis refers to cell migration in response to the gradient of mechanical stiffness of the substrate [40], haptotaxis refers to cell migration in response to the gradient of adhesive substrates or substrate-bound chemokines [41], galvanotaxis refers to cell migration in response to the gradient of electric fields [42] (Figure 2.3).

Except for the basic mechanism of cell migration, directed migration follows other principles terms as the ‘four pillars of directed migration’. The four pillars refer to the four events that must happen during all types of directed migration, including the generation of the gradient signal, sensing of the signal, transmission of the signal, and execution of the signal [43].

- **Chemotaxis**

Chemotaxis is the directed migration towards the gradients of soluble chemical cues, such as growth factors or chemokines.

The chemotactic gradient can be self-generated by the migrating cells themselves. Cells degrade the homogeneous chemoattractant produced initially and form the gradient with low chemoattractant concentration at the high cell density region and high concentration at the surrounding region [44]. In this case, cells keep chasing the high level of chemoattractant and create robust self-generated gradients constantly at the direction of cell movement [45]. Alternatively, cells can secrete migration-enhancing factors at the front and positively stimulate the neighboring cells or leader cells themselves, in an autocrine and paracrine manner [46].

Chemotaxis is the best understood type of directed migration. The chemotaxis mechanisms have been studied in various cell types, such as *Dictyostelium*, immune cells, germ cells, neurons, and tumor cells. To sense and trigger the chemotactic signal, the receptors on the membrane of migrating cells bind the chemotactic cues to trigger the intracellular signal [47]. The activation of receptors in the cell region with higher chemoattractant concentration is stronger than in the low concentration region. The asymmetric activation leads to the polarised downstream intracellular signals. The specific signals accumulated at the cell front and rear promote directed migration [48].

- **Durotaxis**

  Durotaxis is the directed migration towards the stiffness gradients.

  The stiffness gradient can be self-generated by the surrounding or migrating cells themselves. For example, in the mouse limb bud, the stiffness gradient can be generated through *Wnt5a* mediated fibronectin expression [49]. The stiffness gradient also can be created by stiffening or softening the existing ECM. For example, the lysyl oxidase enzymes can stiffen the environment by crosslinking collagen and other ECM components to stabilize ECM and increase stiffness [50]. The matrix metalloproteinases can soften the environment by degrading the ECM proteins to reduce the external stiffness [51]. Stiffness gradients has been observed *in vivo*, and the stiffness has been shown to be related to cell density. During *Xenopus* gastrulation, the increased cell density below the neural crest leads to the increased head mesoderm stiffness and triggers collective migration of *Xenopus* neural crest cells [52].

To sense the mechanical force of durotactic cues, integrin-based focal adhesions (FAs) are important. The FAs generate the high traction force to ECM by the focal adhesion kinase (FAK)-phosphopaxillin-vinculin pathway. The traction force generated by FAs senses the stiffness of the ECM in a dynamic and fluctuating manner and leads to directed cell migration towards stiffer ECM [53]. Together with the integrins, the mechanosensitive ion channel Piezo1 also contributes to stiffness sensing and is involved in the durotactic response in neuronal growth [54]. The actin cytoskeleton-related small GTPases [55, 56] and regulators [57] are critical mechanical sensors for durotaxis, because they control the dynamics of protrusions and adhesions at the front and the retraction at the rear.

- **Haptotaxis**

  Haptotaxis is the directed migration towards gradients of adhesive substrates or substrate-bound chemical cues.

  Cells can secrete ECM components and form adhesive substrate gradients to drive haptotaxis naturally [58, 59, 60]. The migrating cells can also secrete chemical factors that diffuse across extracellular spaces and bind to ECM proteins from substrate-bound immobilized gradients for haptotaxis [61] [62]. As the migrating cells have the ability to remodel the matrix, the haptotactic gradient can be modified by the migrating cells themselves via various processes. For example, the deposition of laminin 5 onto dermal collagen in keratinocytes changes adhesive signals required for keratinocytes migration during wound healing [63]. Endothelial cells degrade local fibronectin and produce fibronectin gradient to migrate by haptotaxis during angiogenesis [64]. Compared to chemotactic cues, haptotactic cues are more long-lasting, since the gradients with immobilized factors are more stable.

  The substrate-bond haptotactic cues can be sensed by the receptor on the cell surface, which is similar to the mechanism in chemotaxis. The haptotactic cues composed of ECM components can be sensed by integrins. The nascent adhesions at the leading edge recruit specific signals which are critical for ECM haptotaxis. The activation of integrins at the nascent adhesions promotes FAK, SFK signalings and the RAC-WAVE regulatory complex (WRC)-ARP2/3 complex feedback loop, thus facilitating the formation of lamellipodia protrusions. The lamellipodia protrusions formed towards higher ECM concentrations are reinforced by the feedback loop to drive directed haptotaxis migration [65].

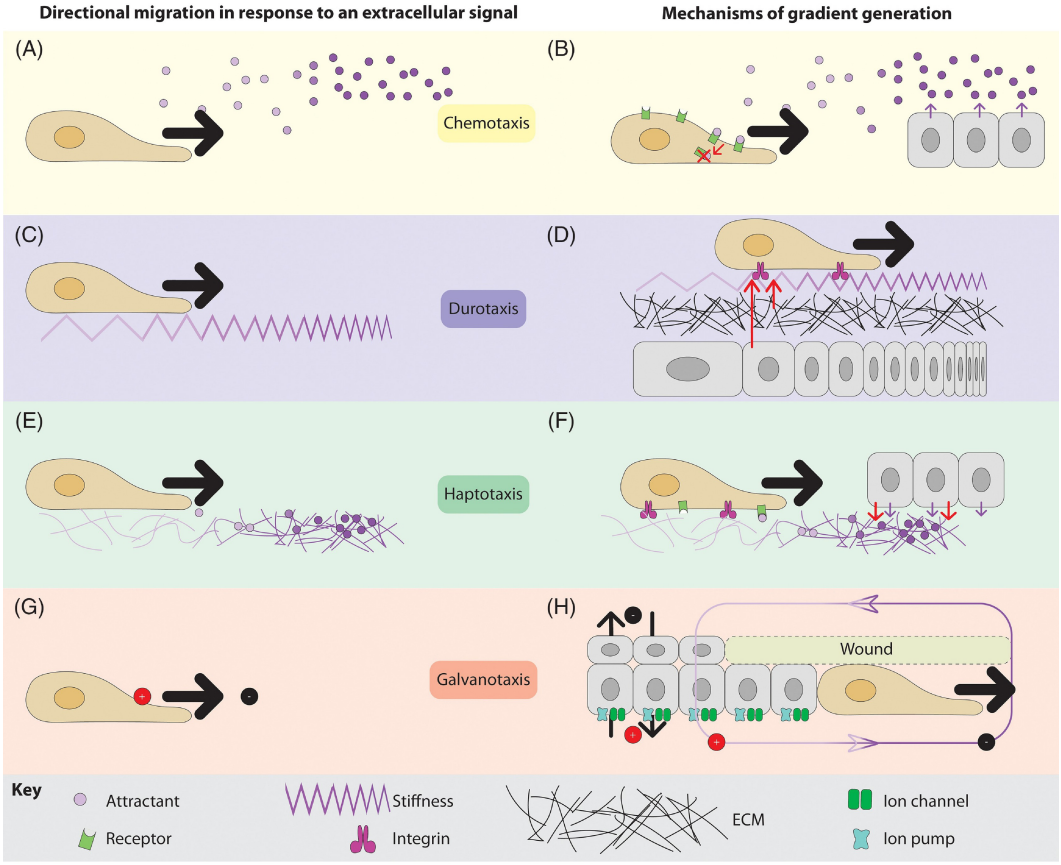


**Figure 2.3: Directed migration in response to different extracellular cues.** Modified from [37]. **A-B**, In chemotaxis, cells migrate towards or from soluble chemical cues produced by the migratory cells themselves, or by others. **C-D**, In durotaxis, cells migrate along a gradient of extracellular stiffness generated by modifying the extracellular matrix or cell density. Stiffness is mechanically sensed by integrins. **E-F**, In haptotaxis, cells migrate along a gradient of adhesive substrates or substrate-bound cues, the underlying mechanistic principles are similar to **B** or **D**. **G-H**, In galvanotaxis, cells migrate in response to an electric field generated by the ion leakage from the wound tissue.

Interestingly, the ARP2/3-mediated lamellipodial protrusions are crucial for haptotaxis, but dispensable for chemotaxis [66]. Myosin IIB is also required for the steering and stabilizing the polarity of cell migration during haptotaxis [67].

- **Galvanotaxis**

  Galvanotaxis is the directional migration towards the gradient of electric fields. The endogenous electric fields are present in many biological tissues. When the epithelium layer is disrupted by injury, the endogenous electric fields are generated immediately, by the asymmetric flows of charged particles and ions [42]. During embryogenesis, electric fields are established through trans-epithelial ion transport [68]

  To sense the galvanotactic cues, membrane depolarization through the activation of transmembrane voltage-gated ion channels can active the intracellular signaling pathways that affect cell polarisation and lead to directed migration [69].

  Another model for galvanotactic sensing and transduction is the electrophoretic redistribution of membrane components within the plasma membranes of the migrating cells, towards or away from the cathode. The redistribution of membrane components induces cellular polarity, and the activation of intracellular signaling pathways are commonly identified to play a role in chemotaxis to guide directed cell migration [70].

*In vivo*, cells need to sense different environmental cues and migrate towards or away from these cues correctly, during a variety of physiological processes. Failure to migrate in the proper way leads to defects in neuronal development, immune deficiencies, and incomplete wounds healing. Improperly initiated or misdirected cell migration can lead to invasive metastatic cancer and autoimmune diseases. In addition, cells are being exposed to multiple directional cues *in vivo* and directed migration is likely to cooperate and guide cell movement simultaneously [71]. But how cells respond to the complex environment and how these different cues cooperate in regulating cell migration remains to be investigated.

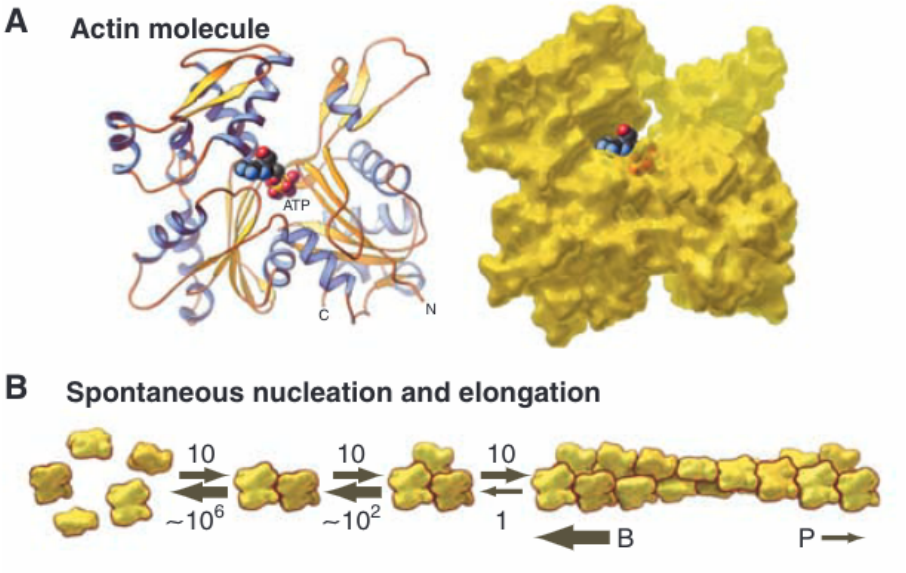


**Figure 2.4: Strcture of actin monomer and actin filament assembly.** Modified from [72]. **A**, Ribbon and space-filling models of the actin monomer with a deep cleft for nucleotide-binding. **B**, Unstable actin monomers spontaneously nucleate and polymerize into stable filaments with a helical arrangement. Actin filaments are polar since all subunits in the filament point in the same direction, and the barbed end of the filament grows much faster than the pointed end.

## 2.2 Actin dynamics

### 2.2.1 Actin and actin filaments

Actin is a highly abundant and conserved protein in all eukaryotes. Actin monomers form actin filaments to provide mechanical support for cells. Actin filaments participate in various biological processes, such as cell migration, vesicle trafficking, cytokinesis, and exocytosis.

Actin monomer is a 42 kDa globular protein (G-actin) with 4 subdomains and a deep cleft for ATP or ADP binding [73] [72]. In physiological conditions, actin monomers can polymerize and form long, stable double-stranded helical actin filaments (F-actin) spontaneously [74]. To start the polymerization reaction, the unstable actin dimers composed of two monomers are stabilized by forming a trimer or tetramer. This process is called the nucleation phase [75]. The initial process is slow, but once the nucleation is complete, actin polymerizes rapidly into actin filaments (F-actin), which is called the elongation phase. During the elongation process, actin filament is assembled with actin monomers at the barbed end and depolymerized at the pointed end. The barbed end grows ten times faster than the pointed end [76] (Figure 2.4).

Actin monomer binds to adenine nucleotide ATP or ADP. During the polymerization process, once the actin monomer is assembled into filament, the ATP that binds to the actin monomer is hydrolyzed and slowly dissociates with inorganic phosphate (Pi). The hydrolysis of ATP results in the stable ADP-Pi bound filament at the barbed end for elongation, and dissociation of Pi destabilizes the filament at the pointed end for depolymerization [77]. The steady-state with ATP-actin assembling at the barbed end and ADP-actin disassembling at the pointed end is called ‘treadmilling’, which is essential for cell motility [14] (Figure 2.5).

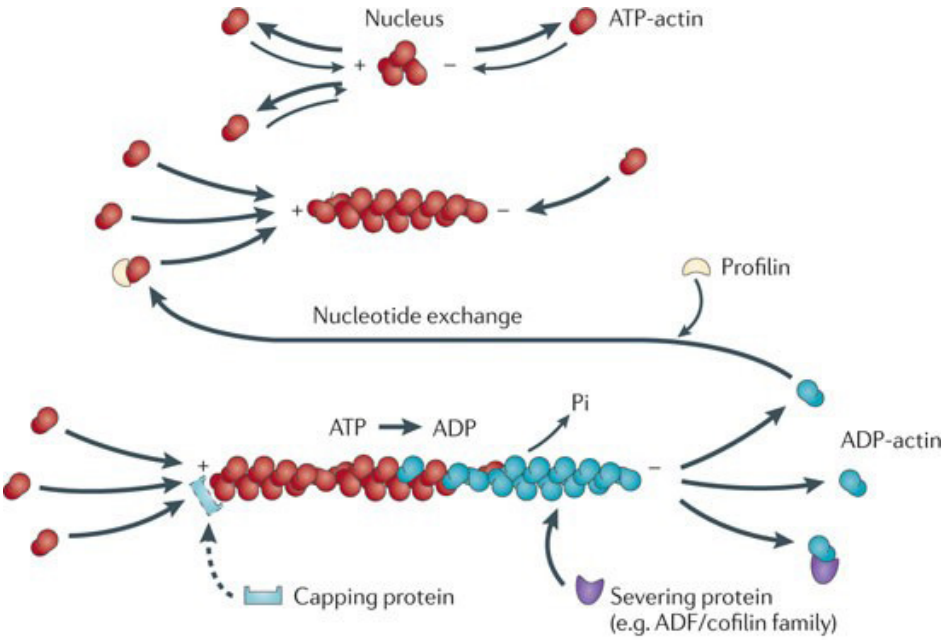


**Figure 2.5: Actin nucleation, elongation and recycling** Modified from [78]. The actin polymerization is initiated once three ATP-actin monomers assemble into a nucleus. Then the ATP-actin monomers polymerize quickly at the barbed end (+), leading to the elongation of actin filaments. Actin depolymerizes at the pointed end (-) and releases ADP-actin monomers. The dynamics of actin filament assembly are regulated by many factors, including profilin which promotes the exchange of ADP to ATP on actin monomers, capping protein that inhibits filament elongation, and severing proteins that disassemble actin filaments.

### 2.2.2 The regulation of actin filaments

Cells tightly control the polymerization and depolymerization of actin filaments for the needs of different functions.

Compared to the fast elongating process, the nucleation process is a slow and rate-limiting step since actin dimer is unstable, and actin monomers are commonly sequestered by actin monomer-binding factors such as profilin and thymosin-$\beta$4, to prevent spontaneous nucleation of new filaments [79]. To break the kinetic barrier and form a stable trimer or tetramer for nucleation, actin nucleators are recruited to mimic the trimer/tetramer state and promote the formation of actin filaments. The actin-related protein (ARP) 2/3 and formins are the best-studied actin nucleating factors [80]. Furthermore, capping protein terminates filament growth.

#### Actin binding proteins

**Profilin** is a small actin monomer binding protein that is involved in actin polymerization in most eukaryotes [81]. Most of the non-polymerized actin monomers in the cytoplasm are bound to profilin with a stoichiometry of 1:1. The profilin-actin complex provides the major pool for actin polymerization [14]. Profilin-bound actin monomers only can be added to the barbed end but not to the pointed end, which promotes the elongation at the barbed end and prevent polymerization at the pointed ends [82], thus leading to the polarity of growing actin filaments [83]. Profilin also can catalyze the exchange of ADP for ATP in actin, which refills the pool of ATP-actin monomers for efficient polymerization [84].

Except for profilin, actin monomer can be sequestered by **thymosin-$\beta$4**, another small actin monomer binding protein in many eukaryotes [85]. Thymosin-$\beta$4 has a higher binding affinity to ATP-actin than ADP-actin and binds to actin monomer in equimolar amounts [86]. Different from profilin, thymosin-$\beta$4 inhibits the exchange of the nucleotide bound to actin and stabilizes actin in monomeric form, thus preventing actin monomers from adding to the filament [87] [88].

While thymosin-$\beta$4 and profilin have comparable affinities to ATP-actin, thymosin-$\beta$4 protein expression is more abundant than profilin in cells [89, 79]. Most of the ATP-actin monomers in resting cells are held by thymosin-$\beta$4 as a pool which is ready for polymerization [86]. Once the polymerization is activated in cells, the free profilin competes with

thymosin-$\beta$4 for binding to ATP-actin and forms profilin-actin monomer pool for efficient actin polymerization [90].

The actin monomer pool can be regulated by actin filament assembly and disassembly dynamics. **Actin depolymerizing factors (ADF/cofilin)** are a family of actin-binding proteins which are essential in regulating actin filaments disassembly and actin network turnover [91]. ADF/cofilin is abundant in almost all types of eukaryotic cells [92]. ADF/cofilin can bind to the barbed end of both actin monomers and to actin filaments. ADF/cofilin binds to ADP-actin with higher affinity and inhibits nucleotide exchange [93]. It was originally shown that ADF/cofilin can increase actin filament depolymerization by promoting actin dissociation at the pointed end [91]. The main function of ADF/cofilin is to break down actin filaments by fragmentation or severing, which is different from the depolymerization mechanism [94]. ADF/cofilin cooperatively binds to the side of actin filaments with a higher affinity with ADP-actin than ATP-actin or ADP-Pi actin. The ADF/cofilin-actin binding contributes to the increased dissociation rate of Pi from actin subunits, which leads to faster aging of actin filament from ATP- to ADP-actin subunits [95]. Actin filament severed by ADF/cofilin increases the number of free filament ends for actin polymerization and depolymerization, resulting in increased general actin filament assembly dynamics [96].

The **capping protein** is a heterodimer that can bind to actin filaments. The capping protein tightly binds to the existing actin filament at the fast-growing barbed ends and prevents the actin monomer addition at the barbed ends, thus regulating elongation of filaments and actin monomer pool [97, 98]. The micromolar concentration of capping protein in the cytoplasm makes that most actin filament barbed ends are capped [99]. The capped barbed ends are essential for efficient depolymerization of the filaments at pointed ends in cooperation with other actin-binding proteins, like profilin and ADF/cofilin [100].

### Actin nucleators

As mentioned above, actin monomer binding factors sequester actin monomers to prevent spontaneous nucleation of new filaments, but enable fast addition of actin monomers for the elongation of existing filaments. Thus, nucleation process is a slow and rate-limiting step for filament formation *in vivo*. To break the nucleation barriers, cells express a variety of actin nucleators that respond to different cellular signals and regulate filament formation at a specific timing and subcellular locations [101] (Figure 2.6).

### The Formins

The Formins is a group of actin nucleators that can initiate the nucleation of linear actin filaments at the barbed end. Formins are a family of proteins that involve in the assembling of a variety of actin structures *in vivo*, such as cytokinetic actin rings, actin cables, filopodia, and stress fibers [102, 103]. Formins contain an N-terminal proline-rich formin homology 1 (FH1) domain, and a unique and highly conserved C-terminal formin homology 2 (FH2) domain. Formins can stabilize spontaneously formed unstable actin dimers and trimers through their donut-shaped dimeric FH2 domains [104]. After nucleation, the formin FH2 domain remains bound to the filaments and moves with the growing barbed ends, thereby protecting them from capping proteins [105, 106]. The processive binding of FH2 domain to the barbed end combined with the association of FH1 domain with profilin allows the rapid addition of new actin monomers at barbed ends. Moreover, the FH1-profilin-barbed end interaction further stabilizes formin at the barbed ends by preventing the force-sensitive dissociation after actin addition [107].

### The ARP2/3 complex

The ARP2/3 complex (Actin-related protein 2/3 complex) is the unique actin nucleator of branched actin filaments at the surface of membranes.

- **Charactrization of the ARP2/3 complex**

  The ARP2/3 complex was first described in *Acanthamoeba castellanii* and has been identified in almost all eukaryotes [108]. The ARP2/3 complex is a heteroheptameric protein complex composed of seven conserved subunits: two actin-related proteins, ARP2 and ARP3, that are highly similar to actin, and five smaller subunits referred to as ARPC1, ARPC2, ARPC3, ARPC4, and ARPC5 (actin-related protein 1-5). In many higher eukaryotes, several ARP2/3 subunits are encoded by more than one isoform. For example, in mammals, ARPC1 and ARPC5 are represented by two isoforms, ARPC1A/ARPC1B and ARPC5/ARPC5L, with 67% identity [109]. The ARP2/3 complex containing of different subunit isoforms may have different functions in nucleating.

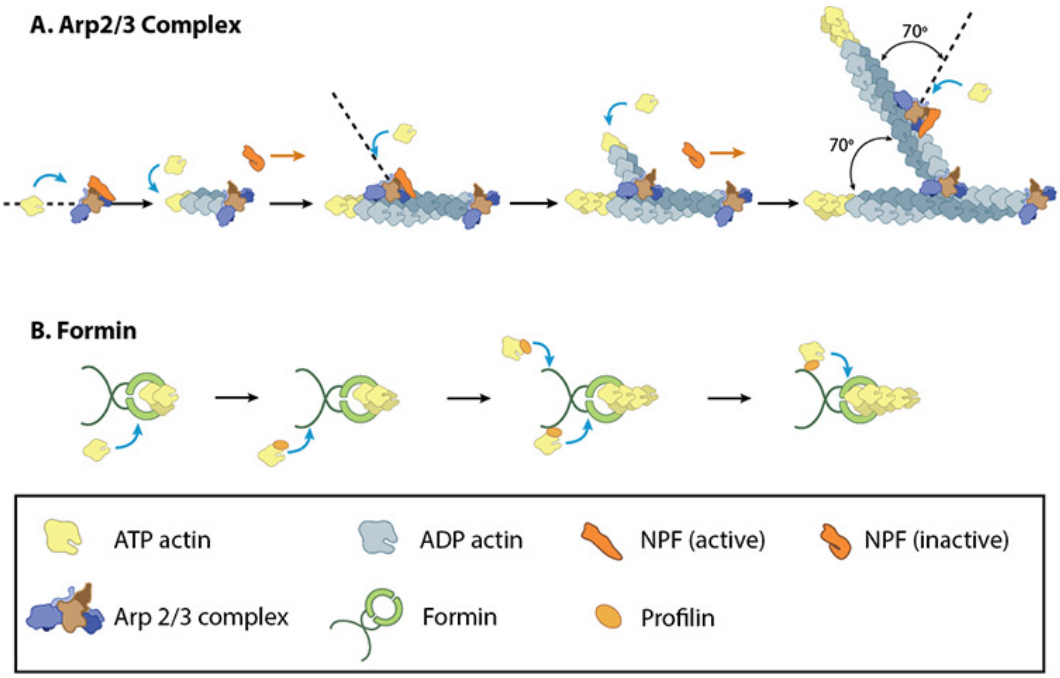


**Figure 2.6: Different actin nucleators in regulating filaments nucleation** **A**, ARP2/3 complex nucleates new branches filaments from the side of pre-existing filaments with the help of nuclear promoting factors (NPFs). **B**, Formin nucleates new linear actin filaments at the barbed ends by cooperating with profilin. Modified from https://www.mechanobio.info/cytoskeleton-dynamics/what-is-the-cytoskeleton/what-are-actin-filaments/how-does-arp23-mediate-the-nucleation-of-branched-filaments/

- **Cellular functions of the ARP2/3 complex**

  As the unique branched actin nucleator, ARP2/3 complex initiates the branched actin nucleation by binding to the side of a pre-existing filament (mother filament) and nucleating the branch filament (daughter filament) at a $\sim 70^{\circ}$ angle with a new barbed end facing the membrane surface [110, 80].

  ARP2/3 complex is involved in a variety of processes by generating branched actin networks at diverse subcellular locations. ARP2/3 complex is critical for cell migration by promoting the formation of lamellipodia and the initiation of filopodia at the leading edge of spreading cells [111, 112]. In 3D environments, the ARP2/3 complex contributes to cell invasion and matrix degradation by generating invasive finger-like protrusions at the leading edge, such as invadopodia in cancer cells or podosomes in hematopoietic and endothelial cells [113, 114]. ARP2/3 complex also plays an important role in endocytosis and phagocytosis by generating branched actin networks involved in endosomes and phagosomes [115, 116]. At the cell-cell adherens junctions, ARP2/3 complex-dependent branched actin networks generate protrusive force to push against each other and maintain cell-cell adhesion [117]. ARP2/3 complex can also produce continuous actin flow to drive the cytoplasmic streaming [118]. In the nucleus, ARP2/3 complex mediates actin polymerization that occurs at the damaged chromatin undergoing homology-directed repair, which is required for chromatin movement necessary for clustering the double-strand breaks [119]. The branched actin networks generated by the ARP2/3 complex also contribute to the nuclear movement from center to periphery in skeletal myofibre for proper muscle function [120].

- **The regulation of the ARP2/3 complex**

  ARP2/3 complex is intrinsically inactive and can be activated by nucleation promoting factors (NPF) [121, 122, 123].

  In the inactive conformation of the ARP2/3 complex, ARP2 and ARP3 are maintained distant from each other. Under the activation signaling, the ARP2/3 complex changes its conformation by bringing ARP2 and ARP3 close to each other to mimic the end of a new actin filament. Then, the ARP2/3 complex with activated conformation interacts with a pre-existing actin filament at the side to initiate the elongation of a new branch filament [110, 124]. The activated ARP2/3 complex acts as a branched junction of two actin filaments.

To activate ARP2/3 complexes, **nucleation promoting factors (NPFs)** are required. Most NPFs in mammals are from the WASP (Wiskott-Aldrich Syndrome Protein) family, which are called class-I NPFs. Several groups of NPFs have been identified in a specific region of cells to promote ARP2/3 mediated branched actin networks: WASP and N-WASP, WAVE1-3, WASH, WHAMM/JMY, and the newly identified WHIMP [125, 126]. These NPFs all share the homology VCA/WCA domain at the C-terminal. The VCA/WCA domain contains the Verprolin homology domain (also called WH2 for WASP homology 2), Cofilin homology domain (also called the central domain), and C-terminal Acidic domain [127, 128]. The C and A domains allow NPFs to bind the ARP2/3 complex, which promotes the conformational change of the ARP2/3 complex with closed ARP2 and ARP3. The V domain allows NPFs to bind an actin monomer and bring actin monomer to the closed ARP2 and ARP3 conformation, thus creating the structure that mimics the actin trimer nucleus that allows the initiation of daughter filament elongation. By interacting with the mother actin filament and the NPF, the ARP2/3 complex is stably maintained in the active conformation [122, 129] (Figure 2.7).

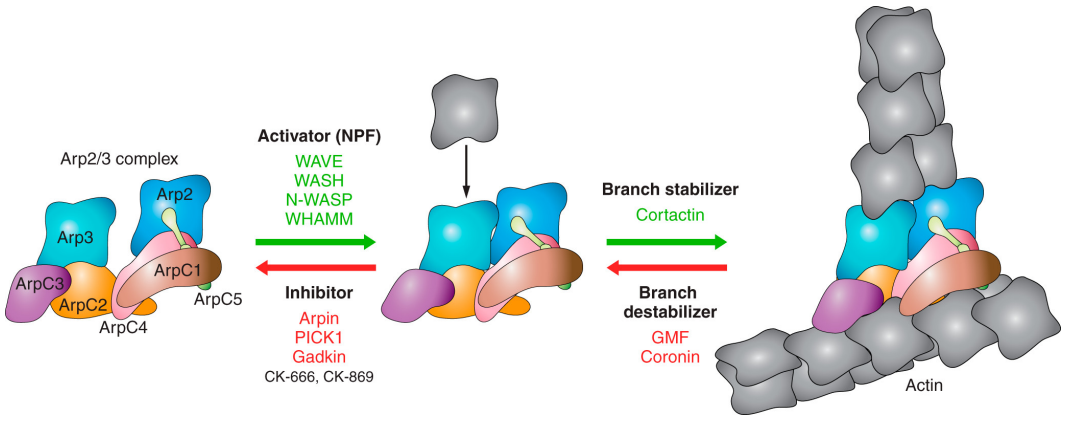


**Figure 2.7: Conformations of the ARP2/3 complex and the regulators between them.** Modified from [124]. The inactive ARP2/3 complex shows a conformation, where ARP2 and ARP3 are away from each other. Upon activation, the ARP2/3 complex rearranges its structure and brings ARP2 and ARP3 together to mimic the end of an actin filament. This active conformation allows the ARP2/3 complex to bind to the pre-existing filament and nucleate the new actin filament from the side. The ARP2/3 complex can be regulated by various factors which are represented above and below the arrows.

ARP2/3 complex is not only controlled by activators but also by inhibitory factors. Several **ARP2/3 inhibitory proteins** are found in different regions of the cell: Arpin, Gadkin, and PICK1.

**Arpin (ARP2/3 inhibitory protein)** is localized at the lamellipodium tip. Arpin contains an acidic domain at its C-terminal. With its A domain, Aprin interacts with the ARP2/3 complex and competes with NPF for ARP2/3 binding, thus sequestering the complex in the inactive conformation [130]. A recent high-resolution cryo-EMs study reveals the structure of Arpin bound to ARP2/3 complex and shows that Arpin contains both C and A domains at its C-terminal, similar to NPFs. But unlike the C and A domains of NPFs that bind to two sites(ARP2-ARPC1 and ARP3) on the ARP2/3 complex, the CA region of Arpin only binds to ARP3. The C domain of Arpin restricts its binding to the ARP3 subunit and stabilizes the C-terminal tail of ARP3. Thus allows to maintain the complex in the inactive conformation and to antagonize the binding of NPFs [131].

**Gadkin**, also known as $\gamma$-BAR, is another acidic domain-containing protein localized at the surface of endosomes. Gadkin directly binds to the ARP2/3 complex through its A domain but cannot activate ARP2/3-dependent actin polymerization. Gadkin is thought to sequester the ARP2/3 complex to endosomal vesicles without inhibiting the activity of the complex, thereby inhibiting cell spreading and motility in dendritic cells [132, 133].

**PICK1 (Protein interacting with C-kinase 1)** contains N-terminal PDZ domain, central BAR domain, and C-terminal acidic domain. PICK1 has been suggested to inactivate ARP2/3 at the surface of clathrin-coated endocytic pits [134]. However, the regulation is complex since it also has been shown that PICK1 does not bind nor inhibit ARP2/3 complex *in vitro* [135].

In addition, some proteins can interact with the ARP2/3 complex as **branch regulators**. These proteins regulate the assembly and disassembly of branched actin networks instead of regulating the activity of the Arp2/3 complex itself.

**Cortactin** is a branch-stabilizing protein that can bind both actin filaments and the ARP2/3 complex. Cortactin stabilizes the branched actin network by competing for ARP2/3 complex binding with NPF after branch nucleation [136, 137].

**GMF (Glial maturation factor)** is a branch destabilizing protein that belongs to the actin-depolymerizing factor (ADF)/cofilin family. However, in contrast to cofilin, GMF is shown to bind the ARP2 subunit of the ARP2/3 complex, instead of actin. GMF inhibits branch nucleation and promotes debranching by inserting itself between ARP2 and daughter filament at the branch junction [138, 139].

**Coronin** is also a debranching protein that can bind to both the ARP2/3 complex and actin filaments. Coronin destabilizes actin branches generated by ARPC1A/ARPC5-containing ARP2/3 complex but not ARPC1B/ARPC5L. Coronin debranches the filaments by stopping the ARP2/3 complex from binding the actin filaments [140, 109].

With the ARP2/3 and branch regulators, cells can control the actin network remodeling, depending on the specific cellular context (Figure 2.8).

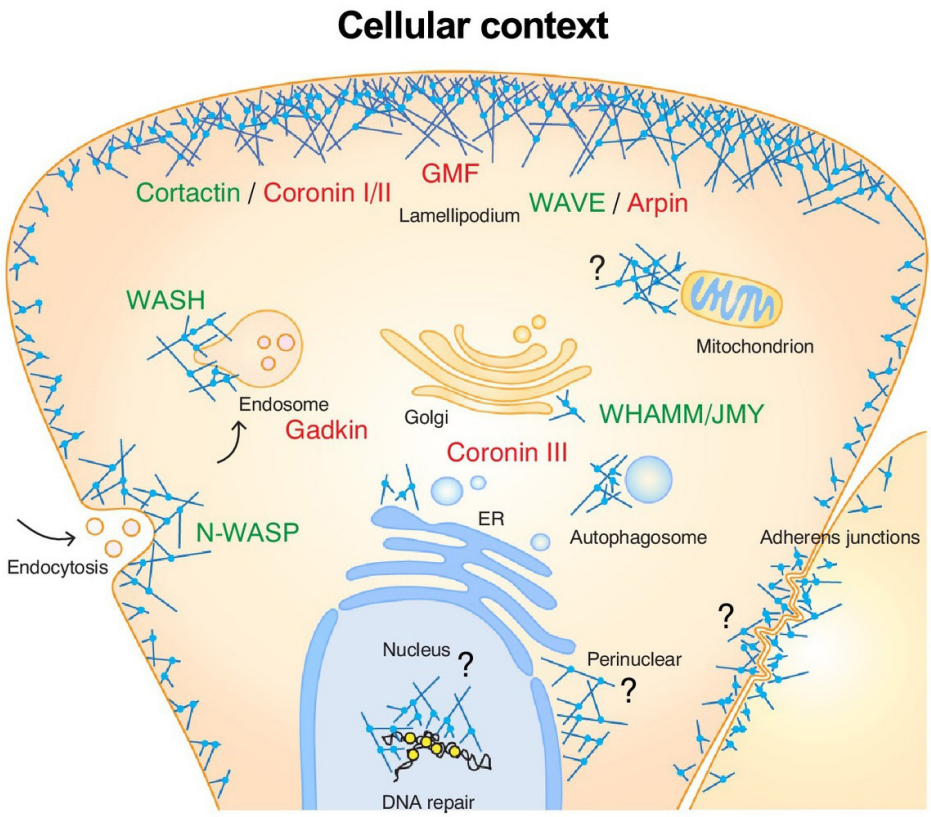


**Figure 2.8: Cellular context of the activators, inhibitors, and branch regulators of ARP2/3 complex.** Modified from [141]. NPFs and branch stabilizers are in green and inhibitors and branch destabilizers are in red.

### 2.2.3 The nucleation promoting factors (NPFs)

As mentioned above, NPFs act as ARP2/3 complex activators to promote branched actin filament nucleation via their conserved VCA domain at the C-terminal. The VCA domain is sufficient to activate the ARP2/3 complex *in vitro*. In cells, the VCA domains are masked in an autoinhibited conformation or embedded into a stable multi-protein complex to keep NPFs in inactive form. NPFs can be modified upon activation signals and expose their VCA domains for ARP2/3 complex activation. Based on the divergent domains at the N terminal, NPFs can be classified into different families that activate the ARP2/3 complex at various subcellular locations to exert specific functions, thus regulating ARP2/3-dependent branched actin network formation spatially and temporally throughout the cells [125]. Four types of NPFs are identified as N-WASP, WAVE, WASH, and WHAMM/JMY families in the human genome (Figure 2.9).

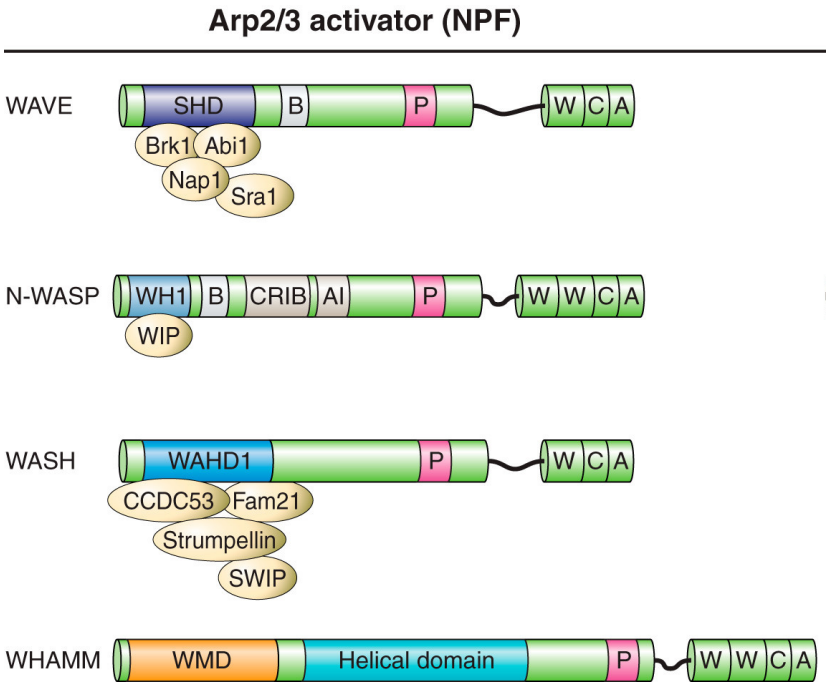


**Figure 2.9: Modular organization of NPFs.** Modified from [124]. All NPFs contain a VCA/WCA domain at the C-terminal, which can bind and activate the ARP2/3 complex. The N-terminal of NPFs are different. SHD/WHD, Scar/WAVE homology domain. B, basic domain. P, proline-rich region. WH1, WASP homology 1. CRIB, CDC42 and RAC1 interactive binding region. AI, autoinhibition domain. WAHD1, WASH homology domain 1. WMD, WHAMM membrane-interacting domain.

### The WASP and N-WASP family

WASP (Wiskott-Aldrich syndrome protein) was originally identified as a mutated gene in the Wiskott-Aldrich syndrome [142]. WASP is expressed specifically in hematopoietic cells in mammals. N-WASP (Neuronal Wiskott-Aldrich syndrome protein) is homologous to WASP but expressed in most cell types, and especially abundant in

the brain [143]. The following description will focus on N-WASP, the more ubiquitous one.

N-WASP is composed of several functional domains from N to C terminus: WH1 domain (WASP homology domain 1), basic (B) domain, GBD domain (GTPase binding domain), PRD domain (Proline-rich domain), and VCA domain. *in vivo*, the native N-WASP is autoinhibited since its VCA domain is masked by the N-terminal regulatory domains [144]. The N-WASP is stabilized at an inactive state by forming the heterodimeric complex with WIP (WASP-interacting protein) or a related protein CR16 through its WH1 domain [145].

To activate the N-WASP/WIP complex, the small GTPase CDC42 and phosphoinositide PIP2 (Phosphatidylinositol-4,5-bisphosphate) work synergistically as N-WASP activators by binding to the GBD domain and basic domain of N-WASP, respectively [146, 147]. In addition, many SH3 domain-containing proteins, such as adaptor proteins NCK1/2 (Non-catalytic kinase 1 and 2), membrane-deforming factor TOCA1 (Transducer of Cdc42-dependent actin assembly protein 1), and the kinase-interacting protein ABI1 (ABL interactor 1), contribute to N-WASP activation by binding to the PRD domain of N-WASP [148, 149, 150]. By binding to the activator, the VCA domain of N-WASP is released from the autoinhibited conformation. Then, the released VCA domain interacts with both actin monomer and ARP2/3 complex to promote the nucleation of branched actin filaments. N-WASP also can be phosphorylated at different sites to increase its affinity of the VCA domain to the ARP2/3 complex [151]. The multiple activation mechanisms can work cooperatively to activate N-WASP with high efficiency [125].

In response to diverse signals, N-WASP-ARP2/3-dependent branched actin networks participate in multiple cellular processes. N-WASP mediated actin polymerization is involved in the filopodia formation, thus promoting cell migration [93]. N-WASP contributes to clathrin-mediated endocytosis by promoting internalization of clathrin-coated vesicles [152, 153]. The N-WASP localizes at the surface of endosomal vesicles and promotes the motility of intracellular vesicles by forming actin comet tails at the tip [154]. N-WASP plays an essential role in the invasive phenotype of macrophages and cancer cells by forming dynamic actin-rich podosomes and invadopodia structures, respectively [155, 113].

### The WASH family

The WASH (Wiskott-Aldrich Syndrome protein and scar homologue) protein is a VCA domain-containing protein identified as the product of a subtelomeric gene that presents extensive duplication in the human genome [156]. The WASH protein is composed of an N-terminal region including WAHD1 domain (WASH homology domain 1) and TBR (Tubulin-binding region), followed by a proline-rich domain and a C-terminal VCA domain. The WASH protein activates ARP2/3 complex by embedding into a stable pentameric WASH complex with the other four proteins, FAM21 (Family with sequence similarity 21), Strumpellin, SWIP (Strumpellin and WASH Interacting protein), and CCDC53 (Coiled-coil domain containing protein 53) [157, 158]. In the WASH complex, SWIP, Strumpellin and CCDC53 are encoded by a single gene, while WASH and FAM21 are encoded by paralogous genes in the mammalian genome. In addition, the WASH complex recruits the heterodimer of capping protein (CP) through the CP interaction (CPI) motif at the C-terminal of FAM21 [159]. The CP interaction has been shown to be important for WASH function in the amoeba *Dictyostelium* [160].

The stability of the WASH complex depends on all subunits. The loss of one of the subunits or the CP heterodimer leads to the destabilization of the entire complex. As a multiprotein complex, the WASH complex is required to be assembled before performing its function. HSBP1 (Heat shock factor binding protein 1) is identified as a critical assembly factor that controls the level of the WASH complex. The homotrimeric HSBP1 binds to and dissociates the precursor CCDC53 homotrimer to form a mixed heterotrimer with a single CCDC53 molecule. The homo to hetero trimer transition contributes a single CCDC53 subunit to assemble WASH complex [161].

Even though WASH protein can induce ARP2/3-mediated actin nucleation *in vitro*, the WASH complex is inactive in the native form with a masked VCA domain [158]. To expose the VCA domain and activate the WASH complex, WASH protein undergoes K63-linked ubiquitination, which is important for modifying protein function. The WASH ubiquitination is mediated by E3 ubiquitin ligase TRIM27 and enhanced by MAGE-L2 [162]. In addition, the endosomal phospholipid PI3P (Phosphatidylinositol 3-phosphate) and PI4P (Phosphatidylinositol 4-phosphate) also contribute to WASH activation, but the details are not clear [163, 164].

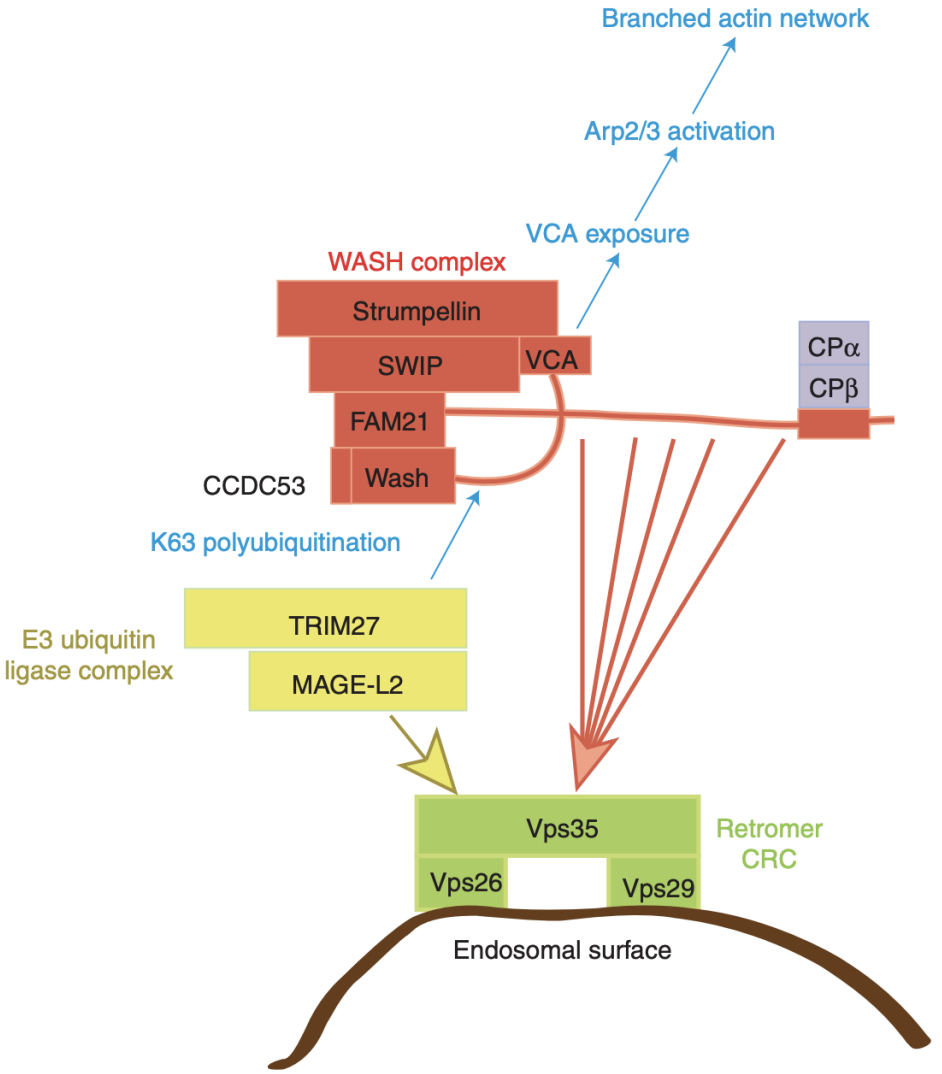


**Figure 2.10: Regulation of the WASH complex.** Modified from [165]. The WASH complex can be recruited to the surface of endosomes by interacting with the retromer complex on the endosomes via its FAM21 subunit. The WASH complex is activated by K63 ubiquitination mediated by the E3 ubiquitin ligase TRIM27 and its enhancer MAGEL2. The activated WASH complex releases its VCA domain, thus activating the ARP2/3 complex and promoting the branched actin network formation on the endosomal surface.

The WASH complex has been shown to be recruited to the surface of the endosome through the FAM21 subunit, which contains multiple binding sites of the retromer, an essential complex in orchestrating cargo sorting within the endosomal network [166, 167]. The WASH complex and retromer have been shown to label specific areas of the endosomal membrane, referred to as microdomains, for further activation of ARP2/3 complex and actin polymerization [168, 165]. The actin networks mediated by the WASH-ARP2/3 complex at the endosome surface are required for endosomal fission and sorting, which is critical for receptor trafficking in cells (Figure 2.10).

A recent study reveals that the WASH complex contributes to actin polymerization at the surface of endosomes by directly binding and activating the ARP2/3 complex and converting the dynactin complex into a seed for the mother filament simultaneously. The dynactin complex is a multiprotein complex that contains an actin-like minifilament with the capped barbed end. The WASH complex subunit FAM21 can bind and uncap dynactin complex via its capping protein interaction (CPI) motif. Once the capping protein is released, the dynactin minifilament elongates from the barbed end and creates a mother filament. Then another WASH complex recruits and activates the ARP2/3 complex on the side of the dynactin-associated filament, thus promoting actin polymerization [169] [170].

The WASH and ARP2/3 complex are also detected at the centrosome, which is known as the main microtubule organizing centre (MTOC), in interphase cells [171]. The actin nucleation at the centrosome is required for the regulation of lymphocyte polarity. In resting lymphocytes, the ARP2/3 complex-mediated actin networks are generated at the centrosome to promote the attachment of the centrosome to the nucleus. However, in active lymphocytes, the level of ARP2/3 complex and actin networks are decreased at the centrosome, which allows the centrosome detachment from the nucleus and its subsequent recruitment to the immune synapse [172]. The density of the centrosomal actin network also affects the growth of the microtubule at the centrosome. The balance of actin network and microtubule at the centrosome may play important roles in the capacity of cells to sense and adapt to external cues [173] [174].

### The WHAMM/JMY family

WHAMM (WASP homolog associated with actin, membranes, and microtubules) and JMY ( Junction mediating regulatory protein) are two homologous proteins with nearly 35% identity. WHAMM and JMY share similar domain organizations: the N-terminal domain, a long central proline-rich domain, and the C-terminal VCA domain. Both of these two proteins are expressed in various tissues and cell types in mammals [125].

WHAMM is composed of an N-terminal WHAMM membrane interaction domain (WMD) required for the interaction with the membrane, a central coiled-coil domain (CC) required for microtubule (MT) binding, and a C-terminal VCA domain with two WH2 domains involved in regulating actin nucleation [175]. Different from other NPFs, WHAMM is not self-inhibited. By binding to MTs, WHAMM undergoes a structural change by exposing the N-terminal WMD for vesicle recruiting and tubular structure remodeling, and masking the C-terminal VCA domain for actin polymerization inhibition. The ability of WHAMM in coordinating actin and MT cytoskeleton networks plays an important role in regulating the membrane dynamics in cells [176, 177]

JMY is identified to have a C-terminal VCA domain consisting of three actin-binding WH2 domains. With the three actin-binding domains, JMY can bring together three actin monomers, which enables JMY to nucleate unbranched actin filament independently of ARP2/3 complex *in vitro*. JMY is the unique NPF protein that has the actin nucleating ability both in ARP2/3-dependent and ARP2/3-independent manners [178, 179].

WHAMM and JMY both localize at the endoplasmic reticulum (ER) and the Golgi, cis-Golgi for WHAMM and trans-Golgi for JMY, and contribute to the vesicle trafficking process [175, 180]. In addition, WHAMM and JMY play critical roles in regulating apoptotic cell death and contribute to autophagosome biogenesis and motility in an ARP2/3-dependent manner [181, 182, 183].

### The WAVE family

WAVE (WASP family Verprolin homolog) protein, which is also known as SCAR (Suppressor of cyclic AMP receptor), was identified by sequence homology with WASP protein and also plays an essential role in regulating actin polymerization via ARP2/3 complex [184, 185]. There are three isoforms of WAVE protein expressed in mammalian cells: WAVE1, WAVE2, and WAVE3. WAVE2 is ubiquitously expressed in all human tissues, while WAVE1 and WAVE3 are expressed in specific tissues, mainly enriched in brain [186].

The WAVE protein is composed of an N-terminal SHD/WHD (SCAR/WAVE homology domain), followed by a basic domain (B), a proline-rich domain domain (PRD), and a C-terminal VCA domain. WHD is a coiled-coil region in all WAVEs and is responsible for heterocomplex formation. The WAVE protein is constitutively present within a complex called WRC (WAVE regulatory complex) for its NPF function. The WRC is a $\sim$ 400 kDa complex composed of five subunits: WAVE, ABI (ABL interactor), CYFIP/SRA (Cytoplasmic FMR1-interacting protein/Specifically RAC1-associated protein), NCKAP (NCK-associated protein), and HSPC300 (Hematopoietic stem progenitor cell 300, also known as BRK1) [187].

The WRC is intrinsically inactive in resting cells, since the VCA domain on WAVE protein is masked by interacting with other subunits in the complex. A large number of proteins can interact with WRC directly to regulate the activity of WRC, thus promoting ARP2/3 activation. WRC-mediated actin networks play many essential functions in various cellular processes, and the aberrant WRC expression is related to cancer cell invasion and metastasis [124].

*A detailed description of the WAVE regulatory complex will be presented in the next section.*

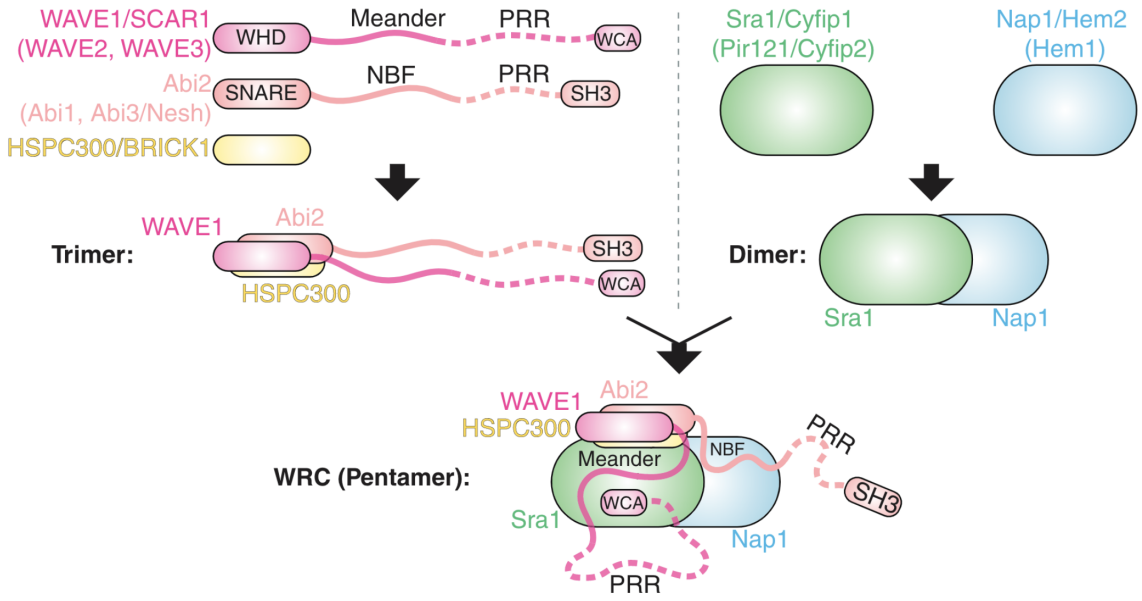


**Figure 2.11: Composition and *in vitro* assembly of the WRC.** Modified from [188]. The scheme illustrates how the WRC is assembled through the reconstitution *in vitro*. Curved lines and dotted lines indicate flexible sequences and unstructured sequences, respectively. NBF, NAP1-binding fragment. WHD, WAVE homology domain. WCA/VCA, WH2 central acidic domain.

## 2.3 The WAVE Regulatory Complex (WRC)

### 2.3.1 Composition of WRC

The WRC is a heteropentameric complex composed of WAVE, CYFIP/SRA, NCKAP, ABI, BRK1/HSP300 proteins at a 1:1:1:1:1 molar ratio. These five subunits are highly conserved in most eukaryotes. Several orthologs are known for four of the WRC subunits, including CYFIP1 and CYFIP2; NCKAP1/NAP1 and NCKAP1L/HEM1; WAVE1, 2, and 3; ABI1, 2, and 3. ABI1 also undergoes alternative splicing to produce different variants [189]. The orthologs of each subunit are supposed to be exchangeable, even though different orthologs are differentially expressed in specific tissues, thus creating the combinatorial complexity of WRC [190, 191]. In addition, all five subunits need to co-exist during evolution. An organism either expresses all five WRC subunits or none of them, like in yeast [188].

The WRC is a stable complex. The stability of WRC components is inter-dependent. Depletion of any of its components reduces the levels of the other components, a phenomenon which occurs in various organisms [192, 193, 194]. The majority of the WRC subunits exist as a complex in the cytosol except for BRK1, which can exist in excess, forming a homotrimer through its C-terminal coiled-coil domain [187, 194, 195]. To assemble the complex, the homotrimeric pool of BRK1 serves as a precursor, even though BRK1 presents as a single molecule in the assembled WRC complex. Single BRK1 dissociates from its homotrimeric precursor to bind the N-terminal of WAVE and ABI and assemble the trimeric subcomplex that contains a single molecule of each subunit. *In vitro* reconstitution and crystal structure of WRC reveals that the complex is assembled with the combination of two subcomplexes: a dimer formed by two large subunits CYFIP-NCKAP and a trimer formed by WAVE-ABI-BRK1. The CYFIP-NCKAP dimer serves as a platform to associate with WAVE-ABI-BRK1 trimer along the long axis [196, 195] (Figure 2.11).

Despite the recombinant WAVE protein being active with the exposed VCA domain, [185, 197], the WRC is maintained in an inactive form by masking its VCA domain via interacting with other subunits *in vivo* [198]. In response to the upstream signals, such as the binding of GTPase RAC to CYFIP1, WRC undergoes a conformational change by releasing the sequestered VCA domain from WAVE to active the ARP2/3 complex, without dissociating the complex [199, 200].

The Nudel protein is identified as an assembly factor of WRC. Nudel stabilizes the subcomplexes subunits of WRC, including CYFIP1, NCKAP1, ABI1, and BRK1 against degradation through its dynamic interaction with CYFIP1 and tightly interaction with BRK1 [201]. However, the details about how the entire WRC is assembled from subunits synthesized in cells and how cells regulate the protein levels of the different subunits for efficient assembling remain to be elucidated.

### 2.3.2 Functions of WRC

The first-characterized function of WRC is to generate ARP2/3-dependent branched actin networks at the lamellipodia and membrane ruffles of migrating cells, which can significantly promote the efficiency of cell migration in various cell types. The ubiquitously expressed WAVE2 contributes to the formation of lamellipodia. WAVE1 promotes the formation of 'dorsal ruffles' and stabilizes lamellipodia [202, 203]. WAVE3 is shown to be enriched at the lamellipodium tip and contributes to lamellipodia formation [204]. The actin remodeling mediated by WRC-ARP2/3 signaling at the plasma membrane is crucial for morphogenetic processes in different systems, such as cancer or immune cells, zebrafish, fruit flies, nematode worms, and *Dictyostelium*. The WRC-related plasma membrane protrusions can coordinate with intracellular traffic processes. The WRC has been shown to participate in the biogenesis of transporters involved in the TGN-to-endosomes transport pathway and in specific types of endocytosis where the direct interaction between WRC and receptors is required [205]. In epithelial cells, the RAC-WRC-ARP2/3 mediated actin reorganization plays an important role in the cadherin-dependent cell-cell junction formation and maintenance [206]. The WRC activity is also shown to be involved in cytokinesis. The activated WRC at the polar cortex of dividing cells is essential for the separation of daughter cells [207].

Consistent with multiple and diverse functions of the WRC-ARP2/3 mediated actin polymerization pathway in cells, aberrant expression or mutations of WRC subunits are associated with many diseases. Depletion of the ubiquitously expressed WRC subunits, like CYFIP1, WAVE2, NCKAP1, and ABI1 in mammals leads to embryonic lethality, whereas a depletion of their tissue-specific orthologs, like brain-specific WAVE1 or hematopoietic cell-specific NCKAP1L, leads to the neural or immune function deficiency [188]. Overexpression of the WRC components is frequently found in many types of cancers and is usually associated with a poor prognosis for the patients. All three WAVE proteins have been found to be overexpressed in various cancer types, such as the breast, colon, liver, lung, ovary, and prostate

cancers [124], except for WAVE3 overexpression in colorectal cancers, which is associated with a better prognosis [208]. Overexpression of ABI1 or BRK1 has been shown to associate with poor prognosis in breast and ovary cancers or lung cancer, respectively [209, 210, 211]. Overexpression of NCKAP1 and NCKAP1L has been shown to associate with poor prognosis in breast cancer and leukemia, respectively [212, 213]. The missense mutations of WRC subunits found in patients are associated with human diseases. Structural analysis reveals that most missense mutations are spatially clustered as hotspots in the complex. There are three mutation hotspots in CYFIP2, identified in patients with neurodevelopmental disorders. Mutations near the RAC binding sites of CYFIP2 may disrupt the WRC autoinhibition and/or affect its binding to RAC [214]. A hotspot in NCKAP1L/HEM1 has been identified in patients with immune dysregulation disease, which causes the loss of NCKAP1L/HEM1 protein and WRC or disrupts the ARF1-mediated WRC activation, thus leading to impaired actin polymerization in synapse formation, and deficient immune cell migration [215].

As WRC is the only known NPF for the ARP2/3 complex in plant cells, the complex plays an important role in various processes in plants. Even though dynamic membrane protrusions are lacking in plant cells, the dynamic actin cytoskeleton is required for multiple functions in plant cells [216]. It has been shown that the WRC-ARP2/3 mediated actin polymerization contributes to various processes of plant growth and development, including asymmetric cell division, cell morphogenesis [217, 218], trichome morphology, root growth, intercellular junctions [219, 220], infection thread formation and plant symbiosis [221, 222, 223].

The WAVE complex also has additional roles in cell morphogenesis beyond ARP2/3 complex activation. A recent study reveals that the WRC may form linear oligomers with a preference for saddle curvatures and enriches the necks of membrane invaginations and transepithelial holes [224].

### 2.3.3 The regulation of WRC

The VCA domain responsible for ARP2/3 activation is present at the C-terminal of WAVE proteins. The VCA domain in WAVE is inhibited within the WRC by binding to the surface of CYFIP subunit. To promote ARP2/3-mediated actin polymerization, the WRC needs to be recruited to the plasma membrane and activated at the lamellipodium tip. The WRC recruitment and activation can be mediated by small GTPases, acidic phospholipids, phosphorylation, and protein-protein interactions [34] (Figure 2.12). These regulators are shown to be present simultaneously and to function in a highly cooperative manner for efficient WRC activation [225, 226].

- **WRC regulation by small GTPases and phospholipids**

  WRC activation plays a central role in its regulation. The Rho family GTPase RAC1 (Ras-related C3 botulinum toxin substrate 1) is the ubiquitous activator of WRC, and its activity is required for membrane protrusions at the lamellipodium tip [227]. Activated RAC1 triggers the activation of WRC by releasing the masked VCA domain from the complex, thus promoting ARP2/3 complex-mediated actin polymerization [228].

  A crystal structure of WRC proposed a RAC1 binding site named the A site on CYFIP subunit [196]. Then, a recent cryo-EM analysis revealed the WRC-RAC1 complex structure and identified another RAC1 binding site named the D site (the A and D sites stand for Adjacent or Distant to the VCA domain binding sites, respectively). The A and D are two different and physically distant sites on the opposite side of the CYFIP subunit. Two activated RAC1 molecules can bind to these two sites simultaneously with $\sim$ 40-fold different affinity, and both interactions are essential for the activation of WRC towards ARP2/3 complex *in vitro* [200]. Nevertheless, cellular studies in mammals and *Dictyostelium* show that the low-affinity A site is the main site for allosteric activation of WRC, while the high-affinity D site is dispensable for WRC activation but required for optimizing WRC function to generate lamellipodial protrusions efficiently, which indicates that the regulation of WRC *in vivo* is much more complicated than *in vitro* [229].

  Given the essential and complex role of the RAC-WRC-ARP2/3 pathway in regulating actin polymerization, it is not surprising that another RAC1-binding protein family

called CYRI (CYFIP-related Rac interactor, also known as Fam49) was recently discovered as a local inhibitor of actin polymerization. CYRI binds to RAC1 through its DUF1394 domain shared with CYFIP. CYRI competes for RAC1 binding with the WRC by this specific domain, thus inhibiting RAC1-mediated WRC activation [230, 231].

Aside from RAC, there are some other GTPases involved in WRC regulation. The ARF family GTPases ARF1 and ARF6 have been shown to cooperate with RAC1 for WRC activation [232]. The RAC-related Rho family GTPases RhoG and CDC42 (Cell division control protein 42) also can fine-tune the WRC activity through the upstream RAC or WRC binding [233]. However, these GTPases are not enough to activate the WRC by themselves and need to work together with RAC to stimulate WRC activity efficiently. This effect may be important for connecting RAC-WRC-ARP2/3 signaling to other processes regulated by these GTPases.

To trigger ARP2/3 complex-mediated actin polymerization, WRC needs to be recruited to the plasma membrane. PIP3 and IRSp53 are involved in the recruitment of the WRC to the plasma membrane. PIP3 (Phosphatidylinositol 3,4,5-trisphosphate) is the membrane lipid produced by PI3K (Phosphatidylinositol 3-kinase). During chemotaxis, the cells sense the chemoattractant gradient and produce PIP3 at the leading edge to establish cell polarity. PIP3 can directly bind to the WRC at the basic region of WAVE and recruit the complex to the polarized membrane. This WRC recruitment by PIP3 enhances WRC activation by RAC1 and is crucial for lamellipodia formation at the leading edge [234]. CHC (Clathrin heavy chain) was also shown to have the ability to bind and recruit the WRC to the plasma membrane, promoting lamellipodia formation [235].

IRSp53 (Insulin receptor substrate of 53 kDa) is described as an inverse BAR domain-containing protein that links RAC and WAVE at the plasma membrane and participates in lamellipodia formation [236, 225]. However, IRSp53 was also found to inhibit the barbed end growth and switch the formation of lamellipodia to filopodia in cells by recruiting and clustering Ena/VASP at the leading edge [237]. Moreover, a recent study shows that IRSp53 requires its interaction with WRC to be enriched at the lamellipodia, but IRSp53 is dispensable for the the proper localization and function of WRC at the lamellipodia [224].

Lamellipodin is also identified as a RAC effector and contributes to WRC regulation.

Lamellipodin directly binds active RAC1, which positively regulates the interaction of lamellipodin with WRC at the SH3 domain of ABI, thus promoting lamellipodia formation and the persistence of cell migration [238].

NHSL1 (Nance-Horan Syndrome-like 1 protein) is a newly identified WRC binding partner, which can directly interact with the SH3 domain of ABI in WRC and negatively regulate WRC activity. The NHS family, which is of particular interest for this study, will be discussed later in the Introduction.

- **WRC regulation by phosphorylation**

  Phosphorylation of the WRC subunits, controlled by multiple extracellular and intracellular signals, plays an important role in regulating the WRC activity. Various kinases promote WRC activation and trigger WRC conformation change by phosphorylating WAVE and ABI in different regions. Phosphorylation in the proline-rich regions may regulate their interactions with other proteins, and phosphorylation in the meander region of WAVE can destabilize its interactions with CYFIP and lead to the release of the VCA domain and the WRC activation [196].

  A tyrosine kinase ABL phosphorylates WAVE and ABI and localizes the complex at the leading edge. ABL phosphorylates WAVE at the meander region and disrupts its interaction with CYFIP, thereby releasing the masked VCA domain. Moreover, the binding of ABI to ABL promotes the phosphorylation of WAVE by ABL [226, 239, 240]. A tyrosine kinase SRC phosphorylates WAVE and activates the WRC in a similar way [241].

  A neuron-specific serine/threonine kinase CDK5 (Cyclin-dependent kinase 5) phosphorylates multiple serine sites in WAVE1 proline-rich region, contributing to the inhibition of WRC and negatively regulating the dendritic spine formation. CDK5 phosphorylates one serine site in the WAVE2 meander region, leading to activated WRC and increased oligodendrocyte precursor migration [242, 243].

  A constitutively active serine/threonine kinase CK2 phosphorylates five serine sites of WAVE2 in the acidic motif of the VCA domain. Phosphorylation of the first two sites inhibits the activity of WRC for ARP2/3 complex activation, whereas phosphorylation of the last three sites increases the negative charge of the acidic motif, thus increasing the affinity of the WRC for ARP2/3 complex [244, 245].

JNKs (JUN N-terminal kinases) and ERKs (Extracellular signal-regulated kinases) also phosphorylate serine and threonine sites in the proline-rich region of WAVE2, which is essential for regulating cell polarity during migration. ERK can phosphorylate both WAVE2 and ABI1 to regulate WRC activity [246, 247, 248].

- **WRC regulation by membrane receptors**

  The WRC can be recruited to the plasma membrane by diverse transmembrane or membrane-associated receptors containing a short peptide motif called WIRS (WRC interacting receptor sequence). The WIRS motif can directly interact with the conserved surface of the WRC composed of CYFIP1 and ABI2. The WIRS-containing proteins also seem to act as scaffolds and play different roles in regulating the WRC activity by cooperating with other WRC regulators like RAC or kinases [199].

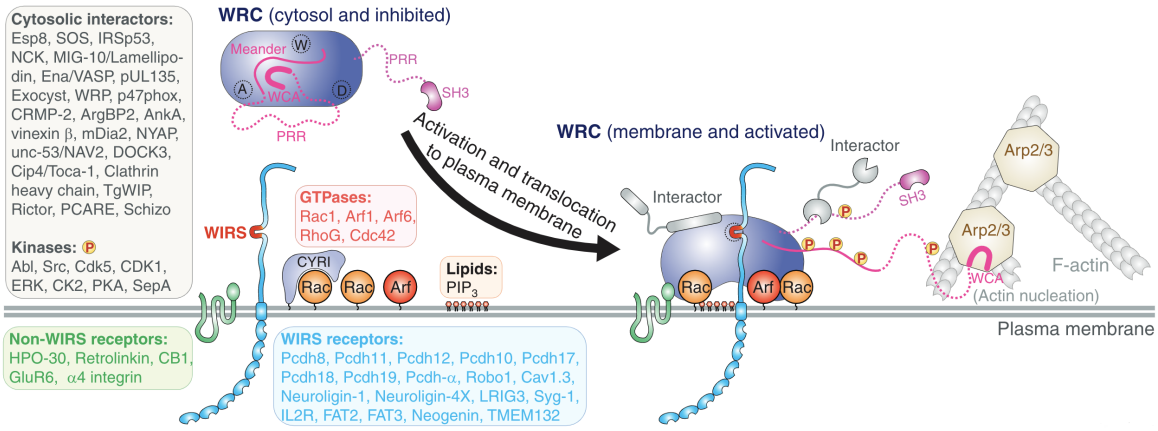


**Figure 2.12: Regulation of the WRC at the plasma membrane.** Modified from [188]. The WRC needs to be recruited to the plasma membrane for its activation. Various factors work cooperatively for the recruitment and activation of WRC at the plasma membrane, leading to the release of the VCA from the inhibited complex. Activated WRC binds to the ARP2/3 complex to promote actin nucleation and the formation of branched actin networks.

## 2.4 PPP2R1A

PPP2R1A is one of the scaffolding subunits that belongs to a well-known serine/threonine phosphatase complex PP2A (Protein phosphatase 2A), which accounts for $\sim$ 1% of total cellular proteins and is responsible for the majority of serine/threonine phosphatase activity in eukaryotic cells.

### 2.4.1 The PP2A complex

**The structure and composition of PP2A complex**

- The PP2A is a heterotrimeric complex composed of a scaffolding A subunit, a regulatory B subunit, and a catalytic C subunit. In vertebrates, each subunit of PP2A is represented by several isoforms. There are two isoforms for the catalytic C subunit, PPP2CA (C$\alpha$) and PPP2CB (C$\beta$), and two isoforms for the scaffolding A subunit, PPP2R1A (A$\alpha$) and PPP2R1B (A$\beta$). The isoforms of A and C subunits have 87% and 97% homology, respectively [249]. PPP2R1A (A$\alpha$) and PPP2CA (C$\alpha$) are more abundant and compose the majority of PP2A complex in most cells [250, 251]. The regulatory B subunit proteins can be classified into four families: B family (B55/PR55, gene symbol PPP2R2 series), B$'$ family (B56/PR61, PPP2R5 series), B$''$ family (PR72/PR130, PPP2R3 series), and B$'''$ family (Striatins/PR93/PR110, STRN), each family contains 2-5 isoforms, and splice variants, which leads to over 100 distinct combinations of the PP2A complex [252, 82, 253].

  Different from the A and C subunits which are expressed ubiquitously, the B subunits show differential cellular localization and variable expression across different cell types and tissues. The substrate specificity and subcellular localization of B subunits determine the diverse functions of the PP2A complex. In view of the diversity of PP2A subunits, the PP2A complex is actually a family of enzymes instead of a single enzyme [254].

- The PP2A A subunit is composed of 15 tandem HEAT (Huntingtin, EF3, PP2A A subunit, and TOR1) repeats. Each repeat contains about 40 amino acid residues, organized into two anti-parallel helices [255]. These 15 repeats form a hook-shaped structure to bind B and C subunits at different ends. The C subunit is globular in structure and contains catalytic phosphatase activity. The B subunits contain the binding sites both

for the substrate and for the A subunit, thus directing the PP2A activity to distinct sets of substrates [256].

To compose the PP2A holoenzyme, the A subunit interacts with an unstable monomeric C subunit to generate the AC dimer, which is called the core enzyme. In the core enzyme, the C subunit binds the A subunit at its HEAT repeats 11–15 and exposes its active site away from the ridge of the A subunit HEAT repeats. Then the core enzyme is ready to interact with a specific B family protein. To form the active holoenzyme, A subunit exhibits conformational flexibility by shifting its HEAT repeats when binding to the other subunits [256].

Crystal structures for the PP2A complex with different B family subunits have been published [256] (Figure 2.13). These studies show that a B family subunit binds to the core enzyme at two interfaces of the A subunit, at HEAT domains 3-7, and HEAT repeats 1-2. The B′ family subunit binds to the core enzyme by both binding to the A subunit at HEAT repeats 2-8 and the C subunit. The B″ family subunit binds to the core enzyme with the HEAT repeats 1-7 of the A subunit at and the C subunit near the active site [257, 258, 259]. The B‴ family protein striatin constitutes the large non-canonical phosphatase STRIPAK (Striatin-interacting phosphatase and kinase) complex with PP2A/C dimer and several other components including STRIP1/STRIP2 (STRN-interacting protein 1/2) and MOB4 (MOB family member 4 protein), CCM3 (Cerebral cavernous malformation 3 protein) and recruits one GCKIII family kinase (MST3, MST4, or STK25). In contrast to the canonical trimeric PP2A holoenzyme containing one copy of each subunit, it has been shown that STRN3 binds to the HEAT repeat 1 of PP2A A subunit via its coiled-coil domain and forms a 2:2 heterotetramer complex [260, 261]. A recent study revealed the structure of the STRIPAK complex and found that the STRIPAK contains four copies of STRN3, and the homotetrameric STRN3 with coiled-coil domains provides an elongated scaffold to link the whole complex together [262]. Thus, the B subunits can contribute to the structural diversity of PP2A and its variants.

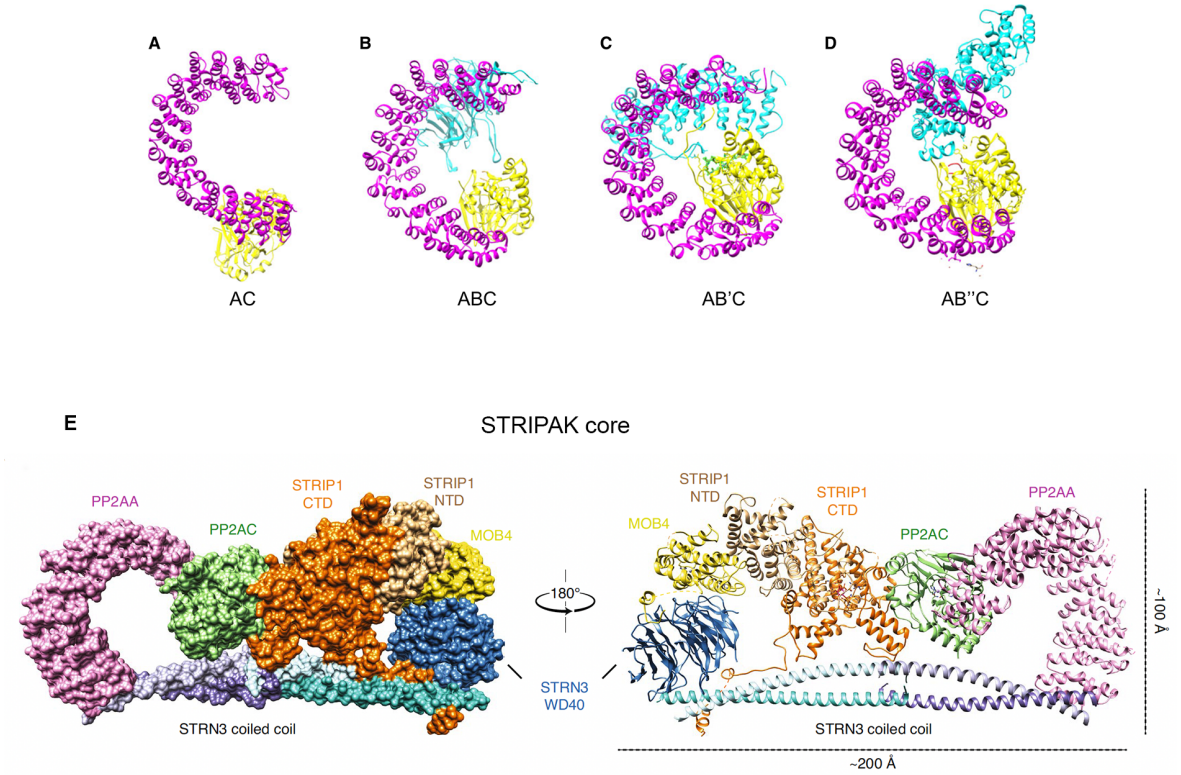


**Figure 2.13: Structures of PP2A core enzyme and holoenzymes.** Modified from [256, 262]. **A**, PP2A core enzyme consists of A$\alpha$ subunit (in magenta) and C$\alpha$ subunit (in yellow). **B,C,D**, PP2A holoenzymes consist of A$\alpha$ subunit, C$\alpha$ subunit, and B subunits (in cyan) from B, B$'$, B$''$ family, respectively. **E**, Structure of STRIPAK core in front and back views with surface (left) and cartoon (right) representations.

**The functions of PP2A complex**

- Given the compositional and structural diversity of PP2A holoenzyme, PP2A has been suggested to dephosphorylate over 300 substrates. These substrates are components involved in various important signaling pathways, key regulators of diverse cellular functions, including but not limited to cell growth and proliferation, cell division, cell death, cell migration, cell metabolism, and cell differentiation [263].

- **PP2A complex in cell migration**

  PP2A was previously shown to be involved in cell migration, based on its phosphatase activity. PP2A promotes YAP1 (Yes-associated protein 1) transcription in response to VEGFR (Vascular endothelial growth factor receptor) signaling or stiffness, and thus contributes to endothelial cell migration during angiogenesis [264]. The inhibition of the phosphatase activity of PP2A by RhoB depletion promotes the AKT1-RAC1 pathway and contributes to mesenchymal cell migration and invasion in lung cells across the 3D matrix [265].

  The large STRIPAK complex composed of both PP2A and various kinases can also be involved in cell migration through some of its components [253]. For example, GCKIII kinases are found to play important roles in cell migration, and are at least partially dependent on the PP2A activity in STRIPAK complex [266]. FGFR1OP2 is also indicated to be important for fibroblast cell migration, and the closure of the wound [267]. Striatin is directly associated with ER$\alpha$ and targets it to the cell membrane. The disruption of the striatin-ER$\alpha$ interaction in cells inhibits PP2A activation, thus leading to abolished estrogen-mediated endothelial cell migration and vascular smooth muscle cell growth [268, 269]. STRIP1 and STRIP2 are also involved in cell migration and morphology in different ways. A knockdown of STRIP1 in PC3 prostate cancer cells leads to increased cortical actin, broader lamellipodium, and reduced cell spreading, while a STRIP2 knockdown in the same cells leads to altered microtubule organization and elongated cell shape [270]. STRIP1 is also shown to be essential for normal mesoderm migration in the mouse embryo, and STRIP1 deficiency in mouse embryonic fibroblasts leads to decreased cell spreading and cell migration speed, and altered actin organization [271].

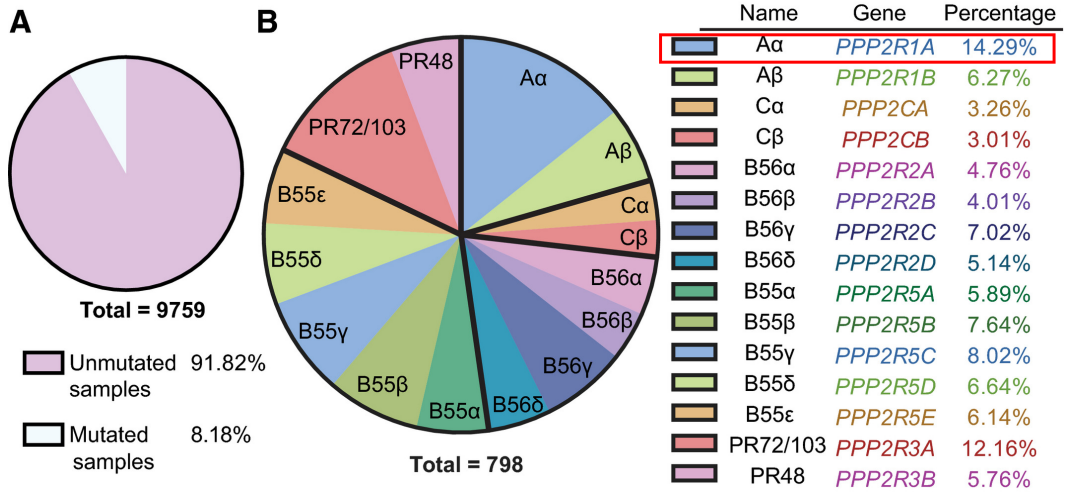


**Figure 2.14: The frequency of PP2A mutations across tumor samples.** Modified from [256]. **A**, Pie chart of the frequency of PP2A mutations across 9759 tumor samples. **B**, Pie chart of the frequency of PP2A mutations divided by PP2A subunit families: A, B, B′, B″ and C. PPP2R1A in the red box shows the highest mutation frequency across all tumor samples.

- **PP2A complex in diseases**

  Consistent with the central role of PP2A in regulating diverse biological functions, the dysregulation of PP2A is observed in many diseases, and PP2A A$\alpha$ and PP2A C$\alpha$ knockout mice undergo embryonic lethality, indicating the importance of PP2A during the development [254].

  As the main serine and threonine phosphatase in the brain, PP2A is essential for neuronal signaling and the development of the nervous system. The dysfunction of PP2A is found to be linked to neurodegenerative disorders such as Alzheimer's disease, by promoting tau hyperphosphorylation, amyloidogenesis, and synaptic deficits [272]. The mutations of PP2A subunits and regulators are also associated with various neurodevelopmental disorders [273].

  PP2A is widely described as a tumor suppressor. Its inactivation is a prerequisite for tumor formation in many studies, and its activity can be selectively inhibited by cancer-promoting chemical okadaic acid (OA) and specific viral oncoproteins: the small tumor antigen (ST) of SV40 and polyomavirus. The OA inhibits PP2A activity by directly interacting with the PP2A C subunit, while the ST inhibits PP2A activity by binding to PP2A A subunit and displacing the B subunit, thereby enhancing protein phosphorylation involved in cell growth [274, 275].

  PP2A is functionally inactivated in cancers. Disruption of the PP2A activity contributes to cancer development through one or several mechanisms. Cancer-associated somatic mutations are commonly detected in genes encoding PP2A A subunits, especially in *PPP2R1A*, which has the highest mutation rate across various cancer types (Figure 2.14). Decreased expression of specific B subunits or PTPA (phosphatase 2A phosphatase activator) and increased expression of endogenous PP2A inhibitors, such as CIP2A (Cancerous inhibitor of PP2A) and SET (Suvar/enhancer of zeste/trithorax), are shown to be associated with cancer progression. Phosphorylation and methylation on C-terminal residues of the C subunit are also important for modulating PP2A activity and contributing to tumorigenesis in humans [276, 254].

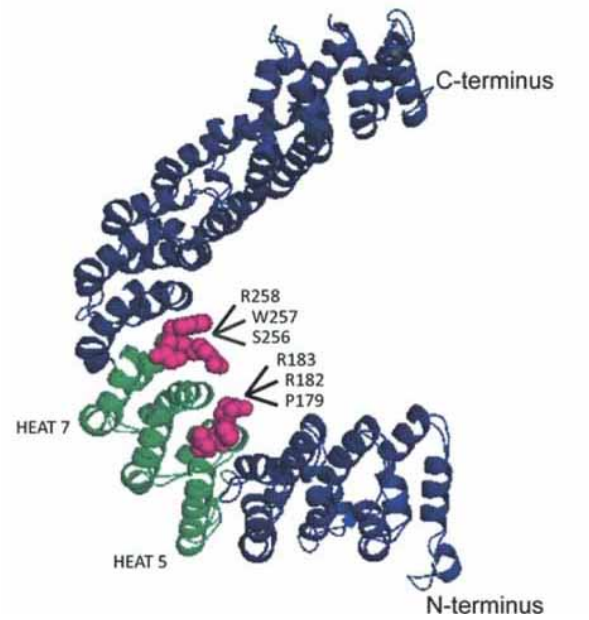


**Figure 2.15: Schematic representation of hotspot mutations in PPP2R1A.** Modified from [277].Three-dimensional protein structure of PPP2R1A. PPP2R1A is composed of 15 repeat HEAT motifs. The HEAT 5 and 7 motifs are highlighted, and amino acid mutants in frequently mutated in cancer patients are annotated.

### 2.4.2 PPP2R1A

As mentioned above, PPP2R1A is one of the A subunits of the PP2A complex. Even though the two isoforms of A subunits, PPP2R1A and PPP2R1B, show similar protein structures and high sequence similarity except for the 12 amino acids extension at the N-terminal of PPP2R1B, the expression levels and tissue distribution of these two isoforms are different. Both isoforms are targets of viral antigens, but only PPP2R1A binds the SV40 ST antigen. Some of PPP2R1B functions are unique and cannot be compensated by PPP2R1A, and an overexpression of PPP2R1A cannot revert tumorigenesis induced by PPP2R1B deficiency, which indicates that these two isoforms are functionally different [249].

**PPP2R1A mutations in cancer**

- *PPP2R1A* has been shown to have the highest mutation occurrence among all PP2A subunits in cancers and is suggested to be a tumor suppressor gene since its cancer-associated mutations in patient samples usually affect only one allele, which results in a state of haploinsufficiency [278]. Around 40% of human high-grade serous type endometrial cancers (type II ECs) have been shown to associate with missense mutations in *PPP2R1A* [277]. A lower frequency of *PPP2R1A* mutations, about 5-10%, are detected in endometrioid-type endometrial cancer (type I ECs), different types of ovarian cancer, breast cancer, lung cancers and melanoma [279, 280]. Most of *PPP2R1A* mutations cluster together in HEAT repeats 5 and 7, which are involved in B subunit binding (Figure 2.15). These PPP2R1A mutations occur at the same residues across different cancer types, forming hotspot mutations: P179R/L, R182W, R183W/Q at HEAT repeat 5, and S256F/Y, W257C/G, R258C/H at HEAT repeat 7, according to the data in COSMIC (Catalogue of somatic mutations in cancer).

  Several of these hotspot mutations of PPP2R1A have been studied. P179R mutation in PPP2R1A is highly specific to the high-grade endometrial cancer subtype, and shows a much higher mutation rate in high-grade endometrial cancer subtype than other cancer types. It has been shown that the P179R mutation in serious endometrial cancer cells leads to a PP2A loss of function effect via the decreased stability of PP2A B and C subunits and disrupted PP2A holoenzyme assembly [281]. Another study based on the endometrial cancer cells shows that the S256F mutation in PPP2R1A leads to increased tumor growth with a dominant-negative mechanism by increasing the binding ability of PPP2R1A to PP2A inhibitor TIPRL1. However, this finding could not be reproduced by others and remains controversial [282]. Among all the human

cancer types, R183 is the most commonly mutated residue, and R183W shows the highest mutation frequency. A study based on KARS-driven colorectal cells shows that R183W mutation leads to loss of PP2A tumor-suppressive activity. PPP2R1A with R183W mutation shows the decreased binding ability to the majority of B subunits, but not to B‴ (striatin) subunits, and this mutation shows no significant impact on PP2A C subunit [283]. Although most of the studies suggest that PPP2R1A mutations in cancer cause a loss of function effect, a study based on endometrial and ovarian cancer cells shows that the W257G mutation in PPP2R1A leads to inhibited tumor growth compared to WT cells, and has no effect on PP2A activity, even though its interaction with PP2A B and C subunits is decreased [284].

In summary, PPP2R1A mutations affect PP2A B or C subunit binding and PP2A activity in different ways, thereby leading to distinct functional consequences, but the mechanistic reasons for these differences remain to be investigated.

**PPP2R1A functions that are independent of PP2A complex**

- So far, most of the functions of PPP2R1A rely on its role in the PP2A complex. But from the quantitative proteome analysis of human cells, the A subunit, especially PPP2R1A (A$\alpha$), is more abundant than the other PP2A subunits [285]. The extra A subunit is thought to bind to the unstable monomeric C subunit and keep its stability and activity in cells, or bind to B subunits for enhanced stability [286, 287, 288]. A recent study also shows that PPP2R1A can localize at the surfaces of melanoma cells and lymphatic endothelial cells and mediate cell-cell interaction by forming homodimers [289]. These studies provided a possibility that the extra PPP2R1A may have other functions, outside of the PP2A complex, which is worth being investigated further.

## 2.5 NHSL1

### 2.5.1 The NHS (Nance-Horan Syndrome) family

The *NHS* gene was identified as the gene mutated in patients with a rare X-linked disorder, Nance-Horan syndrome, which is characterized by congenital cataract, dental anomalies, dysmorphic features, and mental retardation. The null mutations in *NHS* gene are suggested as the cause of the syndrome.

There are at least five isoforms that have been detected in *NHS* gene. Among these isoforms, the NHS-A and NHS-1A are thought to be essential for the pathogenesis of Nance-Horan syndrome, since only these two isoforms contain exon 1 where the null mutations are identified. The NHS-A and NHS-1A isoforms with exon 1 contain the WHD domain at their N-terminal (Figure 2.16). Moreover, the NHS isoforms have been shown to have different distributions in tissues and cells, and only the isoforms containing exon 1 are expressed in epithelia and localize to the cell periphery.

NHSL1 (NHS-like 1) and NHSL2 (NHS-like 2) are another two members identified in the NHS protein family. Even though the overall amino acid conservation between different NHS family members is only $\sim$30%, *NHS*, *NHSL*1, and *NHSL2* are shown to share a similar structure, with several homologous regions. The WHD domain of NHS is suggested to be conserved among the NHS protein family, which indicates that the NHS protein family might have roles in regulating actin dynamics [290, 291].

### 2.5.2 The function of NHS family proteins in cell migration

NHS was shown to localize to the leading edge of lamellipodia and to focal adhesions. The WHD of NHS interacts with ABIs, BRK1, NCKAP1, and CYFIP1, reminiscent of the function of WHD in WAVE proteins. Depletion of NHS results in increased cell spreading and disrupted actin assembly, and overexpression of the NHS isoform with WHD domain inhibits the lamellipodia formation under EGF stimulation, which indicates that NHS may act as a regulator of actin dynamics and cell morphology, by controlling WRC related pathways [292].

NHSL1 is also known to localize to the lamellipodium tip and is involved in regulating cell migration recently. In addition to the conserved WHD domain, same as in NHS, two SH3 binding sites have been identified in NHSL1. NHSL1 can directly interact with the SH3 domain of the ABI subunit in WRC, through these two binding sites. The direct binding

of NHSL1 to WRC is suggested to regulate WRC negatively, and lead to impaired ARP2/3 activity, thus controlling the stability of lamellipodia stability and cell migration efficiency. Moreover, NHSL1 can also interact with active RAC, which indicates that NHSL1 acts as a negative regulator in the RAC-WRC-ARP2/3 pathway. [293].

In addition, NHSL1 contains the FP4 motifs that can be recognized by the EVH1 domain of actin regulator Ena/VASP protein ENAH, suggesting other NHSL1 functions in regulating the actin network remodeling [294].

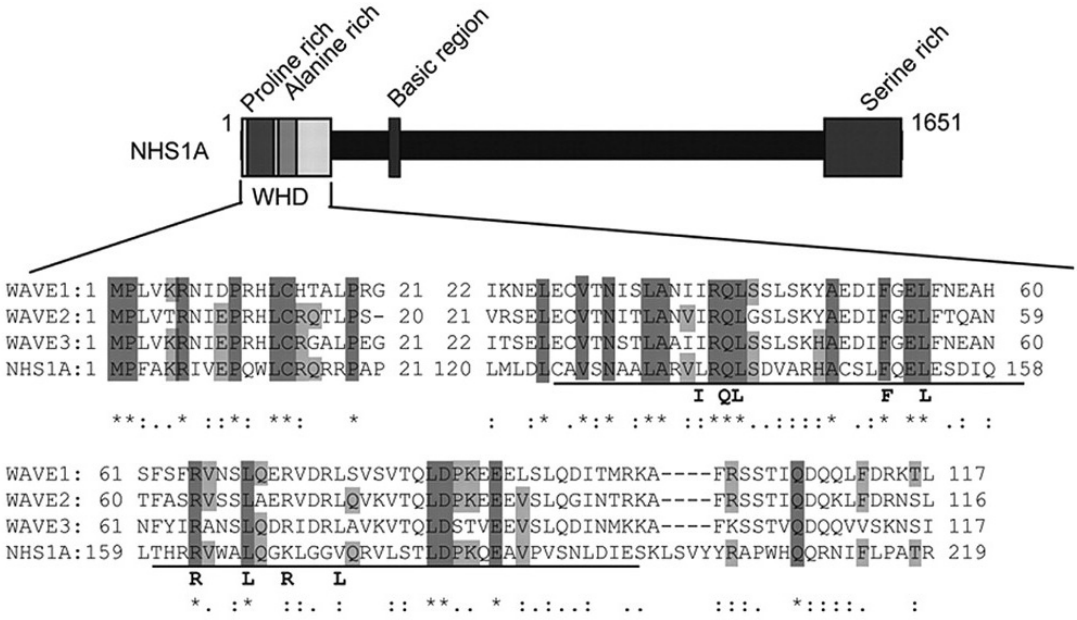


**Figure 2.16: Schematic representation of the identified domains of NHS protein and the alignment of NHS with WAVE1, 2, 3 at the N-terminal.** Modified from [292]. Under the alignment, letters in bold indicate conserved residues in mammalian WAVEs, *Drosophila* SCAR, and *Dictyostelium* SCAR. The underlined region indicates the ABI binding domain.

# Chapter 3

# Objectives of the thesis

Cell migration plays a critical function in various physiological processes. During cell migration, sheet-like protrusions driven by branched actin networks are generated at the leading edge to provide cells with the force to move forward. These actin-based protrusions are called lamellipodia. The lamellipodia formation is governed by the activity of ARP2/3 complex. At the edge of lamellipodia, the small GTPase RAC1 activates the WAVE Regulatory Complex (WRC), which in turn activates the ARP2/3 complex to nucleate branched actin networks. RAC1 maintains its activity when branched actin was previously polymerized, thus composing a positive feedback loop. Hence, cells keep their ability to migrate in the same direction, a phenomenon referred to as migration persistence. RAC1 also activates the ARP2/3 inhibitory protein Arpin at the lamellipodia edge and composes a negative feedback loop by antagonizing the activation of the ARP2/3 complex, which allows cells to brake and turn during migration. By combining the positive and negative feedback loops, cell migration is finely regulated. RAC1-WRC-ARP2/3 driven lamellipodia formation is also required for haptotaxis, the directed migration process towards the gradient of ECMs.

The RAC1-WRC-ARP2/3 pathway is under the control of various factors. Several WRC interacting partners have been identified to associate with the WRC and regulate cell migration persistence in different ways, such as the positive regulator lamellipodin and the newly identified negative regulator NHSL1. CYRI/Fam49, another negative regulator of cell migration, was shown to compete with WRC for RAC1 binding via a specific domain that is structurally similar to the RAC1-interacting domain of CYFIP. However, the regulatory factors that specifically bind to the WRC have not been fully elucidated, especially in the context of differential stimulation of the RAC1-WRC-ARP2/3 pathway.

To dissect the novel factors regulating the WRC, my host lab designed and performed a differential proteomics screen for potential effectors of RAC1-WRC-ARP2/3 signaling in

various conditions. Among the candidates from the screen, PPP2R1A was the strongest, displaying decreased association with WRC when migration is more persistent. PPP2R1A is one of the scaffolding subunits of the PP2A phosphatase complex. The catalytic subunit of the PP2A phosphatase complex was found in the proteomics screen but was not displaying variations in the different conditions, which suggests that PPP2R1A might have a PP2A-independent role in regulating cell migration persistence. PPP2R1A is also a cancer-associated gene, with mutants on several hotspots in various cancer types.

My PhD project aims to understand how PPP2R1A regulates migration persistence in normal and cancer cells and to characterize the molecular mechanisms of this regulatory pathway.

To achieve these goals, I performed experiments of random and directional single-cell migration in 2D and 3D. Tandem Affinity Purification was used to explore the potential partners of PPP2R1A. *In vitro* actin polymerization assay on GTPase-coated beads was established to examine the role of PPP2R1A in regulating actin polymerization. 3D acini assay to mimic the structure of the breast was performed to test how cancer-associated mutations affect the function of PPP2R1A.

Using these approaches, I have shown that PPP2R1A is required for cell migration persistence. Surprisingly, I found that PPP2R1A regulates cell migration by specifically interacting with a novel form of WAVE complex that contained all subunits of the WRC but the WAVE molecule is replaced by a Nance-Horan Syndrome family protein, NHSL1. This new complex was named the WAVE Shell Complex (WSC). In addition, by examining the effect of cancer-associated mutations of PPP2R1A in cells, I found that these mutations dramatically interrupt the interaction between PPP2R1A and WSC and lead to impaired migration persistence and abnormal acini morphology in 3D.

Therefore, in this project, I characterized the role of PPP2R1A as a positive regulator of directional cell migration and demonstrated that a novel multiprotein complex, the WAVE shell complex (WSC) is essential for this function of PPP2R1A.

# Chapter 4

# Results

## 4.1 PPP2R1A regulates migration persistence through the WAVE Shell Complex

*Manuscript is under review at Nature Communications*

**Authors**

**Yanan Wang**[1], Giovanni Chiappetta[2] *, Raphaël Guérois[3] *, Stéphane Romero[1] *, Matthias Krause[4], Claire Dessalles[5], Avin Babataheri[5], Abdul I. Barakatt[5], Joelle Vinh[2], Anna Polesskaya[1] §, Alexis M. Gautreau[1] §

[1]Laboratory of Structural Biology of the Cell (BIOC), CNRS UMR7654, École Polytechnique, Institut Polytechnique de Paris, 91120 Palaiseau, France [2]Biological Mass Spectrometry and Proteomics (SMBP), ESPCI Paris, Université PSL, LPC CNRS UMR8249, 75005 Paris, France [3]Université Paris-Saclay, CEA, CNRS, Institute for Integrative Biology of the Cell (I2BC), 91198, Gif-sur-Yvette, France [4]Randall Centre for Cell and Molecular Biophysics, King's College London, New Hunt's House, Guy's Campus, London, SE1 1UL, UK [5]LadHyX, École Polytechnique, Institut Polytechnique de Paris, 91120 Palaiseau, France *These authors contributed equally to the work
§Corresponding authors:

anna.polesskaya@polytechnique.edu

alexis.gautreau@polytechnique.edu

**Abstract**

The RAC1-WAVE-Arp2/3 signaling pathway generates branched actin networks that power lamellipodium protrusion of migrating cells. Feedback is thought to control protrusion lifetime and migration persistence, but its molecular circuitry remains elusive. Using proteomics, we identified PPP2R1A among proteins differentially associated with the WAVE complex subunit ABI1 when RAC1 was activated and downstream generation of branched actin was blocked. PPP2R1A was found to associate at the lamellipodial edge with a novel form of WAVE complex, the WAVE Shell Complex (WSC), that contains NHSL1 instead of the Arp2/3 activating subunit WAVE as in the canonical WAVE Regulatory Complex (WRC). PPP2R1A was required for persistence in random and directed migration assays and for RAC1-dependent actin polymerization in cell extracts. PPP2R1A requirement was abolished by NHSL1 depletion. PPP2R1A mutations found in tumors impaired WSC binding and migration regulation, suggesting that this novel function of PPP2R1A is critical for its tumor suppressor activity.

**Keywords:** Arp2/3, branched actin, migration persistence, feedback loop, Nance-Horan Syndrome family proteins.

Cell migration is a critical process for animal cells, especially in the embryo, but also in the adult. For example, immune cells constantly patrol the organism to fight infections. Nucleation of branched actin by the Arp2/3 complex fuels membrane protrusions called lamellipodia. This type of cell migration is characterized by its persistence that can be seen even in random migration and measured by the time during which direction is maintained once it is established [1]. Arp2/3-mediated persistence also favors directed migration towards higher concentrations of extracellular matrix (ECM) proteins in a process called haptotaxis [2].

Three WAVE proteins activate Arp2/3 at the cell cortex and in membrane protrusions [3]. WAVE proteins are subunits of the WAVE Regulatory Complex (WRC) that maintains WAVE inactive [4,5]. Upon binding to GTP-bound RAC1, WRC activates Arp2/3 [6,7]. The mechanism involves the exposure of the WCA domain of WAVE that binds and activates Arp2/3 [8,9]. The RAC1-WAVE-Arp2/3 pathway is critical for development and normal adult life but is also involved in cancer [10–12]. Genes encoding subunits of the WAVE and Arp2/3 complexes are overexpressed in a variety of cancers, and this overexpression is associated with high tumor grade and poor patient prognosis [13].

Cell migration is finely regulated at all molecular levels. Each positive component required to generate cortical branched actin, RAC1, WRC and Arp2/3, appears to be counteracted by inhibitory proteins, CYRI [14,15], NHSL1 [16] and ARPIN [17,18], respectively. NHSL1 belongs to the family of Nance-Horan Syndrome (NHS) proteins, which contain an N-terminal WAVE Homology Domain (WHD), as in WAVE proteins [19]. The WHD is the main structural domain that embeds WAVE proteins in the WRC [6,9], raising the possibility that WRC might contain NHS family proteins instead of WAVE proteins at some point in their life cycle. This intriguing possibility, however, has never been reported until now. Instead NHSL1 has been shown to interact with WRC through the C-terminal SH3 domain of the WRC subunit ABI1 [16].

Regulatory circuits of cell migration involve feedback and feedforward loops [20,21]. ARPIN was shown to inhibit Arp2/3 only when RAC1 signaling was on, rendering lamellipodia unstable once they were formed instead of preventing their formation [17]. Positive feedback that sustains membrane protrusion at the front is thought to be responsible for the persistence of cell migration. Indeed, signaling pathways are not linear, and actin polymerization activate WRC further in space and time in propagating waves [22,23] and promotes WRC turn-over [24]. Biochemical signaling in

feedback is constrained by cell mechanics and in particular membrane tension, which appears as a central component to sustain lamellipodial protrusion at the leading edge [25,26]. Feedback signaling is so challenging to dissect that mathematical modeling, computational simulations and machine learning are often required to interpret complex observations that would not fit into simple and linear models [27,28].

Here we used criteria of feedback signaling to uncover a novel molecular machine that regulates migration persistence. Using differential proteomics, we identified the PPP2R1A protein as a novel migration regulator and found that its mode of action involves an interaction with a new multiprotein assembly containing NHSL1 in place of a WAVE subunit, the WAVE Shell Complex (WSC).

## RESULTS

### Identification of PPP2R1A as a Novel Regulator of Migration Persistence

To identify novel partners of WRC, we used proteomics after tandem affinity purification (TAP) of the ABI1 subunit. We reasoned that partners differentially associated with ABI1 when RAC1 is activated and when Arp2/3 is inhibited would be good candidates to regulate migration persistence and feedback signaling. As a model system, we used the human mammary epithelial cell line MCF10A, which is immortalized but not transformed. We thus isolated stable cell lines expressing FLAG-GFP ABI1 from both parental and a genome-edited derivative, where the Q61L mutation affects one allele of *RAC1* and renders the RAC1 GTPase deficient and hence constitutively active. MCF10A cells expressing RAC1 Q61L showed more persistent migration than parental cells [29]. We treated or not both cell lines with the Arp2/3 inhibitory compound CK-666 to modulate the binding of potential WRC partners involved in signaling feedback from branched actin.

After the two successive FLAG and GFP immunoprecipitations (Fig.1a), we identified by mass spectrometry 89 proteins specifically associated with ABI1, but not with FLAG-GFP control (Table S1). We performed label-free quantification of triplicates and calculated the relative abundance of associated proteins in all four conditions after normalization by the amount of the ABI1 bait protein retrieved in each condition. The WRC subunits did not vary considerably in the different conditions, 20 % at most (Fig.1b). Among the hits, we recognized several described functional partners of the WRC such as SRGAP3, also known as WRP [30], the Nance-Horan Syndrome family proteins NHS and NHSL1 [16,19], IRSp53 [31] and lamellipodin, which was 3-fold more associated with WRC when RAC1 was activated, as previously reported [32].

Our attention was drawn to PPP2R1A, a scaffold subunit of the PP2A phosphatase complex, which showed variations in the two-fold range when RAC1 was activated and when CK-666 was applied to cells. The amount of PPP2R1A associated with ABI1 decreased when RAC1 was constitutively activated (Fig.1c). CK-666 induced opposite PPP2R1A variations in parental and RAC1 Q61L cells, probably because the constitutively active RAC1 Q61L does not depend on the feedback of branched actin for its activity. Catalytic subunits of the same PP2A phosphatase

complex, encoded by the two paralogous genes, *PPP2CA* and *PPP2CB*, were also detected in the list of ABI1 partners, but surprisingly these subunits did not show the same variations as PPP2R1A when CK-666 was applied to cells.

We depleted PPP2R1A from MCF10A cells using siRNA pools and tested cells in a 2D random migration assay. Lamellipodia appeared less developed in PPP2R1A-depleted cells, which, as a result, were less spread than control cells (Movie S1). PPP2R1A-depleted cells did not maintain the direction of migration over time as well as controls (Fig.1d). In contrast, this decrease in migration persistence upon PPP2R1A depletion was not significant when the same assay was performed using MCF10A cells expressing RAC1 Q61L (Fig.1e, Movie S2). This was surprising given that migration persistence is increased in MCF10A RAC1 Q61L [29], but was in agreement with our observation that PPP2R1A interacts less with ABI1 when RAC1 is constitutively active. We then isolated a stable MCF10A cell line that expresses FLAG-GFP PPP2R1A. The overexpression of tagged PPP2R1A was moderate, estimated by densitometry of PPP2R1A Western blots to be less than two-fold ($1.96 \pm 0.32$, mean ± sem of 3 triplicates, $P < 0.05$, t-test), with a concomitant decrease in endogenous PPP2R1A (Fig.1f). PPP2R1A expression was, however, sufficient to increase migration persistence in the 2D random migration assay (Movie S3). The loss- and gain-of-function experiments in MCF10A cells thus indicate that migration persistence depends on PPP2R1A levels.

To validate our findings in another cell system, we used the invasive breast cancer cell line MDA-MB-231 that we embedded in 3D collagen gels. PPP2R1A depletion dramatically decreased migration persistence in this setting as well (Fig.1g, Movie S4). Overexpression of PPP2R1A, however, did not affect migration persistence in either MDA-MB-231 cells, or in MCF10A cells expressing RAC1 Q61L (Fig.S1). Migration persistence of cells expressing constitutively active RAC1 Q61L thus appears independent of PPP2R1A levels, unlike parental MCF10A. Other parameters of cell migration necessary for a complete description of cell trajectories, such as cell speed and Mean Square Displacement (MSD), were also altered in some of these genetic perturbations, but inconsistently (Fig.S1), as previously reported [17,29], confirming that migration persistence, but not these other parameters, is the primary target of the RAC1-WAVE-Arp2/3 pathway [20].

**PPP2R1A Interacts With the NHSL1-containing WAVE Shell Complex**

To decipher how PPP2R1A regulated migration of MCF10A and MDA-MB-231 cells, we characterized its partners by proteomics. We purified FLAG-GFP-PPP2R1A by TAP (Fig.2a) and identified its partners by mass spectrometry (Table S2). As expected, we detected in MCF10A and MDA-MB-231 cells the catalytic phosphatase subunit and numerous regulatory subunits of PP2A complexes (PPP2R1B, PPP2R2D, PPP2R3B, PPP2R5A, PPP2R5B, PPP2R5C, PPP2R5D, PPP2R5E) as well as its larger STRIPAK derivatives (STRN, STRIP2, STRN4, MOB4). PPP2R3C was detected associated with PPP2R1A in MCF10A, but not MDA-MB-231 cells. We expected to find the whole WRC in line with the TAP purification of ABI1. However, we detected only 4 of the 5 subunits of the WRC (Fig.2b), namely CYFIP1, NCKAP1, ABI1 and BRK1. BRK1 was only detected in MCF10A and not in MDA-MB-231 cells, but this is likely because BRK1 generates only a few tryptic peptides from its short sequence of 75 amino-acids. Surprisingly, the 3 WAVE proteins were absent from the TAP purification from both cell lines. We searched for NHS family proteins, which were reported to contain an N-terminal WAVE homology domain (WHD) similar to that responsible for WAVE incorporation into WRC [6,19], and found NHSL1 in the TAP purification from both cell lines. We validated the presence of NHSL1 and all WRC subunits except WAVE by Western blots (Fig.2c). We never detected any WAVE protein in TAP purification of PPP2R1A. When NHSL1 was depleted from cells using siRNAs, PPP2R1A immunoprecipitation did not retrieve WRC subunits, but still retrieved the PP2A catalytic subunit (Fig.2d). This result suggests that NHSL1 is the subunit of this alternative complex that is recognized by PPP2R1A.

To examine the composition of the alternative complex devoid of WAVE, we performed TAP to select for the presence of both PPP2R1A and the WRC subunit BRK1. We performed sequential FLAG - PC immunoprecipitations from the stable MCF10A cell line expressing both FLAG-GFP-PPP2R1A and PC-HA-BRK1. We indeed retrieved the WRC without WAVE but containing NHSL1 instead (Fig.2e, Table S3). This TAP purification of both PPP2R1A and BRK1 did not completely exclude PP2A subunits, since it also contained a subset of the subunits found in TAP of PPP2R1A alone, namely PPP2CA, PPP2R2A, PPP2R5D, PPP2R5E and STRN. This result suggests that PPP2R1A can bind to this alternative WRC while being part of PP2A complexes. To our knowledge, a physiological form of WRC without a WAVE subunit and

containing an NHS family protein instead, has not previously been reported. NHSL1 was recently reported to interact with the complete canonical WRC through the ABI1 SH3 domain [16]. PPP2R1A thus does not bind to all pools of NHSL1 molecules, but appears to select a specific conformation of NHSL1, where NHSL1 fully replaces WAVE within its complex. We call this alternative to WRC, the WAVE Shell Complex (WSC), to emphasize that this multiprotein complex, which normally embeds WAVE and regulates its activity, has lost its WAVE subunit.

The HHpred program that detects remote homology [33] indeed predicted with a high probability (99.9 %) that NHSL1 contains a WAVE homology domain (WHD) in its N-terminus (residues 30-90; Fig.S2). A high-confidence structural model generated by the AlphaFold2 program [34–36] showed how NHSL1 could interact with the CYFIP1, NCKAP1, BRK1 and ABI2 subunits (Fig.2f). In this model, NHSL1 forms a triple coiled-coil with BRK1 and ABI2 as the N-terminal helix of the WAVE1 subunit in the WRC [6,37]. Unlike WAVE1 in the WRC, no other region of NHSL1, beyond the Pro97, is predicted to interact with WSC subunits. Three hydrophobic residues of NHSL1, upstream of its WHD, interact with CYFIP1 and contribute to the WSC assembly (Fig.S2).

To examine whether the PP2A complex can dephosphorylate WSC, or WRC, we performed TAP purification of ABI1 in the presence or absence of PPP2R1A (Fig.S3) and analyzed phosphosites by mass spectrometry. We detected phosphosites in ABI1, WAVE2, NHS, NHSL1 and IRSp53, among the well-characterized proteins of the pathway (Table S4). Label-free quantification of phosphosites is not as reliable as that of proteins, which are quantified by several peptides. Nevertheless, we quantified phosphosites when the WSC was connected to PP2A complexes via PPP2R1A or not. All but one phosphosite were either present in similar amounts in both conditions or decreased in the absence of PPP2R1A, which is inconsistent with the lack of association with a phosphatase in this condition. Only the phosphorylation of WAVE2 on Ser308 was found to be increased by 2.6-fold upon PPP2R1A depletion, as if this phosphosite was dephosphorylated by PP2A complexes. This phosphorylated residue, however, was not consistently detected in all technical repeats of the experiment. We attempted to validate this variation in phosphorylation using phosphospecific antibodies, but no increase in phosphorylation was detected in the absence of PPP2R1A (Fig.S3). The variation in the phosphorylation of WAVE2 Ser308 was in any case inconsistent with PP2A complexes associating with WSC, since

WAVE2 is present in the WRC but not in the WSC. Thus, despite the presence of WSC-associated PP2A subunits, including the catalytic subunit, we found no evidence for WSC- or even WRC-directed phosphatase activity.

We then sought to examine PPP2R1A localization and used for this purpose B16-F1 cells that develop prominent lamellipodia. Cells were transfected with GFP-NHSL1 and mScarlet-PPP2R1A. PPP2R1A was colocalized with NHSL1 at the lamellipodium edge (Fig.3a, Movie S5). NHSL1 was strongly enriched at the lamellipodial edge, whereas PPP2R1A extended far beyond, in the entire width of the lamellipodium (Fig.3b). Arp2/3 is incorporated into branched actin networks and extends backwards through the actin retrograde flow. We thus examined the colocalization of mScarlet-PPP2R1A with the GFP-tagged Arp2/3 subunit ARPC1B. Both proteins colocalized in the width of lamellipodia (Fig.3c, Movie S6), but ARPC1B distribution declined steeply away from the edge, whereas PPP2R1A did not exhibit such a gradient (Fig.3d). These analyses suggest that PPP2R1A is a lamellipodial protein that is likely to interact with WSC at the cell edge.

**The Requirement of PPP2R1A in Cell Migration and Actin Polymerization Depends on the Presence of NHSL1**

NHSL1 was previously described as a negative regulator of cell migration [16]. It was thus surprising to find PPP2R1A and NHSL1 biochemically associated. We have knocked down either PPP2R1A, or NHSL1, as well as both proteins simultaneously in order to study epistasis. In line with previous findings, NHSL1 depletion strongly promoted migration persistence in random migration of single MCF10A cells. The decline of migration persistence upon PPP2R1A depletion was abolished by NHSL1 depletion (Fig.4a, Movie S7). Despite their opposite effects, neither of the two migration regulators appears to take over. The simultaneous depletion of both regulators does not significantly affect migration persistence compared to controls, as if the signaling circuit containing the PPP2R1A and NHSL1 was simply dispensable in this random migration assay. We then examined directional migration in a gradient of fibronectin to further challenge cells. This haptotactic assay was previously shown to depend on Arp2/3 activity [2]. PPP2R1A-depleted cells were strongly impaired in their ability to migrate toward higher concentrations of fibronectin (Fig.4b, Movie S8). In contrast, depletion of the migration inhibitor NHSL1 rendered cells slightly,

but significantly, more efficient at directed migration. In this assay, as in random migration, simultaneous depletion of PPP2R1A and NHSL1 abolished the effects of single depletions. In two different cell migration assays, PPP2R1A and NHSL1 thus depend on each other.

To establish that the effects of the PPP2R1A-NHSL1 signaling circuit were due to actin polymerization, we set up an in vitro reconstitution assay of actin polymerization in extracts prepared from MCF10A cells. Actin polymerization at the surface of glutathione beads was monitored by the incorporation of fluorescent actin. GTP-bound RAC1 Q61L was able to trigger the polymerization of actin structures from the surface of the beads (Fig.5a). These structures were discrete fibers, not the dense meshwork observed around beads displaying CDC42 Q61L (Fig.S4). These actin structures, however, were composed of branched actin, since their formation was impaired by the CK-666 compound, as measured by their total fluorescence and length. These actin structures depended on the WRC, as shown using extracts prepared from NCKAP1-depleted cells, and did not depend on the CDC42 effector N-WASP, since they were not inhibited by the N-WASP inhibitory compound wiskostatin [38] (Fig.S4). Extracts prepared from PPP2R1A-depleted cells did not support actin polymerization from RAC1 Q61L displaying beads (Fig.5b). Yet the extracts prepared from NHSL1-depleted cells and those prepared from cells simultaneously depleted of PPP2R1A and NHSL1 were as competent as wild type extracts in supporting actin polymerization. Both PPP2R1A and NHSL1 were detected associated with GTP-bound RAC1 Q61L (Fig.S4), in line with the fact that both CYFIP1 and NHSL1 harbor binding sites for active RAC1 [7,16]. Together, these results show that PPP2R1A requires NHSL1 to regulate cell migration and actin polymerization.

**Uncoupling PPP2R1A From WSC Impairs Migration Persistence**

To uncouple PPP2R1A from WSC, we mapped PPP2R1A binding sites in NHSL1. NHSL1 was divided in four fragments excluding the WHD. Upon transient transfection of 293T cells with GFP fusion proteins of NHSL1 fragments, we found that the 4$^{th}$ fragment at the C-terminus of NHSL1 retrieved a large amount of PPP2R1A upon GFP immunoprecipitation (Fig.6a). The 2$^{nd}$ fragment of NHSL1 that contains the two previously reported binding sites for the SH3 domain of ABI1 [16] also retrieved PPP2R1A, but to a much lesser extent than the 4$^{th}$ fragment. The AlphaFold2 software predicted with high confidence three motifs in fragment 4 that interact with the PPP2R1A

scaffold or the PPP2R5D regulatory subunit retrieved in the WSC TAP (Fig.6b). The first two motifs recognize the first HEAT repeat of PPP2R1A, but with different binding and probably mutually exclusive modes. The third motif of NHSL1 fragment 4 corresponds to a previously described consensus motif for binding regulatory subunits of the B56 family, such as PPP2R5D [39]. Upstream of the consensus motif, binding is reinforced by a long stretch of 25 residues containing two successive and conserved proline residues (Fig.S5). We isolated MCF10A cells that stably express NHSL1 fragment 4. Migration persistence was dramatically decreased in these cells compared to controls (Fig.6c, Fig.S5, Movie S9), suggesting that coupling PPP2R1A to the WSC is critical to regulate cell migration. To obtain further evidence of this point, we investigated the activity of mutated PPP2R1A.

*PPP2R1A* is frequently mutated in tumors, especially in gynecologic cancers [40]. We first obtained a *PPP2R1A* KO MCF10A cell line by transfecting purified Cas9 and gRNA, and established that both *PPP2R1A* alleles were inactivated by deletions creating a frameshift (Fig.S6). We then isolated stable transfectants from this KO expressing FLAG-GFP PPP2R1A fusion proteins, either wild type or harboring the frequent cancer-associated mutations, P179R, R183W or W257C. GFP immunoprecipitations showed that the three mutations strongly impair binding to the WSC, but not to the PP2A catalytic subunit (Fig.6d). In the 2D cell migration assay, *PPP2R1A* KO MCF10A cells displayed reduced migration persistence, like PPP2R1A knocked-down cells. Whereas wild type PPP2R1A rescued the phenotype, mutated forms of PPP2R1A were unable to restore persistence (Fig.6e, Movie S10). This experiment confirmed that the interaction of PPP2R1A with the WSC is important for migration persistence.

We then differentiated acini from the stable rescued cell lines at the surface of Matrigel. *PPP2R1A* KO MCF10A cells were impaired in their ability to differentiate hollow acini with correct cell polarity, a hallmark of cell transformation (Fig.S6). The multicellular structures formed instead were also less regularly spherical than controls. These phenotypes were rescued by wild type PPP2R1A, but not with the derivatives harboring a mutation. These results confirmed that the tumor-associated mutations are loss-of-function and suggested that the interaction of PPP2R1A with the WSC is important to prevent cancer progression.

## DISCUSSION

In this study, we uncovered a novel regulator of migration persistence, PPP2R1A, using differential proteomics when RAC1 was activated and when the formation of its downstream product, branched actin, was impaired. PPP2R1A is a well-characterized scaffold subunit of the PP2A complex, an abundant and heterogeneous phosphatase that regulates several signaling pathways [41]. PP2A phosphatase activity has previously been connected to cell migration and tumor cell invasion [42–44], but there is no evidence that the precise role of PPP2R1A we report here in regulating migration persistence depends on PP2A phosphatase activity. Indeed, the phosphorylated sites that we identified on WSC or WRC subunits did not depend on the presence of PPP2R1A. PPP2R1A may 'moonlight' and regulate migration persistence independently of PP2A phosphatase activity. Yet there is no mutual exclusivity of PPP2R1A interaction with the WSC and assembly of PP2A complexes, since we detected PP2A catalytic and regulatory subunits when we selected the WSC by TAP. The amounts of PP2A catalytic subunits retrieved by the TAP of ABI1 upon RAC1 activation or inhibition of branched actin did not show the same variations as that of PPP2R1A, suggesting different pools of PPP2R1A with varying degrees of PP2A assembly. In line with this idea, a large-scale proteomics-based quantification of protein abundance has previously revealed that PPP2R1A was almost one order of magnitude more abundant than PP2A catalytic and regulatory subunits with which it associates [45].

The A-type subunit PPP2R1A is composed of 15 HEAT repeats, onto which the catalytic C subunit and one of the various B regulatory subunits assemble to form the PP2A holoenzyme [41]. PPP2R1A is mutated in various cancers, particularly often in endometrial cancers (up to 20 % in some subtypes) [46]. PPP2R1A is considered a tumor suppressor but has atypical characteristics. Tumor-associated PPP2R1A substitutions fall into hotspots, like mutations activating oncogenes. Most point mutations cluster in HEAT repeats 5 and 7, where they have been shown to impair the interaction with B regulatory subunits to a varying extent depending on the mutation and the B subunit considered [47,48]. Only one of the two *PPP2R1A* alleles is mutated in tumors, which is also classical of oncogenes. Haploinsufficiency and dominant negative effects are thought to account for PPP2R1A inactivation [47,49]. Here, using a *PPP2R1A* knock-out cell line and examining the rescue provided by wild type or mutated forms (P179R and R183W in HEAT repeat 5 and W257C in HEAT repeat 7), we unambiguously showed that these tumor-associated mutations inactivate

PPP2R1A with respect to this new function in migration persistence as well as in the assay of differentiating acini in Matrigel. Inactivating mutations are consistent with the tumor suppressor nature of PPP2R1A and haploinsufficiency.

Tumor-associated mutations of PPP2R1A impair binding to the here uncovered WSC, where NHSL1 replaces the WAVE subunit. This alternative form of WAVE complex was suspected for a long time, based on the presence of a WAVE homology domain in Nance-Horan Syndrome family proteins [19], but was not previously reported. NHSL1 also associates with WRC through two binding sites for the SH3 domain of ABI1 [16]. It is probably because NHSL1 exists in different pools and complexes, as does PPP2R1A, that these two proteins can regulate migration persistence in opposite ways, positive for PPP2R1A and negative for NHSL1. PPP2R1A, however, selects a specific conformation of NHSL1, where this largely unstructured protein occupies the "shell" composed of all WRC subunits but WAVE. NHSL1 interactions within WSC appear less extensive than WAVE interactions within WRC. NHSL1 is thus unlikely to chase WAVE away but would rather occupy its position when WAVE is not there.

The WSC likely corresponds to a novel intermediate in the WRC life cycle, possibly as a way of activating WAVE. We have obtained evidence that PPP2R1A is required for polymerization of branched actin in cell extracts and for persistence in random and directed migration assays. The surprise is that this requirement of PPP2R1A is not compulsory and depends on the presence of NHSL1 in all assays. The PPP2R1A-WSC interaction may contribute to WRC activation in addition to the primary mechanism, which has been reconstituted *in vitro* without PPP2R1A or NHSL1: Active RAC1 activates the WRC through a conformational change that exposes the Arp2/3 activating WCA domain of WAVE [6,7]. Even if NHSL1 cannot chase WAVE away, the existence of the WSC suggests that the WAVE subunit can dissociate from the WRC that maintains it inactive [4,5]. Freeing WAVE from WRC would be another way to expose its Arp2/3 activating WCA motif. It is difficult to anticipate the mechanism by which WAVE would disengage from the WRC. WAVE proteins were reported to be degraded by proteasomes upon cell activation and ubiquitylated on a specific lysine residue in their WHD [50,51]. But these reports do not demonstrate that this is a free form of WAVE that is degraded after activation. There are many possible views of the WSC role in the WAVE life cycle. The in vitro reconstitution assay of RAC1-

dependent branched actin structures we report here using cell extracts is likely to play an important role in testing different scenarios for a multistep WAVE activation cycle.

Migration persistence is thought to depend on positive feedback [20], which is manifested in propagating waves of branched actin polymerization [22]. Positive feedback has been observed at multiple molecular levels. The simple fact that the product of the Arp2/3 reaction is a new actin filament that can become the substrate of a new Arp2/3-dependent branching reaction is a positive feedback referred to as an autocatalytic reaction [52]. The WRC turns over at the lamellipodium edge due to elongation of actin filaments that it contributes to generating [24,53]. Coronin1A decorates lamellipodial actin and further activates RAC1 via its association with ArhGEF7 [54]. Similarly, we found PPP2R1A in the width of the lamellipodium, ideally localized to sense lamellipodial actin, whereas PPP2R1A association with the WSC is likely to take place at the lamellipodial edge, where NHSL1 is localized, and where new actin filaments are nucleated by the Arp2/3 (Fig.6f). This does not fully demonstrate involvement in feedback, but we initially focused on PPP2R1A, among the many ABI1 partners, because its interaction with the WSC was regulated by branched actin. It is worth noting in this respect that simulations using molecular dynamics have revealed that the HEAT-repeat scaffold of PPP2R1A is particularly elastic and might play a role in mechanotransduction [55]. Furthermore, PPP2R1A is dispensable for migration persistence when RAC1 is constitutively activated by the Q61L mutation. All of this evidence points to a possible role for PPP2R1A, and the WSC it associates with, in a positive feedback that sustains directional migration through continuous actin polymerization at the leading edge. Future work should aim to find ways to dissect, at the molecular level, the complex circuitry that mediates feedback and persistence.

## Author Contributions

YW performed most of the experiments and participated in writing of the manuscript. GC performed the mass spectrometry under the direction of JV. SR performed live localizations of fluorescent fusion proteins. RG generated the structural models. MK generated NHSL1 expression plasmids. CD, AB and AIB helped to set up the haptotaxis assay. AMG and AP have jointly supervised the work and wrote the manuscript.

## Acknowledgments

We thank Vassilis Koronakis for guidance in reconstitution assays using cell extracts. We thank Anna Castro, Gregory Giannone and Emmanuel Derivery for critical reading of the manuscript. This work was supported by grants from Agence Nationale de la Recherche (ANR-20-CE13-0016-01) and Fondation ARC pour la Recherche sur le Cancer (ARC PJA 2021 060003815). Mass spectrometry equipment was subsidized by Conseil Régional d'Ile-de-France (Sesame N°10022268). The PhD of YW was supported by fellowships provided by Fondation pour la Recherche Médicale and by Fondation ARC pour la Recherche sur le Cancer.

**References**


1. Petrie, R. J., Doyle, A. D. & Yamada, K. M. Random versus directionally persistent cell migration. *Nature Reviews Mol Cell Biol* 10, 538–549 (2009).

2. Wu, C. *et al.* Arp2/3 is critical for lamellipodia and response to extracellular matrix cues but is dispensable for chemotaxis. *Cell* 148, 973–987 (2012).

3. Alekhina, O., Burstein, E. & Billadeau, D. D. Cellular functions of WASP family proteins at a glance. *Journal of Cell Science* 130, 2235–2241 (2017).

4. Ismail, A. M., Padrick, S. B., Chen, B., Umetani, J. & Rosen, M. K. The WAVE regulatory complex is inhibited. *Nature Structural & Molecular Biology* 16, 561–563 (2009).

5. Derivery, E., Lombard, Be., Loew, D. & Gautreau, A. The Wave complex is intrinsically inactive. *Cell Motility and the Cytoskeleton* 66, 777–790 (2009).

6. Chen, Z. *et al.* Structure and control of the actin regulatory WAVE complex. *Nature* 468, 533–538 (2010).

7. Chen, B. *et al.* Rac1 GTPase activates the WAVE regulatory complex through two distinct binding sites. *eLife* 6, W529 (2017).

8. Schaks, M., Giannone, G. & Rottner, K. Actin dynamics in cell migration. *Essays Biochem* 63, 483–495 (2019).

9. Rottner, K., Stradal, T. E. B. & Chen, B. WAVE regulatory complex. *Curr Biol* 31, R512–R517 (2021).

10. Kansakar, U., Wang, W., Markovic, V. & Sossey-Alaoui, K. Elucidating the molecular signaling pathways of WAVE3. *Ann Transl Medicine* 8, 900 (2020).

11. Rana, P. S., Alkrekshi, A., Wang, W., Markovic, V. & Sossey-Alaoui, K. The Role of WAVE2 Signaling in Cancer. *Biomed* 9, 1217 (2021).

12. Nikolaou, S. & Machesky, L. M. The stressful tumour environment drives plasticity of cell migration programmes, contributing to metastasis. *J Pathology* 250, 612–623 (2020).

13. Molinie, N. & Gautreau, A. The Arp2/3 Regulatory System and Its Deregulation in Cancer. *Physiological Reviews* 98, 215–238 (2018).

14. Fort, L. *et al.* Fam49/CYRI interacts with Rac1 and locally suppresses protrusions. *Nature Cell Biology* 20, 1159–1171 (2018).

15. Yelland, T. *et al.* Structural Basis of CYRI-B Direct Competition with Scar/WAVE Complex for Rac1. *Structure* 29, 226-237.e4 (2021).

16. Law, A.-L. *et al.* Nance-Horan Syndrome-like 1 protein negatively regulates Scar/WAVE-Arp2/3 activity and inhibits lamellipodia stability and cell migration. *Nat Commun* 12, 5687 (2021).

17. Dang, I. *et al.* Inhibitory signalling to the Arp2/3 complex steers cell migration. *Nature* 503, 281–284 (2013).

18. Fregoso, F. E. *et al.* Molecular mechanism of Arp2/3 complex inhibition by Arpin. *Nat Commun* 13, 628 (2022).

19. Brooks, S. P. *et al.* The Nance-Horan syndrome protein encodes a functional WAVE homology domain (WHD) and is important for co-ordinating actin remodelling and maintaining cell morphology. *Human molecular genetics* 19, 2421–2432 (2010).

20. Krause, M. & Gautreau, A. Steering cell migration: lamellipodium dynamics and the regulation of directional persistence. *Nature Reviews Mol Cell Biol* 15, 577–590 (2014).

21. Graziano, B. R. *et al.* A module for Rac temporal signal integration revealed with optogenetics. *J Cell Biol* 216, 2515–2531 (2017).

22. Weiner, O. D., Marganski, W. A., Wu, L. F., Altschuler, S. J. & Kirschner, M. W. An actin-based wave generator organizes cell motility. *PLoS Biology* 5, e221 (2007).

23. Millius, A., Dandekar, S. N., Houk, A. R. & Weiner, O. D. Neutrophils establish rapid and robust WAVE complex polarity in an actin-dependent fashion. *Current Biology* 19, 253–259 (2009).

24. Mehidi, A. *et al.* Forces generated by lamellipodial actin filament elongation regulate the WAVE complex during cell migration. *Nat Cell Biol* 23, 1148–1162 (2021).

25. Houk, A. R. *et al.* Membrane tension maintains cell polarity by confining signals to the leading edge during neutrophil migration. *Cell* 148, 175–188 (2012).

26. Lee, K. *et al.* Functional Hierarchy of Redundant Actin Assembly Factors Revealed by Fine-Grained Registration of Intrinsic Image Fluctuations. *Cell Systems* 1, 37–50 (2015).

27. Danuser, G., Allard, J. & Mogilner, A. Mathematical Modeling of Eukaryotic Cell Migration: Insights Beyond Experiments. *Annual Review of Cell and Developmental Biology* 29, 501–528 (2013).

28. Wang, C. *et al.* Deconvolution of subcellular protrusion heterogeneity and the underlying actin regulator dynamics from live cell imaging. *Nat Commun* 9, 1688 (2018).

29. Molinie, N. *et al.* Cortical branched actin determines cell cycle progression. *Cell Research* 29, 432–445 (2019).

30. Soderling, S. H. *et al.* The WRP component of the WAVE-1 complex attenuates Rac-mediated signalling. *Nature Cell Biology* 4, 970–975 (2002).

31. Suetsugu, S. *et al.* Optimization of WAVE2 complex–induced actin polymerization by membrane-bound IRSp53, PIP3, and Rac. *J Cell Biology* 173, 571–585 (2006).

32. Law, A.-L. *et al.* Lamellipodin and the Scar/WAVE complex cooperate to promote cell migration in vivo. *J Cell Biology* 203, 673–689 (2013).

33. Gabler, F. *et al.* Protein Sequence Analysis Using the MPI Bioinformatics Toolkit. *Curr Protoc Bioinform* 72, e108 (2020).

34. Jumper, J. *et al.* Highly accurate protein structure prediction with AlphaFold. *Nature* 596, 583–589 (2021).

35. Evans, R. *et al.* Protein complex prediction with AlphaFold-Multimer. *Biorxiv* 2021.10.04.463034 (2022) doi:10.1101/2021.10.04.463034.

36. Mirdita, M. *et al.* ColabFold - Making protein folding accessible to all. *Biorxiv* 2021.08.15.456425 (2022) doi:10.1101/2021.08.15.456425.

37. Derivery, E. *et al.* Free Brick1 is a trimeric precursor in the assembly of a functional wave complex. *PLoS ONE* 3, e2462 (2008).

38. Peterson, J. R. *et al.* Chemical inhibition of N-WASP by stabilization of a native autoinhibited conformation. *Nat Struct Mol Biol* 11, 747–755 (2004).

39. Hertz, E. P. T. *et al.* A Conserved Motif Provides Binding Specificity to the PP2A-B56 Phosphatase. *Mol Cell* 63, 686–695 (2016).

40. Remmerie, M. & Janssens, V. PP2A: A Promising Biomarker and Therapeutic Target in Endometrial Cancer. *Frontiers Oncol* 9, 462 (2019).

41. Amin, P. *et al.* PP2A-B55: substrates and regulators in the control of cellular functions. *Oncogene* 41, 1–14 (2022).

42. Wang, Y., Xia, Y., Kuang, D., Duan, Y. & Wang, G. PP2A regulates SCF-induced cardiac stem cell migration through interaction with p38 MAPK. *Life Sci* 191, 59–67 (2017).

43. Zhang, L. *et al.* Protein phosphatase 2A regulates the p38 signaling pathway to affect the migration of astrocytes. *Mol Med Rep* 18, 4328–4334 (2018).

44. Li, J., Enomoto, A., Weng, L., Sun, L. & Takahashi, M. Dephosphorylation of Girdin by PP2A inhibits breast cancer metastasis. *Biochem Bioph Res Co* 513, 28–34 (2019).

45. Beck, M. *et al.* The quantitative proteome of a human cell line. *Mol Syst Biol* 7, 549–549 (2011).

46. Levine, D. A. *et al.* Integrated genomic characterization of endometrial carcinoma. *Nature* 497, 67–73 (2013).

47. Haesen, D. *et al.* Recurrent PPP2R1A Mutations in Uterine Cancer Act through a Dominant-Negative Mechanism to Promote Malignant Cell Growth. *Cancer Res* 76, 5719–5731 (2016).

48. Taylor, S. E. *et al.* The highly recurrent PP2A Aα-subunit mutation P179R alters protein structure and impairs PP2A enzyme function to promote endometrial tumorigenesis. *Cancer Research* (2019) doi:10.1158/0008-5472.can-19-0218.

49. Chen, W., Arroyo, J. D., Timmons, J. C., Possemato, R. & Hahn, W. C. Cancer-Associated PP2A Aα Subunits Induce Functional Haploinsufficiency and Tumorigenicity. *Cancer Res* 65, 8183–8192 (2005).

50. Joseph, N. *et al.* A conformational change within the WAVE2 complex regulates its degradation following cellular activation. *Sci Rep* 7, 44863 (2017).

51. Hirschhäuser, A., Cann, M. van & Bogdan, S. CK1α protects WAVE from degradation to regulate cell shape and motility in immune response. *J Cell Sci* (2021) doi:10.1242/jcs.258891.

52. Pollard, T. D. Regulation of actin filament assembly by Arp2/3 complex and formins. *Annual Review of Biophysics and Biomolecular Structure* 36, 451–477 (2007).

53. Millius, A., Watanabe, N. & Weiner, O. D. Diffusion, capture and recycling of SCAR/WAVE and Arp2/3 complexes observed in cells by single-molecule imaging. *Journal of Cell Science* 125, 1165–1176 (2012).

54. Castro-Castro, A. *et al.* Coronin 1A promotes a cytoskeletal-based feedback loop that facilitates Rac1 translocation and activation. *The EMBO Journal* 30, 3913–3927 (2011).

55. Grinthal, A., Adamovic, I., Weiner, B., Karplus, M. & Kleckner, N. PR65, the HEAT-repeat scaffold of phosphatase PP2A, is an elastic connector that links force and catalysis. *Proc National Acad Sci* 107, 2467–2472 (2010).

Wang et al., Figure 1

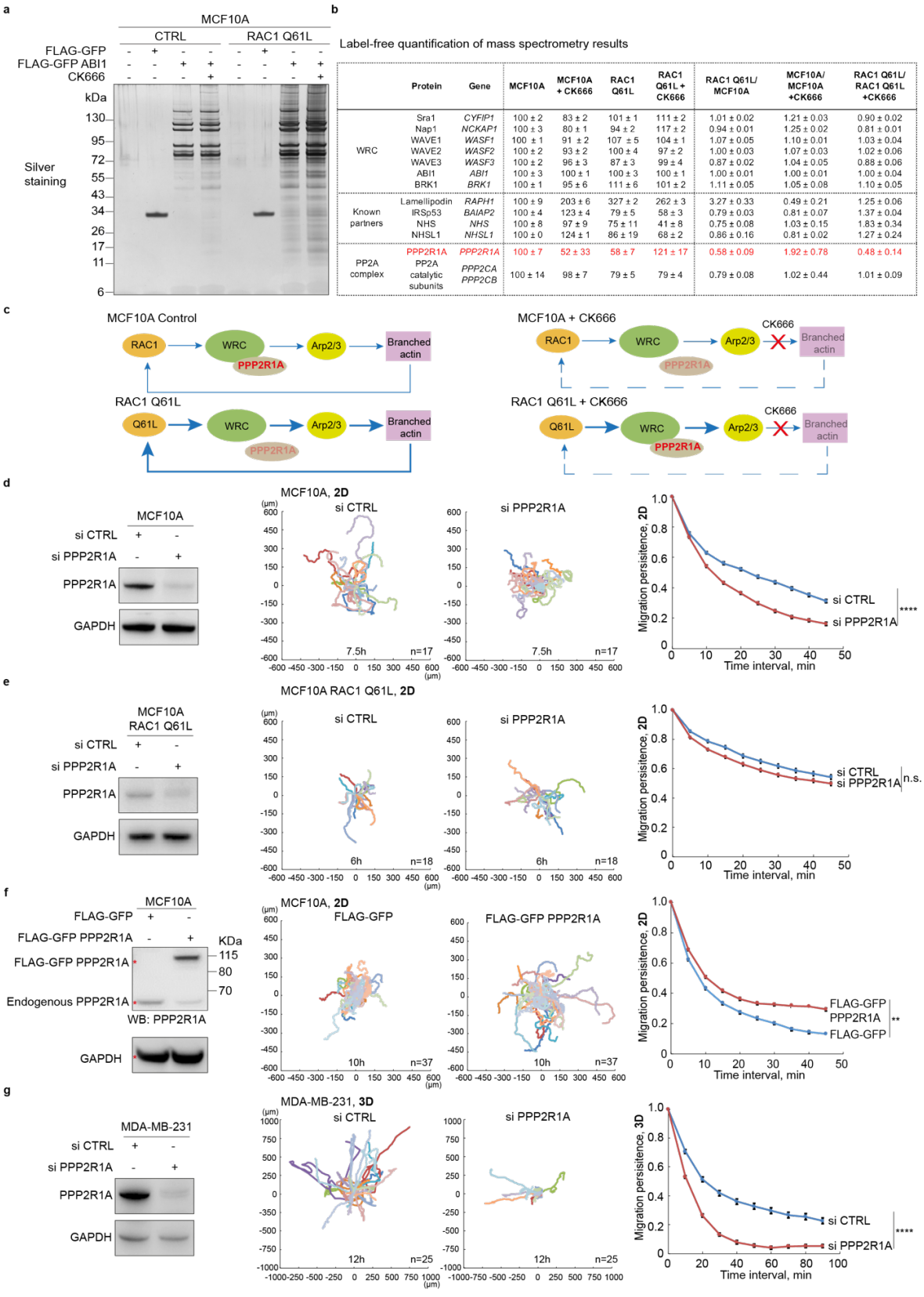


| | Protein | Gene | MCF10A | MCF10A + CK666 | RAC1 Q61L | RAC1 Q61L + CK666 | RAC1 Q61L/ MCF10A | MCF10A/ MCF10A +CK666 | RAC1 Q61L/ RAC1 Q61L +CK666 |
|---|---|---|---|---|---|---|---|---|---|
| WRC | Sra1 | *CYFIP1* | 100 ± 2 | 83 ± 2 | 101 ± 1 | 111 ± 2 | 1.01 ± 0.02 | 1.21 ± 0.03 | 0.90 ± 0.02 |
| | Nap1 | *NCKAP1* | 100 ± 3 | 80 ± 1 | 94 ± 2 | 117 ± 2 | 0.94 ± 0.01 | 1.25 ± 0.02 | 0.81 ± 0.01 |
| | WAVE1 | *WASF1* | 100 ± 1 | 91 ± 2 | 107 ± 5 | 104 ± 1 | 1.07 ± 0.05 | 1.10 ± 0.01 | 1.03 ± 0.04 |
| | WAVE2 | *WASF2* | 100 ± 2 | 93 ± 2 | 100 ± 4 | 97 ± 2 | 1.00 ± 0.03 | 1.07 ± 0.03 | 1.02 ± 0.06 |
| | WAVE3 | *WASF3* | 100 ± 2 | 96 ± 3 | 87 ± 3 | 99 ± 4 | 0.87 ± 0.02 | 1.04 ± 0.05 | 0.88 ± 0.06 |
| | ABI1 | *ABI1* | 100 ± 3 | 100 ± 1 | 100 ± 3 | 100 ± 1 | 1.00 ± 0.01 | 1.00 ± 0.01 | 1.00 ± 0.04 |
| | BRK1 | *BRK1* | 100 ± 1 | 95 ± 6 | 111 ± 6 | 101 ± 2 | 1.11 ± 0.05 | 1.05 ± 0.08 | 1.10 ± 0.05 |
| Known partners | Lamellipodin | *RAPH1* | 100 ± 9 | 203 ± 6 | 327 ± 2 | 262 ± 3 | 3.27 ± 0.33 | 0.49 ± 0.21 | 1.25 ± 0.06 |
| | IRSp53 | *BAIAP2* | 100 ± 4 | 123 ± 4 | 79 ± 5 | 58 ± 3 | 0.79 ± 0.03 | 0.81 ± 0.07 | 1.37 ± 0.04 |
| | NHS | *NHS* | 100 ± 8 | 97 ± 9 | 75 ± 11 | 41 ± 8 | 0.75 ± 0.08 | 1.03 ± 0.15 | 1.83 ± 0.34 |
| | NHSL1 | *NHSL1* | 100 ± 0 | 124 ± 1 | 86 ± 19 | 68 ± 2 | 0.86 ± 0.16 | 0.81 ± 0.02 | 1.27 ± 0.24 |
| PP2A complex | PPP2R1A | *PPP2R1A* | 100 ± 7 | 52 ± 33 | 58 ± 7 | 121 ± 17 | 0.58 ± 0.09 | 1.92 ± 0.78 | 0.48 ± 0.14 |
| | PP2A catalytic subunits | *PPP2CA* *PPP2CB* | 100 ± 14 | 98 ± 7 | 79 ± 5 | 79 ± 4 | 0.79 ± 0.08 | 1.02 ± 0.44 | 1.01 ± 0.09 |

**Figure 1. Identification of PPP2R1A as an ABI1 partner that regulates migration persistence.** **(a)** MCF10A parental cells or genome-edited MCF10A cells where a *RAC1* allele encodes the active RAC1 Q61L mutant form were stably transfected with plasmids expressing FLAG-GFP or FLAG-GFP ABI1. Cells were treated or not with CK666 in order to block the polymerization of branched actin and thus the suspected feedback loop that mediates migration persistence. FLAG-GFP proteins were then purified by Tandem Affinity Purification and associated proteins were revealed by silver staining of SDS-PAGE gels. **(b)** PPP2R1A associates with ABI1 differently upon RAC1-dependent Arp2/3 activation. Label-free quantification of selected proteins identified by mass spectrometry to be associated with ABI1. 3 technical repeats, mean ± sem. **(c)** Schematic representations of the association of PPP2R1A with the WRC in different conditions. **(d)** MCF10A cells were transfected with pools of control (CTRL) or PPP2R1A siRNAs and analyzed by Western blots with PPP2R1A and GAPDH antibodies. Cell trajectories and migration persistence extracted from 2D migration of single MCF10A cells transfected with indicated siRNAs. **(e)** Same experiment as in (a) with MCF10A RAC1 Q61L cells. **(f)** MCF10A cells were stably transfected with plasmids expressing FLAG-GFP or FLAG-GFP PPP2R1A. Migration was analyzed as in (a). **(g)** Same experiment as in (a) with MDA-MB-231 cells analyzed in collagen type I gels. Most cell trajectories upon PPP2R1A depletion are so short that they cannot be well distinguished, because they overlap in the center of the graph. 3 biological repeats of each experiment yielded similar results, only one is displayed. **P<0.01; ****P<0.0001; n.s. not significant.

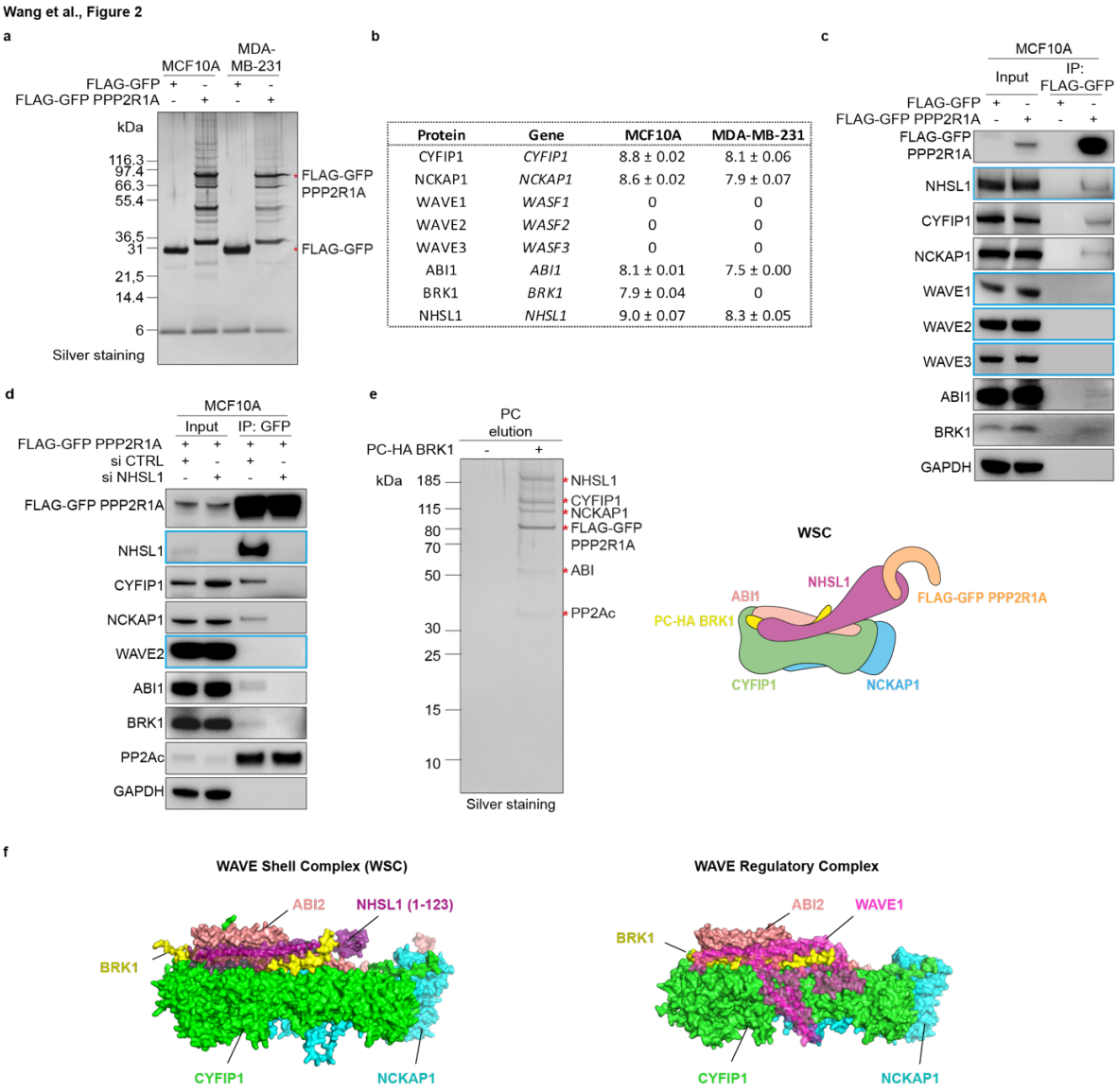


**Figure 2. PPP2R1A interacts with the WAVE Shell Complex (WSC) that contains NHSL1 instead of WAVE proteins. (a)** MCF10A or MDA-MB-231 cells stably expressing FLAG-GFP or FLAG-GFP PPP2R1A were subjected to FLAG-GFP Tandem Affinity Purification and purified proteins were resolved by SDS-PAGE and silver stained. The same samples were used for mass spectrometry and Western blots. **(b)** Label-free quantification of proteins identified by mass spectrometry. In both cell lines, NHSL1 is present at the expense of WAVE subunits. 3 technical repeats, mean ± sem. **(c)** Western blots with the indicated antibodies. 3 biological repeats with similar results. **(d)** PPP2R1A associates with the WSC through NHSL1. MCF10A cells expressing FLAG-GFP PPP2R1A were transfected with pools of siRNAs targeting NHSL1 or non-targeting siRNAs (CTRL). GFP immunoprecipitates were analyzed by Western blots. 3 biological repeats

with similar results. **(e)** An MCF10A cell line stably transfected with two plasmids expressing FLAG-GFP PPP2R1A and PC-HA BRK1 was subjected to FLAG-PC Tandem Affinity Purification to purify the WSC. WSC composition was analyzed by mass spectrometry. Silver stained SDS PAGE of purified WSC. The identity of WSC subunits and the lack of WAVE2 was confirmed using Western blots. 3 biological repeats with similar results. **(f)** Comparison of the structural model of the WSC obtained using Alphafold2 with the X-ray crystal structure WAVE Regulatory Complex (PDB:3P8C). The WSC was composed of NHSL1 (1-123) (purple), CYFIP1 (green), NCKAP1 (cyan), BRK1 (yellow) and ABI2 (1-160) (salmon).

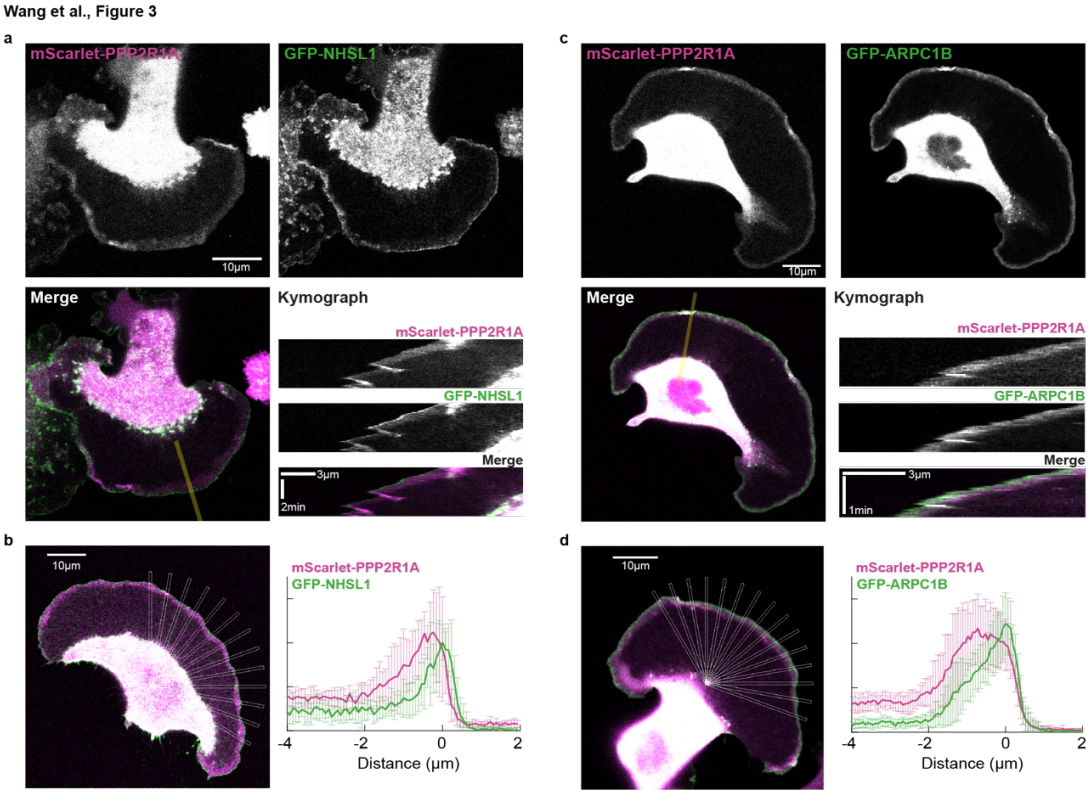


**Figure 3. PPP2R1A colocalizes with branched actin in the width of the lamellipodium and colocalizes with NHSL1 at the lamellipodium edge. (a)** B16-F1 cells were transiently transfected with mScarlet-PPP2R1A and GFP-NHSL1. A kymograph was drawn along the line shown on the merge. **(b)** Overlap of PPP2R1A and NHSL1 over multiple radial line scans registered to the cell edge. **(c)** B16-F1 cells were transiently transfected with mScarlet-PPP2R1A and the Arp2/3 subunit GFP-ARPC1B. A kymograph was drawn along the line shown on the merge. **(d)** Overlap of PPP2R1A and ARPC1B over multiple radial line scans registered to the cell edge.

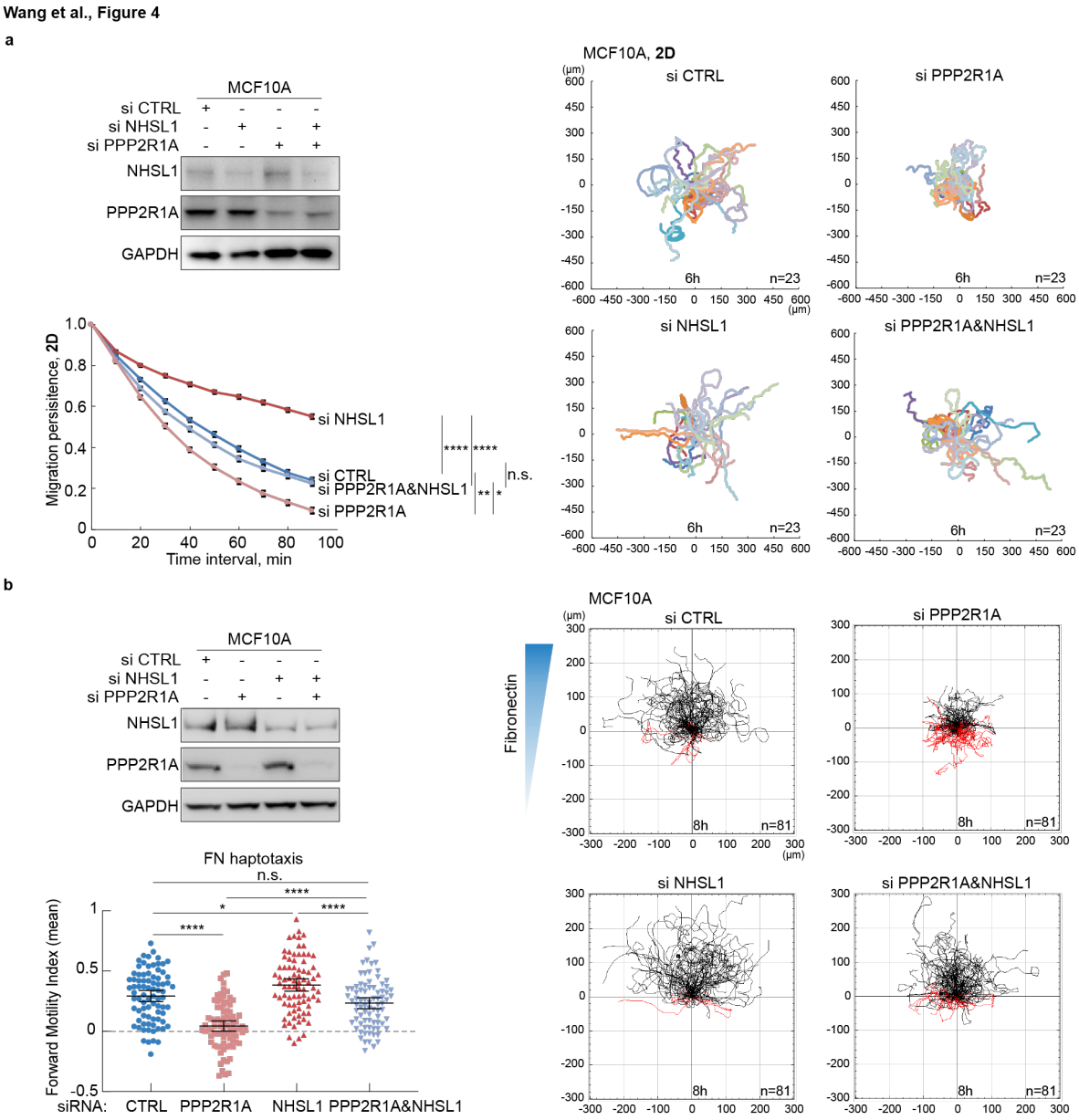


**Figure 4. PPP2R1A depends on NHSL1 to regulate cell migration.** MCF10A cells were transfected with pools of siRNAs targeting PPP2R1A, NHSL1 or both. Non-targeting siRNAs were transfected as controls (CTRL). Western blots were used to validate depletion. **(a)** 2D cell trajectories and migration persistence of single MCF10A cells transfected with indicated siRNAs, n=23. 3 biological repeats with similar results, only one is displayed. **(b)** Haptotaxis of MCF10A cells along a gradient of fibronectin. Cell trajectories of MCF10A cells transfected with indicated siRNAs. 3 biological repeats with similar results. All tracked cells from the 3 experiments were pooled to reach n=81 cells. Mean ± 95% confidence intervals of Forward Motility Index are plotted. *P<0.05; **P<0.01; ****P<0.0001

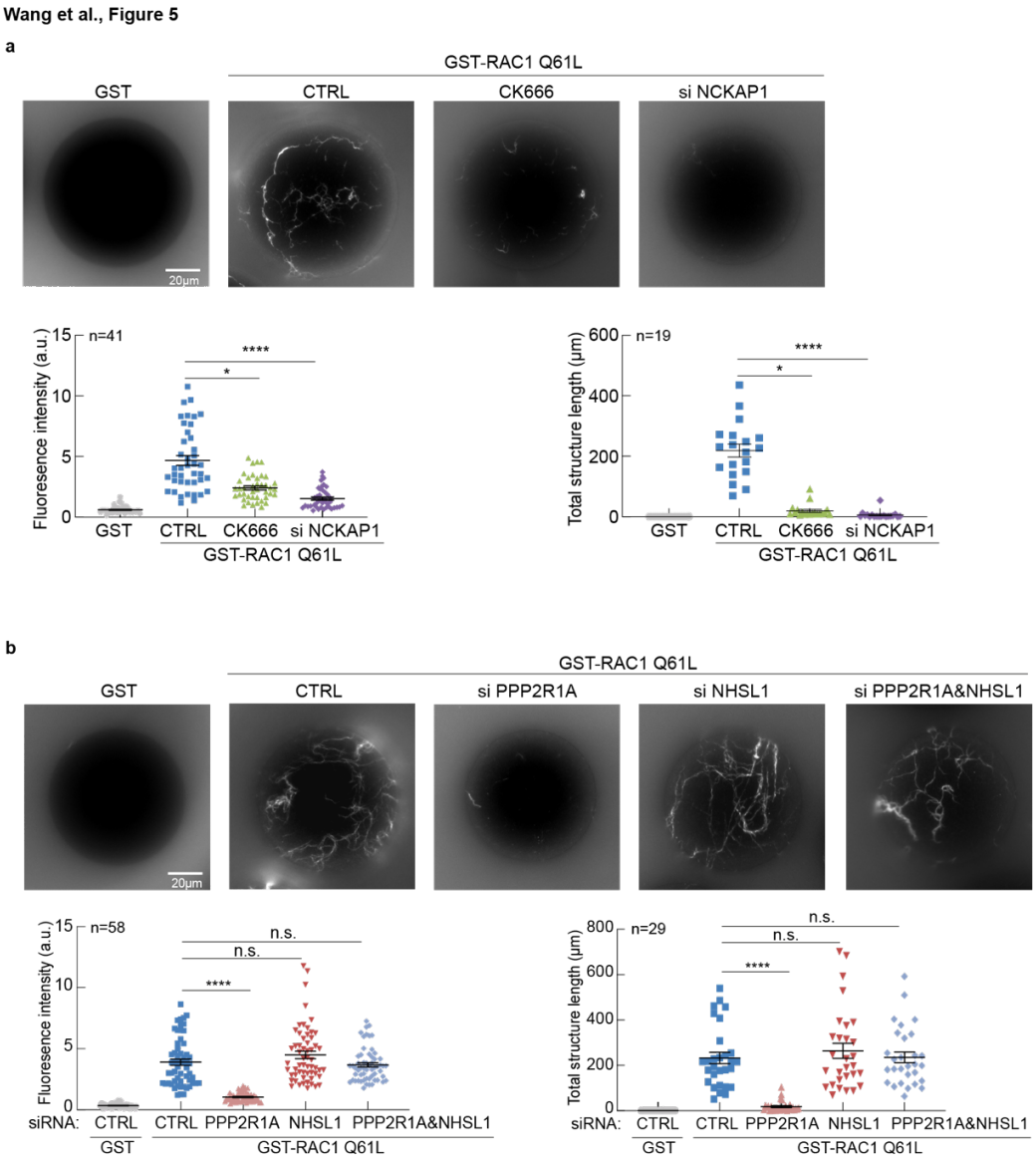


**Figure 5. PPP2R1A is required for RAC1-induced actin polymerization in cell-free extracts.** **(a)** Beads coated with GST or GST-RAC1 Q61L were incubated with cytosolic extracts of MCF10A cells treated with 200 μM CK666 or depleted of NCKAP1. Rhodamine-labeled actin structures polymerized on the beads were examined by fluorescent microscopy and quantified by average florescence intensity and total structure length. **(b)** Similar experiment performed with cytosolic extracts of MCF10A cells depleted of PPP2R1A, NHSL1 or both. 3 biological repeats with similar results for both experiments. n corresponds to the number of beads used for quantification from all 3 experiments.

Wang et al, Figure 6

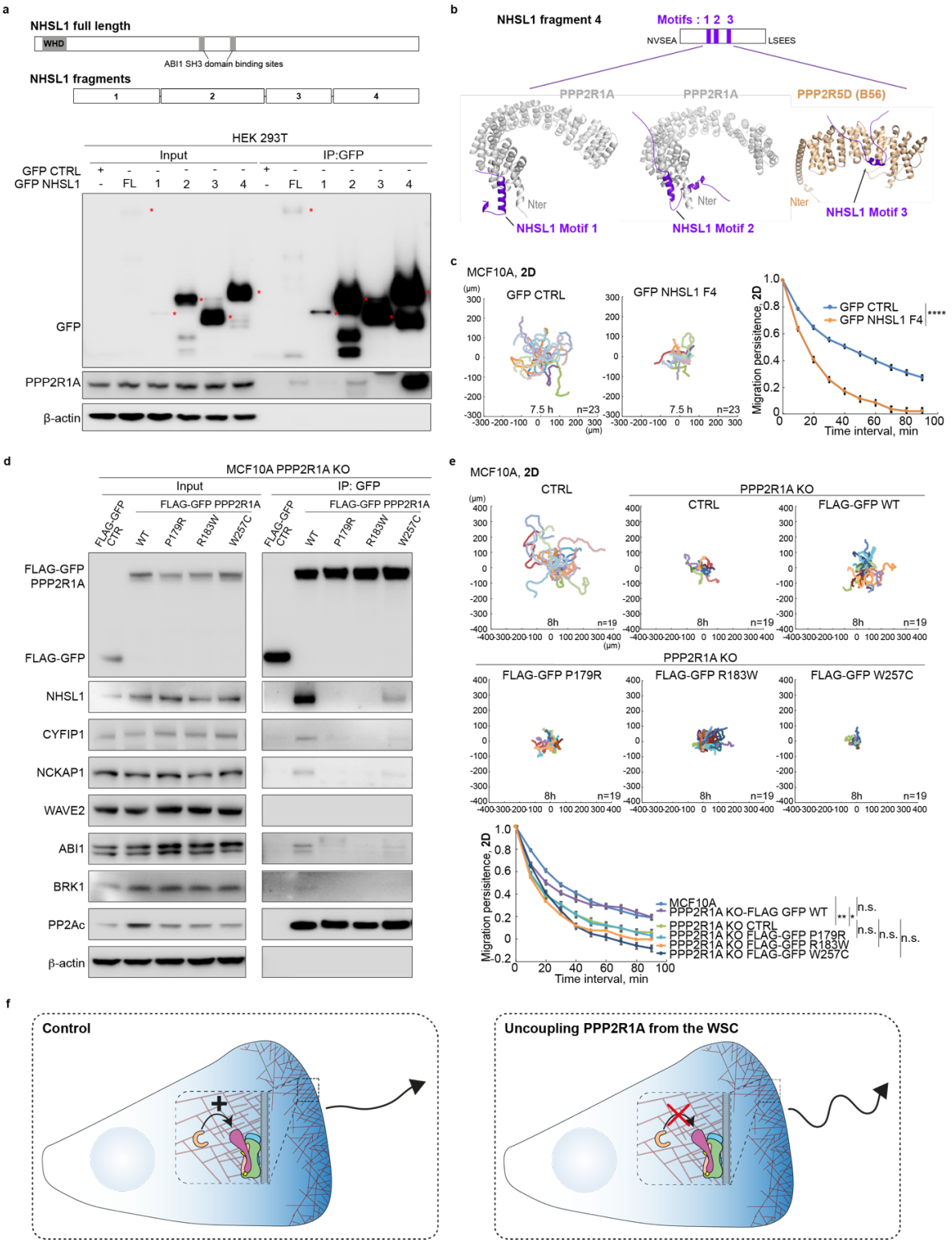

**Figure 6. Uncoupling PPP2R1A from the WSC prevents PPP2R1A from regulating migration persistence. (a)** Scheme of NHSL1 FL and fragments. WHD: WAVE homology domain. HEK 293T cells were transiently transfected with GFP-NHSL1 FL or NHSL1 fragments. Transfected cells were subjected to GFP immunoprecipitation. Western blots with the indicated antibodies. 3 biological repeats of the same experiment with similar results, only one is displayed. **(b)** Prediction of 3 structural motifs that recognize the scaffolding subunit PPP2R1A or the regulatory subunit PPP2R5D of the PP2A complex using Alphafold2. Cartoon representations of the complexes between PPP2R1A (grey) and motif 1($P_{1380}$SRP-DD$H_{1410}$ of NHSL1 in violet or motif 2 ($A_{1430}$SP-EP$S_{1490}$ of NHSL1 in violet). Motif 3 ($S_{1522}$LS-EP$V_{1569}$ of NHSL1 in violet) interacts with PPP2R5D (wheat). **(c)** Cell trajectories, migration persistence, cell speed and MSD were extracted from 2D random migration of MCF10A cells stably expressing GFP-NHSL1 fragment 4, n=23. 2 biological repeats of the same experiment with similar results, only one is displayed. **(d)** *PPP2R1A* knockout MCF10A cells were isolated. The KO line was stably transfected with plasmids expressing GFP-tagged WT or mutant forms of PPP2R1A from tumors of patients. Extracts were subjected to GFP immunoprecipitation and immunoprecipitates were analyzed by Western blots with antibodies that recognize WRC, WSC and the catalytic subunit of the PP2A phosphatase complex. 3 biological repeats with similar results. **(e)** 2D cell trajectories and migration persistence of MCF10A parental cells, KO and rescue derivatives. 3 biological repeats with similar results, only one is displayed. n=19. **(f)** Model showing that PPP2R1A can be uncoupled from the WSC at the lamellipodial edge using the fragment 4 of NHSL1 or tumor associated mutations. *P<0.05; **P<0.01; ****P<0.0001.

**SUPPLEMENTARY INFORMATION**

## METHODS

### Cells

MCF10A cells were grown in DMEM/F12 medium supplemented with 5% horse serum, 20 ng/mL epidermal growth factor, 10µg/mL insulin, 100 ng/mL cholera toxin, 500 ng/mL hydrocortisone and 100U/mL penicillin/streptomycin. MDA-MB-231 and B16-F1 cells were grown in DMEM medium with 10% FBS and 100 U/mL penicillin/streptomycin. Medium and supplements were from Life Technologies and Sigma. Cells were incubated at 37°C in 5% CO2.

### Plasmids

The following plasmids were built using a building block method [1]:

MXS AAVS1L SA2A Puro bGHpA EF1FLAG GFP Blue2 Sv40pA AAVS1R (control)

MXS AAVS1L SA2A Puro bGHpA EF1 FLAG GFP ABI1 Sv40pA AAVS1R

MXS AAVS1L SA2A Puro bGHpA EF1 FLAG GFP PPP2R1A Sv40pA AAVS1R

MXS PGK Blasti bGHpA CAG PC HA Blue2 Sv40pA (control)

MXS PGK Blasti bGHpA CAG PC HA BRK1 Sv40pA

MXS PGK ZeoM bGHpA EF1Flag mScarlet PPP2R1A SV40pA

The plasmid pCAG-EGFP-NHSL1-IRES-Puro encoding GFP fusion with FL NHSL1 containing the WHD (1-1639). FL NHSL1 corresponds to the isoform X6 (XP_047275069.1) with 7 substitutions T440I, A449V, T891A, G1082E, A1123T, P1329S and S1466N. The fragments 1 (MVVFI…KSRDH), 2 (LISRH…EGSGT), 3 (MKKLD…VEPAE) and 4 (NVSEA…LSEES) correspond to the isoform X19 (XP_047275073.1) with 7 substitutions T363I, A372V, T814A, G1005E, A1046T, P1252S and S1389N and were expressed as GFP fusion proteins from the same plasmid as the full-length NHSL1.

### Stable Cell Lines

Stable transfections of MCF10A and MDA-MB-231 cells were performed using Lipofectamine 3000 (Invitrogen) with the plasmids encoding FLAG-GFP, FLAG-GFP ABI1, FLAG-GFP PPP2R1A, FLAG-GFP NHSL1 Fragment 4. To obtain stable integration at the AAVS1 site, cells were co-transfected with two TALEN constructs (Addgene #59025 and 59026) inducing a double strand break at the AAVS1 locus [2]. Cells were selected with 1µg/mL puromycin (Invivogen) and pooled.

Stable MCF10A double cell line was obtained by transfecting cells stably expressing FLAG-GFP PPP2R1A with PC-HA BRK1 or PC-HA Blue2. Cells were then selected with 10μg/ml of Blasticidin (Invivogen). Single clones were expanded and analyzed by Western blot.

**Knockdown and Knockout**

MCF10A and MDA-MB-231 knockdown cells were obtained by transfecting 20 nM siRNAs (Dharmacon ON-TARGET SMART Pool: L-010259-00-0010 for PPP2R1A, L-032698-00-0010 for NHSL1) with Lipofectamine RNAiMAX (Invitrogen). After 3 days, cells were subjected to videomicroscopy or Western blot.

MCF10A knockout cell lines were generated with CRISPR/Cas9 system. The following gRNAs were used:

*PPP2R1A* 5'-CATAGACGAACTCCGCAATG-3'

*NHSL1* 5'-TCGGCTTTCCTCATCTAGGT-3'

non-targeting 5'-AAAUGUGAGAUCAGAGUAAU-3'.

Cells were transfected with gRNA, tracrRNA and Cas9 protein by Lipofectamine CRISPRMAX™ (all reagents from ThermoFischer Scientific). After 2 days, cells were diluted at 0.8 cells/well in 96-well plates. Single clones were expanded and analyzed by Western blot. The positive clones were confirmed by sequencing.

**Antibodies**

The antibodies used were: anti-PPP2R1A (Bethyl Laboratories, A300-962A); anti-NHSL1 (Sigma-Aldrich, HPA029967); anti-PP2Ac (Bethyl Laboratories, A300-732A); anti-GFP (Roche, 11814460001); anti-NCKAP1 (Bethyl Laboratories, A305-178A); anti-WAVE1 (R&D Systems, AF5514); anti-WAVE3 (R&D Systems, AF5515); anti-phospho-WAVE2 Ser308 (Millipore, 07-1511); anti-GAPDH (Thermo Fisher Scientific, AM4300); anti-β-actin (Thermo Fisher Scientific, AM4302). Home-made CYFIP1, ABI1, WAVE2 antibodies and BRK1 antibody were described previously [3,4].

**Western Blots**

Cells were lysed in XB-NP40 buffer (50mM HEPES, 50mM KCl, 1%NP-40, 10mM EDTA, pH 7.7) supplemented with protease inhibitor (Roche), the lysates were clarified by centrifugation at 13,000 rpm for 15 min and subjected to SDS-PAGE using NuPAGE 4-12% Bis-Tris or 3-8% Tris-Acetate gels (Life Technologies). Nitrocellulose membranes were incubated with primary antibodies, HRP conjugated secondary antibodies (Sigma) and

developed with SuperSignal™ West Femto Substrate (Thermo Fisher Scientific) and ChemiDoc imaging system (BIO-RAD). Densitometry of Western blots was performed with ImageJ.

**Immunoprecipitation and Tandem Affinity Purification**

Cells stably expressing FLAG-GFP ABI1 or FLAG-GFP PPP2R1A were lysed with XB-NP40 buffer (50mM HEPES, 50mM KCl, 1%NP-40, 10mM EDTA, pH 7.7) supplemented with protease inhibitors at 4°C for 30 min. The phosphatase inhibitor cocktail PhosSTOP (Roche) was added for phosphosite analysis. The lysates were clarified by centrifugation at 13,000 rpm for 15 min. Clarified cell extracts were incubated with FLAG-M2 beads (Sigma) at 4°C for 4 h. FLAG-M2 beads were washed with XB-NP40 buffer and eluted with 0.5 mg/ml FLAG peptide (Sigma) in XB (50mM HEPES, 50mM KCl, 10mM EDTA, pH 7.7) overnight at 4°C. FLAG elutions were collected and incubated with GFP-trap beads (Chromotek) at 4°C for 1 h. The GFP-trap beads were washed with XB-NP40 buffer. 20% of the beads were subjected to SDS-PAGE for Western blot or silver staining (SilverQuest™ Silver Staining Kit, Thermo Fisher Scientific). 80% of the beads were analyzed by mass spectrometry.

To purify the WSC, MCF10A cells stably expressing FLAG-GFP PPP2R1A and PC-HA BRK1 were lysed with XB-NP40 buffer (50mM HEPES, 50mM KCl, 1%NP-40, 10mM EDTA, pH 7.7) supplemented with protease inhibitors at 4°C for 1 h, then the lysates were clarified by centrifugation at 13,000 rpm for 15 min. Cell extracts were incubated with FLAG-M2 beads (Sigma) overnight at 4°C. FLAG-M2 beads were washed with XB-NP40 buffer, and eluted with 0.5 mg/ml FLAG peptide (Sigma) in FLAG-elution buffer (50mM HEPES, 50mM KCl, 1mM $CaCl_2$, pH 7.7). FLAG elutions were incubated with PC beads (Anti-Protein C Affinity Matrix, Sigma) overnight at 4°C. PC beads were washed eluted with EGTA-elution buffer (50mM HEPES, 50mM KCl, 10mM EGTA, pH 7.7) overnight. PC elutions were subjected to SDS-PAGE and mass spectrometry.

**Mass Spectrometry**

The resins containing the immunoprecipitated sample were loaded onto a 10 kDa cutoff centrifugal filters (Microcon, Millipore-Merck) and washed with 500 µL of ammonium bicarbonate buffer (50 mM, pH 8.0, AMBIC). Disulfide reduction was performed adding to the centrifugal filters 200 µL of a solution containing 10 mM dithiothreitol in AMBIC for 2h at 37 °C. Thiol alkylation was performed by adding to the previous samples 200 µL of a solution containing 50 mM iodoacetamide in AMBIC for 30 minutes at room temperature. Reagents

were removed by filtration and sample washed three times with 500 µL of AMBIC. Proteins were digested with 1 µg of trypsin/Lys-C (Promega) in 100 µL of AMBIC overnight at 37 °C. The resulting peptide mixture was filtered and acidified with trifluoro acetic acid at a final concentration of 0.1%. Technical triplicates were systematically analyzed.

For each fraction, 6 µL of sample was concentrated on a C18 cartridge (Dionex Acclaim PepMap100, 5 µm, 300 µm i.d. x 5 mm) and eluted on a capillary reverse-phase column (C18 Dionex Acclaim PepMap100, 3 µm, 75 µm i.d. x 50 cm) at 220 nL/min, with a gradient of 2% to 38% of buffer B in 60 min (buffer A: 0.1% aq. Formic Acid/Acetonitrile 98:2 (v/v); buffer B: 0.1% aq. Formic Acid/Acetonitrile 10:90 (v/v)), coupled with a quadrupole-Orbitrap mass spectrometer (Q Exactive HF, ThermoFisher Scientific) using a Top 20 data-dependent acquisition MS experiment: 1 survey MS scan (400-2,000 m/z; resolution 70,000) followed by 20 MS/MS scans on the 20 most intense precursors (dynamic exclusion of 30 s, resolution 17,500).

Protein identification was performed with MaxQuant search engine v.1.5.3.30 against the human Swiss-Prot database (updated in 07/2020), with the following parameter: methionine oxidation, cysteine carbamidomethylation, asparagine/glutamine deamidation and serine/threonine/tyrosine phosphorylation as variable modifications, first search error tolerance 20 ppm, main error tolerance 6 ppm, MS/MS error tolerance 20 ppm, FDR 1%. Quantification was performed in label-free LFQ normalization mode, using at least 2 Razor or unique peptide per protein. Quantities were estimated using LFQ intensities. Significant changes in protein amounts were estimated by ANOVA with Bonferroni's Post-Hoc test using a p-value cutoff threshold of 0.05.

Raw files of the LC-MSMS analyses and the database researches have been deposited in PRIDE (https://www.ebi.ac.uk/pride/) with the accession number PXD031584. Files with the reference number 170414 refer to the TAP purification of FLAG-GFP-ABI1, 181220 to the TAP purification of FLAG-GFP-PPP2R1A, 210415 to the TAP purification of the WSC and 200120 to the identification of phosphosites in the TAP purification of FLAG-GFP-ABI1. These files can be downloaded using the following username: reviewer_pxd031584@ebi.ac.uk, and password: DsEdCLt8.

**Migration and Videomicroscopy**

Random cell migration assays were performed in µ-Slide 8 well ibidi dishes. For 2D migration assays, cells were seeded on the dishes coated with 20µg/ml Fibronectin (Sigma). For 3D migration assays, cells were sandwiched between two layers of 2mg/ml collagen (rat tail

collagen type I, Corning). After seeding cells for 24h, videomicroscopy was performed on an inverted Axio Observer microscope (Zeiss) equipped with a Pecon Zeiss incubator XL multi S1 RED LS (Heating Unit XL S, Temp module, CO2 module, Heating Insert PS and CO2 cover), a definite focus module and a Hamamatsu camera C10600 Orca-R2. Images were acquired every 5 or 10 min for 24 h with 10x objective for 2D migration, and every 10 min for 48 h with 20x objective for 3D migration. Individual cells were tracked by ImageJ software-Manual Tracking plug-in. DiPer software was used to analyze the cell migration parameters [5].

Fibronectin gradients were prepared with PRIMO photopatterning system (Alvéole). 35mm ibidi dishes with glass bottom were treated with plasma for 1 min. PDMS stencils (Alvéole) with three 3x3mm wells were stacked on each plasma-treated dish immediately. PDMS stencil wells were coated with PLL-g-PEG for 1 h and rinsed 3 times with PBS. Then photoinitiator (PLPP) (Alvéole) was added to the PDMS stencil wells for micropatterning. LEONARDO photopatterning software was used to design the micropatterns (width 645µm, height 1031µm with 100% to 0% grayscale gradient). The dishes with PDMS stencils were placed onto the microscope holder (Nikon ECLIPSE Ti2) with PRIMO module, and the patterns were projected to the surface at a UV dose of 1500 mg/mm$^2$. PDMS stencil wells were rinsed 3 times with PBS and coated with 50µg/ml Fibronectin/Fibrinogen-Alexa647 (Invitrogen) for 30 minutes at 37°C. The Fibronectin/Fibrinogen-Alexa647 were only adsorbed on the previously illuminated areas. After rinsing the wells 3 times with PBS, MCF10A cells were seeded in the coated PDMS stencil wells. Cells were washed once with medium after adhering for 2 h. After 24 h, videomicroscopy was performed on an inverted Axio Observer microscope (Zeiss) with the 10x objective. Images were acquired every 10 min for 24 h. Individual cells were tracked by ImageJ software-Manual Tracking plug-in. The tracks obtained were analyzed by the chemotaxis tool (Ibidi) to extract the FMI values and cell trajectory plots. The FMI values were plotted by GraphPad Prism software as mean ± 95% confidence intervals.

B16-F1 cells were transiently transfected with GFP and mScarlet plasmids and analyzed by videomicroscopy after 2 days. Videos were acquired using a confocal laser scanning microscope (TCS SP8, Leica) equipped with a high NA oil immersion objective (HC PL APO 63×/ 1.40, Leica), a white light laser (WLL, Leica) and controlled by the LasX software. Images were taken every 10 seconds for about 5-10 min. Kymographs were drawn using Multi Kymograph tool in ImageJ. To analyze the localization of proteins, radial line scans were performed and analyzed as described [6].

**3D Acini**

Single cells were seeded on a 1 mm thick solidified layer of Matrigel (growth factor reduced, Thermo Fisher Scientific, #CB-40230C) in the 8-well glass chamber (Merck, #PEZGS0816) and grown for 3 weeks in MCF10A medium with 1% horse serum, 5 ng/mL EGF and 2% Matrigel. Then the acini were fixed and stained with indicated antibodies. Images were acquired using a confocal laser scanning microscope (TCS SP8, Leica) equipped with a high NA oil immersion objective (HC PL APO 63×/ 1.40, Leica), a white light laser (WLL, Leica) and controlled by the LasX software.

**Protein Purification**

GST-fusion RAC1 WT, RAC1 Q61L and CDC42 Q61L were expressed in and purified from *E. coli* BL21. After 3 hours induction at 37°C with 1mM IPTG, cells were resuspended and lysed in lysis buffer (50mM Tris-HCl, 100mM NaCl, 2.5mM $CaCl_2$, 10mM $MgCl_2$, 1%Triton X100, 5% glycerol, 0.5 mg/ml lysozyme, 10µg/ml DNAseI, 1mM DTT, pH8.0, protease inhibitors) at 4°C for 1 h. The lysates were clarified by centrifugation at 13,000 rpm for 30 min. The supernatants were incubated with Glutathione Sepharose beads (GE healthcare) at 4°C for 3 h. The beads were washed with TBS buffer (50mM Tris, 100mM NaCl, 2.5mM $CaCl_2$, 5mM $MgCl_2$, 1mM DTT, pH8.0), then the bounded proteins were eluted with GST elution buffer (50mM Tris-HCl, 5mM $MgCl_2$, 10mM glutathione, pH8.0). The elutions were dialyzed in buffer (50mM Tris, 5mM $MgCl_2$, 20% glycerol, pH8.0) and kept at -80°C until use.

**GST Pull-Down**

MCF10A cell extracts were prepared with XB-NP40 buffer as described previously. 20µg purified GST-fusion proteins were incubated with 20µl Glutathione Sepharose beads (GE healthcare) in 500µl incubation buffer (50mM Tris-HCl, 100mM NaCl, 2.5mM $CaCl_2$, 10mM $MgCl_2$, 1%Triton X100, 5% glycerol, 1mM DTT, pH8.0) at 4°C for 1 h. The pre-coated beads were washed and incubated with 1 ml MCF10A cell extract at 4°C for 1 h. The beads were washed with XB-NP40 buffer and subjected to Western blot.

**Actin Polymerization in Cell-Free Extracts**

MCF10A cells were lysed either by nitrogen cavitation (Parr instruments, 500 Psi for 20 minutes) in buffer (50mM HEPES, 50mM NaCl, 5mM $MgCl_2$, 0.1mM EDTA, 1mM DTT, pH 7.7, protease inhibitor), or with NP40 containing buffer (50mM HEPES, 50mM KCl, 5mM $MgCl_2$, 1%NP-40, pH 7.7, protease inhibitor) at 4°C for 30 min. The NP40 containing extract

supported RAC1 Q61L-induced actin polymerization, whereas extract obtained by nitrogen cavitation supported CDC42 Q61L-induced actin polymerization. The extracts were clarified by centrifugation at 13,000 rpm for 15 min. 10µl clarified cell extract was supplemented with 2µl energy mix (20mM ATP, 150mM creatine phosphate, 20mM $MgCl_2$, 2mM EGTA) and 0.75µl rhodamine-actin (1mg/ml, Cytoskeleton, Inc.). The mixture was centrifuged 5 min at 13,000 rpm. To trigger the reaction, 1µl Glutathione Sepharose beads bound with 2µg GST-RAC1 Q61L or GST-CDC42 Q61L were added to 10µl reaction mix. After 1 h incubation at room temperature, the reaction was squashed in between a coverslip and the microscope slide. The coverslip was sealed with melted VALAP (Vaseline-Lanoline-Paraffin). The beads were observed under an inverted microscope (Olympus IX83) with 60x oil objective. Fluorescence intensity and structure length on the surface of the beads were measured using ImageJ.

**Structural Modeling**

Sequences of human CYFIP1, NCKAP1, BRK1, ABI2, PPP2R1A and PPP2R5D were retrieved from UniProt database [7] and the full-length NHSL1 cloned in plasmid pCAG were used as input of mmseqs2 homology search program [8] with 3 iterations to generate a multiple sequence alignment (MSA) against the UniRef30 clustered database. Homologs sharing less than 25% sequence identity or less than 50% of coverage of the aligned region with their respective query, were discarded. In case several homologs belonged to the same species, only the one sharing highest sequence identity to the query was kept. Full-length sequences of selected homologs were retrieved and realigned with mafft [9]. To model WSC structure, concatenated MSAs of CYFIP1, NCKAP1, ABI2 (1-160), BRK1 and NHSL1 (1-95, 1-123, or 1-200) were analyzed. Homologs of different subunits belonging to the same species were aligned in a paired manner otherwise in concatenated MSAs. Final concatenated MSAs of WSC contained 2711 positions and 1577 species. MSAs of NHSL1 motif 1 ($P_{1380}$SRP-$DDH_{1410}$), motif 2 ($A_{1430}$SP-$EPS_{1490}$) were similarly concatenated with that of PPP2R1A and MSA of motif 3 ($S_{1522}$LS-$EPV_{1569}$) with that of PPP2R5D (80-530), yielding 3 MSAs from 1733 and 2445 species, respectively. Each concatenated MSA was then used as input to run 5 independent runs of the AlphaFold2 algorithm with 6 iterations each time [10] in order to generate 5 structural models using a local version of the ColabFold interface [11] trained on the multimer dataset [12] on a local HPC equipped with NVIDIA Ampere A100 80Go GPU cards. Best models of each of the 5 runs converged toward similar conformations for each of the 4 modeled molecular systems. High-confidence quality scores of pLDDT in the range of [84.6, 86.2], [91.8, 93.1], [88.3, 88.9], [87.2, 88.9] and pTMscore in the range [0.807, 0.833], [0.816, 0.842], [0.785, 0.8],

[0.844, 0.854] were obtained for WSC and the complexes involving NHSL1 motifs 1, 2 and 3, respectively. For each of the four models, the models with highest pTMscores were relaxed using Rosetta relax protocols to remove steric clashes [13] with strong backbone constraints (std dev. of 0.5 Å for atomic positions) and were used for structural analysis.

The models of i) the Wave Shell Complex (WSC) composed of NHSL1(1-95), CYFIP1, NCKAP1, BRK1 and ABI2(1-160), ii) the NHSL1(1382-1410)-PPP2R1A complex, iii) the NHSL1(1430-1490)-PPP2R1A complex and iv) NHSL1(1522-1569)-PPP2R5D(80-530) complex, are available in ModelArchive (modelarchive.org) with the accession codes ma-agzek (passwd: nFB3QBkRYT), ma-ne9d4 (passwd: KJO5ik7Ksw), ma-sx8ix (passwd: Ozduh9k3eW) and ma-rop1i (passwd: BKiXtzlnG9), respectively.

**Statistics**

Migration persistence for individual cells is evaluated based on the exponential decay and plateau fit as shown below.

$$P = (1 - b) * e^{-\frac{t}{a}} + b$$

Where, $P$ is the migration persistence, $b$ is plateau value, $t$ is the time interval and $a$ is the decay constant. Then the related statistical analysis was conducted through custom-made R programs, as previously described [14].

For other statistical analysis, GraphPad Prism software and Microsoft Excel were used. ANOVA followed by post hoc Tukey's multiple comparison test or Kruskal-Wallis test followed by post hoc Dunn's multiple comparison test were applied based on the Shapiro-Wilk normality test.

Four levels of significance were distinguished: *P < 0.05, **P < 0.01, ***P < 0.001, ****P < 0.0001.

# SUPPLEMENTARY FIGURES

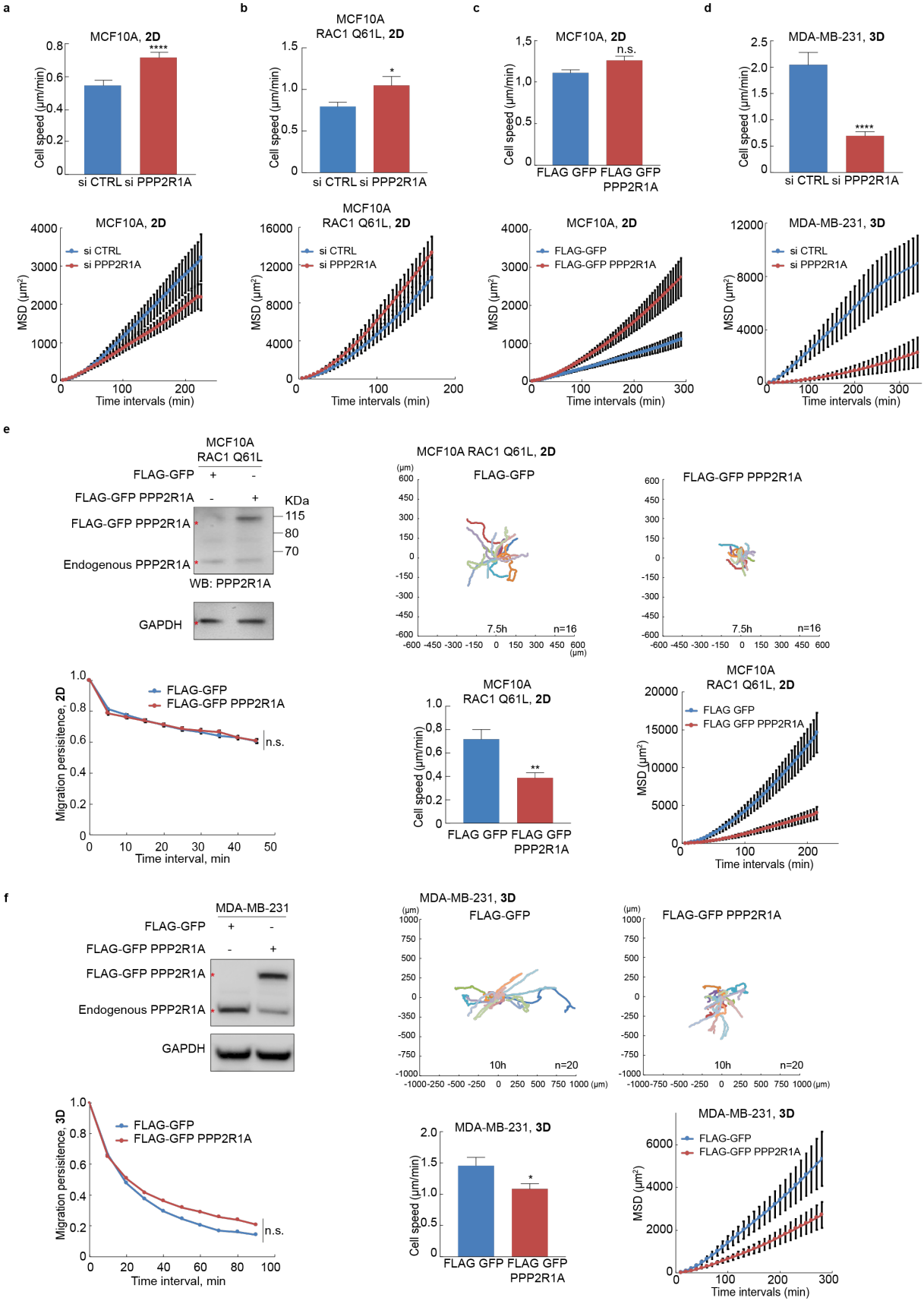

**Figure S1, related to figure 1. Migration parameters of MCF10A and MDA-MB-231. (a-d)** Cell speed and MSD extracted from cell trajectories displayed in corresponding panels of figure 1. 3 biological repeats of the same experiment with similar results, only one is displayed. **(e)** Cell speed and MSD extracted from random migration of single MCF10A cells expressing FLAG-GFP or FLAG-GFP PPP2R1A in 2D, n=16. 2 biological repeats with similar results, only one is displayed. **(f)** MDA-MB-231 cell lines were stably transfected with plasmids expressing FLAG-GFP or FLAG-GFP PPP2R1A and analyzed by Western blots with PPP2R1A or GAPDH antibodies. Cell trajectories, migration persistence, speed and MSD extracted from 3D migration of single MDA-MB-231 cells in collagen type I gels, n=20. 3 biological repeats with similar results, only one is displayed. *P<0.05; ** P<0.01; ****P<0.0001

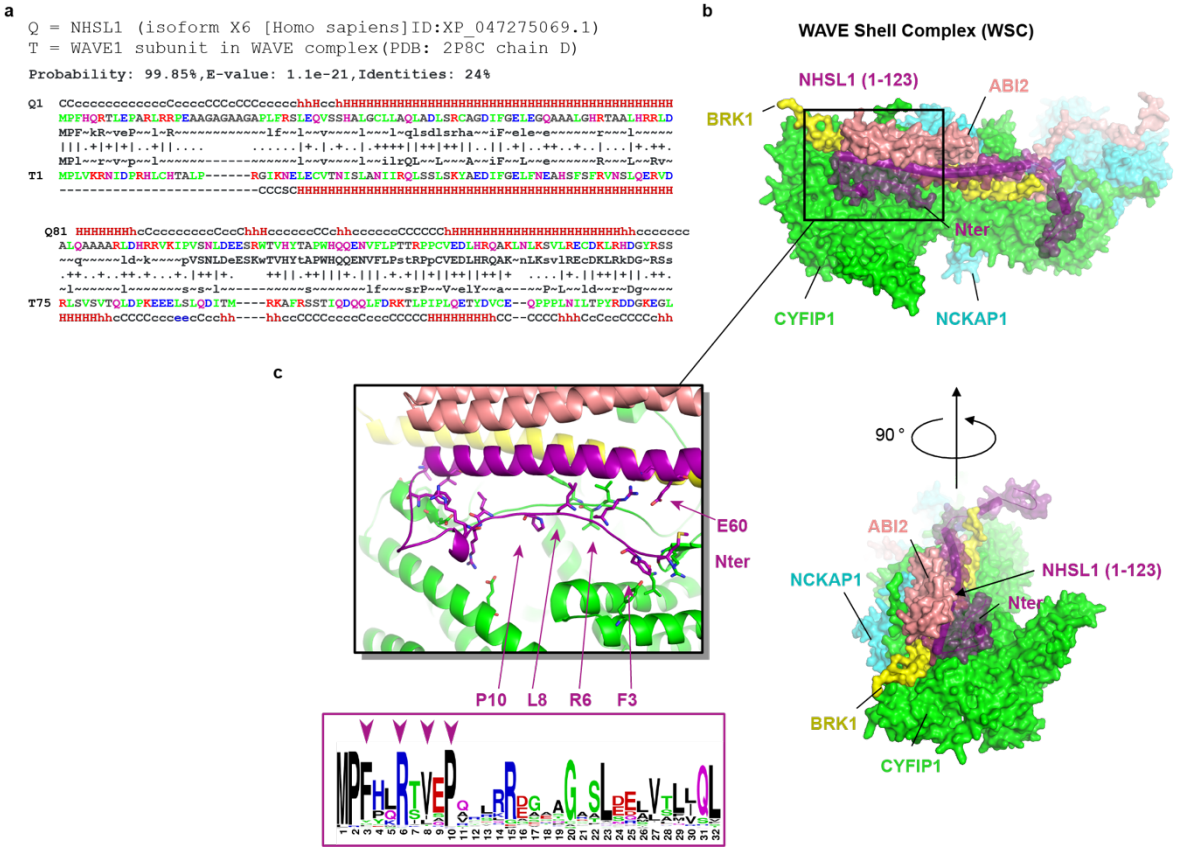


**Figure S2. Structural model of the WSC. (a)** Sequence alignment between the profile of NHSL1 (line Q, 1-160 region) and that of the WAVE1 subunit (line T) extracted from the structure of the WAVE Regulatory Complex (PDB:3P8C). **(b)** Surface representation of the structural model of the WSC generated by AlphaFold2. The model is composed of NHSL1 (1-123) (purple), full-length CYFIP1 (green), NCKAP1 (cyan), BRK1 (yellow) and ABI2 (1-160) (salmon) and is displayed under two views rotated by 90° around the vertical axis. Sensitivity and precision of AlphaFold2 decreases when using long inputs as full WSC. Therefore we also explored potential binary complexes that could be formed between NHSL1 and either CYFIP1 or NCKAP1. These binary structural models with either CYFIP1 or NCKAP1 were very similar to the structural model obtained with full WSC. This suggests that additional interactions downstream of the displayed region of NHSL1 are unlikely. **(c)** Close-up view with cartoon representation. Side chains of amino-acids highlighted as sticks correspond to conserved residues in the N-terminus of NHSL1. Conservation pattern represented in a logo plot using WebLogo[15] indicate the highlighted residues by purple triangles.


| Protein | Gene names | Number of Phospho (STY) | Position with highest probablity | Probability that the different STY residues are phosphorylated | Ctrl | shPPP2R1A |
|---|---|---|---|---|---|---|
| ABI1 | *ABI1* | 1 | 183 | TNPPTQKPPS(1)PPMSGR | 100 ± 12 | 73 ± 9 |
| ABI1 | *ABI1* | 2 | 183 | T(0.004)NPPT(0.015)QKPPS(0.964)PPMS(0.509)GRGT(0.508)LGR | 100 ± 9 | 0 |
| ABI1 | *ABI1* | 1 | 200 | NT(0.013)PY(0.053)KT(0.934)LEPVKPPTVPNDYMTSPAR | 100 ± 49 | 0 |
| ABI1 | *ABI1* | 2 | 183 | TNPPTQKPPS(0.998)PPMS(0.244)GRGT(0.758)LGR | 100 ± 34 | 0 |
| NHSL1 | *NHSL1* | 1 | 1229 | AVPS(0.986)PT(0.011)T(0.003)GEEGSVHSR | 100 ± 6 | 75 ± 9 |
| NHSL1 | *NHSL1* | 1 | 324 | LDSDAGFHS(1)LPR | 100 ± 47 | 46 ± 0 |
| NHSL1 | *NHSL1* | 2 | 1384 | NHS(0.984)PS(0.988)PPVT(0.029)PTGAAPSLASPK | 100 ± 15 | 105 ± 0 |
| NHSL1 | *NHSL1* | 1 | 1186 | SPGAPSAGEAEARPS(0.001)PS(0.002)T(0.002)T(0.002)PLPDS(0.583)S(0.355)PS(0.054)R | 100 ± 0 | 106 ± 45 |
| NHSL1 | *NHSL1* | 1 | 209 | RKT(0.997)IT(0.003)GVPDNIQK | 100 ± 31 | 64 ± 14 |
| WAVE2 | *WASF2* | 1 | 293 | RS(0.209)S(0.765)VVS(0.026)PSHPPPAPPLGSPPGPK | 100 ± 19 | 53 ± 12 |
| WAVE2 | *WASF2* | 1 | 308 | SSVVS(0.004)PS(0.003)HPPPAPPLGS(0.992)PPGPK | 100 ± 0 | 262 ± 97 |
| WAVE3 | *WASF3* | 1 | 235 | LSQSVYHGAS(0.001)S(0.002)EGS(0.017)LS(0.918)PDT(0.063)R | 100 ± 14 | 57 ± 13 |

**Figure S3. Analysis of phosphorylated sites in WRC and WSC in presence or absence of PP2R1A. (a)** MCF10A stably expressing FLAG-GFP ABI1 were transfected with siRNAs targeting PPP2R1A or control siRNAs. TAP purification of ABI1 was analyzed by SDS-PAGE and by mass spectrometry. Label-free quantification of phosphosites identified by mass spectrometry in relevant subunits of WRC and WSC. 3 technical repeats, mean ± sem. **(b)** Western blots of WRC and WSC subunits including phospho-serine 308 of WAVE2.

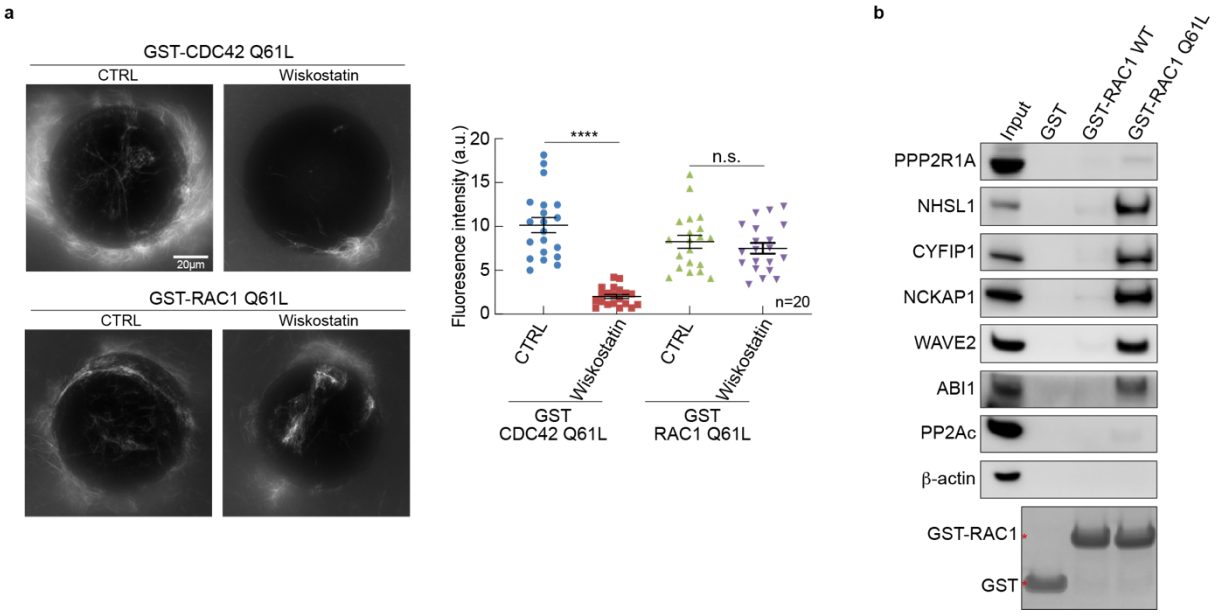


**Figure S4, related to Fig.5. Actin polymerization at the surface of beads displaying GST fusion proteins with small GTPases. (a)** Beads coated with GST-CDC42 Q61L or GST-RAC1 Q61L were incubated with the cell extracts of MCF10A treated or not with 10 µM wiskostatin. Structures containing rhodamine-labeled actin were examined at the surface of beads by epifluorescence and their intensity quantified. **(b)** Beads coated with GST, GST-RAC1 WT or GST-RAC1 Q61L were incubated with MCF10A cell extracts, then subjected to GST pull down. Western blots with the indicated antibodies. For both experiments, 3 biological repeats with similar results, only one is displayed. n corresponds to the total number of beads quantified in all 3 experiments. ****P<0.0001.

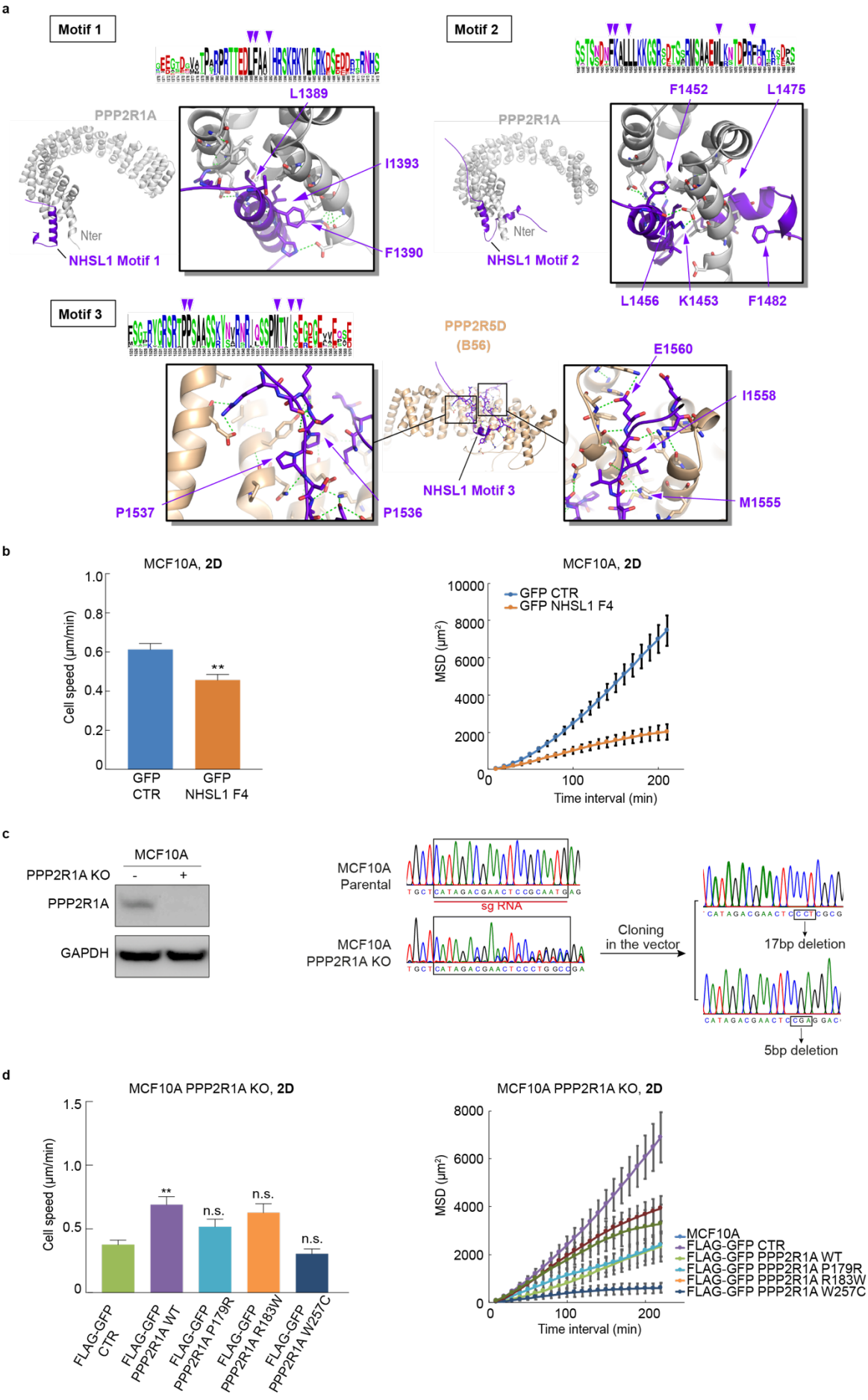
a
Motif 1
L1389
PPP2R1A
I1393
Nter
F1390
NHSL1 Motif 1
Motif 2
F1452
L1475
PPP2R1A
Nter
NHSL1 Motif 2
L1456
K1453
F1482
Motif 3
PPP2R5D
(B56)
E1560
I1558
NHSL1 Motif 3
P1537
P1536
M1555
b
MCF10A, 2D
Cell speed (μm/min)
1.0
0.8
0.6
0.4
0.2
0
**
GFP CTR
GFP NHSL1 F4
MCF10A, 2D
MSD (μm²)
10000
8000
6000
4000
2000
0
GFP CTR
GFP NHSL1 F4
0
100
200
Time interval (min)
c
MCF10A
PPP2R1A KO
-
+
PPP2R1A
GAPDH
MCF10A
Parental
sg RNA
MCF10A
PPP2R1A KO
Cloning
in the vector
17bp deletion
5bp deletion
d
MCF10A PPP2R1A KO, 2D
Cell speed (μm/min)
1.5
1.0
0.5
0
**
n.s.
n.s.
n.s.
FLAG-GFP CTR
FLAG-GFP PPP2R1A WT
FLAG-GFP PPP2R1A P179R
FLAG-GFP PPP2R1A R183W
FLAG-GFP PPP2R1A W257C
MCF10A PPP2R1A KO, 2D
MSD (μm²)
8000
6000
4000
2000
0
0
100
200
Time interval (min)
MCF10A
FLAG-GFP CTR
FLAG-GFP PPP2R1A WT
FLAG-GFP PPP2R1A P179R
FLAG-GFP PPP2R1A R183W
FLAG-GFP PPP2R1A W257C

**Figure S5, related to figure 6. Structural motifs of NHSL1 fragment 4 and characterization of the PPP2R1A KO clone. (a)** Prediction of three motifs of NHSL1 by AlphaFold2 that interact with PPP2R1A or PPP2R5D subunits of the PP2A complex. Cartoon representation with interacting residues of NHSL1 highlighted as sticks. The conservation pattern represented in a logo plot using WebLogo[15] indicates the highlighted residues by purple triangles. Displayed complexes are for motif 1, PPP2R1A (grey) and the region $P_{1380}$SRP-DD$H_{1410}$ in NHSL1 (violet); for motif 2, PPP2R1A (grey) and the region $A_{1430}$SP-EP$S_{1490}$ in NHSL1 (violet); for motif 3, PPP2R5D (wheat) and the region $S_{1522}$LS-EP$V_{1569}$ in NHSL1 (violet). **(b)** Cell speed and MSD extracted from cell trajectories displayed in Fig.6c. 3 biological repeats of the same experiment with similar results, only one is displayed. **(c)** Characterization of the PPP2R1A KO MCF10A clone. Western blots of PPP2R1A and GAPDH as a loading control. Both alleles contain a deletion that induces a frameshift (17 bp and 5 bp). **(d)** Cell speed and MSD were extracted from random migration of MCF10A parental cells, *PPP2R1A* knockout cells or KO clones expressing wild type or mutants of PPP2R1A, n=19. Related to the corresponding experiment displayed in Fig.7e. 3 biological repeats of the same experiment with similar results, only one is displayed. ** $P<0.01$

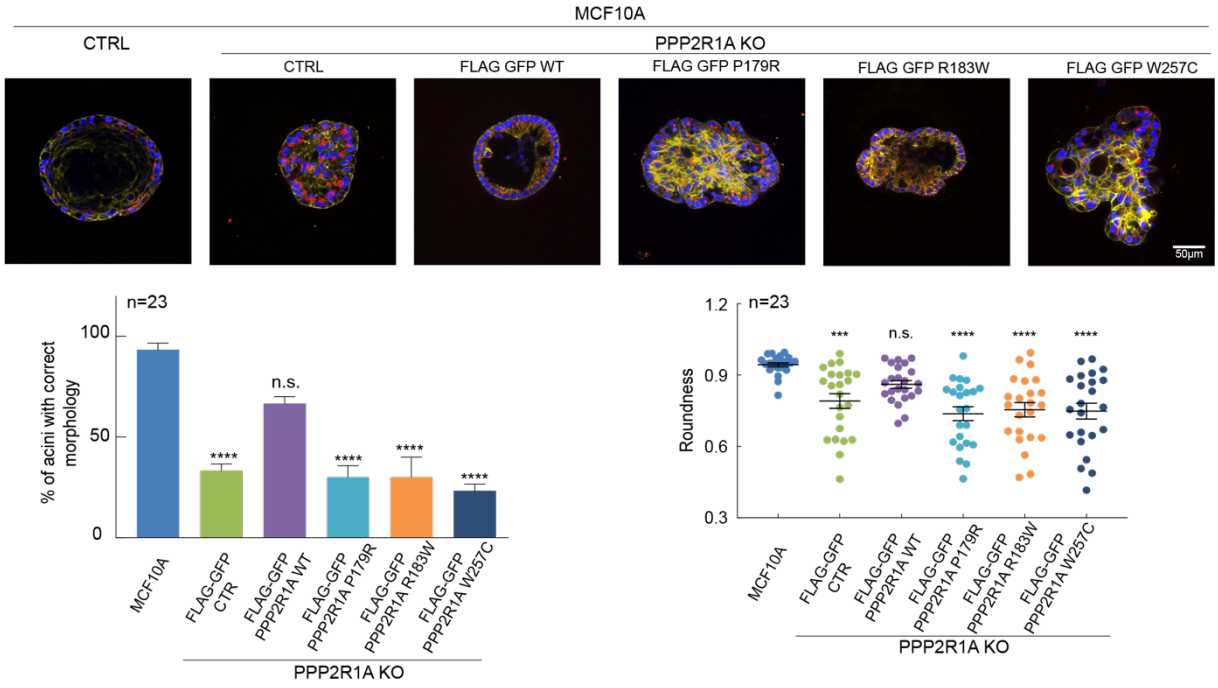


**Figure S6. Development of acini by MCF10A parental cells, *PPP2R1A* KO and rescue derivatives.** Cells were seeded onto Matrigel and grown for 3 weeks. Acini were fixed and stained with DAPI (blue), phalloidin (green) and antibodies targeting the apical Golgi marker GM130 (red). Multicellular structures were observed using confocal microscopy. 3 biological repeats with similar results. Acini with altered polarity or no lumen were scored as abnormal. Roundness of acini outlines, based on central confocal sections. Quantification of the 3 biological repeats. n=23. ***P<0.001; ****P<0.0001

**MOVIE LEGENDS**

**Movie S1, related to figure 1d. Effect of PPP2R1A depletion on the migration persistence of MCF10A cells.**
MCF10A cells transfected with pools of control (CTRL) or PPP2R1A siRNAs were recorded and tracked. Scale bar: 40µm.

**Movie S2, related to figure 1e. Effect of PPP2R1A depletion on the migration persistence of MCF10A RAC1 Q61L cells.**
MCF10A RAC1 Q61L cells transfected with pools of control (CTRL) or PPP2R1A siRNAs were recorded and tracked. Scale bar: 40µm

**Movie S3, related to figure 1f. Effect of PPP2R1A overexpression on the migration persistence of MCF10A cells.**
MCF10A cells stably expressing FLAG-GFP or FLAG-GFP PPP2R1A were recorded and tracked. Scale bar: 40µm.

**Movie S4, related to figure 1g. Effect of PPP2R1A depletion on the migration persistence of MDA-MB-231 cells in 3D.**
MDA-MB-231 cells transfected with pools of control (CTRL) or PPP2R1A siRNAs were seeded in 3D collagen gels and recorded. Scale bar: 40µm.

**Movie S5, related to figure 3a. Localization of PPP2R1A and NHSL1 in B16-F1 cells.**
B16-F1 cells transiently transfected with mScarlet-PPP2R1A and GFP-NHSL1 were recorded. Scale bar: 10µm.

**Movie S6, related to figure 3c. Localization of PPP2R1A and ARPC1B in B16-F1 cells.**
B16-F1 cells transiently transfected with mScarlet-PPP2R1A and GFP-ARPC1B were recorded. Scale bar: 10µm.

**Movie S7, related to figure 4a. Effect of PPP2R1A and NHSL1 combined depletion on the migration persistence of MCF10A cells.**
MCF10A cells transfected with indicated siRNA pools were recorded and tracked. Scale bar: 40µm.

**Movie S8, related to figure 4b. Effect of PPP2R1A and NHSL1 combined depletion on the haptotaxis of MCF10A cells along the fibronectin gradient.**
MCF10A cells transfected with indicated siRNA pools were recorded and tracked. Scale bar: 40µm.

**Movie S9, related to figure 6c. Effect of NHSL1 fragment 4 on the migration persistence of MCF10A cells.**
MCF10A cells stably transfected with GFP or GFP-NHSL1 fragment 4 were recorded and tracked. Scale bar: 40µm.

**Movie S10, related to figure 6f. Effect of PPP2R1A mutations on the migration persistence of MCF10A cells.**

*PPP2R1A* knockout cells were generated in MCF10A. Then the knockout cells were stably transfected with WT or mutant forms of PPP2R1A. Cells for each condition were recorded and tracked. Scale bar: 40μm.

**SUPPLEMENTARY REFERENCES**


1. Sladitschek, H. L. & Neveu, P. A. MXS-Chaining: A Highly Efficient Cloning Platform for Imaging and Flow Cytometry Approaches in Mammalian Systems. *PLoS ONE* 10, e0124958-20 (2015).

2. González, F. *et al.* An iCRISPR platform for rapid, multiplexable, and inducible genome editing in human pluripotent stem cells. *Cell stem cell* 15, 215–226 (2014).

3. Gautreau, A. *et al.* Purification and architecture of the ubiquitous Wave complex. *Proceedings of the National Academy of Sciences of the United States of America* 101, 4379–4383 (2004).

4. Derivery, E. *et al.* Free Brick1 is a trimeric precursor in the assembly of a functional wave complex. *PLoS ONE* 3, e2462 (2008).

5. Gorelik, R. & Gautreau, A. Quantitative and unbiased analysis of directional persistence in cell migration. *Nature Protocols* 9, 1931–1943 (2014).

6. Dang, I. *et al.* Inhibitory signalling to the Arp2/3 complex steers cell migration. *Nature* 503, 281–284 (2013).

7. Consortium, T. U. *et al.* UniProt: the universal protein knowledgebase in 2021. *Nucleic Acids Res* 49, D480–D489 (2020).

8. Steinegger, M. & Söding, J. MMseqs2 enables sensitive protein sequence searching for the analysis of massive data sets. *Nat Biotechnol* 35, 1026–1028 (2017).

9. Katoh, K. & Standley, D. M. MAFFT Multiple Sequence Alignment Software Version 7: Improvements in Performance and Usability. *Mol Biol Evol* 30, 772–780 (2013).

10. Jumper, J. *et al.* Highly accurate protein structure prediction with AlphaFold. *Nature* 596, 583–589 (2021).

11. Mirdita, M. *et al.* ColabFold - Making protein folding accessible to all. *Biorxiv* 2021.08.15.456425 (2022) doi:10.1101/2021.08.15.456425.

12. Evans, R. *et al.* Protein complex prediction with AlphaFold-Multimer. *Biorxiv* 2021.10.04.463034 (2022) doi:10.1101/2021.10.04.463034.

13. Leman, J. K. *et al.* Macromolecular modeling and design in Rosetta: recent methods and frameworks. *Nat Methods* 17, 665–680 (2020).

14. Simanov, G. *et al.* Arpin Regulates Migration Persistence by Interacting with Both Tankyrases and the Arp2/3 Complex. *Int J Mol Sci* 22, 4115 (2021).

15. Crooks, G. E., Hon, G., Chandonia, J.-M. & Brenner, S. E. WebLogo: A Sequence Logo Generator. *Genome Res* 14, 1188–1190 (2004).

# Chapter 5

# Discussion

## 5.1 PPP2R1A, a novel regulator of cell migration persistence

During cell migration, the RAC1-WRC-ARP2/3 pathway is essential for cells to control their directional persistence. This pathway is regulated by both positive and negative factors, such as lamellipodin, ARPIN, CYRI, and NHSL1. In this study, we addressed the question of identification of novel, previously unknown regulatory proteins involved in the RAC1-WRC-ARP2/3 pathway by associating with the ARP2/3 activator, the WRC. By performing a proteomic screen, several proteins were identified to be differentially associated with WRC when the RAC1-WRC-ARP2/3 pathway is activated or inhibited. Interestingly, PPP2R1A protein turned out to be one of the strongest candidates. PPP2R1A is one of the scaffolding subunits of a well-known phosphatase complex, PP2A, but the function of PP2A has not been specifically implicated in the RAC1-WRC-ARP2/3 pathway. It is known that the PP2A complex works as a holoenzyme composed of 3 subunits to play its phosphatase activity in various cellular processes, and the substrate-specificity of the PP2A complex depends on the diversity of its regulatory subunits. However, in our experiments, we have never detected any of the regulatory subunits of the PP2A complex. Even though we have detected the catalytic subunits of PP2A, their interaction with WRC shows no variation in different cell migration conditions. The differential recruitment to WRC is strictly specific to PPP2R1A.

Although most of the studies about PPP2R1A are focused on its role in the PP2A complex, PPP2R1A has been shown to form a homodimer at the cell surface by itself, and promote lymphatic-melanoma cell interaction independently of the PP2A complex [289]. In addition,

the quantitative proteomic analysis of human cells shows that PPP2R1A is much more abundant than the other PP2A subunits [285], indicating that the extra PPP2R1A may form other complexes and function independently of the PP2A complex. Therefore, we have attempted to understand the novel role of the PPP2R1A protein in the regulation of WRC.

To this end, we analyzed the role of PPP2R1A in the migration of human normal epithelial cells in 2D conditions and found that the loss of PPP2R1A led to a significant decrease in cell migration persistence, or the ability of cells to sustain their movement at the same direction, whereas even a two-fold overexpression of this protein increased it. Moreover, in cancer cells, depletion of PPP2R1A decreased the migration persistence dramatically in 3D conditions. Other parameters of cell migration were also analyzed in our experiments, such as cell speed and Mean Square Displacement (MSD). Although the speed and MSD were affected by the PPP2R1A level in cells, their differences were not consistent, in full agreement with the previous findings, which showed that these parameters are not the main target of the RAC1-WRC-ARP2/3 pathway [34]. Thus, it became clear that PPP2R1A is indeed a positive regulator of WRC within the RAC1-WRC-ARP2/3 pathway that controls migration persistence in cells.

## 5.2 WAVE Shell Complex: a novel multiprotein complex

To further dissect how PPP2R1A interacts with the WRC, we analyzed all the potential partners of PPP2R1A in normal or cancer human cells by mass spectrometry. Surprisingly, we found that PPP2R1A was associated with a novel form of the WAVE complex, which contains four subunits of the canonical WRC, NCKAP1, CYFIP, ABI1, and BRK1, but lacks the WAVE subunit. Further immunoprecipitation assay validated the MS data and revealed that another WHD containing protein, NHSL1 was required for the association of PPP2R1A with the four remaining subunits of the canonical WRC. For this reason, we proposed that there existed a novel form of WRC, which contains NHSL1 instead of WAVE protein, and named this novel complex the WAVE Shell Complex (WSC). Interestingly, we observed that the function of PPP2R1A in regulating migration persistence was totally dependent on the presence of NHSL1, since the depletion of NHSL1 abolished the effect of PPP2R1A in cell migration. This effect was not only detected in the random cell migration, but also in the directed cell migration on the gradient of fibronectin, which is known as haptotaxis. As the RAC1-WRC-ARP2/3 mediated actin polymerization is critical in random and haptotaxis, we

performed the *in vitro* actin polymerization assay and found that PPP2R1A depletion dramatically impaired the actin polymerization on the surface of RAC1 Q61L coated beads, a phenomenon that was abolished by depleting PPP2R1A and NHSL1 simultaneously. These results indicated that the function of PPP2R1A in regulating migration persistence fully depended on the WSC.

The canonical WRC is composed of five subunits, and all of these subunits are essential for the stability of the complex [194]. A structural model has revealed that the WRC assembly relies on two intermediate subcomplexes, CYFIP-NCKAP and WAVE-ABI-BRK1 [196, 195]. The WRC switches to the active conformation by exposing the VCA domain of the WAVE subunit, in order to activate the ARP2/3 complex for branched actin nucleation at the leading edge. After the nucleation event, the WRC dissociates from the ARP2/3 complex at the branch junctions and might undergo recycling in cytosol [295, 296]. For example, the Nudel protein is identified as a WRC assembly factor via its interaction with CYFIP1 and BRK1, thus stabilizing the subcomplexes against degradation [201]. But the details about how the entire complex is assembled from single subunits and recycled from the leading edge for multiple rounds of ARP2/3 activation, and whether any other intermediate subcomplexes exist for efficient WRC assembly, are still not clear.

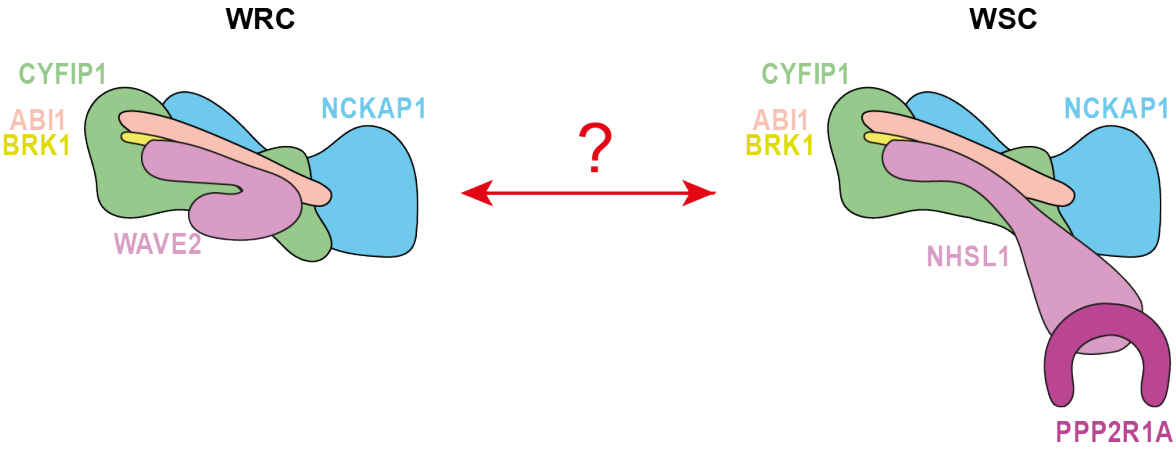


**Figure 5.1: Schematic representation of the WRC and WSC.**

Our observation provided more possibilities for the assembly of WRC. It is possible that the WSC participates in the turnover of the WRC during cell migration, and that the NHSL1 protein serves as a scaffold and a hub to ensure the transition between the canonical WRC and the WSC. One hypothesis is that when the WRC is released from the branch junctions

after activating the ARP2/3 complex, the WAVE subunit may detach from the complex, and the cells will need a new WAVE protein or a replacement (for example, the NHSL1, a protein with the WHD domain) to preserve the remaining subunits of WRC from degradation, thus facilitating further WRC formation through an energy-saving mechanism. The WSC may act as an intermediate subcomplex pool during the WRC assembly, and once cells need the WRC for ARP2/3 activation, the NHSL1 in the pool of WSC can be replaced by WAVE protein, to promote fast and efficient WRC assembly. More studies are needed to elucidate these hypotheses to clarify how these two complexes co-exist and cooperate in normal and cancer cell physiology (Figure 5.1).

## 5.3 The complexity of NHSL1

NHS family proteins have been identified to contain the WHD domain, which is conserved in WAVE proteins and is important for the interaction of WAVE proteins with other WRC subunits. NHS has been shown to interact with the WRC subunits ABI1, BRK1, NCKAP1, and CYFIP1 via its WHD domain. And overexpression of the WHD domain-containing isoforms of NHS was shown to inhibit the lamellipodia formation under the stimulation of EGF in MTLn3 breast cancer cells [292].

A recent study also found that the NHSL1 protein acts as an inhibitor of directional cell migration via interacting with the canonical WRC [293]. In this research, by studying a specific NHSL1 isoform without the WHD domain, two SH3 domain binding sites were identified in NHSL1 and shown to be important for the interaction of NHSL1 with ABI1. Through the binding with ABI1, NHSL1 was shown to interact with all subunits of WRC.

Our results suggest that the role of NHSL1 is more complex. In our work, NHSL1 is not only a regulator of the canonical WRC, but it also can replace the WAVE subunit in WRC and compose a novel complex, the WAVE Shell Complex. The WSC can be selectively recognized by PPP2R1A and is essential for the PPP2R1A to play a role in regulating migration persistence. By mapping the exact interacting region of NHSL1 with PPP2R1A, we found that even though the middle region with ABI1 binding sites was important for the interaction of NHSL1 with WRC, the C-terminal region of NHSL1 specifically interacted with PPP2R1A. A stable expression of this C-terminal fragment in cells dramatically decreased cell migration persistence, which indicated a dominant-negative effect that mimics the interruption of the PPP2R1A-NHSL1 interaction. This result clearly showed the importance of the interaction of PPP2R1A to NHSL1/WSC in regulating efficient cell migration.

Together, it seems that NHSL1 can regulate cell migration in different ways by forming distinct complexes, but how NHSL1 selects the different complexes for proper function in migrating cells remains to be investigated. In addition, as the WHD and ABI1 binding sites are highly conserved in the NHS protein family (NHS, NHSL1, NHSL2), it will be interesting to study NHS and NHSL2 for their potential functions in regulating cell migration. For example, the observed absence of functional redundancy between NHS and NHSL1, even though they are usually co-expressed in the same cells, is indeed very curious.

## 5.4 PPP2R1A cancer-associated mutations

*PPP2R1A* has been shown to mutate in various cancer types [256]. Most of the mutations are clustered in the near region in *PPP2R1A* and form mutation hotspots in multiple cancer types. *PPP2R1A* is suggested to be a tumor suppressor gene through a haploinsufficiency effect since most of its cancer-associated mutations usually happen only in one allele [278].

Some of the PPP2R1A mutations have been studied previously, but mostly with regard to the role of PPP2R1A in PP2A activity. The effect of different PPP2R1A mutations on the PP2A complex varies and leads to different functional consequences. For example, the P179R mutation is suggested to affect the stability of PP2A B and C subunits, thus disrupting the PP2A holoenzyme activity [281, 282], the R183W mutation is suggested to impair the binding ability to the majority of PP2A B subunits but has no significant impact on PP2A C subunit [283], the S256F mutation is shown to increase the binding ability to PP2A inhibitor TIPRL1 and increases tumor growth with a dominant-negative mechanism [282], the W257G mutation is shown to decrease PP2A B and C subunits and leads to inhibited tumor growth, but has no effect on PP2A activity [284].

To investigate whether these cancer-associated mutations in PPP2R1A affect its role in cell migration in our system, we generated the PPP2R1A knockout cell line with human breast epithelial cells and then rescued the KO cells by wild-type or mutant PPP2R1A. In the 2D migration assay, we observed a significant decrease in migration persistence in PPP2R1A knockout cells, and this effect was only rescued by the wild-type PPP2R1A but not by the mutant forms of PPP2R1A. Immunoprecipitation experiment showed that PPP2R1A mutations specifically interrupted the interaction between PPP2R1A and NHSL1, but had no effect on the interaction with PP2A C subunit. These results indicated that the impaired cell migration persistence caused by PPP2R1A cancer-associated mutations was likely due to a specific loss of interaction with NHSL1, and thus with other WSC subunits.

By examining the oncogenic transformation potential of PPP2R1A mutations with a classical long-term acini formation assay in human breast epithelial cells, we found that the mishappen morphology caused by PPP2R1A knockout can be partially restored by the wild-type PPP2R1A, but not by the cancer-derived mutants, which suggested that the tumor suppressor function of PPP2R1A might be related to its specific role in the regulation of cell migration. Hence, our study highlights the potential role of PPP2R1A-regulated cell migration in cancer progression.

# Chapter 6

# Conclusions and Perspectives

In conclusion, my work characterized the function of a novel cell migration regulator - PPP2R1A, which was originally identified by my host lab via a differential proteomic screen. I first studied the effect of PPP2R1A in cell migration and found that PPP2R1A is required for both directional persistence in random cell migration and directional cell migration along fibronectin gradients. I further demonstrated that PPP2R1A regulates cell migration by specifically interacting with a novel complex, which contains four subunits of the canonical WRC, but the WAVE subunit is replaced by NHSL1. We named it the WAVE Shell Complex (WSC). NHSL1 is required for the association of PPP2R1A with other WSC subunits, and for the function of PPP2R1A in regulating cell migration and cell-free actin polymerization. In addition, I studied the effect of PPP2R1A cancer-associated mutations in regulating cell migration and found that the mutant PPP2R1A exhibits impaired migration persistence and decreased interaction with WSC. Together, this study revealed a novel multiprotein complex, the WSC, that has a critical role in regulating migration persistence in normal and cancer cells.

My work has revealed the importance of PPP2R1A and WSC in regulating migration persistence, but the underlying molecular mechanisms are not fully elucidated yet. More studies should be done, in order to investigate the exact role of WSC in migrating cells. For example, a structural analysis of the complex by cryo-EM would be important to understand the exact composition and conformation of the WSC. This analysis can be done either by purifying the complex from human cells, as I have done in this study, or by reconstituting the WSC *in vitro*. *in vivo*, putting cells in over-activated or fully inhibited cell migration conditions can be useful to understand how WSC and WRC cooperate and regulate their relative abundance in cells. Studying the turnover of PPP2R1A or of the complete WSC at the lamellipodium tip, by advanced imaging of live cells, will be helpful to examine the dynamics of these

molecules during cell migration. All this work, challenging but very interesting, awaits to be done in the future.

# Chapter 7

# Annex

## 7.1 CYFIP2-containing WAVE complexes inhibit cell migration by a competition mechanism

*Manuscript is submitted to bioRxiv*

**Authors**

Anna Polesskaya[1], Arthur Boutillon[2 #], Sheng Yang[3 #], **Yanan Wang**[1], Stéphane Romero[1], Yijun Liu[3], Marc Lavielle[4], Sophie Vacher[5], Anne Schnitzler[5], Nicolas Molinie[1], Nathalie Rocques[1], Artem Fokin[1], Raphaël Guérois[6], Ivan Bièche[5], Baoyu Chen[3], Nicolas B. David[2], Alexis M. Gautreau[1]

[#] co-second author [1]CNRS UMR7654, Institut Polytechnique de Paris, 91120 Palaiseau, France. [2]INSERM U1182, CNRS UMR7645, Institut Polytechnique de Paris, 91120 Palaiseau, France. [3]Roy J. Carver Department of Biochemistry, Biophysics and Molecular Biology, Iowa State University, Ames, IA 50011, USA. [4]INRIA Saclay & Center for Applied Mathematics (CMAP), Institut Polytechnique de Paris, 91120 Palaiseau, France. [5]Pharmacogenomics Unit, Department of Genetics, Institut Curie, 26 rue d'Ulm, 75005 Paris, France. [6]Institute for Integrative Biology of the Cell (I2BC), CEA, CNRS, University Paris-Saclay, CEA-Saclay, 91190 Gif-sur-Yvette, France.

**Keywords**

Patient cohort, multiprotein complexes, Zebrafish embryo, Scar/WAVE, WAVE Regulatory Complex, Arp2/3

# CYFIP2-containing WAVE complexes inhibit cell migration by a competition mechanism

Anna Polesskaya[1], Arthur Boutillon[2, #], Sheng Yang[3, #], Yanan Wang[1], Stéphane Romero[1], Yijun Liu[3], Marc Lavielle[4], Sophie Vacher[5], Anne Schnitzler[5], Nicolas Molinie[1], Nathalie Rocques[1], Artem Fokin[1], Raphaël Guérois[6], Ivan Bièche[5], Baoyu Chen[3], Nicolas B. David[2], Alexis M. Gautreau[1]

# co-second author

[1] CNRS UMR7654, Institut Polytechnique de Paris, 91120 Palaiseau, France.

[2] INSERM U1182, CNRS UMR7645, Institut Polytechnique de Paris, 91120 Palaiseau, France.

[3]Roy J. Carver Department of Biochemistry, Biophysics and Molecular Biology, Iowa State University, Ames, IA 50011, USA.

[4] INRIA Saclay & Center for Applied Mathematics (CMAP), Institut Polytechnique de Paris, 91120 Palaiseau, France.

[5] Pharmacogenomics Unit, Department of Genetics, Institut Curie, 26 rue d'Ulm, 75005 Paris, France.

[6] Institute for Integrative Biology of the Cell (I2BC), CEA, CNRS, University Paris-Saclay, CEA-Saclay, 91190 Gif-sur-Yvette, France.

Correspondence concerning mathematical modeling should be addressed to ML (Marc.Lavielle@inria.fr)

Correspondence concerning biomedical aspects and material requests should be addressed to the lead contact, AMG (alexis.gautreau@polytechnique.edu)

Running title: CYFIP2 inhibits cell migration

Keywords: Patient cohort, multiprotein complexes, Zebrafish embryo, Scar/WAVE, WAVE Regulatory Complex, Arp2/3.

Abbreviations: BIC, Bayesian Information Criteria; KD, knock-down; KO, knock-out; MFS, metastasis-free survival; RFS, Relapse-free survival.

## ABSTRACT

Branched actin networks polymerized by the Arp2/3 complex are critical for cell migration. The WAVE complex is the major Arp2/3 activator at the leading edge of migrating cells. However, multiple distinct WAVE complexes can be assembled in a cell, due to the combinatorial complexity of paralogous subunits. When systematically analyzing the contribution of each WAVE complex subunit to the metastasis-free survival of breast cancer patients, we found that overexpression of the CYFIP2 subunit was surprisingly associated with good prognosis. Gain and loss of function experiments in transformed and untransformed mammary epithelial cells, as well as in prechordal plate cells in gastrulating zebrafish embryos, revealed that lamellipodium protrusion and cell migration were always inversely related to CYFIP2 levels. The role of CYFIP2 was systematically opposite to the role of the paralogous subunit CYFIP1 or of the NCKAP1 subunit, which determines levels of WAVE complexes. CYFIP2 showed no difference from CYFIP1 in assembling WAVE complexes or binding to active RAC1. CYFIP2-containing WAVE complexes, however, were less able to activate the Arp2/3 complex in response to RAC1 binding. CYFIP1- and CYFIP2-containing WAVE complexes thus compete for active RAC1 and produce different outcomes. Therefore, cell migration, lamellipodium protrusion and Arp2/3 activity are controlled by relative levels of CYFIP1 and CYFIP2.

## INTRODUCTION

Vertebrate genomes are the result of two genome-wide duplications [1]. This explains why many protein families are encoded by up to four paralogous genes in the human genome, but by a single gene in invertebrates such as *Drosophila* or *C. elegans*. The availability of several paralogous genes in the human genome has permitted the emergence of new regulations or specialized functions of specific paralogs. In cancers, alteration of gene expression or mutation usually concerns a single specific member of the family, which has to be identified.

Ten to twenty percent of human proteins form stable multiprotein complexes [2]. These complexes are often referred to as molecular machines to emphasize that they perform elaborate functions through the coordination of their subunits [3]. When several subunits are encoded by paralogous genes, a combinatorial complexity arises. Different complexes, potentially displaying different regulations and functions, stem from the different assemblies of paralogous subunits. If a specific molecular machine is responsible for cancer progression, it is also critical to be able to identify it.

Cell migration is controlled by several multiprotein complexes [4]. The Arp2/3 complex generates branched actin networks, which power membrane protrusions. At the protrusive edge, WAVE complexes activate the Arp2/3 complex [5,6]. The WAVE-Arp2/3 pathway depends on the activity of the small GTPase RAC1, which is necessary and sufficient to generate lamellipodia [7]. The RAC1-WAVE-Arp2/3 pathway controls protrusion lifetime and migration persistence through numerous feedback and feedforward loops [8]. This pathway has been implicated in the migration and invasion of tumor cells in various model systems [4].

The combinatorial complexity of WAVE complexes is daunting. A WAVE complex is composed of 5 generic subunits, hereafter referred to as WAVE, ABI, BRK, NAP and CYFIP. Except BRK, all human subunits are encoded by paralogous genes, 3 for WAVE and ABI, and 2 for NAP and CYFIP [9]. There are as many as 3x3x2x2, *i.e.* 36, possible WAVE complexes, just by combining the different paralogous subunits. Furthermore, the *ABI1* gene has been shown to be alternatively spliced and the resulting isoforms do not possess the same ability to mediate macropinocytosis, which, like lamellipodium formation, depends on the ability of branched actin to drive protrusions [10]. In mouse embryonic fibroblasts, WAVE2 is critical for the formation of peripheral ruffles, whereas WAVE1 is critical for dorsal ruffles [11]. Thus, evidence already exists for functional specialization among WAVE complexes.

WAVE complex subunits have been mostly reported to be overexpressed in tumors [4]. In line with their function in promoting cell migration and invasion, their overexpression is generally associated with high grades and poor prognosis. High levels of WAVE subunits is of poor prognosis for patients in breast, ovary, lung and liver cancers [12–16]. The overexpression of WAVE3 in colorectal cancers, however, is associated with good prognosis [17]. Similar to the general trend, high expression of the NAP paralogs, NCKAP1 and NCKAP1L, has been associated with poor prognosis in breast cancer and leukemia, respectively [18,19]. High expression of ABI1 has also been associated with poor prognosis in breast and ovary cancers [20,21].

Whereas most studies, including cancer studies, focused on one subunit, we measured the expression levels of all the paralogous genes encoding subunits in a large cohort of breast cancer patients, in an attempt to tackle the complexity of the WAVE complex. This systematic endeavor allowed us to examine each of the 36 possible WAVE complexes for their possible association with metastasis-free survival (MFS). We found no evidence for the involvement of a specific WAVE complex assembly. The first order determinant of MFS was whether WAVE complexes contained the NCKAP1 subunit. The second order determinant was whether WAVE complexes contained the CYFIP2 subunit. Surprisingly, however, we found that high levels of *CYFIP2* were associated with good prognosis. This unexpected effect on MFS could be accounted for by the fact that CYFIP2-containing complexes specifically impair cell migration in a variety of cell systems. CYFIP2-containing WAVE complexes are less activated by RAC1 than CYFIP1-containing WAVE complexes, suggesting that they titrate out the major activator of the WAVE complex.

## RESULTS

### Systematic analysis of WAVE complex subunits in breast cancer

In a cohort of 527 breast cancer patients (Table S1), we measured by qRT-PCR the mRNA levels of the 11 genes encoding WAVE complex subunits. Expression values in tumors were normalized to the expression in healthy breast tissue. We found that the expression of several subunits is profoundly deregulated in breast cancer (Table 1). *CYFIP2*, *NCKAP1L* and *ABI3* were up-regulated in 37%, 22% and 12% of tumors, respectively. Cases of overexpression were in different subgroups of breast cancer patients. *NCKAP1L* is mostly overexpressed in the Hormone Receptor (HR)- ERBB2+ subgroup. *ABI3* is mostly overexpressed in the HR- ERBB2-, triple negative subgroup. *CYFIP2* is mostly overexpressed in the HR+ ERBB2- subgroup and in low-grade tumors of good prognosis (Table S1). *WASF3* and *WASF1* are down-regulated in 46% and 27% of the cohort. Underexpression of these WAVE subunits is also mostly displayed in the good prognosis HR+ ERBB2- subgroup. We then examined if fluctuations in subunit expression were associated with prognosis.

Since the outcome of patients is known in the cohort and given the role of the WAVE complex in tumor cell invasion, we were especially interested in the metastasis-free survival (MFS). MFS starts at the date of surgery and terminates at the date of the last news from the patient, of metastasis diagnostic, or of death. We applied to these right-censored data a classical Cox univariate model using the expression level of each subunit as the variable. We sorted the different subunit genes according to increasing p-values (Fig. S1). The first three genes were *NCKAP1*, *CYFIP2* and *NCKAP1L*. The levels of *NCKAP1* mRNA, within their natural fluctuations, were significantly associated with MFS (p=0.012, Fig. S1). Indeed, we previously reported that high levels of *NCKAP1* were associated with poor MFS [18]. Levels of *CYFIP2* and *NCKAP1L* also appeared significantly associated with MFS, but with a lower significance, p=0.138 and 0.288, respectively.

Our goal when measuring expression levels of all WAVE subunits in the cohort was to examine whether a particular combination of subunits would create a specific WAVE complex conferring invasive properties to tumor cells. This is why we chose to perform highly accurate measurements by qRT-PCR in our cohort of 527 patients, even if global analyses were already available in public databases containing a larger number of patients. To analyze the association of various WAVE assemblies with MFS, we needed to transform and normalize our variables, i.e. subunit levels. Using a monotonous function of the type $\log(x\text{-}c)$, levels of each subunit fitted a Gaussian distribution. Then we normalized transformed variables around 0 with a variance of 1, to allow a better comparison between different subunit levels. Transformation and normalization did not change the relative association of subunit levels with MFS, since, by univariate Cox analysis, the 3 most powerful subunits to predict MFS were still, first, *NCKAP1* with a p-value of 0.005, second, *CYFIP2* with a p-value of 0.059, just above the classical 5% significance level, but far above the third subunit, *NCKAP1L*, with a p-value of 0.397 (Fig. S1).

During these simple Cox analyses of the original subunit levels or of the transformed and normalized variables, we were struck by the fact that *NCKAP1* and *CYFIP2* had opposite coefficients for the association with MFS. Indeed, high levels of *NCKAP1* were associated with poor MFS, whereas high levels of *CYFIP2* were associated with good MFS (Fig.S1).

Using transformed and normalized variables, we were able to perform a multivariate Cox analysis to analyze the association of each of the 36 possible WAVE complexes with MFS (Fig.S1). We sorted the 36 WAVE complexes according to increasing p-values. The 18 best combinations all contained NCKAP1 as the NAP subunit, while the best 9 combinations also contained CYFIP2 as the CYFIP subunit, suggesting that NCKAP1 is the first order predictor, whereas CYFIP2 is the second order predictor in our cohort. The multivariate Cox analysis does not suggest a specific WAVE assembly that would be particularly associated with MFS, what seems to matter is whether the assembly contains NCKAP1 and/or CYFIP2. Computer simulations using random permutations of values confirmed that the prediction powers of NCKAP1 and CYFIP2 cannot be attributed to chance (Fig.S1).

We then evaluated further multivariate Cox models by adding up to 5 variables using NCKAP1, CYFIP2, WASF3 and ABI2 and BRK1 subunits in this order. The log-likelihood criterium increased when more subunits were introduced, but the log-likelihood always increases when further variables are added. Therefore, we compared the models using Bayesian Information Criteria (BIC). BIC introduces a penalty term for the number of variables used in the model to avoid overfitting. The model with 2 variables, NCKAP1 and CYFIP2, had the smallest BIC (Fig.S1) and thus appeared as the optimal model of MFS in our cohort. MFS over time can be accurately predicted from mRNA levels of *NCKAP1* and *CYFIP2*. In our optimal model, *NCKAP1* is a first order predictor with a p-value of 0.001, whereas *CYFIP2* is the second order predictor with a p-value of 0.012. Importantly, in this multivariate model, as in the initial univariate models, *NCKAP1* and *CYFIP2* have opposite coefficients, indicating that up-regulation of *NCKAP1*, but down-regulation of *CYFIP2*, are associated with poor prognosis. In the model, the higher the *CYFIP2* value, the better the MFS, for a given value of *NCKAP1*. To illustrate how the second order predictor *CYFIP2* modulates the MFS, we ran the model with expression levels found in patient tumors populating the outskirts of the distribution (Fig.1A). The extreme values of *NCKAP1* dominate the predicted MFS when *CYFIP2* values are

intermediate (Fig.1B). In contrast, extreme values of *CYFIP2* significantly oppose the effect of *NCKAP1*, when *NCKAP1* values are not extreme.

To validate the prediction of our statistical model that NCKAP1 and CYFIP2 control MFS, we used a public database of breast cancer patients, where the transcriptome of more than 3900 tumors, was analyzed by Affymetrix chips [22]. Given the large number of patients, more genes encoding WAVE complex subunits were significantly associated with relapse-free survival (RFS) than in our cohort containing slightly more than 500 patients. However, the two most strongly associated ones were *NCKAP1* and *CYFIP2*, as in our analyses. As our model predicted, high levels of NCKAP1 were associated with poor RFS, whereas high levels of CYFIP2 were associated with good RFS (Fig.1C). All these results together indicate that CYFIP2 should have a function at odds with the major function of WAVE complexes, that is to promote cell migration [4].

**The WAVE complex subunit CYFIP2 inhibits the migration of mammary carcinoma cells**

Since the expression of WAVE subunits CYFIP2 and NCKAP1 are associated with opposite prognoses in breast cancer patients, we sought to compare their function in mammary carcinoma cells. Moreover, we compared the two paralogous subunits CYFIP1 and CYFIP2 in two classical breast cancer cell lines, MCF7, which is HR+ ERBB2-, and MDA-MB-231, which is HR- ERBB2- (triple negative).

Depletion of the different subunits using RNAi had different impact on WAVE complex levels. Indeed, WAVE complexes are stable when fully assembled, providing an explanation as to why depletion of a subunit usually destabilizes the multiprotein complex it should be part of [9]. Depletion of NCKAP1 in MCF7 cells leads to a severe downregulation of WAVE complex subunits, including CYFIP1 and CYFIP2 (Fig.2A). This result shows a key role of NCKAP1 for the stability of CYFIP1- and CYFIP2-containing WAVE complexes in cells. Depletion of CYFIP1 leads to a significant destabilization of the WAVE complex, which can be appreciated on NCKAP1, WAVE2 and BRK1 levels. In contrast, depletion of CYFIP2 does not lead to a visible depletion of the same subunits. Since MCF7 cells have conserved their epithelial organisation, we assessed cell migration in a wound healing assay. CYFIP1 or NCKAP1 depleted cells failed to close the wound before 78-81h compared to 30 h for control cells (Fig. 2A and Movie S1). In sharp contrast, CYFIP2 depleted cells were not impaired in their ability to close the wound and were in fact significantly faster than controls (20 h vs. 30 h).

We then turned to MDA-MB-231 cells, which displayed the same overall pattern of subunit expression upon depletion of NCKAP1 or CYFIP1/2 as MCF7 cells (Fig.2B). Briefly, WAVE complexes were destabilized upon NCKAP1 or CYFIP1 depletion, but not upon CYFIP2 depletion. We thus decided to measure levels of CYFIP1 and 2 using purified CYFIP1- or CYFIP2-containing WAVE complexes as standards, serial dilutions and Western blots in their linear range (Fig.S2). We found that MDA-MB-231 express roughly 6-times more CYFIP1 than CYFIP2 (Fig.2C), providing a first level of explanation as to why CYFIP1 depletion affects more the stability of other subunits than CYFIP2. However, this was not the

only effect, since the depletion of each CYFIP protein resulted in approximately 50 % up-regulation of its remaining CYFIP paralog. These up-regulations of the paralogous CYFIP proteins were not observed at the mRNA level and might represent stabilization of CYFIP subunits with other WAVE complex subunits when the paralogous CYFIP protein is not expressed (Fig.S3).

We first evaluated in the Transwell assay the migration of MDA-MB-231 cells when CYFIP1, 2, or NCKAP1 were depleted using pools of siRNAs. Depletion of NCKAP1 and CYFIP1 significantly decreased the number of cells able to migrate through the filter, whereas the depletion of CYFIP2 had the converse effect (Fig.2D). The effect of transient siRNA-mediated depletions was confirmed using stable MDA-MB-231 lines expressing either a shRNA targeting NCKAP1 or CYFIP2 [5](Fig.S4). We then attempted to obtain stable MDA-MB-231 lines overexpressing NCKAP1 or CYFIP2. We obtained lines expressing GFP-tagged CYFIP2, but repeatedly failed in obtaining clones expressing NCKAP1 in parallel selection schemes. The overexpression of CYFIP2 slightly decreased cell migration in the Transwell assay, whereas CYFIP2 depletion increased it (Fig.S4). Loss- and gain-of function of CYFIP2 thus yield opposite phenotypes.

MDA-MB-231 cells are mesenchymal, unlike epithelial MCF7 cells. Nonetheless, in a wound healing assay, CYFIP2 depleted MDA-MB-231 closed the wound faster than controls, and MDA-MB-231 cells depleted of NCKAP1 and CYFIP1 were significantly delayed in doing so (Fig.S4), exactly as we had observed in MCF7 cells. We then turned to a more physiopathological assay for MDA-MB-231. We seeded isolated MDA-MB-231 cells in 3D gels of collagen type I. In these settings, mimicking invasion of the mesenchyme, differences in cell migration were more dramatic (Fig. 2E). NCKAP1 depleted cells hardly migrated at all, as evidenced by strongly decreased Mean Squared Displacement (MSD), mostly due to reduced speed. NCKAP1 depleted cells ended up entering into apoptosis during the first 24 h (Movie S2). CYFIP1 depleted cells were not significantly affected in their ability to migrate, even though they also appeared prone to die in these settings. CYFIP1 and NCKAP1 depleted cells formed significantly fewer protrusions than controls (Fig.2E). In contrast, CYFIP2 depleted cells often explored a significantly larger territory than controls. The increased MSD of CYFIP2 depleted cells could be accounted for by the dramatically increased migration persistence. The protrusive activity of CYFIP2 depleted cells was significantly increased compared to controls. Finally, CYFIP2 depleted cells had no issue of survival in 3D collagen, unlike cells depleted of NCKAP1 or CYFIP1.

In conclusion, in all the assays performed with the two breast cancer cell lines, the opposite roles of NCKAP1 and CYFIP2 were consistently observed and in line with their association with their prognostic roles in the metastasis-free survival of breast cancer patients.

**CYFIP2 inhibits cell migration of untransformed cells**

We wondered if the anti-migratory role of CYFIP2 was its normal function or rather associated with cell transformation. To address this question, we used the immortalized, but not transformed, MCF10A mammary cell line. MCF10A expressed approximately 6-fold more CYFIP1 than CYFIP2 (Fig.3A). CYFIP2 is thus less abundant than CYFIP1 in two cell lines, MCF10A and MDA-MB-231. As in MDA-MB-231, siRNA-mediated depletion of NCKAP1 and CYFIP1 from MCF10A cells significantly decreased protein levels of WAVE complex subunits, but not their mRNA levels (Fig.3B, Fig.S3), whereas CYFIP2 depletion did not affect the overall stability of WAVE complexes.

MCF10A cells are more epithelial than MDA-MB-231 cells. They establish cell-cell junctions and form epithelial islets. However, they are plastic epithelial cells. In 2D cultures, in their regular culture medium, which contains EGF, MCF10A cells display cell-cell junctions, but also frequently migrate as single cells. We depleted MCF10A cells with siRNA pools targeting either NCKAP1, CYFIP1 or CYFIP2. Cells depleted of NCKAP1 appeared as small and organized as a tight epithelium, whereas the cells depleted of CYFIP2 appeared larger with membrane protrusions, even if they remained associated with one another (Fig.3B, Movie S3). CYFIP1 depletion did not have a pronounced effect on cell morphology. We then recorded MCF10A cells to analyze cell migration. Trajectories corresponding to single cells were plotted (Fig.3C). NCKAP1 depleted single cells migrated much less than controls, an effect which was mostly due to decreased cell speed. In contrast, CYFIP2 depleted cells did not explore a wider territory than controls, nor did they migrate faster, but they significantly increased migration persistence. Importantly, same results were obtained with two single siRNA sequences for each gene (Fig.S5), indicating that these results were not due to off-targets. Such a phenotype, characterized by increased migration persistence of single MCF10A cells, was previously observed upon activation of RAC1 or upon depletion of the Arp2/3 inhibitory protein ARPIN [23].

To study differentiation of acini in Matrigel, we isolated *CYFIP2* knock-out (KO) clones using CRISPR-Cas9. From about 100 independent MCF10A clones, we selected two CYFIP2 negative clones, which turned out to be KO on both alleles due to insertions/deletions changing the ORF (Fig.S6A). As expected, *CYFIP2* KO clones displayed increased migration persistence (Fig.S6BC). The initial KO of CYFIP2 led to an increase of the level of WAVE complex subunits, as previously shown for siRNA assays, but this effect disappeared in long-term cultures (Fig.S6DE). The differentiation of *CYFIP2* KO clones was then assayed in Matrigel, where MCF10A cells develop acini structures. *CYFIP2* inactivation did not affect the morphogenetic program, nor cell polarity, but resulted in significantly larger 3D structures containing more cells than the control (Fig.3D). Similar results were previously obtained when ARPIN was inactivated [23]. CYFIP2 thus behaves like this well-established inhibitory protein of cell migration, ARPIN. This result on acini structures is consistent with the fact that the RAC1-WAVE-Arp2/3 pathway controls cell cycle progression [23].

To validate the anti-migratory function of CYFIP2 in a physiological system and to test whether this function is specific to breast cells or more general, we turned to the zebrafish embryo, and in particular to prechordal plate cells, which stereotypically migrate during

gastrulation [24,25]. Prechordal plate cells migrate from the fish organizer (shield) to the animal pole of the embryo by forming actin-rich protrusions. These RAC1 dependent protrusions are the 3D equivalents of 2D lamellipodia and are easily distinguished from thin, filopodia-like extensions [26,27]. We assessed the function of CYFIP1, CYFIP2 and NCKAP1 using both morpholino-mediated loss-of-function and mRNA over-expression.

We first analyzed prechordal plate cell trajectories, in embryos injected with morpholino and/or mRNA for CYFIP1, CYFIP2 and NCKAP1 (Fig.4A). Experiments were performed in a goosecoid:GFP transgenic line, allowing easy identification of prechordal plate cells. Nuclei were labelled by expression of a Histone2B–mCherry construct, the cells were tracked (Movie S5), and cell trajectories were plotted. Similar to what was observed using human cell lines, CYFIP2 depletion increased migration persistence as compared to injection of a control morpholino. This effect was rescued by co-injection of a morpholino-insensitive CYFIP2 mRNA, demonstrating the specificity of the phenotype. Consistently, overexpression of CYFIP2, i.e. injection of the same amount of mRNA as for the rescue but without the corresponding morpholino, decreased cell persistence. In contrast to CYFIP2, downregulation of CYFIP1 or NCKAP1 reduced cell persistence, both effects being rescued by the co-injection of the corresponding mRNAs.

We then used cell transplants to look for cell autonomous defects and analyzed cell dynamics and protrusivity. Few prechordal plate cells from a donor embryo injected with morpholino and/or mRNA were transplanted to the prechordal plate of an uninjected host embryo (Fig.4B). Actin-rich protrusions were highlighted by the enrichment of the LifeAct-mCherry marker (Fig.4B, Movie S6). CYFIP2 depletion doubled the number of protrusions compared to cells injected with a control morpholino (Fig.4B). This effect was rescued by a morpholino-insensitive CYFIP2 mRNA. Consistently, CYFIP2 overexpression decreased the number of protrusions, much like the depletion of NCKAP1 and CYFIP1. CYFIP2 depletion also significantly and specifically increased protrusion length (Fig.4B).

The results using zebrafish embryos are thus perfectly in line with those obtained in human breast cells and demonstrate that the unexpected anti-migratory function of CYFIP2 is a general and conserved function of this subunit, at least across vertebrates.

### CYFIP2 rescues lamellipodium formation in *CYFIP1/2* double KO cells

To examine whether CYFIP2 was a functional subunit of the WAVE complex, we re-expressed CYFIP2 in B16-F1 *CYFIP1/2* double knock-out cells (DKO) [28]. GFP-CYFIP2 clearly rescued lamellipodium formation in DKO cells, like GFP-CYFIP1, even if CYFIP1 appeared to induce more prominent lamellipodia than CYFIP2 (Fig.5AB, movie S6). We also analyzed two point mutations of CYFIP2, R87C and I664M, that are recurring mutations found in patients affected by intellectual disability [29]. These two point mutations did not impair the ability of CYFIP2 to induce lamellipodia. On the opposite, the mutations seemed to induce more prominent lamellipodia (movie S7).

We quantitatively analyzed the effect of CYFIP2 and of its mutated derivatives on protrusions using line scans. The expression of CYFIP2 was unable to restore the full speed of

protrusions observed in parental B16-F1 cells or in CYFIP1-rescued DKO cells (Fig.5C). R87C and I664M mutations rendered CYFIP2 significantly more efficient at rescuing the protrusion rate, up to the level of parental or CYFIP1 reconstituted cells. We then analyzed the width of lamellipodia, using immunofluorescence of the ARPC2 subunit of the Arp2/3 complex and of cortactin, a protein that stabilizes the Arp2/3 at the branched junction between filaments [4]. In line with their faster protrusions, CYFIP1, R87C and I664M CYFIP2 induced lamellipodia deeper into the cell than wild type CYFIP2 (Fig.5DE). So CYFIP2 is a functional CYFIP protein, but less active than CYFIP1, and point mutations that induce developmental defects in patients alleviate this restrained activity of CYFIP2.

### CYFIP2 containing WAVE complexes are poorly activated by active RAC1

CYFIP2 is 88 % identical to CYFIP1. So we replaced CYFIP1 with CYFIP2 in the molecular model of the WAVE complex derived from crystallography of a reconstitued complex containing a WAVE1 form lacking the central proline-rich region and a truncated ABI2 lacking the the disordered C-terminus [30]. We mapped on this model the WIRS binding site that allows the WAVE complex to interact with various transmembrane receptors [31]. None of these binding sites was affected by the substitutions in CYFIP2 (Fig.6A). Consistently, we observed by ultracentrifugation on sucrose gradients that CYFIP2 was incorporated into the native WAVE complex, which sediments at around 11 Swedbergs (Fig.6B)[32]. Two binding sites exist for active RAC1 at the surface of the WAVE complex: the so-called A site, which shares structural homology with the CYRI-B protein [33,34], and the D site [35]. None of the RAC1 binding sites was affected by substitutions in CYFIP2. To examine the binding to RAC1 and activation by RAC1, we reconstituted a WAVE complex with either CYFIP1 or CYFIP2 using a previously described procedure [36]. Both complexes interacted equally well with GTP-bound RAC1 (Fig.6C and D). In pyrene-actin polymerization assays, however, the CYFIP2-containing WAVE complex was poorly activated by RAC1 compared to the CYFIP1-containing WAVE complex (Fig.6E). These in vitro data are thus consistent with the observation that in cells CYFIP2 promotes lamellipodium formation, but not as well as CYFIP1.

## DISCUSSION

Here we have systematically analyzed the expression levels of WAVE complex subunits in a cohort of breast cancer patients. *Ad hoc* statistical modeling, taking into account assembly rules among paralogous subunits, increased the statistical power of the analysis and revealed the unique role of the CYFIP2 subunit, whose overexpression is associated with good prognosis for metastasis-free survival. These findings were validated using an independent cohort of breast cancer patients available in public databases. *CYFIP2* had previously been implicated in pathologies, since it is mutated in children affected with intellectual disability and epileptic encephalopathy [37,38]. In zebrafish, CYFIP2 loss-of-function mutations result in defective axonal pathfinding in retinal ganglion cells [39]. This function of CYFIP2 is also not redundant with the one of the paralogous subunit, CYFIP1, which is involved in axon growth [40].

We have experimentally validated the prediction of our model, which implies a protective role of CYFIP2 overexpression in breast cancer. CYFIP2 is at odds with other subunits, since it is the first subunit of the WAVE complex that is ever reported to oppose cell migration. Indeed, we found that CYFIP2 opposes cell migration in a variety of cell systems, MCF10A, MDA-MB-231 and prechordal plate cells from the zebrafish embryo. In these experiments, CYFIP2 depletion enhances cell migration, whereas CYFIP2 overexpression decreases cell migration. We were struck by this anti-migratory role of CYFIP2, which to our knowledge was never reported before, even if depletion of different subunits of the WAVE complex did not always give the same phenotype [41–45].

In all cell systems we studied here, the main parameter that CYFIP2 controls is migration persistence, which relates to the persistence of lamellipodial protrusions [8]. In fact, the role of CYFIP2 is very similar to the Arp2/3 inhibitory protein Arpin that directly inhibits the Arp2/3 complex at the leading edge [46]. In neuronal growth cones, CYFIP2 was found to localize at the tip of filopodia, structures composed of linear actin and not of branched actin [40], in line with an inhibitory function of CYFIP2 on branched actin formation we suggest here.

CYFIP2 is highly related to CYFIP1, with 88 % identity. Both CYFIP proteins incorporate into WAVE complexes [47–49]. Accordingly, we found here that CYFIP2 depends on NCKAP1 for its stability, like CYFIP1 and that CYFIP2 is found into the same WAVE complex migrating at 11 Swedbergs as CYFIP1. Importantly, the residues of CYFIP1 that are involved in binding active RAC1 are all conserved in CYFIP2. However, we found that CYFIP2-containing WAVE complexes were less activatable by active RAC1 than CYFIP1-containing WAVE complexes. This property accounts for the observed phenotypes. Indeed, depletion of CYFIP2 can render available more active RAC1 to activate more CYFIP1-containing WAVE complexes, which are easily activatable (Fig.6F).

Another effect is expected to increase migration upon CYFIP2 depletion and to decrease it upon CYFIP1 depletion. In RNAi experiments, CYFIP1-depleted cells were found to overexpress CYFIP2, whereas CYFIP2-depleted cells were found to overexpress CYFIP1. This compensatory expression of the paralogous CYFIP was marginally observed at the mRNA level in some cases and more significantly at the protein level, suggesting that CYFIP proteins might be stabilized by the availability of partner subunits [9]. However, this compensatory expression of CYFIP1 is lost over time in the *CYFIP2* KO clones that we isolated from MCF10A cells, while enhanced migration persistence of *CYFIP2* KO clones is sustained, strongly suggesting that this effect has a minor contribution compared to the poor activation of CYFIP2-containing complexes by active RAC1.

This modulation of phenotypes based on subunit composition of complexes was previously described for the Arp2/3 complex [50]. The paralogous subunits ARPC1B and ARPC5L assemble Arp2/3 complexes, which are more activatable than the ones assembled around ARPC1A and ARPC5. The situation is perfectly analogous to the one described here for the WAVE complex assembled with CYFIP1 and CYFIP2 paralogous subunits. Vertebrate genomes encoding paralogous subunits for many stable multiprotein complexes thus offer numerous opportunities to fine tune cellular responses. The two examples of WAVE and Arp2/3 complexes illustrate that each cell of a vertebrate organism can regulate levels of cortical

branched actin, polymerized in response to signaling inputs, based on the expression of the paralogous genes that regulate the "activatability" of these molecular machines.

## METHODS

### Patient cohort for mRNA analysis

All patients (mean age 60.9 years, range 29-91 years) met the following criteria: primary unilateral nonmetastatic breast carcinoma for which complete clinical, histological and biological data were available; no radiotherapy or chemotherapy before surgery; and full follow-up at Institut Curie - Hospital René Huguenin. All patients before 2007 were informed that their tumor samples might be used for scientific purposes and had the opportunity to decline. Since 2007, patients treated in our institution have given their approval by signed informed consent. This study was approved by the local ethics committee (Breast Group of René Huguenin Hospital). Treatment (information available for 524 patients) consisted of modified radical mastectomy in 320 cases (61%) or breast-conserving surgery plus locoregional radiotherapy in 204 cases (39%). The patients had a physical examination and routine chest radiotherapy every 3 months for 2 years, then annually. Mammograms were done annually. Adjuvant therapy was administered to 416 patients, consisting of chemotherapy alone in 130 cases, hormone therapy alone in 178 cases and both treatments in 108 cases. During a median follow-up of 10.5 years (range 1 month to 36.3 years), 210 patients developed metastasis. Sixteen specimens of adjacent normal breast tissue from breast cancer patients or normal breast tissue from women undergoing cosmetic breast surgery were used as sources of normal RNA.

### qRT-PCR

Specific mRNAs were quantified from the cycle number (Ct value) at which the increase in the fluorescence signal started to be detected by the laser detector of the ABI Prism 7900 sequence detection system (Perkin-Elmer Applied Biosystems, Foster City, CA) as previously described [52]. Specific transcripts were quantified using the following primers: WASF1-U (5'-CCTCTCATTTTGAAACAAGACCTCAG-3') and WASF1-L (5'-CTAAATGGCAAGGCAGAAAGTGAGT-3') for the *WASF1* gene (PCR product of 79 pb); WASF2-U (5'- AAAGCTGGGGACTTCTGGGTATC-3') and WASF2-L (5'-GTGAAGAAGCAGAGTCTGACTGTGGT-3') for the *WASF2* gene (PCR product of 122 pb); WASF3-U (5'- GAGTGATAAGCCACCGCCTCTG-3') and WASF3-L (5'-GCCCATCCTTCTTGTCATCTCTGTA-3') for the *WASF3* gene (PCR product of 62 pb); ABI1-U (5'-GGGGAACACTGGGACGGAAT-3') and ABI1-L (5'-GCTGTCCTGCCTGGACTATGCT-3') for the *ABI1* gene (PCR product of 124 pb); ABI2-U (5'-CCGTGGGCTCCACGTTCTTACT-3') and ABI2-L (5'-TCCTTCCTGAAAGGACAGCTCATCT-3') for the *ABI2* gene (PCR product of 90 pb); ABI3-U (5'-TGCTGCGGGTCGCTGACTA-3') and ABI3-L (5'-

GCGCCTTCCGCTTGTCTGT-3') for the *ABI3* gene (PCR product of 63 pb); BRK1-U (5'-AAAATCGCAGACTTTCTCAACTCGT-3') and BRK1-L (5'-TTCAAGGGCTGTCAATTTCTCGT-3') for the *BRK1* gene (PCR product of 84 pb); NCKAP1-U (5'-AGTGTACCCTTAGTGACCAGTTGCT-3') and NCKAP1-L (5'-TCAGGTTCCCCTTTCTTACCAGT-3') for the *NCKAP1* gene (PCR product of 106 pb); NCKAP1L-U (5'- GAAAAGTCCATGGAACCATCTCTCA-3') and NCKAP1L-L (5'-GTACTGGTCCTAAATGTTGCGTGCT-3') for the *NCKAP1L* gene (PCR product of 91 pb); CYFIP1-U (5'-CACGAGTACGGCTCTCCTGGTATC-3') and CYFIP1-L (5'-CCGCAGGTTCTGGAAGCACA-3') for the *CYFIP1* gene (PCR product of 102pb); CYFIP2-U (5'-CCCACGTCATGGAGGTGTACTCT-3') and CYFIP2-L (5'-TAATTGTAGCGTGTGGCTCTCTCA-3') for the *CYFIP2* gene (PCR product of 112pb); TBP-U (5'-TGCACAGGAGCCAAGAGTGAA-3') and TBP-L (5'-CACATCACAGCTCCCCACCA-3') for the *TBP* gene (PCR product of 132 bp), which was the reference gene used for normalization. Over and under-expression were defined as >3 and <0.33, respectively, the expression compared to the median expression of normal samples.

Public transcriptomics data on breast cancer [22] were interrogated using the kmplot website (http://kmplot.com) on June 26, 2019 using best cut-offs for JetSet determined best probes (*NCKAP1* 207738_s_at, *CYFIP2* 220999_s_at, [51].

**Cell lines, transfection and establishment of stable clones**

MCF10A cells were grown in DMEM/F12 medium supplemented with 5% horse serum, 20 ng/mL epidermal growth factor, 10 µg/mL insulin, 500 ng/mL hydrocortisone, and 100 ng/mL cholera toxin. MDA-MB-231 were grown in DMEM medium with 10% FBS. Medium and supplements were from Life Technologies and Sigma. Cells were incubated at 37°C in 5% $CO_2$. MCF10A and MDA-MB-231 were from the collection of breast cell lines organized by Thierry Dubois (Institut Curie, Paris).

Stable MCF10A cells expressing CYFIP2 were obtained by transfecting MCF10A cells, with the home-made plasmid MXS AAVS1L SA2A Puro bGHpA EF1Flag GFP CYFIP2 Sv40pA AAVS1R, or MXS AAVS1L SA2A Puro bGHpA EF1Flag GFP Blue Sv40pA AAVS1R as a control. Transfection was performed with Lipofectamine 2000 (Invitrogen). To obtain stable integration of the MXS plasmid at the AAVS1 site, cells were cotransfected with two TALEN plasmids inducing DNA double strand breaks at the AAVS1 locus (Addgene #59025 and 59026; [52]. Cells were selected with 1 µg/mL puromycine (Invivogen) and pooled. Stable MCF10A cells expressing shRNA were obtained by transfection with previously described pSUPER-Retro-Puro plasmids [5] and puromycin selection.

The stable 293 Flp-In cell line expressing Flag-HA-CYFIP1 were previously described [53]. An equivalent cell line expressing Flag-HA-CYFIP2 was obtained according to a published procedure[54].

MDA-MB-231 and MCF10A were depleted by siRNAs (OnTarget Smart Pools, Dharmacon), transfected at 20 nM final concentration using Lipofectamine RNAiMAX (Invitrogen), and re-

transfected 72h later, for the total of 6 days. This protocol was necessary due to an unusually long half-life of CYFIP2 protein (AP, unpublished observations).

The MCF10A CYFIP2 knockout cell line was generated with CRISPR/Cas9 system. The targeting sequence 5'-CAUUUGUCACGGGCAUUGCA-3' was used to induce the double strand break. For the negative control the non-targeting sequence 5'-AAAUGUGAGAUCAGAGUAAU-3' was used. Cells were transfected with crRNA:trackRNA duplex and the purified Cas9 protein by Lipofectamine CRISPRMAX™ Cas9 Transfection Reagent (all reagents from Thermofisher Scientific). The next day, cells were subjected to dilution at 0.8 cells/well in 96 well plates. Single clones were expanded and analyzed by CYFIP2 Western blot. 2 positive clones were identified. The PCR products amplified from genomic DNA containing the gRNA recognition site were then cloned (Zero Blunt PCR Cloning Kit, Thermofisher Scientific) and sequenced. A frameshift of +1 and a -1 in the 3rd exon of the CYFIP2 gene in both clones was confirmed by sequencing (see Fig. S6 for details).

**Antibodies and Western blot**

Cells were lysed in RIPA buffer and analyzed by Western blot. SDS-PAGE was performed using NuPAGE 4-12% Bis-Tris and 3-8% Tris-Acetate gels (Life Technologies). Nitrocellulose membranes were developed with horseradish peroxidase (HRP) coupled antibodies (Sigma) and SuperSignal West Femto chemiluminescent substrate (Thermo Fisher Scientific). Home-made rabbit polyclonal antibodies CYFIP1, ABI1, WAVE2 were previously described [32]. The mouse monoclonal antibody, 231H9, targeting BRK1 was previously described [55]. The antibodies targeting CYFIP-2 (Sigma SAB2701081), NCKAP1 (Bethyl A305-178A), cortactin (Millipore 4F11), ARPC2 (Millipore 07-227) and tubulin (Sigma T9026) were purchased. Quantification of wb was performed by densitometry, using the ImageJ software.

**Sucrose gradient**

For sucrose gradient analysis of WAVE subunits, Nitrogen cavitation (Parr instruments, 500 Psi for 20 min) followed by centrifugation (16,000 × g, 20 min) and ultracentrifugation (150,000 × g, 60 min) were used to prepare cytosolic extracts from cells trypsinized from two 15 cm dishes and resuspended in the XB buffer (20 mM HEPES, 100mM NaCl, 1mM MgCl2, 0.1 mM EDTA, 1mM DTT, pH 7.7). 200 µL of extract was loaded on the 11 mL 5–20% sucrose gradient in the XB buffer and subjected to ultracentrifugation for 17 h at 197,000 ×g in the swinging bucket rotor SW41 Ti (Beckman). 0.5 mL fractions were collected and concentrated by using trichloroacetic acid precipitation with insulin as a carrier. The samples were washed with acetone, dried and then resuspended in the 1x LDS loading buffer with 2.5% of β-ME for Western blot analysis.

**Migration assays**

Transwell migration assays were performed using FluoroBlok inserts with 8 µm holes (Corning, 351152), covered with 20 µg/ml fibronectin (Sigma, F1141). MDA-MB-231 cells

were plated in serum-free medium and allowed to migrate towards serum-containing medium for 16 h, incubated with 4 µg/ml calcein AM (Sigma, C1359) for 1 h, and images of fluorescent cells were acquired and quantified using ImageJ software.

2D migration was performed using 8 chamber Ibidi dishes (Biovalley 80826) covered with 20 µg/ml fibronectin. 3D migration was performed in 2 mg/ml collagen gel polymerized at 37°C (rat tail collagen type I, Corning 354263), with the cells sandwiched between the two layers of collagen. An inverted Axio Observer microscope (Zeiss) equipped with a Pecon Zeiss incubator XL multi S1 RED LS (Heating Unit XL S, Temp module, $CO_2$ module, Heating Insert PS and $CO_2$ cover), a definite focus module and a Hamamatsu camera C10600 Orca-R2 was used to perform videomicroscopy. Pictures were taken every 5 min for 24 h for 2D migration, and every 20 min for 48 h for 3D migration. Random migration of single cells and migration persistence, based on the angular shift between frames, was analyzed as previously described [46] using DiPer programs [56].

**Rescue of DKO cells**

B16-F1 mouse melanoma cells that are *CYFIP1/2* double KO were a kind gift of Klemens Rottner (Helmholtz-Zentrum für Infektionsforschung, Braunschweig). GFP-tagged human CYFIP1 or CYFIP2 (wild type or mutant) were transiently transfected into the DKO cells, and 48 h later, 10-minute videos (images taken every 10 seconds) were acquired using a confocal laser scanning microscope (TCS SP8, Leica) equipped with a high NA oil immersion objective (HC PL APO 63×/ 1.40, Leica), a white light laser (WLL, Leica) and controlled by the LasX software. Protrusion speed was measured using the Multi Kymograph tool in ImageJ software. For the LineScan analysis, images of fixed, stained cells were obtained, and analyzed as described in [46] and [23].

**Zebrafish embryos, cell transplantation and imaging**

Embryos were obtained by natural spawning of *Tg(-1.8gsc:GFP)ml1* adult fishes [57]. All animal studies were done in accordance with the guidelines issued by the Ministère de l'Education Nationale, de l'Enseignement Supérieur et de la Recherche and were approved by the Direction Départementale des Services Vétérinaires de l'Essonne and the Ethical Committee N°59.

Translation blocking morpholinos (Gene Tool LLC Philomath) were designed against zebrafish *CYFIP1* (AAAAACTATCCGCTTCGACTGTTCA) and *CYFIP2* (CGACACAGGTTCACTCACAAAACAG). The *NCKAP1* morpholino (CCGAGACATGGCTCAAACGACCGTC) was described in [58]. The control morpholino is a standard control (CCTCTTACCTCAGTTACAATTTATA). mRNAs were synthesized using pCS2+ plasmids containing the human genes described in [32] and the mMessage mMachine SP6 kit (Thermo Fischer).

For cell migration quantification, embryos were injected at the one-cell stage with 1.5 nl of a solution containing Histone2B-mCherry mRNA (30 ng/µl) and either control morpholino (0.1, 0.2 or 0.8mM), MoCYFIP1 (0.2mM), MoCYFIP2 (0.1mM) or MoNCKAP1 (0.8mM), with or

without mRNAs encoding either human CYFIP1 (10ng/µl), human CYFIP2 (10ng/µl) or human NCKAP1 (10ng/µl). Injected embryos were mounted in 0.2% agarose in embryo medium and imaged between 60% and 80% epiboly (6.5-8.5 hpf) under an upright TriM Scope II (La Vision Biotech) two photon microscope equipped with an environmental chamber (okolab) at 28°C using a 25x water immersion objective. Visualization of 3D movies and nuclei tracking were done using Imaris (Bitplane). Cell migration parameters were extracted using custom Matlab (Math Works) code and autocorrelation was computed using published Excel macros [56].

For protrusion analysis, embryos were injected in one cell at the four-cell stage with 1.5 nl of a solution containing Lifeact-mCherry mRNA (50 ng/µl) and either control morpholino (0.5 mM), MoCYFIP1 (0.2mM), MoCYFIP2 (0.1mM) or MoNCKAP1 (0.8mM), with or without mRNAs encoding either human CYFIP1 (10ng/µl), human CYFIP2 (10ng/µl) or human NCKAP1 (10ng/µl). Small cell groups were transplanted at shield stage (6 hpf) from the shield of an injected embryo to the shield of an untreated host. Embryos were then cultured in embryo medium [59] with 10 U/mL penicillin and 10 µg/mL streptomycin. Transplanted embryos were mounted in 0.2% agarose in embryo medium and imaged between 60% and 80% epiboly (6.5-8.5 hpf) under an inverted TCS SP8 confocal microscope equipped with environmental chamber (Leica) at 28°C using a HC PL APO 40x/1.10 W CS2 objective. Visualization of images was done on ImageJ, lamellipodia-like actin rich protrusions being quantified on the basis of morphological criteria as described in [26].

**Reconstitution of WAVE complexes and in vitro assays**

Recombinant WAVE complexes containing full-length human CYFIP1 or CYFIP2, full-length NCKAP1, full-length BRK1, ABI2 (1-158) and WAVE1 (1-230)-$(GGS)_6$-WCA (485-559), referred to as WRC230WCA were purified as previously described [35,36]. CYFIP1- and CYFIP2-containing WAVE complexes behaved similarly during expression and purification by various chromatographic steps. Other proteins, including the Arp2/3 complex, actin, WAVE1 WCA, Tev, GST-RAC1 (Q61L P29S, 1-188), and untagged RAC1 (Q61L P29S, 1-188) were purified as previously described [35].

GST pull-down experiments were performed as previously described [35]. Briefly, 200 pmol of GST-RAC1 and 200 pmol of WAVE complex were mixed with 20 µL of Glutathione Sepharose beads (GE Healthcare) in 1 mL of binding buffer (10 mM HEPES pH 7, 50 or 100 mM NaCl, 5% (w/v) glycerol, 2 mM $MgCl_2$, 1 mM DTT, and 0.05% Triton X100) at 4 °C for 30 min, followed by three washes using 1 mL of the binding buffer in each wash. Finally, the bound proteins were eluted with GST elution buffer (100 mM Tris-HCl pH 8.5, 30 mM reduced glutathione, and 2 mM $MgCl_2$) and examined on SDS-PAGE gels.

GST equilibrium pull-down assays were performed in the EPD buffer (10 mM HEPES pH 7, 50 mM NaCl, 5% (w/v) glycerol, 2 mM $MgCl_2$, and 1 mM DTT) as previous described (Chen et al., 2017). Essentially, each 100 µL of reaction contained 0.1 µM WRC230WCA, varying concentrations of GST-Rac1(Q61L P29S, 1-188), 30 µL of the Glutathione Sepharose beads, and 0.05% Triton X100. All protein samples and beads were first dialyzed or equilibrated in the EPD buffer prior to use. After gentle mixing at 4°C for 30 min, the beads were pelleted by a brief centrifugation, and the supernatant was immediately transferred to SDS loading buffer

and analyzed by Coomassie blue-stained SDS-PAGE gels. Total intensity of the CYFIP1/2 and NCKAP1 bands was quantified by ImageJ to determine the unbound WAVE complex. The derived fractional occupancy from several independent experiments was pooled and globally fitted to obtain the binding isotherms and the apparent dissociation constants $K_D$.

Actin polymerization assays were performed as previously described [35] with slight modifications. Each reaction (120 µL) contained 4 µM actin (5% pyrene labeled), 10 nM Arp2/3 complex, 100 nM WRC230WCA or WAVE1 WCA, and desired concentration of untagged RAC1 (Q61L P29S, 1-188) in NMEH20GD buffer (50 mM NaCl, 1 mM $MgCl_2$, 1 mM EGTA, 10 mM HEPES pH7.0, 20% (w/v) glycerol, and 1 mM DTT). Pyrene-actin fluorescence was recorded every 5 seconds at 22 °C using a 96-well flat-bottom black plate (Greiner Bio-One™) in a Spark plater reader (Tecan), with excitation at 365 nm and emission at 407 nm (15 nm bandwidth for both wavelengths).

**Statistical analyses**

Patient cohort. Relationships with mRNA levels and clinical parameters were identified using the $\chi^2$ test. Statistical analyses using univariate and multivariate Cox proportional hazard models were performed with the R computing environment (R Development Core Team, 2017). Codes are available upon request.

Migration persistence. Exponential decay and plateau fit ($y = (1 - b) * e^{-\frac{t}{a}} + b$) was performed for all individual cells. Coefficients were then compared using one-way ANOVA. Statistical analysis was performed in R using linear mixed-effect models to take into account the resampling of the same statistical unit.

Significance. Differences were considered significant at confidence levels greater than 95% ($p < 0.05$). Four levels of statistical significance were distinguished: *P<0.05; **P<0.01; ***P<0.001; ****P<0.0001.

## Acknowledgements

We thank Nelia Cordeiro for technical support, Theresia Stradal for sharing shRNA plasmids targeting NCKAP1 and CYFIP2, Klemens Rottner for the *CYFIP1/2* DKO cells, and Chuang Yu for his help with statistical tools. This work was supported by grants from the Agence Nationale de la Recherche (ANR-15-CE13-0016-01 for AMG and NBD), from the fondation ARC pour la Recherche sur le Cancer (PGA120140200831 for AMG and IB and DOC20170505494 to NM), from National Institute of Health (grant R35 GM128786) to BC, from Institut National du Cancer (INCA_6521 for AMG and IB, and INCA_11508 for AMG, IB and ML). We thank the Polytechnique Bioimaging Facility for assistance with live imaging on their equipment partly supported by Région Ile-de-France (interDIM) and Agence Nationale de la Recherche (ANR-11-EQPX-0029 Morphoscope2, ANR-10-INBS-04 France BioImaging)

## Conflict of interest

The authors declare no conflict of interest

## Author contributions

AP performed *in vitro* experiments of cell migration and wrote the manuscript. AB and NBD performed *in vivo* experiments in zebrafish embryos. ML performed statistical modeling. SV, AS and IB performed qRT-PCR measurements of WAVE complex expression. NM constructed the integrative plasmid used to overexpress CYFIP2. NR quantified CYFIP1/2 protein expression in cell lines. AF and YW isolated the CYFIP2 knockout clones and performed experiments with these clones. YW performed the sucrose gradient experiments. RG performed the structural comparison of CYFIP1/2 proteins. SR performed the confocal microscopy of B16-F1 cells and helped with the data analysis. SY, YL, and BC reconstituted CYFIP1/2 containing WAVE complexes and performed RAC1 binding and pyrene actin assays. AMG supervised the study and wrote the manuscript. All authors have commented on the manuscript and approved the submission.

## REFERENCES

1. Dehal, P., and Boore, J.L. (2005). Two Rounds of Whole Genome Duplication in the Ancestral Vertebrate. PLoS Biology *3*, e314-9.

2. Ruepp, A., Waegele, B., Lechner, M., Brauner, B., Dunger-Kaltenbach, I., Fobo, G., Frishman, G., Montrone, C., and Mewes, H.W. (2010). CORUM: the comprehensive resource of mammalian protein complexes--2009. Nucleic Acids Research *38*, D497-501.

3. Alberts, B. (1998). The cell as a collection of protein machines: preparing the next generation of molecular biologists. Cell *92*, 291–294.

4. Molinie, N., and Gautreau, A. (2018). The Arp2/3 Regulatory System and Its Deregulation in Cancer. Physiological Reviews *98*, 215–238.

5. Steffen, A., Rottner, K., Ehinger, J., Innocenti, M., Scita, G., Wehland, J., and Stradal, T.E.B. (2004). Sra-1 and Nap1 link Rac to actin assembly driving lamellipodia formation. The EMBO Journal *23*, 749–759.

6. Lai, F.P.L., Szczodrak, M., Block, J., Faix, J., Breitsprecher, D., Mannherz, H.G., Stradal, T.E.B., Dunn, G.A., Small, J.V., and Rottner, K. (2008). Arp2/3 complex interactions and actin network turnover in lamellipodia. The EMBO Journal *27*, 982–992.

7. Steffen, A., Koestler, S.A., and Rottner, K. (2014). Requirements for and consequences of Rac-dependent protrusion. European Journal of Cell Biology *93*, 184–193.

8. Krause, M., and Gautreau, A. (2014). Steering cell migration: lamellipodium dynamics and the regulation of directional persistence. Nature Reviews Mol Cell Biol *15*, 577–590.

9. Derivery, E., and Gautreau, A. (2010). Generation of branched actin networks: assembly and regulation of the N-WASP and WAVE molecular machines. BioEssays : news and reviews in molecular, cellular and developmental biology *32*, 119–131.

10. Dubielecka, P.M., Cui, P., Xiong, X., Hossain, S., Heck, S., Angelov, L., and Kotula, L. (2010). Differential Regulation of Macropinocytosis by Abi1/Hssh3bp1 Isoforms. PLoS ONE *5*, e10430.

11. Suetsugu, S., Yamazaki, D., Kurisu, S., and Takenawa, T. (2003). Differential Roles of WAVE1 and WAVE2 in Dorsal and Peripheral Ruffle Formation for Fibroblast Cell Migration. Dev Cell *5*, 595–609.

12. Iwaya, K., Norio, K., and Mukai, K. (2007). Coexpression of Arp2 and WAVE2 predicts poor outcome in invasive breast carcinoma. Modern Pathology *20*, 339–343.

13. Zhang, J., Tang, L., Shen, L., Zhou, S., Duan, Z., Xiao, L., Cao, Y., Mu, X., Zha, L., and Wang, H. (2012). High level of WAVE1 expression is associated with tumor aggressiveness and unfavorable prognosis of epithelial ovarian cancer. Gynecologic oncology *127*, 223–230.

14. Semba, S., Iwaya, K., Matsubayashi, J., Serizawa, H., Kataba, H., Hirano, T., Kato, H., Matsuoka, T., and Mukai, K. (2006). Coexpression of actin-related protein 2 and Wiskott-Aldrich syndrome family verproline-homologous protein 2 in adenocarcinoma of the lung. Clinical cancer research : an official journal of the American Association for Cancer Research *12*, 2449–2454.

15. Yang, L.Y., Tao, Y.M., Ou, D.P., Wang, W., Chang, Z.G., and Wu, F. (2006). Increased Expression of Wiskott-Aldrich Syndrome Protein Family Verprolin-Homologous Protein 2 Correlated with Poor Prognosis of Hepatocellular Carcinoma. Clinical cancer research : an official journal of the American Association for Cancer Research *12*, 5673–5679.

16. Ji, Y., Li, B., Zhu, Z., Guo, X., He, W., Fan, Z., and Zhang, W. (2015). Overexpression of WAVE3 promotes tumor invasiveness and confers an unfavorable prognosis in human hepatocellular carcinoma. Biomedicine & pharmacotherapy = Biomédecine & pharmacothérapie *69*, 409–415.

17. Zhang, Y., Guan, X.-Y., Dong, B., Zhao, M., Wu, J.-H., Tian, X.-Y., and Hao, C.-Y. (2012). Expression of MMP-9 and WAVE3 in colorectal cancer and its relationship to clinicopathological features. Journal of Cancer Research and Clinical Oncology *138*, 2035–2044.

18. Lomakina, M.E., Lallemand, F., Vacher, S., Molinie, N., Dang, I., Cacheux, W., Chipysheva, T.A., Ermilova, V.D., Koning, L.D., Dubois, T., et al. (2016). Arpin downregulation in breast cancer is associated with poor prognosis. British journal of cancer *114*, 545–553.

19. Joshi, A.D., Hegde, G.V., Dickinson, J.D., Mittal, A.K., Lynch, J.C., Eudy, J.D., Armitage, J.O., Bierman, P.J., Bociek, R.G., Devetten, M.P., et al. (2007). ATM, CTLA4, MNDA, and HEM1 in High versus Low CD38-Expressing B-Cell Chronic Lymphocytic Leukemia. Clinical cancer research : an official journal of the American Association for Cancer Research *13*, 5295–5304.

20. Wang, C., Tran-Thanh, D., Moreno, J.C., Cawthorn, T.R., Jacks, L.M., Wang, D.-Y., McCready, D.R., and Done, S.J. (2010). Expression of Abl interactor 1 and its prognostic significance in breast cancer: a tissue-array-based investigation. Breast Cancer Research and Treatment *129*, 373–386.

21. Zhang, J., Tang, L., Chen, Y., Duan, Z., Xiao, L., Li, W., Liu, X., and Shen, L. (2015). Upregulation of Abelson interactor protein 1 predicts tumor progression and poor outcome in epithelial ovarian cancer. Human pathology *46*, 1331–1340.

22. Győrffy, B., Lanczky, A., Eklund, A.C., Denkert, C., Budczies, J., Li, Q., and Szallasi, Z. (2009). An online survival analysis tool to rapidly assess the effect of 22,277 genes on breast cancer prognosis using microarray data of 1,809 patients. Breast Cancer Research and Treatment *123*, 725–731.

23. Molinie, N., Rubtsova, S.N., Fokin, A., Visweshwaran, S.P., Rocques, N., Polesskaya, A., Schnitzler, A., Vacher, S., Denisov, E.V., Tashireva, L.A., et al. (2019). Cortical branched actin determines cell cycle progression. Cell Research *29*, 432–445.

24. Montero, J.-A., Kilian, B., Chan, J., Bayliss, P.E., and Heisenberg, C.-P. (2003). Phosphoinositide 3-kinase is required for process outgrowth and cell polarization of gastrulating mesendodermal cells. Current Biology *13*, 1279–1289.

25. Dumortier, J.G., Martin, S., Meyer, D., Rosa, F.M., and David, N.B. (2012). Collective mesendoderm migration relies on an intrinsic directionality signal transmitted through cell contacts. Proceedings of the National Academy of Sciences of the United States of America *109*, 16945–16950.

26. Diz-Muñoz, A., Krieg, M., Bergert, M., Ibarlucea-Benitez, I., Muller, D.J., Paluch, E., and Heisenberg, C.-P. (2010). Control of Directed Cell Migration In Vivo by Membrane-to-Cortex Attachment. PLoS Biology *8*, e1000544-12.

27. Petrie, R.J., Gavara, N., Chadwick, R.S., and Yamada, K.M. (2012). Nonpolarized signaling reveals two distinct modes of 3D cell migration. The Journal of Cell Biology *197*, 439–455.

28. Schaks, M., Singh, S.P., Kage, F., Thomason, P., Klünemann, T., Steffen, A., Blankenfeldt, W., Stradal, T.E., Insall, R.H., and Rottner, K. (2018). Distinct Interaction Sites of Rac GTPase with WAVE Regulatory Complex Have Non-redundant Functions in Vivo. Current Biology *28*, 3674-3684.e6.

29. Zweier, M., Begemann, A., McWalter, K., Cho, M.T., Abela, L., Banka, S., Behring, B., Berger, A., Brown, C.W., Carneiro, M., et al. (2019). Spatially clustering de novo variants in CYFIP2, encoding the cytoplasmic FMRP interacting protein 2, cause intellectual disability and seizures. Eur J Hum Genet *27*, 747–759.

30. Chen, Z., Borek, D., Padrick, S.B., Gomez, T.S., Metlagel, Z., Ismail, A.M., Umetani, J., Billadeau, D.D., Otwinowski, Z., and Rosen, M.K. (2010). Structure and control of the actin regulatory WAVE complex. Nature *468*, 533–538.

31. Chen, B., Brinkmann, K., Chen, Z., Pak, C.W., Liao, Y., Shi, S., Henry, L., Grishin, N.V., Bogdan, S., and Rosen, M.K. (2014). The WAVE regulatory complex links diverse receptors to the actin cytoskeleton. Cell *156*, 195–207.

32. Gautreau, A., Ho, H.H., Li, J., Steen, H., Gygi, S.P., and Kirschner, M.W. (2004). Purification and architecture of the ubiquitous Wave complex. Proceedings of the National Academy of Sciences of the United States of America *101*, 4379–4383.

33. Fort, L., Batista, J.M., Thomason, P.A., Spence, H.J., Whitelaw, J.A., Tweedy, L., Greaves, J., Martin, K.J., Anderson, K.I., Brown, P., et al. (2018). Fam49/CYRI interacts with Rac1 and locally suppresses protrusions. Nature Cell Biology *20*, 1159–1171.

34. Yelland, T., Le, A.H., Nikolaou, S., Insall, R., Machesky, L., and Ismail, S. (2021). Structural Basis of CYRI-B Direct Competition with Scar/WAVE Complex for Rac1. Structure *29*, 226-237.e4.

35. Chen, B., Chou, H.-T., Brautigam, C.A., Xing, W., Yang, S., Henry, L., Doolittle, L.K., Walz, T., and Rosen, M.K. (2017). Rac1 GTPase activates the WAVE regulatory complex through two distinct binding sites. eLife *6*, W529.

36. Chen, B., Padrick, S.B., Henry, L., and Rosen, M.K. (2014). Biochemical reconstitution of the WAVE regulatory complex. Methods in Enzymology *540*, 55–72.

37. Nakashima, M., Kato, M., Aoto, K., Shiina, M., Belal, H., Mukaida, S., Kumada, S., Sato, A., Zerem, A., Sagie, T.L., et al. (2018). De novo hotspot variants in CYFIP2 cause early-onset epileptic encephalopathy. Annals of neurology *83*, 794–806.

38. Zweier, M., Begemann, A., McWalter, K., Cho, M.T., Abela, L., Banka, S., Behring, B., Berger, A., Brown, C.W., Carneiro, M., et al. (2019). Spatially clustering de novo variants in CYFIP2, encoding the cytoplasmic FMRP interacting protein 2, cause intellectual disability and seizures. European journal of human genetics : EJHG, 1–13.

39. Pittman, A.J., Gaynes, J.A., and Chien, C.-B. (2010). nev (cyfip2) is required for retinal lamination and axon guidance in the zebrafish retinotectal system. Developmental Biology *344*, 784–794.

40. Cioni, J.-M., Wong, H.H.-W., Bressan, D., Kodama, L., Harris, W.A., and Holt, C.E. (2018). Axon-Axon Interactions Regulate Topographic Optic Tract Sorting via CYFIP2-Dependent WAVE Complex Function. Neuron *97*, 1078-1093.e6.

41. Blagg, S.L., Stewart, M., Sambles, C., and Insall, R.H. (2003). PIR121 Regulates Pseudopod Dynamics and SCAR Activity in Dictyostelium. Current Biology *13*, 1480–1487.

42. Ibarra, N., Blagg, S.L., Vazquez, F., and Insall, R.H. (2006). Nap1 Regulates Dictyostelium Cell Motility and Adhesion through SCAR-Dependent and -Independent Pathways. Current Biology *16*, 717–722.

43. Pollitt, A.Y., and Insall, R.H. (2008). Abi Mutants in Dictyostelium Reveal Specific Roles for the SCAR/WAVE Complex in Cytokinesis. Current Biology *18*, 203–210.

44. Litschko, C., Linkner, J., Brühmann, S., Stradal, T.E.B., Reinl, T., Jänsch, L., Rottner, K., and Faix, J. (2017). Differential functions of WAVE regulatory complex subunits in the regulation of actin-driven processes. European Journal of Cell Biology *96*, 715–727.

45. Korobova, F., and Svitkina, T. (2008). Arp2/3 complex is important for filopodia formation, growth cone motility, and neuritogenesis in neuronal cells. Molecular Biology of the Cell *19*, 1561–1574.

46. Dang, I., Gorelik, R., Sousa-Blin, C., Derivery, E., Guérin, C., Linkner, J., Nemethova, M., Dumortier, J.G., Giger, F.A., Chipysheva, T.A., et al. (2013). Inhibitory signalling to the Arp2/3 complex steers cell migration. Nature *503*, 281–284.

47. Stradal, T., Courtney, K.D., Rottner, K., Hahne, P., Small, J.V., and Pendergast, A.M. (2001). The Abl interactor proteins localize to sites of actin polymerization at the tips of lamellipodia and filopodia. Curr Biol *11*, 891–895.

48. Kumar, V., Kim, K., Joseph, C., Kourrich, S., Yoo, S.-H., Huang, H.C., Vitaterna, M.H., Villena, F.P.-M. de, Churchill, G., Bonci, A., et al. (2013). C57BL/6N mutation in cytoplasmic FMRP interacting protein 2 regulates cocaine response. Science *342*, 1508–1512.

49. Wan, C., Borgeson, B., Phanse, S., Tu, F., Drew, K., Clark, G., Xiong, X., Kagan, O., Kwan, J., Bezginov, A., et al. (2015). Panorama of ancient metazoan macromolecular complexes. Nature *525*, 339–344.

50. Abella, J.V.G., Galloni, C., Pernier, J., Barry, D.J., Kjær, S., Carlier, M.-F., and Way, M. (2016). Isoform diversity in the Arp2/3 complex determines actin filament dynamics. Nature Cell Biology *18*, 76–86.

51. Bieche, I., Parfait, B., Laurendeau, I., Girault, I., Vidaud, M., and Lidereau, R. (2001). Quantification of estrogen receptor alpha and beta expression in sporadic breast cancer. Oncogene *20*, 8109–8115.

52. González, F., Zhu, Z., Shi, Z.-D., Lelli, K., Verma, N., Li, Q.V., and Huangfu, D. (2014). An iCRISPR platform for rapid, multiplexable, and inducible genome editing in human pluripotent stem cells. Cell stem cell *15*, 215–226.

53. Derivery, E., Lombard, Be., Loew, D., and Gautreau, A. (2009). The Wave complex is intrinsically inactive. Cell Motility and the Cytoskeleton *66*, 777–790.

54. Derivery, E., and Gautreau, A. (2010). Assaying WAVE and WASH complex constitutive activities toward the Arp2/3 complex. Methods in Enzymology *484*, 677–695.

55. Derivery, E., Fink, J., Martin, D., Houdusse, A., Piel, M., Stradal, T.E., Louvard, D., and Gautreau, A. (2008). Free Brick1 is a trimeric precursor in the assembly of a functional wave complex. PLoS ONE *3*, e2462.

56. Gorelik, R., and Gautreau, A. (2014). Quantitative and unbiased analysis of directional persistence in cell migration. Nature Protocols *9*, 1931–1943.

57. Doitsidou, M., Reichman-Fried, M., Stebler, J., Köprunner, M., Dörries, J., Meyer, D., Esguerra, C.V., Leung, T., and Raz, E. (2002). Guidance of primordial germ cell migration by the chemokine SDF-1. Cell *111*, 647–659.

58. Biswas, S., Emond, M.R., and Jontes, J.D. (2010). Protocadherin-19 and N-cadherin interact to control cell movements during anterior neurulation. The Journal of Cell Biology *191*, 1029–1041.

59. Hans, S., Christison, J., Liu, D., and Westerfield, M. (2007). Fgf-dependent otic induction requires competence provided by Foxi1 and Dlx3b. BMC developmental biology *7*, 5.

Table 1: Tumours showing up- or down-regulation of WAVE complex subunits in breast cancer (> 3 or < 0.3)

| Generic name | Gene name | All tumours | | HR+ ERBB2- | | HR+ ERBB2+ | | HR- ERBB2- | | HR- ERBB2+ | |
|---|---|---|---|---|---|---|---|---|---|---|---|
| | | % down | % up | % down | % up | % down | % up | % down | % up | % down | % up |
| WAVE | ***WASF1*** | **27** | 2 | **37** | 1 | 10 | 2 | 10 | 3 | 21 | 6 |
| | ***WASF2*** | 3 | 1 | 3 | 0 | 3 | 2 | 2 | 3 | 1 | 0 |
| | ***WASF3*** | **46** | 1 | **56** | 0 | 48 | 0 | 27 | 2 | 25 | 3 |
| ABI | ***ABI1*** | 0 | 1 | 0 | 0 | 0 | 2 | 0 | 3 | 0 | 1 |
| | ***ABI2*** | 3 | 0 | 1 | 0 | 2 | 0 | 7 | 0 | 3 | 0 |
| | ***ABI3*** | 1 | **12** | 1 | 5 | 0 | 17 | 0 | **25** | 3 | 17 |
| BRK | ***BRK1*** | 0 | 4 | 0 | 3 | 0 | 10 | 0 | 4 | 0 | 3 |
| NAP | ***NCKAP1*** | 0 | 2 | 0 | 1 | 0 | 2 | 0 | 6 | 0 | 4 |
| | ***NCKAP1L*** | 0 | **22** | 0 | 15 | 0 | 12 | 0 | 37 | 0 | **39** |
| CYFIP | ***CYFIP1*** | 0 | 4 | 0 | 1 | 0 | 12 | 0 | 6 | 0 | 7 |
| | ***CYFIP2*** | 1 | **37** | 1 | **44** | 0 | 36 | 0 | 30 | 1 | 17 |

## Figures

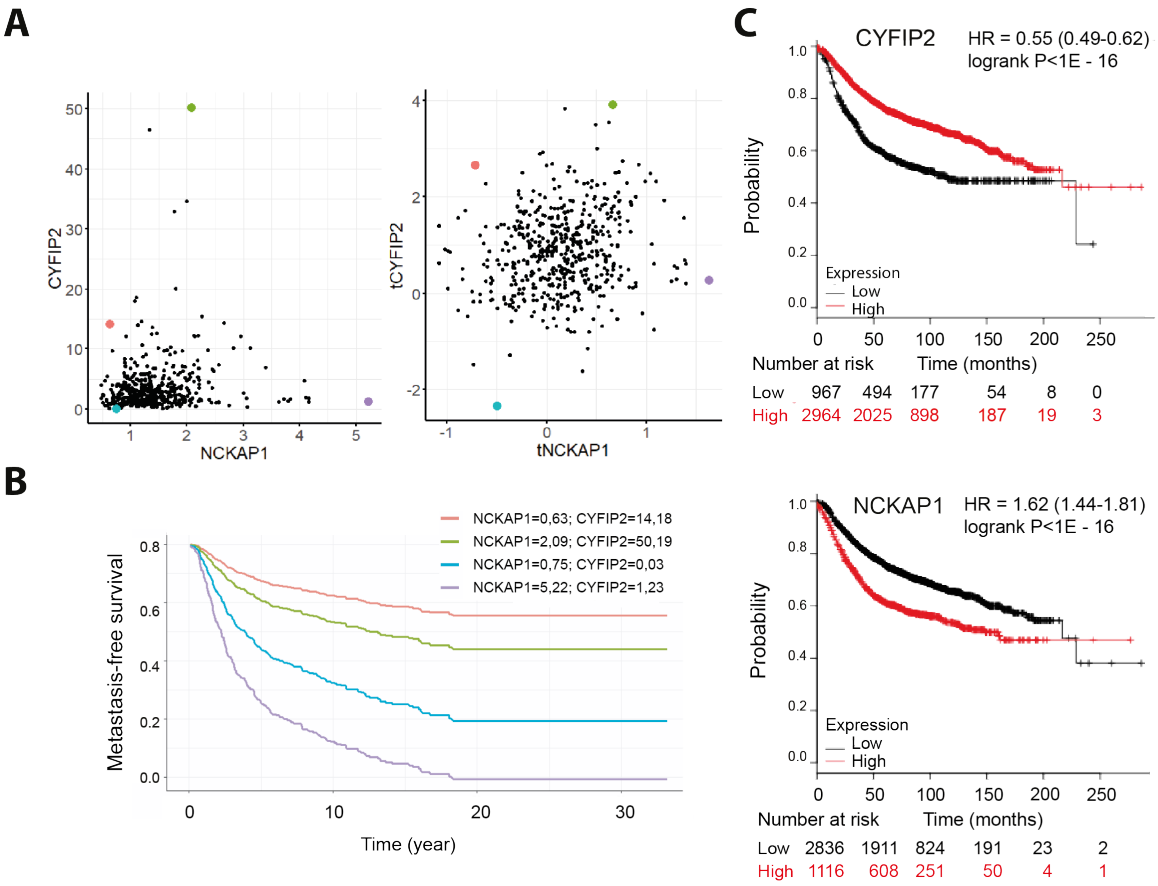


Fig.1, Polesskaya et al.

**Figure 1. CYFIP2 overexpression is associated with good prognosis in breast cancer patients.**

**(A)** Distribution of *NCKAP1* and *CYFIP2* mRNA levels in mammary carcinomas from a cohort of 527 breast cancer patients, before (left panel) or after transformation and normalization (right panel) **(B)** A multivariate Cox model predicting metastasis-free survival (MFS) based on *NCKAP1* and *CYFIP2* mRNA levels as the only two inputs was derived. The 4 highlighted tumors representing the different outskirts of gene expression in the cohort were chosen to run the model. The purple and turquoise patients developed metastases that were diagnosed after 922 and 1487 days, respectively. The red and green patients did not develop metastasis and survived for 4248 and 4146 days, respectively. Even though extreme *NCKAP1* values drive MFS in the red and purple patients, the extreme values of *CYFIP2* rule the outcome of the green and turquoise patients at intermediate values of *NCKAP1*. The model thus predicts that high levels of *NCKAP1* are associated with poor prognosis, whereas high levels of *CYFIP2* are associated with good prognosis. **(C)** Validation of the prediction using a public database, kmplot.com, containing more than 3900 breast cancer patients. Kaplan-Meier representations.

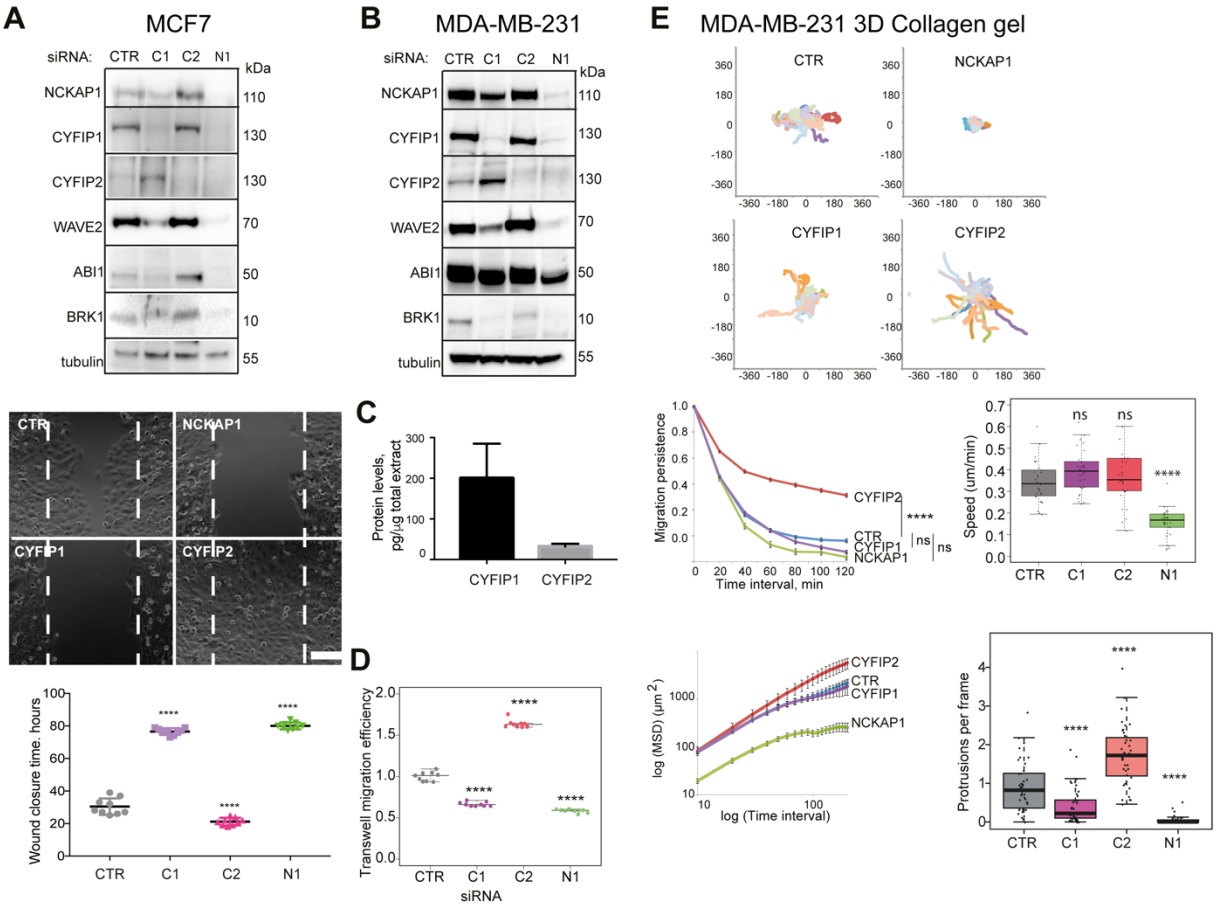


Fig.2, Polesskaya et al.

**Figure 2. CYFIP2 inhibits the migration of human breast cancer cells.** (**A**) MCF7 cells were transfected with pools of siRNAs targeting CYFIP1 (C1), CYFIP2 (C2), NCKAP1 (N1) or non-targeting ones (CTR). Western blots of WAVE complex subunits and tubulin as a loading control. Wound healing of MCF7 cells. Still images corresponding to the time, where the first wound is healed (CYFIP2). Quantification of nine technical repeats. Scale bar: 400 μm. (**B**) MDA-MB-231 cells were transfected with pools of siRNAs and analyzed by Western blots as above. (**C**) Levels of CYFIP1 and CYFIP2 proteins in MDA-MB-231. Mean ± SD of 3 biological repeats. (**D**) Quantification of Transwell migration efficiency of MDA-MB-231 cells, n=9. (**E**) Depleted MDA-MB-231 cells depleted of the indicated proteins were embedded in 3D collagen type I gels and recorded by videomicroscopy. Trajectories, migration persistence, Mean Square Displacement (MSD), and average number of protrusions per frame are plotted, n=30. *P<0.05; **P<0.01; ***P<0.001; ****P<0.0001.

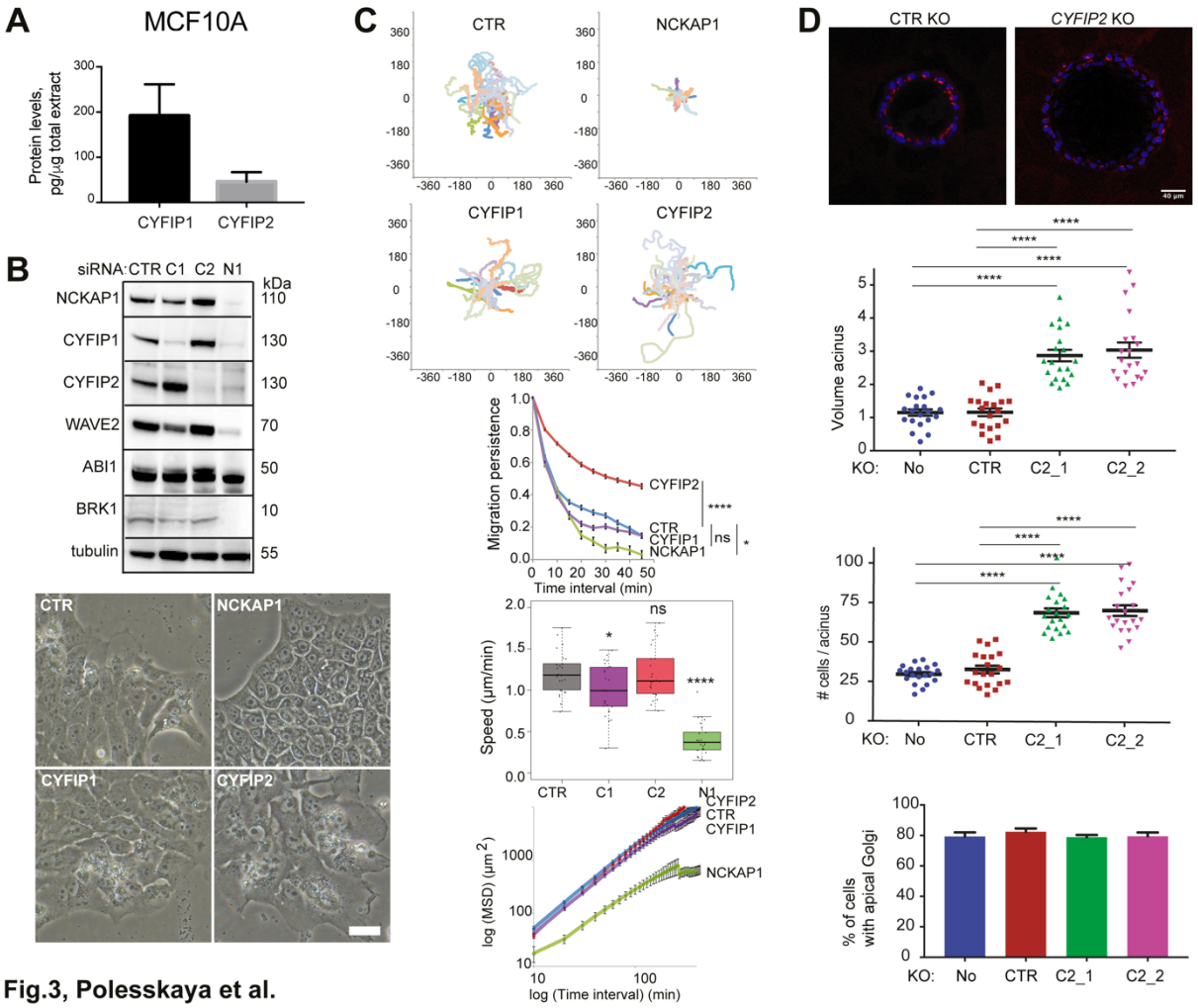


Fig.3, Polesskaya et al.

**Figure 3. CYFIP2 inhibits the migration of normal breast epithelial cells and the growth of 3D acini.** (**A**) Levels of CYFIP1 and CYFIP2 proteins in MDA-MB-231. Mean ± SD of 3 biological repeats. (**B**) MCF10A cells were transfected with pools of CYFIP1 (C1), CYFIP2 (C2), NCKAP1 (N1) or non-targeting siRNAs (CTR). WAVE complex subunits and tubulin as a loading control were analyzed by Western blot. Phase-contrast images of depleted cells. Scale bar: 50 µm. **(C)** Trajectories, migration persistence, speed, MSD extracted from random migration of single MCF10A cells. 2D migration, Fibronectin coating, n=25. (**D**) *CYFIP2* KO cells or parental MCF10A cells were differentiated at the surface of matrigel. Confocal microscopy of acini labeled with DAPI (blue) and the Golgi marker GM130 (red). Scale bar: 40 µm. Quantification of acinus volume and the number of cells per acinus, n=20. (**H**), Quantification of cells' polarity within acini, n=130. *P<0.05; ****P<0.0001.

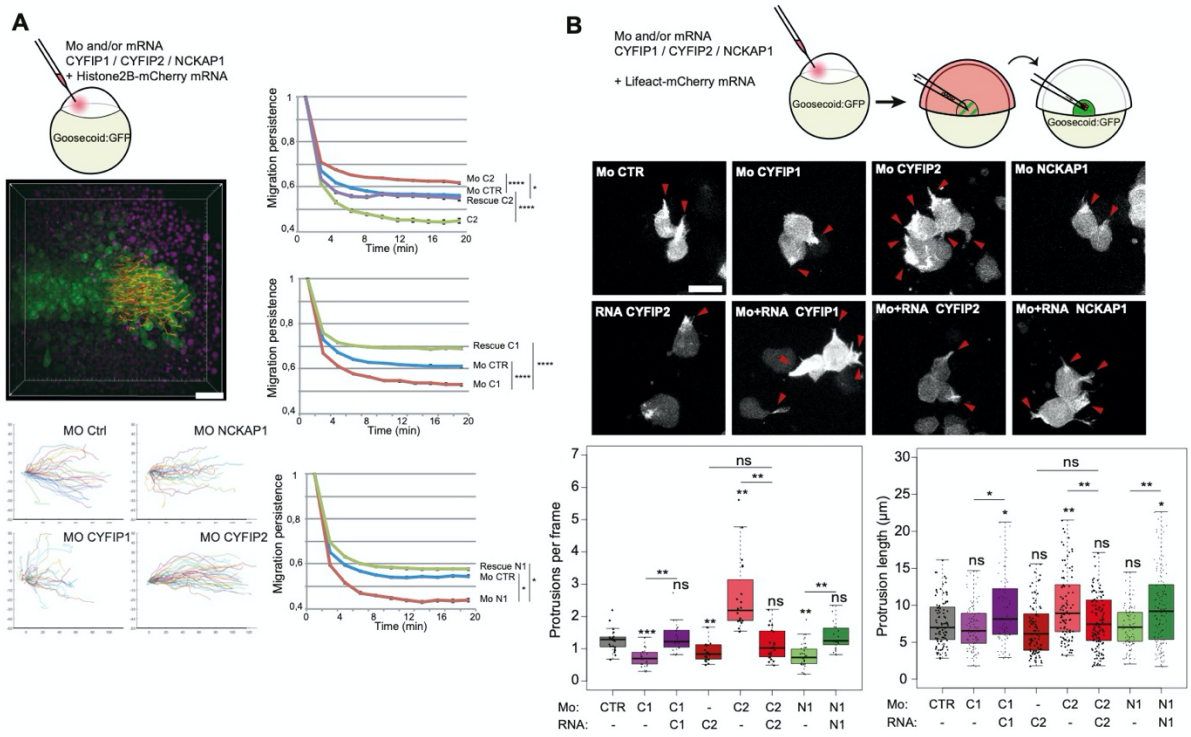


**Figure 4. CYFIP2 inhibits migration persistence and actin rich protrusions in zebrafish embryos during gastrulation.** (A) Scheme of the experimental design. Embryos were injected with Histone2B-mCherry mRNA and morpholinos (Mo) targeting a control sequence (CTR), CYFIP1 (C1), CYFIP2 (C2), NCKAP1 (N1), alone or in combination with mRNAs encoding the same proteins (rescue). Dorsal view of a volume acquisition of a Tg(Gsc:GFP) zebrafish embryo. Scale bar is 50 µm. Animal pole is located at the right. Notochord and prechordal plate cells express GFP (green) and nuclei express histone2B-mCherry (in magenta). Nuclei of prechordal plate cells are 3D-tracked over time (color coded) (Movie S5). Trajectories of 10 first time points (20 min) for 50 randomly selected cells for each condition, plotted at the same origin (axes in µm). Migration persistence of prechordal plate cells injected with the indicated MO and/or mRNA. (B) CYFIP2 inhibits actin rich protrusions in zebrafish embryos during gastrulation. Scheme of the experimental design. Donor embryos were injected with the actin filament marker LifeAct-mCherry mRNA and morpholinos (Mo) targeting a control sequence (CTR), CYFIP1 (C1), CYFIP2 (C2), NCKAP1 (N1), alone or in combination with mRNAs encoding the same proteins. Labeled prechordal plate cells from a donor embryo were transplanted into an uninjected embryo and recorded. Imaged of typical cells described in (A), red arrowheads indicate actin-rich protrusions. Scale bar: 20µm. Quantification of the average number of protrusions per frame, n=17 to 32 cells from 4 to 5 embryos per condition. Quantification of protrusion length, n=95 (randomly selected protrusions per condition). ANOVA on linear mixed model accounting for the sampling biases. ns P>0.05; * P<0.05; ** P<0.01; *** P<0.001. The p-values without a bar refer to comparisons with the control condition.

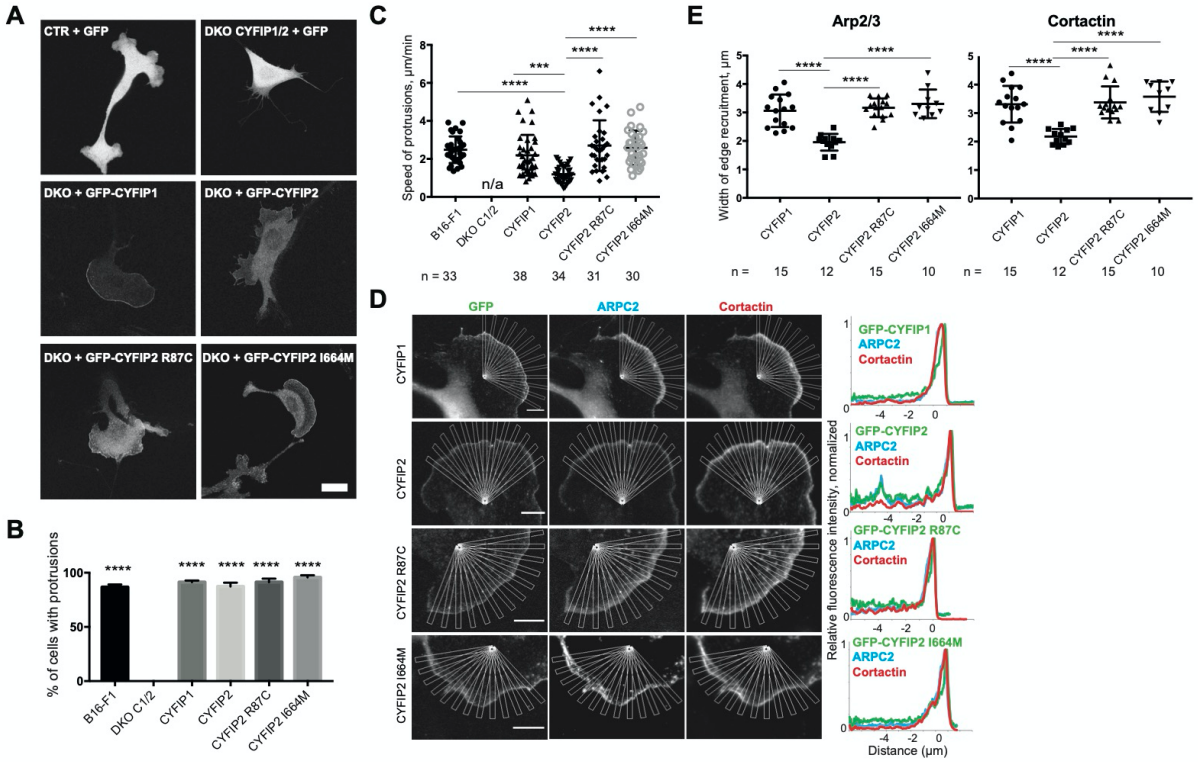


Fig.5, Polesskaya et al.

**Figure 5. CYFIP2 rescues *CYFIP1/2* Double Knock-Out (DKO).** GFP-tagged CYFIP1, CYFIP2, and two CYFIP2 mutants were expressed in B16-F1 control cells and in DKO cells. (A) Distribution of GFP fusion proteins and morphology of transfected cells. Scale bar: 20 µm. (B) Percentage of transfected cells forming protrusions, n=100, analysis by one-way ANOVA and Dunnett's multiple comparisons test. (C) Average speed of protrusions. Only the significant differences as determined by one-way ANOVA and Tukey's multiple comparisons test are indicated. (D) Recruitment of GFP-tagged CYFIP1, CYFIP2, and mutant CYFIP2 assessed by multiple radial line scans. Average profiles of the indicated markers upon registering line scans. Scale bars: 5µm. (E) Width of Arp2/3 and cortactin recruitment. ***P<0.001; ****P<0.0001.

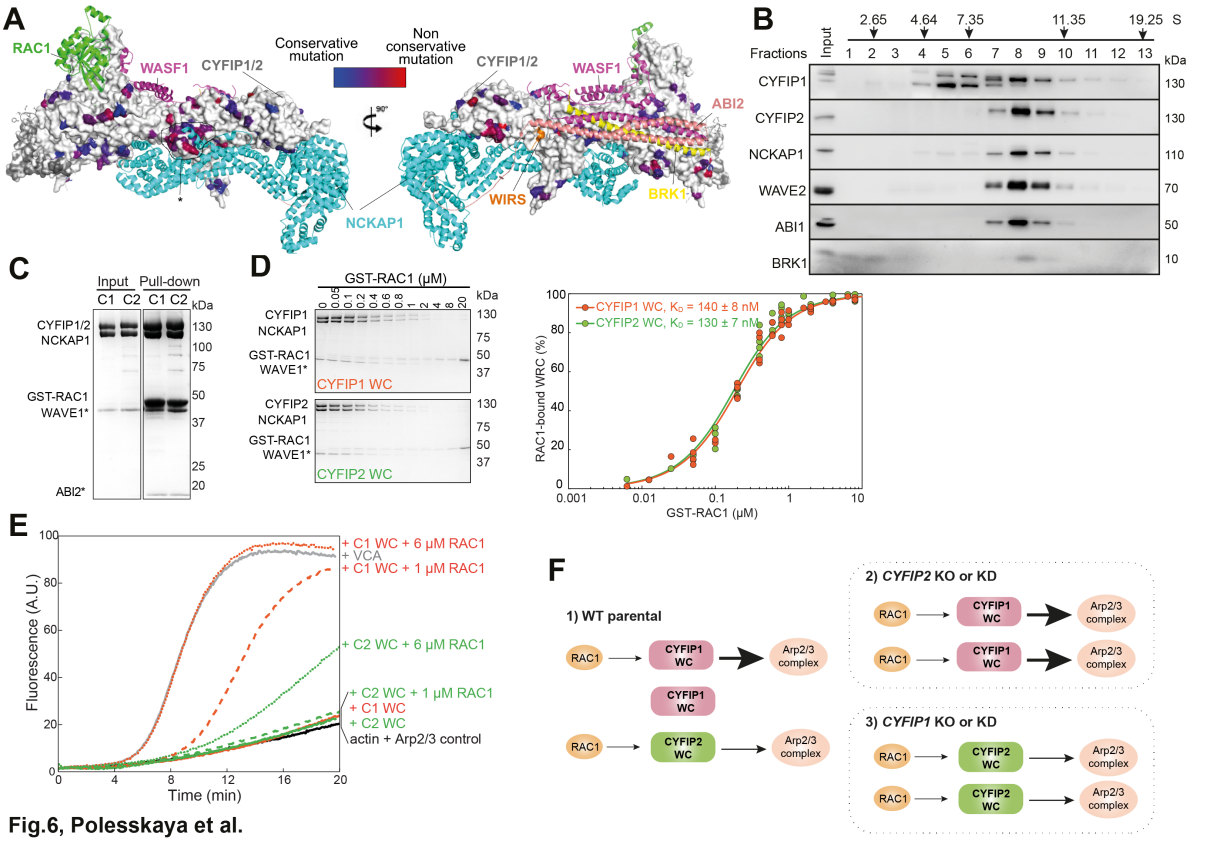


Fig.6, Polesskaya et al.

**Figure 6. CYFIP2-containing WAVE complexes are less activatable by RAC1 than CYFIP1-containing WAVE complexes.** (A) Structural models of CYFIP1 and CYFIP2. Sequence identity between CYFIP1 and CYFIP2 is 88% and non-conserved positions are colour-coded. The vast majority of non conserved residues fall outside of binding sites for known protein partners. WAVE complex subunits and WIRS peptide were obtained from PDB:4N78. RAC1 binding was modelled using the CYRI-B Rac1 complex as template (PDB:7AJK). (B) Ultracentrifugation of MCF10A lysate on a sucrose gradient. WAVE complex subunits are revealed by Western blots. The CYFIP1 antibody cross-reacts with a lower molecular weight band. (C) Coomassie-blue stained SDS-PAGE gels showing reconstitution of WAVE complexes containing CYFIP1 or CYFIP2 and pull-down with GTP-bound RAC1 (GST-RAC1 Q61L P29S). ABI2* and WAVE1* are not full length proteins (See Methods). (D) WAVE complexes containing supernatants upon pull-down with increasing amounts of GST-Rac1 Q61L P29S. Dissociation constants $K_D$ and standard errors are derived from fitting of quantification of 4 independent experiments at various concentrations. (E) Pyrene-actin polymerization assay of CYFIP1- or CYFIP2-containing WAVE complexes. Conditions: 4 μM actin (5% pyrene-labeled), 10 nM Arp2/3 complex, 100 nM WAVE complexes (WC) or WAVE1 WCA, and indicated amounts of untagged Rac1 Q61L P29S. Results are representative of two independent experiments. (F) Model: CYFIP2-containing WAVE complexes activate less Arp2/3 upon RAC1 binding than CYFIP1-containing WAVE complexes. Upon depletion of CYFIP2, Arp2/3 activity increases, because more CYFIP1 containing complexes are activated by RAC1, leading to increased migration. On the opposite, upon depletion of CYFIP1, Arp2/3 activity decreases, despite compensatory increase in CYFIP2 levels, leading to reduced migration.

**Table S1: Characteristics of the breast tumors relative to *CYFIP2* mRNA levels**

| | **Number of patients (%)** | **Number with metastases (%)** | ***p-value*** [a] | ***CYFIP2* mRNA normally expressed** | ***CYFIP2* mRNA over expressed (> 3)** | ***p-value*** [f] |
|---|---|---|---|---|---|---|
| *Total* | 527 (100) | 210 (39.8) | | 332 (63.0) | 195 (37.0) | |
| *Age* | | | | | | |
| <50 | 125 (23.7) | 52 (41.6) | 0.52 (NS) | 82 (65.6) | 43 (34.4) | 0.49 (NS) |
| >50 | 402 (76.3) | 158 (39.3) | | 250 (62.2) | 152 (37.8) | |
| *SBR histological grade* [b,c] | | | | | | |
| I | 60 (11.7) | 12 (20.0) | **0.0019** | 34 (56.7) | 26 (43.3) | **0.011** |
| II | 241 (47.1) | 100 (41.5) | | 141 (58.5) | 100 (41.5) | |
| III | 211 (41.2) | 94 (44.5) | | 150 (71.1) | 61 (28.9) | |
| *Lymph node status* [d] | | | | | | |
| 0 | 159 (30.5) | 48 (30.2) | **<0.0000001** | 96 (60.4) | 63 (39.6) | 0.66 (NS) |
| 1-3 | 250 (47.9) | 88 (35.2) | | 162 (64.8) | 88 (35.2) | |
| >3 | 113 (21.6) | 72 (63.7) | | 70 (61.9) | 43 (38.1) | |
| *Macroscopic tumor size* [e] | | | | | | |
| <25mm | 248 (48.0) | 77 (31.0) | **0.000015** | 154 (62.1) | 94 (37.9) | 0.66 (NS) |
| >25mm | 269 (52.0) | 132 (49.1) | | 172 (63.9) | 97 (36.1) | |
| *ERα status* | | | | | | |
| Negative | 181 (34.3) | 76 (42.0) | 0.10 (NS) | 138 (76.2) | 43 (23.8) | **0.0000052** |
| Positive | 346 (65.7) | 134 (38.7) | | 194 (56.1) | 152 (43.9) | |
| *PR status* | | | | | | |
| Negative | 255 (48.4) | 110 (43.1) | **0.025** | 186 (72.9) | 69 (27.1) | **0.0000047** |
| Positive | 272 (51.6) | 100 (36.8) | | 146 (53.7) | 126 (46.3) | |
| *ERBB2 status* | | | | | | |
| Negative | 397 (75.3) | 153 (38.5) | 0.17 (NS) | 235 (59.2) | 162 (40.8) | **0.0016** |
| Positive | 130 (24.7) | 57 (43.8) | | 97 (74.6) | 33 (25.4) | |
| *Molecular subtypes* | | | | | | |
| HR- ERBB2- | 102 (19.4) | 38 (37.3) | 0.054 (NS) | 71 (69.6) | 31 (30.4) | **0.00011** |
| HR- ERBB2+ | 72 (13.7) | 36 (50.0) | | 60 (83.3) | 12 (16.7) | |
| HR+ ERBB2- | 295 (56.0) | 115 (39.0) | | 164 (55.6) | 131 (44.4) | |
| HR+ ERBB2+ | 58 (11.0) | 21 (36.2) | | 37 (63.8) | 21 (36.2) | |

## Supplemental figures

**A**

| | Original values | | | Transformed and normalized values | | | |
|---|---|---|---|---|---|---|---|
| gene | coefficient | p-value | adjusted p-value | gene | coefficient | p-value | adjusted p-value |
| *NCKAP1* | 0.27 | 0.012 | 0.132 | *NCKAP1* | 0.195 | 0.005 | 0.055 |
| *CYFIP2* | -0.027 | 0.138 | 1 | *CYFIP2* | -0.134 | 0.059 | 0.59 |
| *NCKAP1L* | -0.051 | 0.288 | 1 | *NCKAP1L* | -0.058 | 0.397 | 1 |
| *WASF2* | -0.162 | 0.377 | 1 | *WASF3* | -0.045 | 0.519 | 1 |
| *ABI3* | -0.022 | 0.439 | 1 | *ABI1* | 0.042 | 0.546 | 1 |
| *WASF3* | -0.066 | 0.573 | 1 | *WASF2* | -0.041 | 0.561 | 1 |
| *ABI1* | 0.054 | 0.644 | 1 | *ABI3* | -0.036 | 0.603 | 1 |
| *ABI2* | -0.068 | 0.749 | 1 | *BRK1* | 0.035 | 0.609 | 1 |
| *CYFIP1* | -0.01 | 0.866 | 1 | *CYFIP1* | 0.036 | 0.612 | 1 |
| *WASF1* | 0.009 | 0.930 | 1 | *ABI2* | -0.034 | 0.624 | 1 |
| *BRK1* | 0.004 | 0.962 | 1 | *WASF1* | -0.007 | 0.919 | 1 |

**B**

| Subunit assembled | | | | | |
|---|---|---|---|---|---|
| NAP | CYFIP | ABI | WAVE | BRK | p-value |
| **1** | **2** | 2 | 3 | 1 | 0,0023 |
| **1** | **2** | 2 | 2 | 1 | 0,0032 |
| **1** | **2** | 1 | 3 | 1 | 0,0036 |
| **1** | **2** | 3 | 3 | 1 | 0,0038 |
| **1** | **2** | 1 | 2 | 1 | 0,0044 |
| **1** | **2** | 3 | 2 | 1 | 0,0044 |
| **1** | **2** | 2 | 1 | 1 | 0,0050 |
| **1** | **2** | 1 | 1 | 1 | 0,0069 |
| **1** | **2** | 3 | 1 | 1 | 0,0076 |
| **1** | 1 | 2 | 2 | 1 | 0,0098 |
| **1** | 1 | 2 | 3 | 1 | 0,0115 |
| **1** | 1 | 2 | 1 | 1 | 0,0167 |
| **1** | 1 | 3 | 2 | 1 | 0,0220 |
| **1** | 1 | 1 | 2 | 1 | 0,0246 |
| **1** | 1 | 3 | 3 | 1 | 0,0352 |
| **1** | 1 | 1 | 3 | 1 | 0,0444 |
| **1** | 1 | 3 | 1 | 1 | 0,0470 |
| **1** | 1 | 1 | 1 | 1 | 0,0569 |
| 2 | 2 | 1 | 3 | 1 | 0,2212 |
| 2 | 2 | 1 | 2 | 1 | 0,2464 |
| 2 | 2 | 1 | 1 | 1 | 0,3183 |
| 2 | 2 | 3 | 3 | 1 | 0,3259 |
| 2 | 2 | 2 | 3 | 1 | 0,3649 |
| 2 | 2 | 3 | 2 | 1 | 0,3764 |
| 2 | 2 | 3 | 1 | 1 | 0,4103 |
| 2 | 2 | 2 | 2 | 1 | 0,4154 |
| 2 | 2 | 2 | 1 | 1 | 0,4287 |
| 2 | 1 | 1 | 2 | 1 | 0,5184 |
| 2 | 1 | 2 | 2 | 1 | 0,6576 |
| 2 | 1 | 2 | 3 | 1 | 0,6746 |
| 2 | 1 | 1 | 3 | 1 | 0,6847 |
| 2 | 1 | 3 | 2 | 1 | 0,7330 |
| 2 | 1 | 2 | 1 | 1 | 0,7767 |
| 2 | 1 | 3 | 3 | 1 | 0,7998 |
| 2 | 1 | 1 | 1 | 1 | 0,8247 |
| 2 | 1 | 3 | 1 | 1 | 0,8945 |

**C**

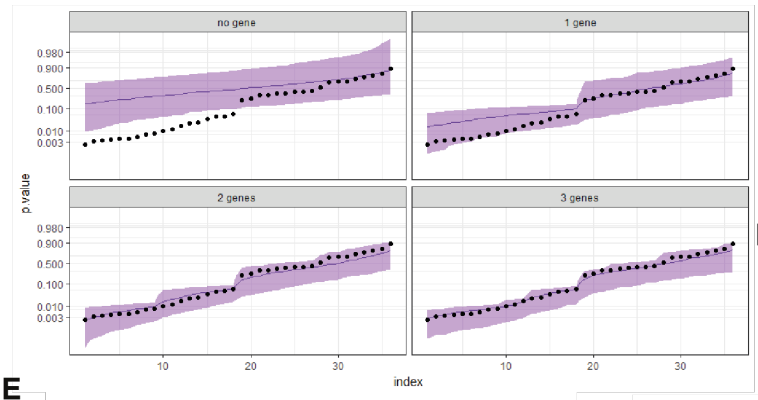


**D**

| Genes | log.likelihood | BIC |
|---|---|---|
| - | -1234.7 | 2469.3 |
| NCKAP1 | -1230.7 | 2466.8 |
| NCKAP1, CYFIP2 | -1227.6 | **2465.8** |
| NCKAP1, CYFIP2, WASF3 | -1226.2 | 2468.4 |
| NCKAP1, CYFIP2, WASF3, ABI2 | -1225.4 | 2472.2 |
| NCKAP1, CYFIP2, WASF3, ABI2, BRK1 | -1224.9 | 2476.6 |

**E**

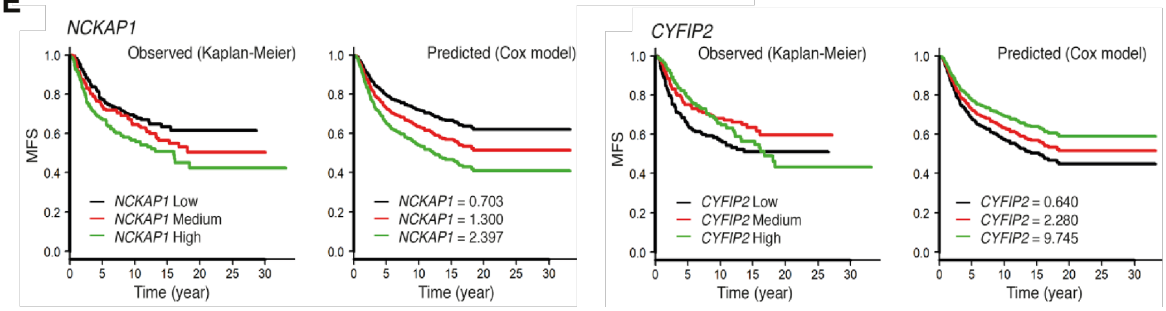


**Figure S1. Statistical modeling of the association of WAVE complexes with metastasis-free survival (MFS). A** Cox univariate analysis before and after transformation and normalization of mRNA levels of WAVE complex subunits. **B** Association of each WAVE assembly with MFS. **C** Random permutations. Experimental p values associated with the 36 WAVE assemblies (black dots) are compared with computed p-values corresponding to hypotheses (purple; 1000 simulations to derive the 90 % confidence interval): all subunits can be permuted (0 gene); all subunits except the most significant one, *NCKAP1*, can be permuted (1 gene); all subunits except the two most significant ones, *NCKAP1* and *CYFIP2*, can be permuted (2 genes); All subunits except the 3 most significant ones (3 genes) can be permuted. The small p-values obtained for the combination *NCKAP1* and *CYFIP2* are not obtained by chance, since computer simulations graphically illustrate the good agreement between what is observed and what is expected according to models when at least two of the most significant genes are fixed. **D** Comparison of the different models with Bayesian Information Criteria (BIC). The model with 2 fixed genes corresponds to the optimal statistical model, <hcih is used below and for Fig.1. **E** Kaplan-Meier of MFS as a function of NCKAP1 or CYFIP2 mRNA levels. Observed survival is modeled with the 2-variable Cox model.

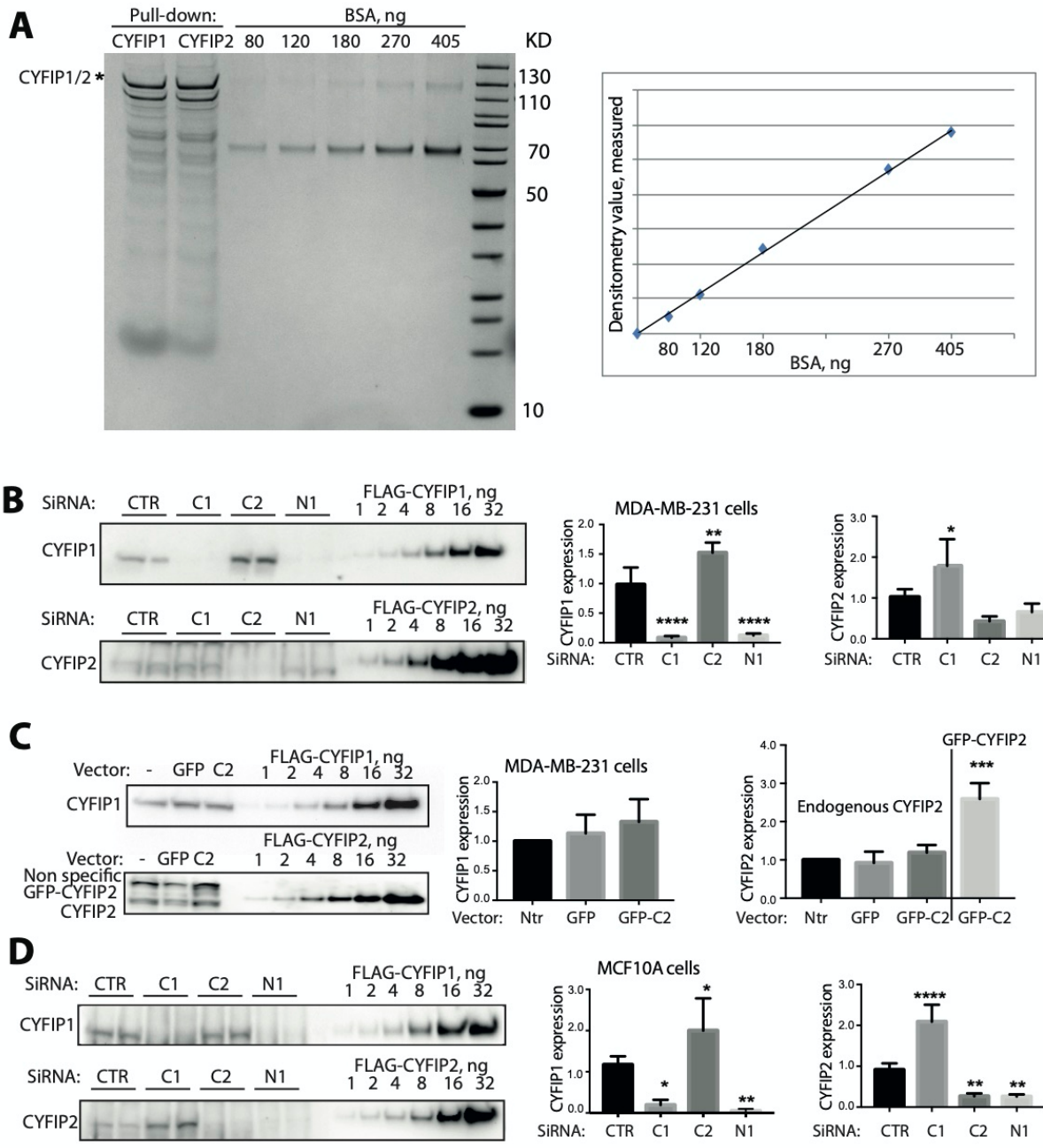


**Figure S2. Quantification of CYFIP1/2 proteins in MDA-MB-231 and MCF10A cells.** (A) Colloidal coomassie-stained gel with FLAG-tagged, purified CYFIP1/2-containing WAVE complexes, and BSA standard. We have purified tagged CYFIP1 or CYFIP2-containing WAVE complexes from stable 293 Flp-In cell lines. (B) Quantification of CYFIP1, CYFIP2 and NCKAP1 levels in MDA-MB-231 cells treated with siRNAs. Duplicate transfections of the siRNA smartpool were analyzed for each gene, the experiment was repeated twice (total n=4). (C) Quantification of CYFIP1, CYFIP2 and NCKAP1 levels in MDA-MB-231 stable cell lines expressing GFP or GFP-CYFIP2, n=3. (D) Quantification of CYFIP1, CYFIP2 and NCKAP1 levels in MCF10A cells treated with siRNAs. Duplicate transfections of the siRNA smartpool were analyzed for each gene, the experiment was repeated twice (total n=4). Mean ± SD. Shown are the statistically significant differences (one-way ANOVA). *P<0.05; **P<0.01; ***P<0.001; ****P<0.0001.

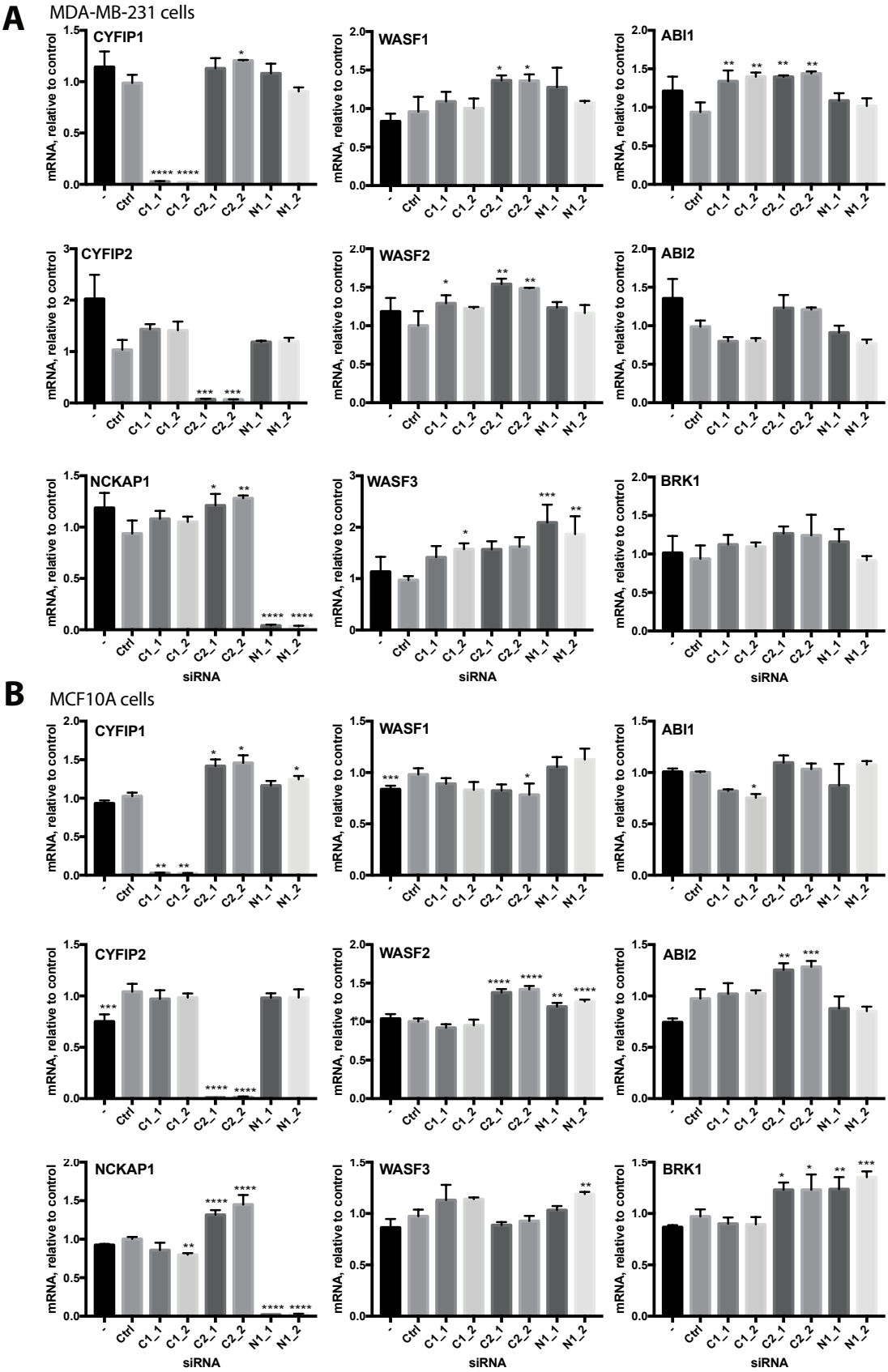


**Figure S3.** qRT-PCR analysis of mRNA levels of WAVE subunits in MDA-MB-231 and MCF10A cells transfected with two independent siRNAs targeting either CYFIP1 (C1),

CYFIP2 (C2), or NCKAP1 (N1). Mean ± SD of n=3 independent biological experiments, shown are the statistically significant differences (one-way ANOVA). *P<0.05; **P<0.01; ***P<0.001; ****P<0.0001.

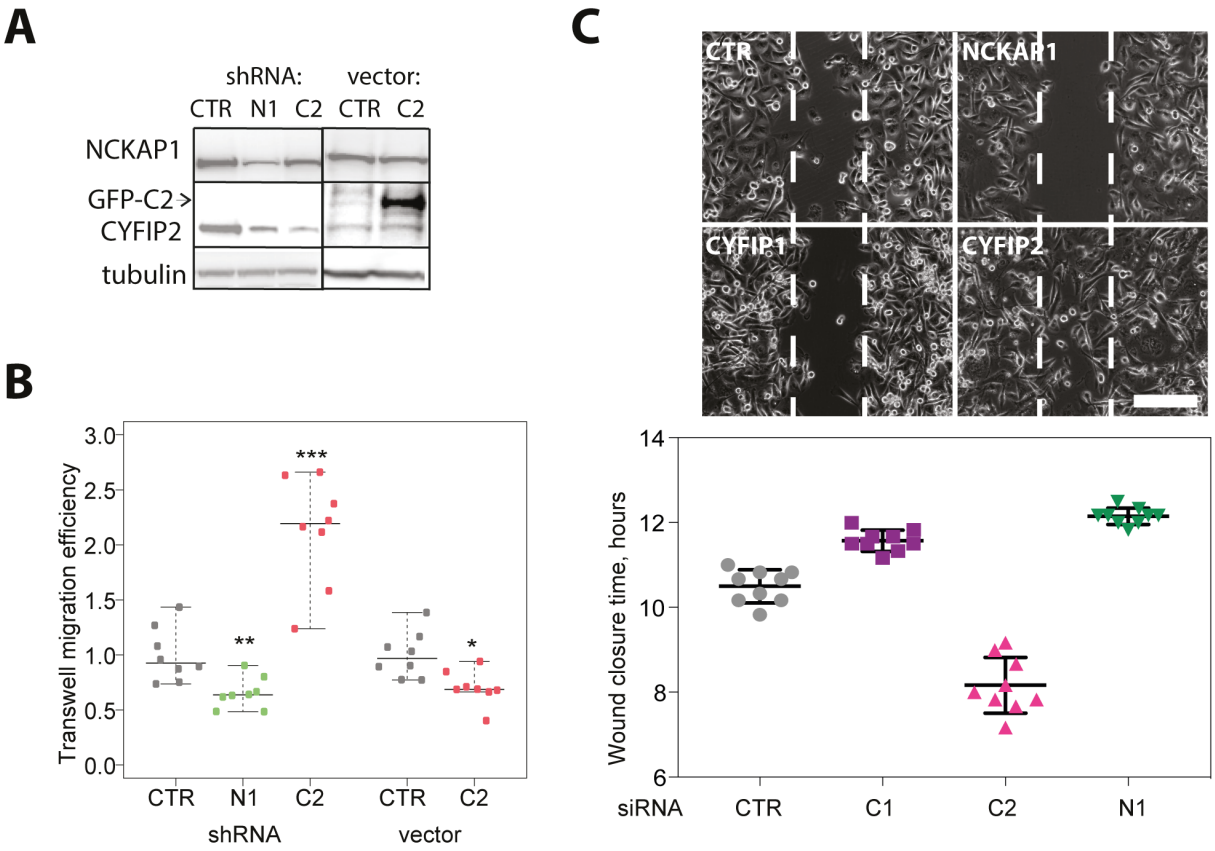


**Figure S4. Wound healing and Transwell migration assays of MDA-MB-231 cells.** (A) stable MDA-MB-231 cell lines expressing either the indicated shRNAs or overexpressing the GFP-CYFIP2 protein (GFP-C2) were analyzed by Western blots with NCKAP1 and CYFIP2 antibodies. (B) Quantification of Transwell migration efficiency of cells shown in (A), mean ± SD of n=9 (technical repeats), statistical analysis by one-way ANOVA. (C) Cells were transfected with indicated siRNAs targeting NCKAP1 (N1), CYFIP1 (C1), CYFIP2 (C2) or non-targeting controls (CTR) for 5 days, and plated on Ibidi dishes with inserts (Molinie & Gautreau, 2018). 24 h later, the inserts were removed, and wound healing was monitored by video microscopy as previously described. A picture was taken every 10 min for 18 h. Still images taken when the first wound is closed. Scale bar, 400 µm. Quantification of the closure time, mean ± SD of n=9 technical repeats, statistical analysis by one-way ANOVA.

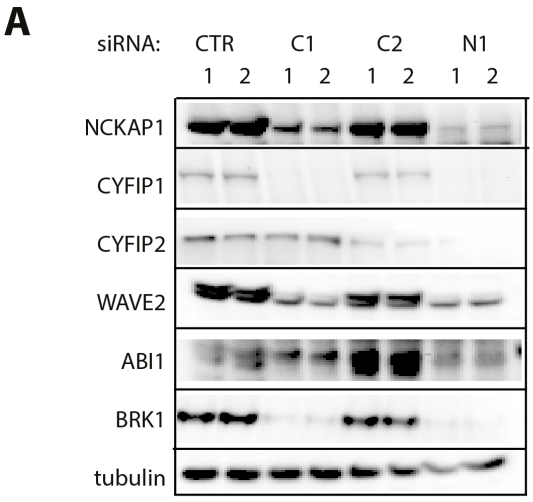


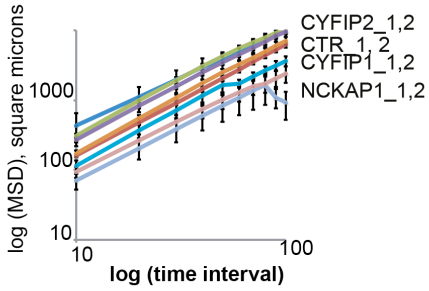


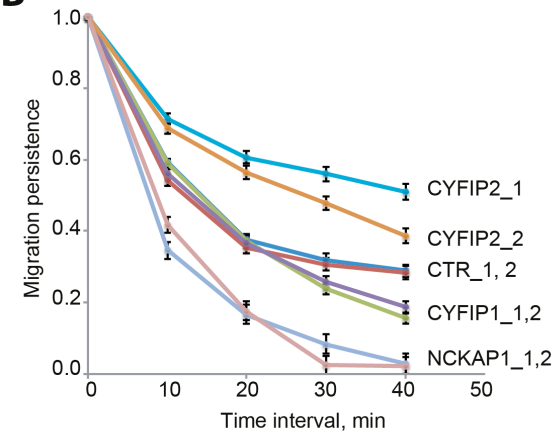


| | comparison | p-value | |
|---|---|---|---|
| 1 | Ctr_1/C1_1 | 0.46 | ns |
| 2 | Ctr_2/C1_1 | 0.82 | ns |
| 3 | Ctr_1/C1_2 | 0.38 | ns |
| 4 | Ctr_2/C1_2 | 0.71 | ns |
| 5 | Ctr_1/C2_1 | 0.0012 | ** |
| 6 | Ctr_2/C2_1 | 0.00023 | *** |
| 7 | Ctr_1/C2_2 | 0.044 | * |
| 8 | Ctr_2/C2_2 | 0.014 | * |
| 9 | Ctr_1/N1_1 | 0.00020 | *** |
| 10 | Ctr_2/N1_1 | 0.00077 | *** |
| 11 | Ctr_1/N1_2 | 0.00049 | *** |
| 12 | Ctr_2/N1_2 | 0.0016 | *** |

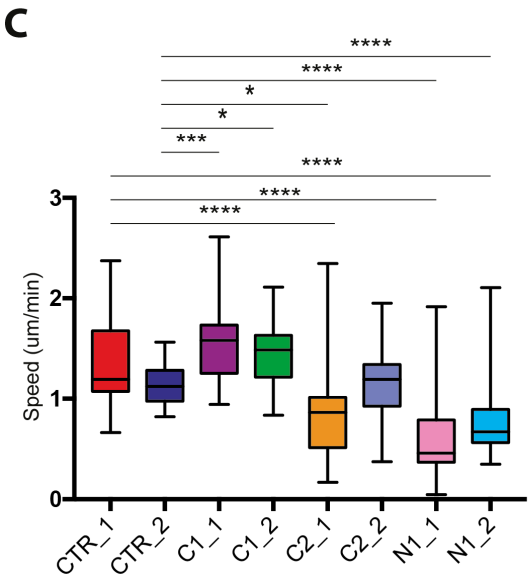

**Figure S5.** Two independent siRNAs targeting *CYFIP1*, *CYFIP2*, and *NCKAP1* were used to deplete the corresponding proteins from MCF10A cells. Depletion was evaluated by Western blot (A). From single cell trajectories of 2D random migration assays, migration persistence, speed and MSD were calculated and plotted (n=30 cells) (B-D). Statistical analysis was carried out by one-way ANOVA. In panel (C), only the significant differences are indicated.

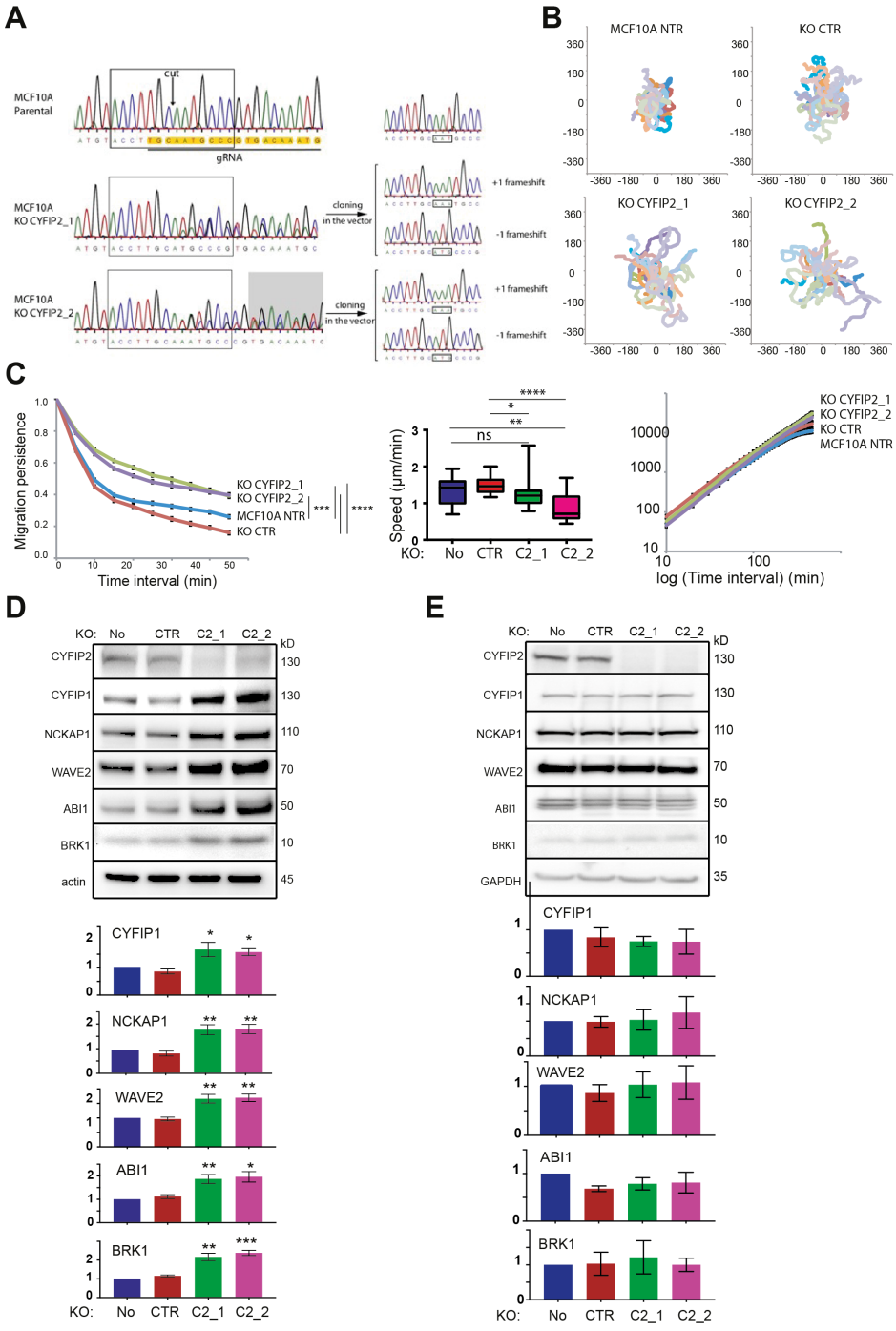


**Figure S6. Characterization of CYFIP2 KO clones 1 and 2 in MCF10A cells**. (**A**) The only two KO clones that were isolated appeared to have the same genetic alterations. Since they were truly independent, they were both analyzed in parallel in all subsequent assays. (**B**) Trajectories of CYFIP2 KO and control cells in 2D random migration assay, n=30. (**C**) Analysis of migration persistence, speed and MSD of cells shown in (**B**). (**D-E**) Expression of WAVE complex subunits and a quantification of three independent western blots in the above-shown cell lines immediately after selection (**D**) and after two months of culture (**E**).

## Supplemental Reference

Molinie N & Gautreau A (2018) Directional Collective Migration in Wound Healing Assays. *Methods in molecular biology (Clifton, NJ)* 1749: 11–19

## Legend to supplemental movies

**Movie S1. CYFIP2 inhibits migration of MCF7 cells in a wound healing assay.** Cells were transfected with indicated siRNAs targeting NCKAP1, CYFIP1, CYFIP2 or non-targeting controls (CTR) for 5 days, and plated on Ibidi dishes with inserts. 24 h later, inserts were removed, and wound healing was monitored by video microscopy. A picture was taken every 20 min. Scale bar: 400 μm.

**Movie S2. CYFIP2 inhibits migration of MDA-MB-231 cells in 3D collagen gel.** Cells transfected with the indicated siRNAs were recorded by phase contrast optics for 48 h with one frame every 20 min. Scale bar: 50 μm.

**Movie S3. CYFIP2 inhibits migration of MCF10A cells.** Cells transfected with the indicated siRNAs were recorded by phase contrast optics for 24 h with one frame every 5 min. For the calculation of migration parameters, only single cells were analyzed. Scale bar: 50 μm.

**Movie S4. Four-dimensional tracking of prechordal plate nuclei.** Nuclei of a Tg(gsc:GFP) embryo were labeled with Histone2B-mCherry (magenta). A Z-stack was acquired every 2 min. Nuclei of prechordal plate cells (identified by GFP expression and morphological criterion), not visible here, were 3D-tracked in time (white squares). Tracks are building up as cells are moving. Animal pole is to the right.

**Movie S5. CYFIP2 inhibits actin rich protrusions in zebrafish embryos during gastrulation.** Donor embryos were injected with the actin filament marker LifeAct-mCherry mRNA and morpholinos (Mo) targeting CYFIP1 (C1), CYFIP2 (C2), NCKAP1 (N1), alone or in combination with mRNAs encoding the same proteins. 1 frame per minute. Scale bar: 25 μm.

**Movie S6. GFP-CYFIP2 restores lamellipodium protrusion and is recruited to the lamellipodial edge.** B16-F1 mouse melanoma cells, control and CYFIP1/2 double knock-out (DKO) were transfected with the indicated GFP plasmids and green fluorescence was recorded every 10 s for 10 min.

**Movie S7. R87C and I664M CYFIP2 restore lamellipodium protrusion and are recruited to the lamellipodial edge.** CYFIP1/2 double knock-out (DKO) B16-F1 cells were transfected with the indicated GFP plasmids and green fluorescence was recorded every 10 s for 10 min.

# References


[1] Juan-Antonio Montero and Carl-Philipp Heisenberg. “Gastrulation dynamics: cells move into focus”. In: *Trends in cell biology* 14.11 (2004), pp. 620–627.

[2] Elena Scarpa and Roberto Mayor. “Collective cell migration in development”. In: *Journal of Cell Biology* 212.2 (2016), pp. 143–155.

[3] Peter Friedl and Bettina Weigelin. “Interstitial leukocyte migration and immune function”. In: *Nature immunology* 9.9 (2008), pp. 960–969.

[4] Hélène D Moreau et al. “Integrating physical and molecular insights on immune cell migration”. In: *Trends in immunology* 39.8 (2018), pp. 632–643.

[5] Li Li et al. “Collective cell migration: Implications for wound healing and cancer invasion”. In: *Burns & trauma* 1.1 (2013), pp. 2321–3868.

[6] Xavier Trepat, Zaozao Chen, and Ken Jacobson. “Cell migration”. In: *Comprehensive Physiology* 2.4 (2012), p. 2369.

[7] Tim Lämmermann and Michael Sixt. “Mechanical modes of ‘amoeboid’cell migration”. In: *Current opinion in cell biology* 21.5 (2009), pp. 636–644.

[8] Oliver T Fackler and Robert Grosse. “Cell motility through plasma membrane blebbing”. In: *The Journal of cell biology* 181.6 (2008), pp. 879–884.

[9] Ewa K Paluch and Erez Raz. “The role and regulation of blebs in cell migration”. In: *Current opinion in cell biology* 25.5 (2013), pp. 582–590.

[10] Kunito Yoshida and Thierry Soldati. “Dissection of amoeboid movement into two mechanically distinct modes”. In: *Journal of cell science* 119.18 (2006), pp. 3833–3844.

[11] Stephen E Malawista, Anne de Boisfleury Chevance, and Laurence A Boxer. “Random locomotion and chemotaxis of human blood polymorphonuclear leukocytes from a patient with Leukocyte Adhesion Deficiency-1: Normal displacement in close quarters via chimneying”. In: *Cell motility and the cytoskeleton* 46.3 (2000), pp. 183–189.

[12] Lillian K Fritz-Laylin, Samuel J Lord, and R Dyche Mullins. "WASP and SCAR are evolutionarily conserved in actin-filled pseudopod-based motility". In: *Journal of Cell Biology* 216.6 (2017), pp. 1673–1688.

[13] Lillian K Fritz-Laylin et al. "Actin-based protrusions of migrating neutrophils are intrinsically lamellar and facilitate direction changes". In: *Elife* 6 (2017), e26990.

[14] Thomas D Pollard and Gary G Borisy. "Cellular motility driven by assembly and disassembly of actin filaments". In: *Cell* 112.4 (2003), pp. 453–465.

[15] Stephanie L Gupton and Frank B Gertler. "Filopodia: the fingers that do the walking". In: *Science's STKE* 2007.400 (2007), re5–re5.

[16] Sharona Even-Ram and Kenneth M Yamada. "Cell migration in 3D matrix". In: *Current opinion in cell biology* 17.5 (2005), pp. 524–532.

[17] Peter Friedl. "Prespecification and plasticity: shifting mechanisms of cell migration". In: *Current opinion in cell biology* 16.1 (2004), pp. 14–23.

[18] Heiko Blaser et al. "Migration of zebrafish primordial germ cells: a role for myosin contraction and cytoplasmic flow". In: *Developmental cell* 11.5 (2006), pp. 613–627.

[19] Tatyana M Svitkina et al. "Analysis of the actin–myosin II system in fish epidermal keratocytes: mechanism of cell body translocation". In: *The Journal of cell biology* 139.2 (1997), pp. 397–415.

[20] Martin Bergert et al. "Cell mechanics control rapid transitions between blebs and lamellipodia during migration". In: *Proceedings of the National Academy of Sciences* 109.36 (2012), pp. 14434–14439.

[21] Peter Friedl and Katarina Wolf. "Plasticity of cell migration: a multiscale tuning model". In: *Journal of Cell Biology* 188.1 (2010), pp. 11–19.

[22] Veronika Te Boekhorst, Luigi Preziosi, and Peter Friedl. "Plasticity of cell migration in vivo and in silico". In: *Annual review of cell and developmental biology* 32 (2016), pp. 491–526.

[23] Yan-Jun Liu et al. "Confinement and low adhesion induce fast amoeboid migration of slow mesenchymal cells". In: *Cell* 160.4 (2015), pp. 659–672.

[24] Brian R Graziano et al. "Cell confinement reveals a branched-actin independent circuit for neutrophil polarity". In: *PLoS biology* 17.10 (2019), e3000457.

[25] Matteo Parri and Paola Chiarugi. "Rac and Rho GTPases in cancer cell motility control". In: *Cell communication and signaling* 8.1 (2010), pp. 1–14.

[26] Peter Friedl and Darren Gilmour. "Collective cell migration in morphogenesis, regeneration and cancer". In: *Nature reviews Molecular cell biology* 10.7 (2009), pp. 445–457.

[27] Roberto Mayor and Sandrine Etienne-Manneville. “The front and rear of collective cell migration”. In: *Nature reviews Molecular cell biology* 17.2 (2016), pp. 97–109.

[28] Adam Shellard and Roberto Mayor. “Supracellular migration–beyond collective cell migration”. In: *Journal of cell science* 132.8 (2019), jcs226142.

[29] Eric Theveneau and Roberto Mayor. “Can mesenchymal cells undergo collective cell migration? The case of the neural crest: The case of the neural crest”. In: *Cell adhesion & migration* 5.6 (2011), pp. 490–498.

[30] Katarina Wolf et al. “Multi-step pericellular proteolysis controls the transition from individual to collective cancer cell invasion”. In: *Nature cell biology* 9.8 (2007), pp. 893–904.

[31] Yael Hegerfeldt et al. “Collective cell movement in primary melanoma explants: plasticity of cell-cell interaction, $\beta$1-integrin function, and migration strategies”. In: *Cancer research* 62.7 (2002), pp. 2125–2130.

[32] Steffi Lehmann et al. “Hypoxia induces a HIF-1-dependent transition from collective-to-amoeboid dissemination in epithelial cancer cells”. In: *Current Biology* 27.3 (2017), pp. 392–400.

[33] Pieta K Mattila and Pekka Lappalainen. “Filopodia: molecular architecture and cellular functions”. In: *Nature reviews Molecular cell biology* 9.6 (2008), pp. 446–454.

[34] Matthias Krause and Alexis Gautreau. “Steering cell migration: lamellipodium dynamics and the regulation of directional persistence”. In: *Nature reviews Molecular cell biology* 15.9 (2014), pp. 577–590.

[35] Michael Abercrombie. “The Croonian Lecture, 1978-The crawling movement of metazoan cells”. In: *Proceedings of the Royal Society of London. Series B. Biological Sciences* 207.1167 (1980), pp. 129–147.

[36] Ryan J Petrie, Andrew D Doyle, and Kenneth M Yamada. “Random versus directionally persistent cell migration”. In: *Nature reviews Molecular cell biology* 10.8 (2009), pp. 538–549.

[37] Adam Shellard and Roberto Mayor. “All roads lead to directional cell migration”. In: *Trends in cell biology* 30.11 (2020), pp. 852–868.

[38] Cécile Arrieumerlou and Tobias Meyer. “A local coupling model and compass parameter for eukaryotic chemotaxis”. In: *Developmental cell* 8.2 (2005), pp. 215–227.

[39] Henry R Bourne and Orion Weiner. “Cell polarity: a chemical compass”. In: *Nature* 419.6902 (2002), pp. 21–21.

[40] Chun-Min Lo et al. “Cell movement is guided by the rigidity of the substrate”. In: *Biophysical journal* 79.1 (2000), pp. 144–152.

[41] Stephen B Carter. “Haptotaxis and the mechanism of cell motility”. In: *Nature* 213.5073 (1967), pp. 256–260.

[42] Min Zhao. “Electrical fields in wound healing—an overriding signal that directs cell migration”. In: *Seminars in cell & developmental biology*. Vol. 20. 6. Elsevier. 2009, pp. 674–682.

[43] Shuvasree SenGupta, Carole A Parent, and James E Bear. “The principles of directed cell migration”. In: *Nature Reviews Molecular Cell Biology* 22.8 (2021), pp. 529–547.

[44] Andrew J Muinonen-Martin et al. “Melanoma cells break down LPA to establish local gradients that drive chemotactic dispersal”. In: *PLoS biology* 12.10 (2014), e1001966.

[45] Luke Tweedy and Robert H Insall. “Self-generated gradients yield exceptionally robust steering cues”. In: *Frontiers in Cell and Developmental Biology* 8 (2020), p. 133.

[46] Ritankar Majumdar, Michael Sixt, and Carole A Parent. “New paradigms in the establishment and maintenance of gradients during directed cell migration”. In: *Current opinion in cell biology* 30 (2014), pp. 33–40.

[47] Kristen F Swaney, Chuan-Hsiang Huang, and Peter N Devreotes. “Eukaryotic chemotaxis: a network of signaling pathways controls motility, directional sensing, and polarity”. In: *Annual review of biophysics* 39 (2010), pp. 265–289.

[48] Fei Wang. “The signaling mechanisms underlying cell polarity and chemotaxis”. In: *Cold Spring Harbor perspectives in biology* 1.4 (2009), a002980.

[49] Min Zhu et al. “Spatial mapping of tissue properties in vivo reveals a 3D stiffness gradient in the mouse limb bud”. In: *Proceedings of the National Academy of Sciences* 117.9 (2020), pp. 4781–4791.

[50] Linyi Cai et al. “The role of the lysyl oxidases in tissue repair and remodeling: A concise review”. In: *Tissue engineering and regenerative medicine* 14.1 (2017), pp. 15–30.

[51] Yunfei Chen et al. “Matrix metalloproteinases in remodeling of lower extremity veins and chronic venous disease”. In: *Progress in molecular biology and translational science* 147 (2017), pp. 267–299.

[52] Elias H Barriga et al. “Tissue stiffening coordinates morphogenesis by triggering collective cell migration in vivo”. In: *Nature* 554.7693 (2018), pp. 523–527.

[53] Sergey V Plotnikov et al. “Force fluctuations within focal adhesions mediate ECM-rigidity sensing to guide directed cell migration”. In: *Cell* 151.7 (2012), pp. 1513–1527.

[54] David E Koser et al. “Mechanosensing is critical for axon growth in the developing brain”. In: *Nature neuroscience* 19.12 (2016), pp. 1592–1598.

[55] Duncan B Wormer et al. “The focal adhesion-localized CdGAP regulates matrix rigidity sensing and durotaxis”. In: *PloS one* 9.3 (2014), e91815.

[56] Joseph HR Hetmanski et al. “Membrane tension orchestrates rear retraction in matrix-directed cell migration”. In: *Developmental cell* 51.4 (2019), pp. 460–475.

[57] Julieann I Puleo et al. “Mechanosensing during directed cell migration requires dynamic actin polymerization at focal adhesions”. In: *Journal of Cell Biology* 218.12 (2019), pp. 4215–4235.

[58] Jason T Smith, James T Elkin, and W Monty Reichert. “Directed cell migration on fibronectin gradients: effect of gradient slope”. In: *Experimental cell research* 312.13 (2006), pp. 2424–2432.

[59] Steve Hsu et al. “Effects of shear stress on endothelial cell haptotaxis on micropatterned surfaces”. In: *Biochemical and biophysical research communications* 337.1 (2005), pp. 401–409.

[60] Guillaume Charras and Erik Sahai. “Physical influences of the extracellular environment on cell migration”. In: *Nature reviews Molecular cell biology* 15.12 (2014), pp. 813–824.

[61] Milka Sarris et al. “Inflammatory chemokines direct and restrict leukocyte migration within live tissues as glycan-bound gradients”. In: *Current Biology* 22.24 (2012), pp. 2375–2382.

[62] Michele Weber et al. “Interstitial dendritic cell guidance by haptotactic chemokine gradients”. In: *Science* 339.6117 (2013), pp. 328–332.

[63] Beth P Nguyen et al. “Deposition of laminin 5 in epidermal wounds regulates integrin signaling and adhesion”. In: *Current opinion in cell biology* 12.5 (2000), pp. 554–562.

[64] Josephine T Daub and Roeland MH Merks. “A cell-based model of extracellular-matrix-guided endothelial cell migration during angiogenesis”. In: *Bulletin of mathematical biology* 75.8 (2013), pp. 1377–1399.

[65] Samantha J King et al. “Lamellipodia are crucial for haptotactic sensing and response”. In: *Journal of cell science* 129.12 (2016), pp. 2329–2342.

[66] Congying Wu et al. “Arp2/3 is critical for lamellipodia and response to extracellular matrix cues but is dispensable for chemotaxis”. In: *Cell* 148.5 (2012), pp. 973–987.

[67] Chun-Min Lo et al. “Nonmuscle myosin IIb is involved in the guidance of fibroblast migration”. In: *Molecular biology of the cell* 15.3 (2004), pp. 982–989.

[68] Kevin B Hotary and Kenneth R Robinson. “Endogenous electrical currents and voltage gradients in Xenopus embryos and the consequences of their disruption”. In: *Developmental biology* 166.2 (1994), pp. 789–800.

[69] Maria E Mycielska and Mustafa BA Djamgoz. “Cellular mechanisms of direct-current electric field effects: galvanotaxis and metastatic disease”. In: *Journal of cell science* 117.9 (2004), pp. 1631–1639.

[70] Greg M Allen, Alex Mogilner, and Julie A Theriot. “Electrophoresis of cellular membrane components creates the directional cue guiding keratocyte galvanotaxis”. In: *Current Biology* 23.7 (2013), pp. 560–568.

[71] David Caballero et al. “Ratchetaxis: long-range directed cell migration by local cues”. In: *Trends in cell biology* 25.12 (2015), pp. 815–827.

[72] Thomas D Pollard and John A Cooper. “Actin, a central player in cell shape and movement”. In: *science* 326.5957 (2009), pp. 1208–1212.

[73] Kenneth C Holmes et al. “Atomic model of the actin filament”. In: *Nature* 347.6288 (1990), pp. 44–49.

[74] Thomas D Pollard. “Actin and actin-binding proteins”. In: *Cold Spring Harbor perspectives in biology* 8.8 (2016), a018226.

[75] David Sept and J Andrew McCammon. “Thermodynamics and kinetics of actin filament nucleation”. In: *Biophysical journal* 81.2 (2001), pp. 667–674.

[76] Jeffrey R Kuhn and Thomas D Pollard. “Real-time measurements of actin filament polymerization by total internal reflection fluorescence microscopy”. In: *Biophysical journal* 88.2 (2005), pp. 1387–1402.

[77] Edward D Korn, Marie-France Carlier, and Dominique Pantaloni. “Actin polymerization and ATP hydrolysis”. In: *Science* 238.4827 (1987), pp. 638–644.

[78] Alexander Nürnberg, Thomas Kitzing, and Robert Grosse. “Nucleating actin for invasion”. In: *Nature Reviews Cancer* 11.3 (2011), pp. 177–187.

[79] Kristen Skruber, Tracy-Ann Read, and Eric A Vitriol. “Reconsidering an active role for G-actin in cytoskeletal regulation”. In: *Journal of cell science* 131.1 (2018), jcs203760.

[80] Thomas D Pollard. “Regulation of actin filament assembly by Arp2/3 complex and formins”. In: *Annu. Rev. Biophys. Biomol. Struct.* 36 (2007), pp. 451–477.

[81] L Carlsson et al. “Actin polymerizability is influenced by profilin, a low molecular weight protein in non-muscle cells”. In: *Journal of molecular biology* 115.3 (1977), pp. 465–483.

[82] Clarence E Schutt et al. “The structure of crystalline profilin–$\beta$-actin”. In: *Nature* 365.6449 (1993), pp. 810–816.

[83] M Pring, A Weber, and MR Bubb. “Profilin-actin complexes directly elongate actin filaments at the barbed end”. In: *Biochemistry* 31.6 (1992), pp. 1827–1836.

[84] CG Dos Remedios et al. “Actin binding proteins: regulation of cytoskeletal microfilaments”. In: *Physiological reviews* 83.2 (2003), pp. 433–473.

[85] Daniel Safer and Vivianne T Nachmias. “Beta thymosins as actin binding peptides”. In: *Bioessays* 16.7 (1994), pp. 473–479.

[86] Marie-France Carlier et al. “Modulation of the interaction between G-actin and thymosin beta 4 by the ATP/ADP ratio: possible implication in the regulation of actin dynamics”. In: *Proceedings of the National Academy of Sciences* 90.11 (1993), pp. 5034–5038.

[87] Pascal J Goldschmidt-Clermont et al. “The control of actin nucleotide exchange by thymosin beta 4 and profilin. A potential regulatory mechanism for actin polymerization in cells.” In: *Molecular biology of the cell* 3.9 (1992), pp. 1015–1024.

[88] Hans Georg Mannherz and Ewald Hannappel. “The $\beta$-thymosins: intracellular and extracellular activities of a versatile actin binding protein family”. In: *Cell motility and the cytoskeleton* 66.10 (2009), pp. 839–851.

[89] A Weber et al. “Interaction of thymosin. beta. 4 with muscle and platelet actin: implications for actin sequestration in resting platelets”. In: *Biochemistry* 31.27 (1992), pp. 6179–6185.

[90] Bo Xue et al. “Structural basis of thymosin-$\beta$4/profilin exchange leading to actin filament polymerization”. In: *Proceedings of the National Academy of Sciences* 111.43 (2014), E4596–E4605.

[91] Marie-France Carlier et al. “Actin depolymerizing factor (ADF/cofilin) enhances the rate of filament turnover: implication in actin-based motility”. In: *The Journal of cell biology* 136.6 (1997), pp. 1307–1322.

[92] Sutherland K Maciver and Patrick J Hussey. “The ADF/cofilin family: actin-remodeling proteins”. In: *Genome biology* 3.5 (2002), pp. 1–12.

[93] Laurent Blanchoin and Thomas D Pollard. “Interaction of actin monomers with AcanthamoebaActophorin (ADF/cofilin) and profilin”. In: *Journal of Biological Chemistry* 273.39 (1998), pp. 25106–25111.

[94] Ernesto Andrianantoandro and Thomas D Pollard. “Mechanism of actin filament turnover by severing and nucleation at different concentrations of ADF/cofilin”. In: *Molecular cell* 24.1 (2006), pp. 13–23.

[95] Wenxiang Cao, Jim P Goodarzi, and M Enrique. “Energetics and kinetics of cooperative cofilin–actin filament interactions”. In: *Journal of molecular biology* 361.2 (2006), pp. 257–267.

[96] Cristian Suarez et al. “Cofilin tunes the nucleotide state of actin filaments and severs at bare and decorated segment boundaries”. In: *Current Biology* 21.10 (2011), pp. 862–868.

[97] Gerhard Isenberg, Ueli Aebi, and Thomas D Pollard. “An actin-binding protein from Acanthamoeba regulates actin filament polymerization and interactions”. In: *Nature* 288.5790 (1980), pp. 455–459.

[98] Marc Edwards et al. “Capping protein regulators fine-tune actin assembly dynamics”. In: *Nature reviews Molecular cell biology* 15.10 (2014), pp. 677–689.

[99] Dorothy A Schafer, Phillip B Jennings, and John A Cooper. “Dynamics of capping protein and actin assembly in vitro: uncapping barbed ends by polyphosphoinositides.” In: *The Journal of cell biology* 135.1 (1996), pp. 169–179.

[100] Laurent Blanchoin, Thomas D Pollard, and R Dyche Mullins. “Interactions of ADF / cofilin, Arp2/3 complex, capping protein and profilin in remodeling of branched actin filament networks”. In: *Current Biology* 10.20 (2000), pp. 1273–1282.

[101] Melissa A Chesarone and Bruce L Goode. “Actin nucleation and elongation factors: mechanisms and interplay”. In: *Current opinion in cell biology* 21.1 (2009), pp. 28–37.

[102] Bruce L Goode and Michael J Eck. “Mechanism and function of formins in the control of actin assembly”. In: *Annu. Rev. Biochem.* 76 (2007), pp. 593–627.

[103] Jan Faix and Robert Grosse. “Staying in shape with formins”. In: *Developmental cell* 10.6 (2006), pp. 693–706.

[104] Martin Pring et al. “Mechanism of formin-induced nucleation of actin filaments”. In: *Biochemistry* 42.2 (2003), pp. 486–496.

[105] Dennis Breitsprecher and Bruce L Goode. “Formins at a glance”. In: *Journal of cell science* 126.1 (2013), pp. 1–7.

[106] Naomi Courtemanche. “Mechanisms of formin-mediated actin assembly and dynamics”. In: *Biophysical reviews* 10.6 (2018), pp. 1553–1569.

[107] Luyan Cao et al. “Modulation of formin processivity by profilin and mechanical tension”. In: *Elife* 7 (2018), e34176.

[108] Laura M Machesky et al. “Purification of a cortical complex containing two unconventional actins from Acanthamoeba by affinity chromatography on profilin-agarose.” In: *The Journal of cell biology* 127.1 (1994), pp. 107–115.

[109] Jasmine VG Abella et al. “Isoform diversity in the Arp2/3 complex determines actin filament dynamics”. In: *Nature cell biology* 18.1 (2016), pp. 76–86.

[110] Isabelle Rouiller et al. “The structural basis of actin filament branching by the Arp2/3 complex”. In: *The Journal of cell biology* 180.5 (2008), pp. 887–895.

[111] Simon A Johnston et al. “Arp2/3 complex activity in filopodia of spreading cells”. In: *BMC cell biology* 9.1 (2008), pp. 1–17.

[112] Farida Korobova and Tatyana Svitkina. “Arp2/3 complex is important for filopodia formation, growth cone motility, and neuritogenesis in neuronal cells”. In: *Molecular biology of the cell* 19.4 (2008), pp. 1561–1574.

[113] Hideki Yamaguchi et al. “Molecular mechanisms of invadopodium formation: the role of the N-WASP–Arp2/3 complex pathway and cofilin”. In: *The Journal of cell biology* 168.3 (2005), pp. 441–452.

[114] Danielle A Murphy and Sara A Courtneidge. “The’ins’ and’outs’ of podosomes and invadopodia: characteristics, formation and function”. In: *Nature reviews Molecular cell biology* 12.7 (2011), pp. 413–426.

[115] Robin C May et al. “Involvement of the Arp2/3 complex in phagocytosis mediated by Fc$\gamma$R or CR3”. In: *Nature cell biology* 2.4 (2000), pp. 246–248.

[116] Claudia Hinze and Emmanuel Boucrot. “Local actin polymerization during endocytic carrier formation”. In: *Biochemical Society Transactions* 46.3 (2018), pp. 565–576.

[117] Nadia Efimova and Tatyana M Svitkina. “Branched actin networks push against each other at adherens junctions to maintain cell–cell adhesion”. In: *Journal of Cell Biology* 217.5 (2018), pp. 1827–1845.

[118] Kexi Yi et al. “Dynamic maintenance of asymmetric meiotic spindle position through Arp2/3-complex-driven cytoplasmic streaming in mouse oocytes”. In: *Nature cell biology* 13.10 (2011), pp. 1252–1258.

[119] Benjamin R Schrank et al. “Nuclear ARP2/3 drives DNA break clustering for homology-directed repair”. In: *Nature* 559.7712 (2018), pp. 61–66.

[120] William Roman et al. “Myofibril contraction and crosslinking drive nuclear movement to the periphery of skeletal muscle”. In: *Nature cell biology* 19.10 (2017), pp. 1189–1201.

[121] Robert C Robinson et al. “Crystal structure of Arp2/3 complex”. In: *science* 294.5547 (2001), pp. 1679–1684.

[122] Avital A Rodal et al. “Conformational changes in the Arp2/3 complex leading to actin nucleation”. In: *Nature structural & molecular biology* 12.1 (2005), pp. 26–31.

[123] Laura M Machesky et al. “Scar, a WASp-related protein, activates nucleation of actin filaments by the Arp2/3 complex”. In: *Proceedings of the National Academy of Sciences* 96.7 (1999), pp. 3739–3744.

[124] Nicolas Molinie and Alexis Gautreau. “The Arp2/3 regulatory system and its deregulation in cancer”. In: *Physiological reviews* 98.1 (2018), pp. 215–238.

[125] Kenneth G Campellone and Matthew D Welch. “A nucleator arms race: cellular control of actin assembly”. In: *Nature reviews Molecular cell biology* 11.4 (2010), pp. 237–251.

[126] Shail Kabrawala, Margaret D Zimmer, and Kenneth G Campellone. “WHIMP links the actin nucleation machinery to Src-family kinase signaling during protrusion and motility”. In: *PLoS genetics* 16.3 (2020), e1008694.

[127] Jean-Baptiste Marchand et al. “Interaction of WASP/Scar proteins with actin and vertebrate Arp2/3 complex”. In: *Nature cell biology* 3.1 (2001), pp. 76–82.

[128] David Chereau et al. “Actin-bound structures of Wiskott–Aldrich syndrome protein (WASP)-homology domain 2 and the implications for filament assembly”. In: *Proceedings of the National Academy of Sciences* 102.46 (2005), pp. 16644–16649.

[129] Erin D Goley et al. “Critical conformational changes in the Arp2/3 complex are induced by nucleotide and nucleation promoting factor”. In: *Molecular cell* 16.2 (2004), pp. 269–279.

[130] Irene Dang et al. “Inhibitory signalling to the Arp2/3 complex steers cell migration”. In: *Nature* 503.7475 (2013), pp. 281–284.

[131] Fred E Fregoso et al. “Molecular mechanism of Arp2/3 complex inhibition by Arpin”. In: *Nature Communications* 13.1 (2022), pp. 1–12.

[132] Tanja Maritzen et al. “Gadkin negatively regulates cell spreading and motility via sequestration of the actin-nucleating ARP2/3 complex”. In: *Proceedings of the National Academy of Sciences* 109.26 (2012), pp. 10382–10387.

[133] Hannah Schachtner et al. “Loss of Gadkin affects dendritic cell migration in vitro”. In: *PLoS One* 10.12 (2015), e0143883.

[134] Daniel L Rocca et al. “Inhibition of Arp2/3-mediated actin polymerization by PICK1 regulates neuronal morphology and AMPA receptor endocytosis”. In: *Nature cell biology* 10.3 (2008), pp. 259–271.

[135] Yadaiah Madasu et al. “PICK1 is implicated in organelle motility in an Arp2/3 complex–independent manner”. In: *Molecular biology of the cell* 26.7 (2015), pp. 1308–1322.

[136] Alissa M Weaver et al. "Cortactin promotes and stabilizes Arp2/3-induced actin filament network formation". In: *Current Biology* 11.5 (2001), pp. 370–374.

[137] Orit Siton et al. "Cortactin releases the brakes in actin-based motility by enhancing WASP-VCA detachment from Arp2/3 branches". In: *Current Biology* 21.24 (2011), pp. 2092–2097.

[138] Qing Luan and Brad J Nolen. "Structural basis for regulation of Arp2/3 complex by GMF". In: *Nature structural & molecular biology* 20.9 (2013), pp. 1062–1068.

[139] Minna Poukkula et al. "Actin-depolymerizing factor homology domain: a conserved fold performing diverse roles in cytoskeletal dynamics". In: *Cytoskeleton* 68.9 (2011), pp. 471–490.

[140] Liang Cai et al. "Coronin 1B antagonizes cortactin and remodels Arp2/3-containing actin branches in lamellipodia". In: *Cell* 134.5 (2008), pp. 828–842.

[141] Alexis M Gautreau et al. "Nucleation, stabilization, and disassembly of branched actin networks". In: *Trends in cell biology* (2021).

[142] Jonathan MJ Derry, Hans D Ochs, and Uta Francke. "Isolation of a novel gene mutated in Wiskott-Aldrich syndrome". In: *Cell* 78.4 (1994), pp. 635–644.

[143] Hiroaki Miki, Kenji Miura, and Tadaomi Takenawa. "N-WASP, a novel actin depolymerizing protein, regulates the cortical cytoskeletal rearrangement in a PIP2-dependent manner downstream of tyrosine kinases." In: *The EMBO journal* 15.19 (1996), pp. 5326–5335.

[144] Annette S Kim et al. "Autoinhibition and activation mechanisms of the Wiskott–Aldrich syndrome protein". In: *Nature* 404.6774 (2000), pp. 151–158.

[145] Hsin-Yi Henry Ho et al. "CR16 forms a complex with N-WASP in brain and is a novel member of a conserved proline-rich actin-binding protein family". In: *Proceedings of the National Academy of Sciences* 98.20 (2001), pp. 11306–11311.

[146] Henry N Higgs and Thomas D Pollard. "Activation by Cdc42 and PIP2 of Wiskott-Aldrich syndrome protein (WASp) stimulates actin nucleation by Arp2/3 complex". In: *The Journal of cell biology* 150.6 (2000), pp. 1311–1320.

[147] Kenneth E Prehoda et al. "Integration of multiple signals through cooperative regulation of the N-WASP-Arp2/3 complex". In: *Science* 290.5492 (2000), pp. 801–806.

[148] Nenad Tomasevic et al. "Differential regulation of WASP and N-WASP by Cdc42, Rac1, Nck, and PI (4, 5) P2". In: *Biochemistry* 46.11 (2007), pp. 3494–3502.

[149] Hsin-Yi Henry Ho et al. "Toca-1 mediates Cdc42-dependent actin nucleation by activating the N-WASP-WIP complex". In: *Cell* 118.2 (2004), pp. 203–216.

[150] Metello Innocenti et al. “Abi1 regulates the activity of N-WASP and WAVE in distinct actin-based processes”. In: *Nature cell biology* 7.10 (2005), pp. 969–976.

[151] Eduardo Torres and Michael K Rosen. “Protein-tyrosine kinase and GTPase signals cooperate to phosphorylate and activate Wiskott-Aldrich syndrome protein (WASP) / neuronal WASP”. In: *Journal of Biological Chemistry* 281.6 (2006), pp. 3513–3520.

[152] Christien J Merrifield et al. “Neural Wiskott Aldrich Syndrome Protein (N-WASP) and the Arp2/3 complex are recruited to sites of clathrin-mediated endocytosis in cultured fibroblasts”. In: *European journal of cell biology* 83.1 (2004), pp. 13–18.

[153] Stefanie Benesch et al. “N-WASP deficiency impairs EGF internalization and actin assembly at clathrin-coated pits”. In: *Journal of cell science* 118.14 (2005), pp. 3103–3115.

[154] Stefanie Benesch et al. “Phosphatidylinositol 4, 5-Biphosphate (PIP2)-induced Vesicle Movement Depends on N-WASP and Involves Nck, WIP, and Grb2* 210”. In: *Journal of Biological Chemistry* 277.40 (2002), pp. 37771–37776.

[155] Kiyohito Mizutani et al. “Essential role of neural Wiskott-Aldrich syndrome protein in podosome formation and degradation of extracellular matrix in src-transformed fibroblasts”. In: *Cancer research* 62.3 (2002), pp. 669–674.

[156] Elena V Linardopoulou et al. “Human subtelomeric WASH genes encode a new subclass of the WASP family”. In: *PLoS genetics* 3.12 (2007), e237.

[157] Emmanuel Derivery et al. “The Arp2/3 activator WASH controls the fission of endosomes through a large multiprotein complex”. In: *Developmental cell* 17.5 (2009), pp. 712–723.

[158] Da Jia et al. “WASH and WAVE actin regulators of the Wiskott–Aldrich syndrome protein (WASP) family are controlled by analogous structurally related complexes”. In: *Proceedings of the National Academy of Sciences* 107.23 (2010), pp. 10442–10447.

[159] Maria Hernandez-Valladares et al. “Structural characterization of a capping protein interaction motif defines a family of actin filament regulators”. In: *Nature structural & molecular biology* 17.4 (2010), pp. 497–503.

[160] Laura Park et al. “Cyclical action of the WASH complex: FAM21 and capping protein drive WASH recycling, not initial recruitment”. In: *Developmental cell* 24.2 (2013), pp. 169–181.

[161] Sai P Visweshwaran et al. “The trimeric coiled-coil HSBP 1 protein promotes WASH complex assembly at centrosomes”. In: *The EMBO journal* 37.13 (2018), e97706.

[162] Yi-Heng Hao et al. “Regulation of WASH-dependent actin polymerization and protein trafficking by ubiquitination”. In: *Cell* 152.5 (2013), pp. 1051–1064.

[163] Rui Dong et al. “Endosome-ER contacts control actin nucleation and retromer function through VAP-dependent regulation of PI4P”. In: *Cell* 166.2 (2016), pp. 408–423.

[164] Amika Singla et al. “Endosomal PI (3) P regulation by the COMMD/CCDC22/CCDC93 (CCC) complex controls membrane protein recycling”. In: *Nature communications* 10.1 (2019), pp. 1–17.

[165] Alexis Gautreau, Ksenia Oguievetskaia, and Christian Ungermann. “Function and regulation of the endosomal fusion and fission machineries”. In: *Cold Spring Harbor perspectives in biology* 6.3 (2014), a016832.

[166] Emmanuèle Helfer et al. “Endosomal recruitment of the WASH complex: active sequences and mutations impairing interaction with the retromer”. In: *Biology of the Cell* 105.5 (2013), pp. 191–207.

[167] Christopher Burd and Peter J Cullen. “Retromer: a master conductor of endosome sorting”. In: *Cold Spring Harbor perspectives in biology* 6.2 (2014), a016774.

[168] Emmanuel Derivery et al. “Actin polymerization controls the organization of WASH domains at the surface of endosomes”. In: *PloS one* 7.6 (2012), e39774.

[169] Artem I Fokin et al. “The Arp1/11 minifilament of dynactin primes the endosomal Arp2/3 complex”. In: *Science advances* 7.3 (2021), eabd5956.

[170] Artem I Fokin and Alexis M Gautreau. “Assembly and activity of the WASH molecular machine: distinctive features at the crossroads of the actin and microtubule cytoskeletons”. In: *Frontiers in Cell and Developmental Biology* 9 (2021), p. 751.

[171] Francesca Farina et al. “The centrosome is an actin-organizing centre”. In: *Nature cell biology* 18.1 (2016), pp. 65–75.

[172] Dorian Obino et al. “Actin nucleation at the centrosome controls lymphocyte polarity”. In: *Nature communications* 7.1 (2016), pp. 1–14.

[173] Francesca Farina et al. “Local actin nucleation tunes centrosomal microtubule nucleation during passage through mitosis”. In: *The EMBO journal* 38.11 (2019), e99843.

[174] Daisuke Inoue et al. “Actin filaments regulate microtubule growth at the centrosome”. In: *The EMBO journal* 38.11 (2019), e99630.

[175] Kenneth G Campellone et al. “WHAMM is an Arp2/3 complex activator that binds microtubules and functions in ER to Golgi transport”. In: *Cell* 134.1 (2008), pp. 148–161.

[176] Qing-Tao Shen et al. “Structural insights into WHAMM-mediated cytoskeletal coordination during membrane remodeling”. In: *Journal of Cell Biology* 199.1 (2012), pp. 111–124.

[177] Tianyang Liu et al. “Structural Insights of WHAMM’s Interaction with Microtubules by Cryo-EM”. In: *Journal of Molecular Biology* 429.9 (2017), pp. 1352–1363.

[178] J Bradley Zuchero et al. “p53-cofactor JMY is a multifunctional actin nucleation factor”. In: *Nature cell biology* 11.4 (2009), pp. 451–459.

[179] Amanda S Coutts, Louise Weston, and Nicholas B La Thangue. “A transcription cofactor integrates cell adhesion and motility with the p53 response”. In: *Proceedings of the National Academy of Sciences* 106.47 (2009), pp. 19872–19877.

[180] Kai Schlüter et al. “JMY is involved in anterograde vesicle trafficking from the trans-Golgi network”. In: *European journal of cell biology* 93.5-6 (2014), pp. 194–204.

[181] Virginia L King et al. “The actin nucleation factors JMY and WHAMM enable a rapid Arp2/3 complex-mediated intrinsic pathway of apoptosis”. In: *PLoS Genetics* 17.4 (2021), e1009512.

[182] David J Kast et al. “WHAMM directs the Arp2/3 complex to the ER for autophagosome biogenesis through an actin comet tail mechanism”. In: *Current Biology* 25.13 (2015), pp. 1791–1797.

[183] Xiaohua Hu and R Dyche Mullins. “LC3 and STRAP regulate actin filament assembly by JMY during autophagosome formation”. In: *Journal of Cell Biology* 218.1 (2019), pp. 251–266.

[184] Hiroaki Miki, Shiro Suetsugu, and Tadaomi Takenawa. “WAVE, a novel WASP-family protein involved in actin reorganization induced by Rac”. In: *The EMBO journal* 17.23 (1998), pp. 6932–6941.

[185] Laura M Machesky and Robert H Insall. “Scar1 and the related Wiskott–Aldrich syndrome protein, WASP, regulate the actin cytoskeleton through the Arp2/3 complex”. In: *Current biology* 8.25 (1998), pp. 1347–1356.

[186] Shiro Suetsugu, Hiroaki Miki, and Tadaomi Takenawa. “Identification of two human WAVE/SCAR homologues as general actin regulatory molecules which associate with the Arp2/3 complex”. In: *Biochemical and biophysical research communications* 260.1 (1999), pp. 296–302.

[187] Alexis Gautreau et al. “Purification and architecture of the ubiquitous Wave complex”. In: *Proceedings of the National Academy of Sciences* 101.13 (2004), pp. 4379–4383.

[188] Klemens Rottner, Theresia EB Stradal, and Baoyu Chen. "WAVE regulatory complex". In: *Current Biology* 31.10 (2021), R512–R517.

[189] Emmanuel Derivery and Alexis Gautreau. "Generation of branched actin networks: assembly and regulation of the N-WASP and WAVE molecular machines". In: *Bioessays* 32.2 (2010), pp. 119–131.

[190] Craig F Stovold, Thomas H Millard, and Laura M Machesky. "Inclusion of Scar/WAVE3 in a similar complex to Scar/WAVE1 and 2". In: *BMC cell biology* 6.1 (2005), pp. 1–12.

[191] Tadaomi Takenawa and Shiro Suetsugu. "The WASP–WAVE protein network: connecting the membrane to the cytoskeleton". In: *Nature reviews Molecular cell biology* 8.1 (2007), pp. 37–48.

[192] Jeffrey C Nolz et al. "The WAVE2 complex regulates actin cytoskeletal reorganization and CRAC-mediated calcium entry during T cell activation". In: *Current biology* 16.1 (2006), pp. 24–34.

[193] Patricia Kunda et al. "Abi, Sra1, and Kette control the stability and localization of SCAR/WAVE to regulate the formation of actin-based protrusions". In: *Current Biology* 13.21 (2003), pp. 1867–1875.

[194] Emmanuel Derivery et al. "Free Brick1 is a trimeric precursor in the assembly of a functional wave complex". In: *PloS one* 3.6 (2008), e2462.

[195] Joern Linkner et al. "High-resolution X-ray structure of the trimeric Scar/WAVE-Complex precursor Brk1". In: *PLoS One* 6.6 (2011), e21327.

[196] Zhucheng Chen et al. "Structure and control of the actin regulatory WAVE complex". In: *Nature* 468.7323 (2010), pp. 533–538.

[197] Sharon Eden et al. "Mechanism of regulation of WAVE1-induced actin nucleation by Rac1 and Nck". In: *Nature* 418.6899 (2002), pp. 790–793.

[198] Emmanuel Derivery et al. "The Wave complex is intrinsically inactive". In: *Cell motility and the cytoskeleton* 66.10 (2009), pp. 777–790.

[199] Baoyu Chen et al. "The WAVE regulatory complex links diverse receptors to the actin cytoskeleton". In: *Cell* 156.1-2 (2014), pp. 195–207.

[200] Baoyu Chen et al. "Rac1 GTPase activates the WAVE regulatory complex through two distinct binding sites". In: *Elife* 6 (2017), e29795.

[201] Shuang Wu et al. "Nudel is crucial for the WAVE complex assembly in vivo by selectively promoting subcomplex stability and formation through direct interactions". In: *Cell research* 22.8 (2012), pp. 1270–1284.

[202] Catherine Yan et al. “WAVE2 deficiency reveals distinct roles in embryogenesis and Rac-mediated actin-based motility”. In: *The EMBO journal* 22.14 (2003), pp. 3602–3612.

[203] Daisuke Yamazaki et al. “A novel function of WAVE in lamellipodia: WAVE1 is required for stabilization of lamellipodial protrusions during cell spreading”. In: *Genes to Cells* 10.5 (2005), pp. 381–392.

[204] Khalid Sossey-Alaoui et al. “Down-regulation of WAVE3, a metastasis promoter gene, inhibits invasion and metastasis of breast cancer cells”. In: *The American journal of pathology* 170.6 (2007), pp. 2112–2121.

[205] Mihaela Anitei and Bernard Hoflack. “Bridging membrane and cytoskeleton dynamics in the secretory and endocytic pathways”. In: *Nature cell biology* 14.1 (2012), pp. 11–19.

[206] Daisuke Yamazaki, Tsukasa Oikawa, and Tadaomi Takenawa. “Rac-WAVE-mediated actin reorganization is required for organization and maintenance of cell-cell adhesion”. In: *Journal of cell science* 120.1 (2007), pp. 86–100.

[207] Jason S King et al. “SCAR/WAVE is activated at mitosis and drives myosin-independent cytokinesis”. In: *Journal of cell science* 123.13 (2010), pp. 2246–2255.

[208] Yi Zhang et al. “Expression of MMP-9 and WAVE3 in colorectal cancer and its relationship to clinicopathological features”. In: *Journal of cancer research and clinical oncology* 138.12 (2012), pp. 2035–2044.

[209] Chunjie Wang et al. “Expression of Abl interactor 1 and its prognostic significance in breast cancer: a tissue-array-based investigation”. In: *Breast cancer research and treatment* 129.2 (2011), pp. 373–386.

[210] Jing Zhang et al. “Upregulation of Abelson interactor protein 1 predicts tumor progression and poor outcome in epithelial ovarian cancer”. In: *Human pathology* 46.9 (2015), pp. 1331–1340.

[211] Xiongwei Cai et al. “Metastatic potential of lung squamous cell carcinoma associated with HSPC300 through its interaction with WAVE2”. In: *Lung Cancer* 65.3 (2009), pp. 299–305.

[212] Maria E Lomakina et al. “Arpin downregulation in breast cancer is associated with poor prognosis”. In: *British journal of cancer* 114.5 (2016), pp. 545–553.

[213] Avadhut D Joshi et al. “ATM, CTLA4, MNDA, and HEM1 in high versus low CD38–expressing B-cell chronic lymphocytic leukemia”. In: *Clinical Cancer Research* 13.18 (2007), pp. 5295–5304.

[214] Anaïs Begemann et al. "New insights into the clinical and molecular spectrum of the novel CYFIP2-related neurodevelopmental disorder and impairment of the WRC-mediated actin dynamics". In: *Genetics in Medicine* 23.3 (2021), pp. 543–554.

[215] Sarah A Cook et al. "HEM1 deficiency disrupts mTORC2 and F-actin control in inherited immunodysregulatory disease". In: *Science* 369.6500 (2020), pp. 202–207.

[216] Makoto Yanagisawa, Chunhua Zhang, and Daniel B Szymanski. "ARP2/3-dependent growth in the plant kingdom: SCARs for life". In: *Frontiers in Plant Science* 4 (2013), p. 166.

[217] Michelle R Facette et al. "The SCAR/WAVE complex polarizes PAN receptors and promotes division asymmetry in maize". In: *Nature Plants* 1.2 (2015), pp. 1–8.

[218] Wenqi Zhou et al. "Homologs of SCAR/WAVE complex components are required for epidermal cell morphogenesis in rice". In: *Journal of experimental botany* 67.14 (2016), pp. 4311–4323.

[219] Dipanwita Basu et al. "DISTORTED3/SCAR2 is a putative Arabidopsis WAVE complex subunit that activates the Arp2/3 complex and is required for epidermal morphogenesis". In: *The Plant Cell* 17.2 (2005), pp. 502–524.

[220] Julia Dyachok et al. "Plasma membrane-associated SCAR complex subunits promote cortical F-actin accumulation and normal growth characteristics in Arabidopsis roots". In: *Molecular plant* 1.6 (2008), pp. 990–1006.

[221] Akira Miyahara et al. "Conservation in function of a SCAR/WAVE component during infection thread and root hair growth in Medicago truncatula". In: *Molecular plant-microbe interactions* 23.12 (2010), pp. 1553–1562.

[222] Liping Qiu et al. "SCARN a novel class of SCAR protein that is required for root-hair infection during legume nodulation". In: *PLoS Genetics* 11.10 (2015), e1005623.

[223] Aleksandr Gavrin et al. "Developmental modulation of root cell wall architecture confers resistance to an oomycete pathogen". In: *Current Biology* 30.21 (2020), pp. 4165–4176.

[224] Anne Pipathsouk et al. "The WAVE complex associates with sites of saddle membrane curvature". In: *Journal of Cell Biology* 220.8 (2021), e202003086.

[225] Andres M Lebensohn and Marc W Kirschner. "Activation of the WAVE complex by coincident signals controls actin assembly". In: *Molecular cell* 36.3 (2009), pp. 512–524.

[226] Yan Leng et al. "Abelson-interactor-1 promotes WAVE2 membrane translocation and Abelson-mediated tyrosine phosphorylation required for WAVE2 activation". In: *Proceedings of the National Academy of Sciences* 102.4 (2005), pp. 1098–1103.

[227] Amine Mehidi et al. “Transient activations of Rac1 at the lamellipodium tip trigger membrane protrusion”. In: *Current Biology* 29.17 (2019), pp. 2852–2866.

[228] Anika Steffen et al. “Rac function is crucial for cell migration but is not required for spreading and focal adhesion formation”. In: *Journal of cell science* 126.20 (2013), pp. 4572–4588.

[229] Matthias Schaks et al. “Distinct interaction sites of Rac GTPase with WAVE regulatory complex have non-redundant functions in vivo”. In: *Current Biology* 28.22 (2018), pp. 3674–3684.

[230] Loic Fort et al. “Fam49/CYRI interacts with Rac1 and locally suppresses protrusions”. In: *Nature cell biology* 20.10 (2018), pp. 1159–1171.

[231] Tamas Yelland et al. “Structural Basis of CYRI-B Direct Competition with Scar/WAVE Complex for Rac1”. In: *Structure* 29.3 (2021), pp. 226–237.

[232] Vassilis Koronakis et al. “WAVE regulatory complex activation by cooperating GTPases Arf and Rac1”. In: *Proceedings of the National Academy of Sciences* 108.35 (2011), pp. 14449–14454.

[233] Matthias Schaks et al. “RhoG and Cdc42 can contribute to Rac-dependent lamellipodia formation through WAVE regulatory complex-binding”. In: *Small GTPases* 12.2 (2021), pp. 122–132.

[234] Tsukasa Oikawa et al. “PtdIns (3, 4, 5) P3 binding is necessary for WAVE2-induced formation of lamellipodia”. In: *Nature cell biology* 6.5 (2004), pp. 420–426.

[235] Jérémie J Gautier et al. “Clathrin is required for Scar/Wave-mediated lamellipodium formation”. In: *Journal of cell science* 124.20 (2011), pp. 3414–3427.

[236] Hiroaki Miki et al. “IRSp53 is an essential intermediate between Rac and WAVE in the regulation of membrane ruffling”. In: *Nature* 408.6813 (2000), pp. 732–735.

[237] Andrea Disanza et al. “CDC42 switches IRSp53 from inhibition of actin growth to elongation by clustering of VASP”. In: *The EMBO journal* 32.20 (2013), pp. 2735–2750.

[238] Ah-Lai Law et al. “Lamellipodin and the Scar/WAVE complex cooperate to promote cell migration in vivo”. In: *Journal of Cell Biology* 203.4 (2013), pp. 673–689.

[239] Jeremy R Stuart et al. “c-Abl interacts with the WAVE2 signaling complex to induce membrane ruffling and cell spreading”. In: *Journal of Biological Chemistry* 281.42 (2006), pp. 31290–31297.

[240] Khalid Sossey-Alaoui, Xiurong Li, and John K Cowell. “c-Abl-mediated phosphorylation of WAVE3 is required for lamellipodia formation and cell migration”. In: *Journal of Biological Chemistry* 282.36 (2007), pp. 26257–26265.

[241] Hazel Ardern et al. “Src-dependent phosphorylation of Scar1 promotes its association with the Arp2/3 complex”. In: *Cell motility and the cytoskeleton* 63.1 (2006), pp. 6–13.

[242] Yong Kim et al. “Phosphorylation of WAVE1 regulates actin polymerization and dendritic spine morphology”. In: *Nature* 442.7104 (2006), pp. 814–817.

[243] Yuki Miyamoto, Junji Yamauchi, and Akito Tanoue. “Cdk5 phosphorylation of WAVE2 regulates oligodendrocyte precursor cell migration through nonreceptor tyrosine kinase Fyn”. In: *Journal of Neuroscience* 28.33 (2008), pp. 8326–8337.

[244] Shirin M Pocha and Giles O Cory. “WAVE2 is regulated by multiple phosphorylation events within its VCA domain”. In: *Cell motility and the cytoskeleton* 66.1 (2009), pp. 36–47.

[245] Seiji Ura et al. “Pseudopod growth and evolution during cell movement is controlled through SCAR/WAVE dephosphorylation”. In: *Current Biology* 22.7 (2012), pp. 553–561.

[246] Christopher M Danson et al. “Phosphorylation of WAVE2 by MAP kinases regulates persistent cell migration and polarity”. In: *Journal of cell science* 120.23 (2007), pp. 4144–4154.

[247] Michelle C Mendoza et al. “ERK-MAPK drives lamellipodia protrusion by activating the WAVE2 regulatory complex”. In: *Molecular cell* 41.6 (2011), pp. 661–671.

[248] Michelle C Mendoza. “Phosphoregulation of the WAVE regulatory complex and signal integration”. In: *Seminars in cell & developmental biology*. Vol. 24. 4. Elsevier. 2013, pp. 272–279.

[249] Pieter JA Eichhorn, Menno P Creyghton, and René Bernards. “Protein phosphatase 2A regulatory subunits and cancer”. In: *Biochimica et Biophysica Acta (BBA)-Reviews on Cancer* 1795.1 (2009), pp. 1–15.

[250] Brian A Hemmings et al. “. alpha.-And. beta.-forms of the 65-kDa subunit of protein phosphatase 2A have a similar 39 amino acid repeating structure”. In: *Biochemistry* 29.13 (1990), pp. 3166–3173.

[251] Stuart R Stone, Jan Hofsteenge, and Brian A Hemmings. “Molecular cloning of cDNAs encoding two isoforms of the catalytic subunit of protein phosphatase 2A”. In: *Biochemistry* 26.23 (1987), pp. 7215–7220.

[252] Regina E Mayer et al. “Structure of the 55-kDa regulatory subunit of protein phosphatase 2A: evidence for a neuronal-specific isoform”. In: *Biochemistry* 30.15 (1991), pp. 3589–3597.

[253] Juyeon Hwang and David C Pallas. "STRIPAK complexes: structure, biological function, and involvement in human diseases". In: *The international journal of biochemistry & cell biology* 47 (2014), pp. 118–148.

[254] Caitlin M O'Connor et al. "Therapeutic targeting of PP2A". In: *The international journal of biochemistry & cell biology* 96 (2018), pp. 182–193.

[255] Matthew R Groves et al. "The structure of the protein phosphatase 2A PR65/A subunit reveals the conformation of its 15 tandemly repeated HEAT motifs". In: *Cell* 96.1 (1999), pp. 99–110.

[256] Jaya Sangodkar et al. "All roads lead to PP 2A: exploiting the therapeutic potential of this phosphatase". In: *The FEBS journal* 283.6 (2016), pp. 1004–1024.

[257] Uhn Soo Cho and Wenqing Xu. "Crystal structure of a protein phosphatase 2A heterotrimeric holoenzyme". In: *Nature* 445.7123 (2007), pp. 53–57.

[258] Yongna Xing et al. "Structure of protein phosphatase 2A core enzyme bound to tumor-inducing toxins". In: *Cell* 127.2 (2006), pp. 341–353.

[259] Nathan Wlodarchak et al. "Structure of the Ca2+-dependent PP2A heterotrimer and insights into Cdc6 dephosphorylation". In: *Cell research* 23.7 (2013), pp. 931–946.

[260] Cuicui Chen et al. "Striatins contain a noncanonical coiled coil that binds protein phosphatase 2A A subunit to form a 2: 2 heterotetrameric core of striatin-interacting phosphatase and kinase (STRIPAK) complex". In: *Journal of Biological Chemistry* 289.14 (2014), pp. 9651–9661.

[261] Yang Tang et al. "Selective inhibition of STRN3-containing PP2A phosphatase restores hippo tumor-suppressor activity in gastric cancer". In: *Cancer Cell* 38.1 (2020), pp. 115–128.

[262] Byung-Cheon Jeong et al. "Cryo-EM structure of the Hippo signaling integrator human STRIPAK". In: *Nature structural & molecular biology* 28.3 (2021), pp. 290–299.

[263] Nathan Wlodarchak and Yongna Xing. "PP2A as a master regulator of the cell cycle". In: *Critical reviews in biochemistry and molecular biology* 51.3 (2016), pp. 162–184.

[264] Xiao Jiang et al. "Protein phosphatase 2A mediates YAP activation in endothelial cells upon VEGF stimulation and matrix stiffness". In: *Frontiers in Cell and Developmental Biology* 9 (2021), p. 1094.

[265] E Bousquet et al. "RhoB loss induces Rac1-dependent mesenchymal cell invasion in lung cells through PP2A inhibition". In: *Oncogene* 35.14 (2016), pp. 1760–1769.

[266] Chris D Madsen et al. "STRIPAK components determine mode of cancer cell migration and metastasis". In: *Nature cell biology* 17.1 (2015), pp. 68–80.

[267] Audrey Lin et al. “Small cytoskeleton-associated molecule, fibroblast growth factor receptor 1 oncogene partner 2/wound inducible transcript-3.0 (FGFR1OP2/wit3. 0), facilitates fibroblast-driven wound closure”. In: *The American journal of pathology* 176.1 (2010), pp. 108–121.

[268] Sophie J Bernelot Moens et al. “Rapid estrogen receptor signaling is essential for the protective effects of estrogen against vascular injury”. In: *Circulation* 126.16 (2012), pp. 1993–2004.

[269] Kazutaka Ueda et al. “Rapid estrogen receptor signaling mediates estrogen-induced inhibition of vascular smooth muscle cell proliferation”. In: *Arteriosclerosis, thrombosis, and vascular biology* 33.8 (2013), pp. 1837–1843.

[270] Siau Wei Bai et al. “Identification and characterization of a set of conserved and new regulators of cytoskeletal organization, cell morphology and migration”. In: *BMC biology* 9.1 (2011), pp. 1–18.

[271] Hisham Bazzi et al. “STRIP1, a core component of STRIPAK complexes, is essential for normal mesoderm migration in the mouse embryo”. In: *Proceedings of the National Academy of Sciences* 114.51 (2017), E10928–E10936.

[272] Jean-Marie Sontag and Estelle Sontag. “Protein phosphatase 2A dysfunction in Alzheimer’s disease”. In: *Frontiers in molecular neuroscience* 7 (2014), p. 16.

[273] Priyanka Sandal et al. “Protein phosphatase 2A–structure, function and role in neurodevelopmental disorders”. In: *Journal of cell science* 134.13 (2021), jcs248187.

[274] Jason D Arroyo and William C Hahn. “Involvement of PP2A in viral and cellular transformation”. In: *Oncogene* 24.52 (2005), pp. 7746–7755.

[275] Marc Mumby. “PP2A: unveiling a reluctant tumor suppressor”. In: *Cell* 130.1 (2007), pp. 21–24.

[276] Hirota Fujiki et al. “The concept of the okadaic acid class of tumor promoters is revived in endogenous protein inhibitors of protein phosphatase 2A, SET and CIP2A, in human cancers”. In: *Journal of cancer research and clinical oncology* 144.12 (2018), pp. 2339–2349.

[277] Melissa K McConechy et al. “Subtype-specific mutation of PPP2R1A in endometrial and ovarian carcinomas”. In: *The Journal of pathology* 223.5 (2011), pp. 567–573.

[278] Wen Chen et al. “Cancer-associated PP2A A$\alpha$ subunits induce functional haploinsufficiency and tumorigenicity”. In: *Cancer research* 65.18 (2005), pp. 8183–8192.

[279] George A Calin et al. “Low frequency of alterations of the $\alpha$ (PPP2R1A) and $\beta$ (PPP2R1B) isoforms of the subunit A of the serine-threonine phosphatase 2A in human neoplasms”. In: *Oncogene* 19.9 (2000), pp. 1191–1195.

[280] Munmun Rahman et al. “PPP2R1A mutation is a rare event in ovarian carcinoma across histological subtypes”. In: *Anticancer research* 33.1 (2013), pp. 113–118.

[281] Sarah E Taylor et al. “The highly recurrent PP2A A$\alpha$-subunit mutation P179R alters protein structure and impairs PP2A enzyme function to promote endometrial tumorigenesis”. In: *Cancer research* 79.16 (2019), pp. 4242–4257.

[282] Dorien Haesen et al. “Recurrent PPP2R1A mutations in uterine cancer act through a dominant-negative mechanism to promote malignant cell growth”. In: *Cancer research* 76.19 (2016), pp. 5719–5731.

[283] Caitlin M O’Connor et al. “Inactivation of PP2A by a recurrent mutation drives resistance to MEK inhibitors”. In: *Oncogene* 39.3 (2020), pp. 703–717.

[284] Ae Lee Jeong et al. “Patient derived mutation W257G of PPP2R1A enhances cancer cell migration through SRC-JNK-c-Jun pathway”. In: *Scientific reports* 6.1 (2016), pp. 1–12.

[285] Martin Beck et al. “The quantitative proteome of a human cell line”. In: *Molecular systems biology* 7.1 (2011), p. 549.

[286] Xinghai Li et al. “B56-associated protein phosphatase 2A is required for survival and protects from apoptosis in Drosophila melanogaster”. In: *Molecular and cellular biology* 22.11 (2002), pp. 3674–3684.

[287] Stefan Strack, J Thomas Cribbs, and Lisa Gomez. “Critical role for protein phosphatase 2A heterotrimers in mammalian cell survival”. In: *Journal of Biological Chemistry* 279.46 (2004), pp. 47732–47739.

[288] Veerle Janssens et al. “Identification and functional analysis of two Ca2+-binding EF-hand motifs in the B “/PR72 subunit of protein phosphatase 2A”. In: *Journal of Biological Chemistry* 278.12 (2003), pp. 10697–10706.

[289] Dawn R Christianson et al. “Ligand-directed targeting of lymphatic vessels uncovers mechanistic insights in melanoma metastasis”. In: *Proceedings of the National Academy of Sciences* 112.8 (2015), pp. 2521–2526.

[290] Kathryn P Burdon et al. “Mutations in a novel gene, NHS, cause the pleiotropic effects of Nance-Horan syndrome, including severe congenital cataract, dental anomalies, and mental retardation”. In: *The American Journal of Human Genetics* 73.5 (2003), pp. 1120–1130.

[291] SP Brooks et al. “Identification of the gene for Nance-Horan syndrome (NHS)”. In: *Journal of medical genetics* 41.10 (2004), pp. 768–771.

[292] Simon P Brooks et al. “The Nance–Horan syndrome protein encodes a functional WAVE homology domain (WHD) and is important for co-ordinating actin remodelling and maintaining cell morphology”. In: *Human molecular genetics* 19.12 (2010), pp. 2421–2432.

[293] Ah-Lai Law et al. “Nance-Horan Syndrome-like 1 protein negatively regulates Scar/WAVE-Arp2/3 activity and inhibits lamellipodia stability and cell migration”. In: *Nature communications* 12.1 (2021), pp. 1–20.

[294] Theresa Hwang et al. “Native proline-rich motifs exploit sequence context to target actin-remodeling Ena/VASP protein ENAH”. In: *eLife* 11 (2022), e70680.

[295] Benjamin A Smith et al. “Three-color single molecule imaging shows WASP detachment from Arp2/3 complex triggers actin filament branch formation”. In: *Elife* 2 (2013), e01008.

[296] Arthur Millius, Naoki Watanabe, and Orion D Weiner. “Diffusion, capture and recycling of SCAR/WAVE and Arp2/3 complexes observed in cells by single-molecule imaging”. In: *Journal of cell science* 125.5 (2012), pp. 1165–1176.

# *Acknowledgements*

First of all, I would like to thank my two supervisors, Dr. Anna Polesskaya and Prof. Alexis Gautreau. Thanks to Prof. Alexis Gautreau for providing me the opportunity to be a member of his team in 2018. Thanks to Dr. Anna Polesskaya for her continuous support and infinite patience during the project. It was really a pleasure to work with Anna and Alexis. They gave me a lot of inspiration on how to organize my ideas clearly and logically, both in the experimental plans and oral presentations. I also learned how to deal with the pressure of scientific research and how to manage my time well. Their enthusiasm and rigor for scientific research have deeply influenced me and keep me thinking about my interests and future career directions. I am sure that the lessons I learned from them will help me a lot in the future.

I would like to thank all the members of my thesis committee. Thanks to Dr. Raphaël Guérois and Dr. Maria-Carla Parrini for following the progress of my thesis and giving me precious suggestions. Thanks to Dr. Matthias Krause for his helpful discussions during my project. Thanks to Prof. Arnaud Echard and Dr. Julie Plastino for having agreed to be the examiner and reviewer of my thesis.

I want to thank all the current and former members of our lab. Thanks to Stéphane Romero for helping me with the nice experiments. Thanks to Artem Fokin and Gleb Simanov for helpful discussions and suggestions. Thanks to Nathalie Rocques, John James, Karina Rysenkova, Nikita Novikov, Maurine Marteau, Nicolas Molinié, and Dmitry Guschin, for allowing me to work in a warm atmosphere. Thanks to everyone in the Structural Biology of the Cell laboratory for their kindness and help.

Thanks to our collaborators Claire Dessalles, Avin Babataheri, Abdul Barakat from LadHyX, Ecole Polytechnique and Giovanni Chiappetta, Joelle Vinh from ESPCI Paris-Université PSL for their help with the interesting experiments in the project.

I would like to thank my parents and my brother. Thanks for their unconditional support of all my decisions and for the warmth and encouragement they gave me whenever I needed it. I feel so lucky to have them by my side. I would also like to thank my fiancé Chuang Yu, who has been with me for more than 10 years. I would like to thank him for encouraging and supporting me to pursue my PhD in France. Thanks to him for being with me when I was stressed, sharing my happiness when I made progress, and encouraging me to believe

in myself when I felt uncertain about the future. Of course, I also want to thank him for the programming he did for my statistical analysis, which saved me a lot of time.

Finally, thanks to Fondation pour la Recherche Médicale and Fondation ARC pour la Recherche sur le Cancer for supporting my work.

ECOLE DOCTORALE

**Titre :** PPP2R1A contrôle la persistance de la migration via le « WAVE Shell Complex ».

**Mots clés :** migration cellulaire, lamellipodes, réseau d'actine branché, ARP2/3, WAVE, PPP2R1A

**Résumé :** Lors de la migration cellulaire, la voie de signalisation RAC1-WAVE-ARP2/3 induit la polymérisation du réseau d'actine branché, qui sert de moteur à la protrusion des lamellipodes. Cette voie est finement régulée par de nombreux signaux de rétroaction qui contrôlent la durée de vie de la protrusion et la persistance de la migration. Nous avons choisi les cellules épithéliales du sein, la lignée MCF10A, afin d'identifier les protéines qui s'associent au complexe WAVE lors d'une migration persistante, mais dont l'association avec WAVE est modulée lorsque la production en aval d'actine branché est inhibée. Ce criblage protéomique différentiel a identifié PPP2R1A (une sous-unité régulatrice de la phosphatase trimérique PP2A) comme le candidat le plus intéressant pour une étude approfondie. J'ai pu démontrer que ce nouveau facteur associé à WAVE est requis pour la persistance de la migration dans les cellules humaines normales et cancéreuses, dans diverses conditions. Notre observation selon laquelle PPP2R1A interagit avec quatre sous-unités du complexe WAVE, mais pas avec WAVE/WASF, a conduit à la purification et à la caractérisation de « WAVE Shell Complex (WSC) », une nouvelle variante de WAVE contenant la protéine régulatrice de la migration NHSL1 qui s'est avérée être nécessaire à l'existence de WSC. Fait intéressant, PPP2R1A est muté sur plusieurs hotspots dans différents types de cancer, et ces mutations abolissent son interaction avec NHSL1 et WSC, suggérant un rôle critique de cette voie non seulement dans les cellules normales, mais aussi dans la progression du cancer.

**Title:** PPP2R1A regulates migration persistence through the WAVE Shell Complex.

**Keywords:** cell migration, lamellipodia, branched actin network, ARP2/3, WAVE, PPP2R1A

**Abstract:** During cell migration, the RAC1-WAVE-ARP2/3 signaling pathway induces the network of branched actin, that serves as a motor for lamellipodia protrusion. This pathway is finely regulated by numerous feed-back and feed-forward signals that control the protrusion lifetime and migration persistence.
We screened in MCF10A human breast epithelial cells for proteins that associate with the WAVE complex during persistent migration, but whose association with WAVE is modulated when the downstream production of branched actin is inhibited. The differential proteomics screen identified PPP2R1A (a regulatory subunit of the PP2A trimeric phosphatase) as the strongest hit and a novel WAVE-associated factor required for migration persistence in normal and cancer human cells, in various conditions. The differential proteomics screen identified PPP2R1A (a regulatory subunit of the PP2A trimeric phosphatase) as the strongest hit and a novel WAVE-associated factor required for migration persistence in normal and cancer human cells, in various conditions. Our observation that PPP2R1A interacts with four WAVE complex subunits, but not with WAVE/WASF, led to a purification and characterization of a "WAVE Shell Complex (WSC)", a novel variant of WAVE containing the migration regulatory protein NHSL1 that turned out to be necessary for the existence of WSC. Interestingly, PPP2R1A is mutated on hotspots in different cancer types, and these mutations abolish its interaction with NHSL1 and WSC, suggesting a critical role of for this pathway not only in normal cells, but also in cancer progression.